Glycosylated nanomaterials: Neutralisation and detection of bacteria and toxins

by

Sarah-Jane Richards

Thesis

Submitted to The University of Warwick

for the degree of

Doctor of Philosophy

MOAC Doctoral Training Centre

December 2014

THE UNIVERSITY OF WARWICK

In loving memory of

Nan Barnes

and

Brian Manifold

Contents

List of Schemes and Figures

Chapter 9   **Glyco-Gold Nanoparticle Libraries for Label-Free, Low-
                   Cost and High Throughput Evaluation of Glycan/Lectin
                   Interactions for Affinity Measurements and Ratiometric
                   Biosensing**

List of Tables

Abbreviations

ATRP	Atom-transfer radical-polymerisation
AIBN	Azobisisobutyronitrile
AuNP	Gold nanoparticle
BSA	Bovine serum albumin
cAMP	Cyclic adenosine monophosphate
CCT	Catalytic chain transfer
CFG	Consortium for Functional Glycomics
CFU	Colony forming units
CMLRP	Copper-mediated living radical polymerisation
Con A	Concanavalin A
CRP	Controlled radical polymerisation
CTx	Cholera toxin
CuAAC	Copper catalysed alkyne azide cycloaddition
Ð	Dispersity
DBU	Diazabicyclo[5.4.0]undec-7-ene
DC-SIGN	Dendritic Cell-Specific Intercellular adhesion molecule-3-Grabbing Non-integrin
DCM	Dichloromethane
DIPEA	Diisopropylethylamine
DLS	Dynamic light scattering
DMF	Dimethylformamide
DMSO	Dimethylsulfoxide
DP	Degree of polymerisation

E. coli	*Escherichia coli*
ELISA	Enzyme-linked immunosorbent assay
ELLA	Enzyme-linked lectin assay
FITC	Fluorescein isothiocyanate
FLSA	Fluorescent-linked sorbent assay
$GalN_3$	β-D-galactose-azide
Gb_3	Globotriaosylceramide
GCS	Galactocerebroside
glycoAuNP	Glycosylated gold nanoparticle
GM1	Monosialotetrahexosylganglioside
GM1os	GM1-oligosaccharide
HBS	HEPES buffered saline
HEPES	4-(2-Hydroxyethyl)piperazine-1-ethanesulfonic acid, N-(2-Hydroxyethyl)piperazine-N′-(2-ethanesulfonic acid)
HIV	Human immunodeficiency virus
HPLC	High pressure liquid chromatography
HSB	Hue, saturation, brightness
IR	Infra-red spectroscopy
ITC	Isothermal calorimetry
K_a	Association rate constant
K_d	Equilibrium binding constant
K_{off}	Disassociation rate constant
LD_{50}	Median lethal dose
LDA	Linear discriminate analysis
$\log P$	Partition coefficient

LSPR	Local surface plasmon resonance
LT	Heat labile enterotoxin
Me_6TREN	Tris[2-(dimethylamino)ethyl]amine
MeOD	Deuterated methanol
MIC_{50}	Minimum concentration required to inhibit 50 % of binding
M_n	Number average molecular weight
MS	Mass spectrometry
M_w	Weight average molecular weight
MWCO	Molecular weight cut-off
NMP	Nitroxide-mediated polymerisation
NMR	Nuclear magnetic resonance spectroscopy
OD	Optical density
OWLS	Optical waveguide lightmode spectroscopy
PAMAM	Polyamidoamine
PBS	Phosphate buffered saline
PCR	Polymerase chain reaction
PEG	Polyethylene glycol
PFP	Pentafluorophenol
pHEA	Poly(*N*-hydroxyethylacrylamide)
PI	Polypropyleneimine
PLG	Poly(L-glutamic acid)
PMMA	Poly(methylmethacrylate)
PNA	Peanut agglutinin
PPE	Poly(*p*-phenylene ethynylene)
PPFMA	Poly(pentafluorophenyl methacrylate)

QCM-d	Quartz crystal microbalance with dissipation monitoring
RAFT	Reversible addition-fragmentation chain-transfer
RCA$_{120}$	*Ricinus communis* agglutinin 120
RGB	Red green blue
ROI	Region of interest
ROMP	Ring opening metathesis polymerisation
S. auerus	*Staphlococcus aureus*
SBA	Soybean agglutinin
SEC	Size exclusion chromatography
SET-LRP	Single-electron transfer living radical polymerisation
SLT	Shiga-like toxin
SPR	Surface plasmon resonance
TBS	Tris buffered saline
TBTA	Tris(benzyltriazolylmethyl)amide
TEA	Triethylamine
TEM	Transmission electron microscopy
THF	Tetrahydrofuran
Tris	Tris(hydroxymethyl)aminomethane),
UEA	*Ulex europeus* agglutinin
V. cholerae	*Vibrio cholerae*
VDMA	2-vinyl-4,4-dimethylmethylazlactone
WGA	Wheat germ agglutinin
ΔD	Change in dissipation
Δf	Change in frequency

Acknowledgements

First, I would like to thank Matt, my supervisor, whose unwavering optimism has led to such a successful project. It is his enthusiasm and positive outlook that has helped me complete this thesis and allowed me to have such an enjoyable time doing it. I would like to thank him for the opportunity to join his (at the time very small) group and be there to watch it grow into a large, vibrant, research team.

Secondly, I'd like to thank my second supervisor, Del Besra at the University of Birmingham for the excellent opportunity to work in his impressive research lab. I'd like to also thank Liz Fullam for helping with the microbiology side of the project at both Birmingham and Warwick.

I have had a wonderful time being part of the Gibson group. My thanks go to Caroline, Dan, Tom and Lucienne for putting up with me in the office, complaining about writing my introduction, amongst many, many other things. I thank you for being there to help, support and bounce ideas off of, but mainly for keeping me sane over the past three and a bit years. Thanks also to all the other Gibson group members past and present who have influenced me during my PhD journey. Matt, Dan, Caroline and Tom I will forever have great memories of the ACS conference in San Francisco.

I'd like to thank Dave Haddleton for his kind words of support and his guidance and the Haddleton group, particularly Kay, (real) Jenny and Danielle who have supported me along the way. My thanks also go to Mat Jones for helping me right at the beginning of the project to get it off the ground.

I'd like to thank those who have given assistant to me with training and guidance on various instruments in the department including, Ben Douglas for his

Declaration

The work presented in this thesis is entirely original and my own work, except where acknowledged in the text. I confirm that this thesis has not been submitted for a degree at another University.

Chapter 2 was published as:

S-J. Richards, M. W. Jones, M. Hunaban, D. M. Haddleton, M. I. Gibson, 'Probing bacterial-toxin inhibition with synthetic glycopolymers prepared by tandem post-polymerisation modification: role of linker length and carbohydrate density', *Angew. Chem. Int. Ed.*, **2012**, *51*, 7932-7936.

Chapter 3 was published as:

M. W. Jones, **S-J. Richards**, D. M. Haddleton, M. I. Gibson, 'Poly(azlactones)s: versatile scaffolds for tandem post-polymerisation modification and glycopolymer synthesis', *Polym. Chem.* **2013**, *4*, 717.

Chapter 4 was published as:

M. W. Jones, L. Otten, **S-J. Richards**, R. Lowery, D. J. Phillips, D. M. Haddleton, M. I. Gibson, 'Glycopolymers with secondary binding motifs mimic glycan branching and display bacterial lectin selectivity in addition to affinity', *Chem. Sci.*, **2014**, *5*, 1611-1616.

Chapter 5 was published as:

Y. Gou, **S-J. Richards**, D. M. Haddleton, M. I. Gibson, *Polym. Chem.*, 'Investigation of glycopolymer-lectin interactions using QCM-d: comparison of surface binding with inhibitory activity', **2012**, *3*, 1634-1640.

Chapter 6 was published as:

L. Otten, **S-J. Richards**, E. Fullam, G. S. Besra, M. I. Gibson, 'Gold nanoparticle-linked analysis of carbohydrate-protein interactions, and polymeric inhibitors, using unlabelled proteins; easy measurement using a 'simple' digital camera', *J. Mater Chem. B.*, **2013**, *1*, 2665-2675.

Chapter 7 was published as:

S-J. Richards, E. Fullam, G. S. Besra, M. I. Gibson, 'Discrimination between bacterial phenotypes using glyconanoparticles and the impact of polymer coating on detection readouts', *J. Mater Chem. B.*, **2014**, *2*, 1490-1498.

Chapter 8 was published as:

S-J. Richards, M. I. Gibson, 'Optimisation of the polymer coating for glycosylated gold nanoparticle biosensors to ensure stability and rapid optical readouts', *ACS Macro Lett.*, **2014**, *3*, 1004-1008.

Chapter 9 is in preparation for:

S-J. Richards, L. Otten and M. I. Gibson, 'Glyco-gold nanoparticle libraries for label-free, low-cost and high throughput evaluation of glycan/lectin interactions for affinity measurements and ratiometric biosensing'

Abstract

The identification and treatment of bacterial infections remains a major healthcare challenge, especially to ensure appropriate application of a limited spectrum of antibiotics. Therefore the development of alternatives to antibiotics and new analytical tools to probe pathogenic infection processes and as point-of-care biosensors is crucial to combat the spread of infectious diseases.

Glycopolymers offer many opportunities for interfacing synthetic materials with biological systems. However, the nature of the interactions between glycopolymers and their biological targets, lectins, and the structural features necessary to obtain high-affinity materials are not fully understood. The application of synthetic glycopolymers to anti-adhesive therapies has so far been limited by their lack of lectin specificity.

Herein a number of tandem post-polymerisation modification methods are utilised to probe the multivalent inhibition of a bacterial toxin as a function of linker length, carbohydrate density, and glycopolymer chain length. Guided by structural-biology information, the binding-pocket depth of the toxin was probed and used as a means to specifically improve inhibition of the toxin by the glycopolymer.

Glycosylated gold nanoparticles that change colour due to lectin-mediated aggregation may find use as biosensors to aid in the detection of infectious diseases and biological warfare agents such as ricin. Here, carbohydrate-functionalised, gold nanoparticles have been used to discriminate between lectins and bacterial phenotypes. Optimisation of the particle coating is required to ensure stability in complex media, but still allow for rapid detection readouts.

Chapter 1

Introduction

1.1 Infectious diseases

Infectious diseases are the second-leading cause of death worldwide and the third-leading cause of death in economically advanced countries.[1] Microbial infection remains one of the most serious complications in several areas, including medical devices, medical equipment and instrumentation, drugs, healthcare and hygiene applications, food packaging and food storage. Reisner and Woods found that that 85-90 % of all clinically reported infections are caused by only seven microorganisms with *Escherichia coli* (*E. coli*) and *Staphylococcus aureus* (*S. aureus*) accountable for approximately half of all infections (Table 1.1).[2]

Table 1.1: The seven organisms found to be the cause of more than 85 % of all clinically reported infections in order of prevalence.[2]

Microorganism	Example Infections
Staphylococcus aureus	Skin infections, respiratory disease, food poisoning
Escherichia coli	Food poisoning, urinary tract infections
Klebsiella spp.	Pneumonia, urinary tract infections, septicaemia, meningitis, diarrhoea
Enterococcus spp.	Urinary tract infections, bacteraemia, bacterial endocarditis, diverticulitis, meningitis
Streptococcus spp.	Pink eye, meningitis, bacterial pneumonia, necrotising fasciitis
Pseudomonas aeruginosa	Urinary tract infections, respiratory infections
Enterobacter spp.	Urinary tract infections

Despite a steady stream of potential targets being discovered through developments in genomics and proteomics, antibiotic development in the pharmaceutical industry is steeply declining (Figure 1.1).[1, 3, 4] Due to the intense use and misuse of antibiotics, antibiotic resistance is now one of the most pressing global healthcare problems facing today's society (Figure 1.1).[3, 5, 6] Since the introduction of effective antibiotics for infectious diseases in the mid-20th century it is difficult to imagine a life without them, however, this is becoming a very real possibility for some infections.[7] Therefore, there is a very pressing need for new methods to combat these bacterial pathogens, faster point-of-care diagnostic techniques and a better understanding of the host interactions required.
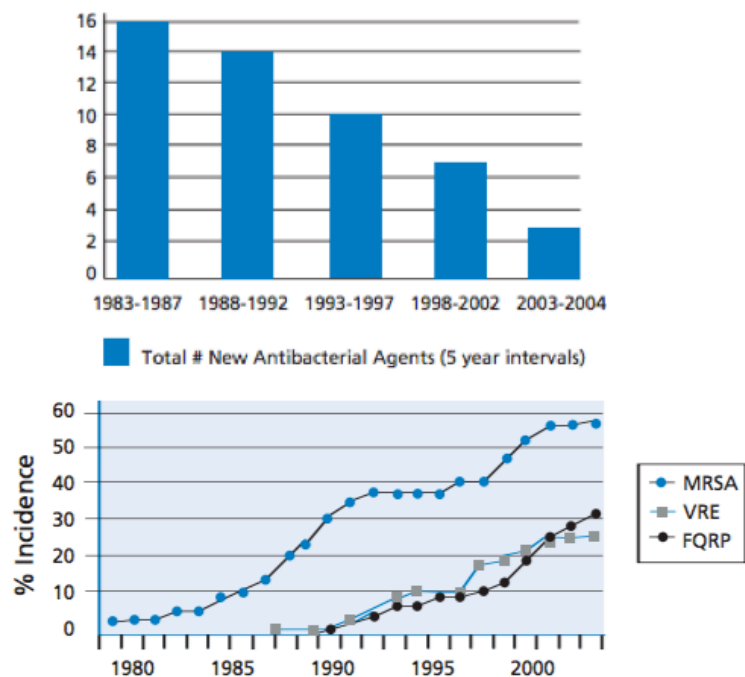
Figure 1.1: Decline in antibiotic development and increase in antibiotic resistance (MRSA = methicillin resistant *Staphlococcus aureus*, VRE = vancomycin resistant *Enterococcus*, FQRP = fluoroquinolone-resistant *Pseudomonas aeruginosa*). Figure adapted from Infectious Disease Society of America 2004 report.

1.2 Protein-carbohydrate interactions

Carbohydrates are one of the four major classes of biomolecules in addition to nucleic acids, protein and lipids. In nature, carbohydrates exist mostly as polysaccharides. These highly complex macromolecules fulfil a variety of tasks ranging from structural and metabolic function to regulating development, cell signalling, cell adhesion, and host–pathogen interactions. Carbohydrates coat most cell types in nature and are used mostly in recognition pathways and signal transduction.[8] The wide range of functions carried out by carbohydrates is reflected in the structural diversity of carbohydrate molecules. Glycan structural and chemical diversity is determined by the specific combination of selected elements from a set of monosaccharide building blocks: the different glycosidic linkages used to link these monosaccharides, the stereochemical configuration of the glycosidic bonds, branching and site-specific modifications lead to the complexity of the glycome.[9]

Carbohydrates are challenging to analyse due to their complex nature, thus technologies to rapidly assess glycan structures are still in the developmental stages. Significant challenges in analysing the glycome come from its enormous structural diversity; of the major classes of biomolecule, carbohydrates are the most structurally diverse, due to different enantiomers, diastereoisomers, anomers and linkages and branching (Figure 1.2). This heterogeneity makes isolation of pure samples, and in sufficient amounts, from biological sources extremely difficult.[10] No single technique can be used to define all aspects of the glycome. Several techniques are typically employed in parallel such as high-performance liquid chromatography (HPLC), mass spectroscopy (MS), and array technologies.[8, 11-16] In contrast, a single technique can be used to interrogate RNA, DNA or proteins. Molecular biology techniques, such as gene mutation, over expression, and silencing allow the

perturbation of specific proteins and their subsequent functional assignment. Fluorescent labelling can be used to tag proteins for visualisation to study localisation.[12] Protease enzymes are available to digest proteins and assignment of the protein sequence can be carried out by MS. A difficulty of MS for glycan characterisation is the discrimination of a number of structural isomers, such as enantiomers (e.g. D/L-glucose), diastereoisomers (e.g. glucose/mannose), anomers (α/β), and linkages and branching (e.g. 1-4/1-6) (Figure 1.2).[14] For DNA, sequencing and microarray technologies can be used. Amplification methods, analogous to the polymerase chain reaction (PCR) for DNA are not available for carbohydrates.[17]

Enantiomers

D-Glucose
180.16 g.mol⁻¹

L-Glucose
180.16 g.mol⁻¹

Diastereoisomers

Glucose
180.16 g.mol⁻¹

Galactose
180.16 g.mol⁻¹

Anomers

beta-Glucose
180.16 g.mol⁻¹

alpha-Glucose
180.16 g.mol⁻¹

Branching

Maltose
342.30 g.mol⁻¹

Isomaltose
342.30 g.mol⁻¹
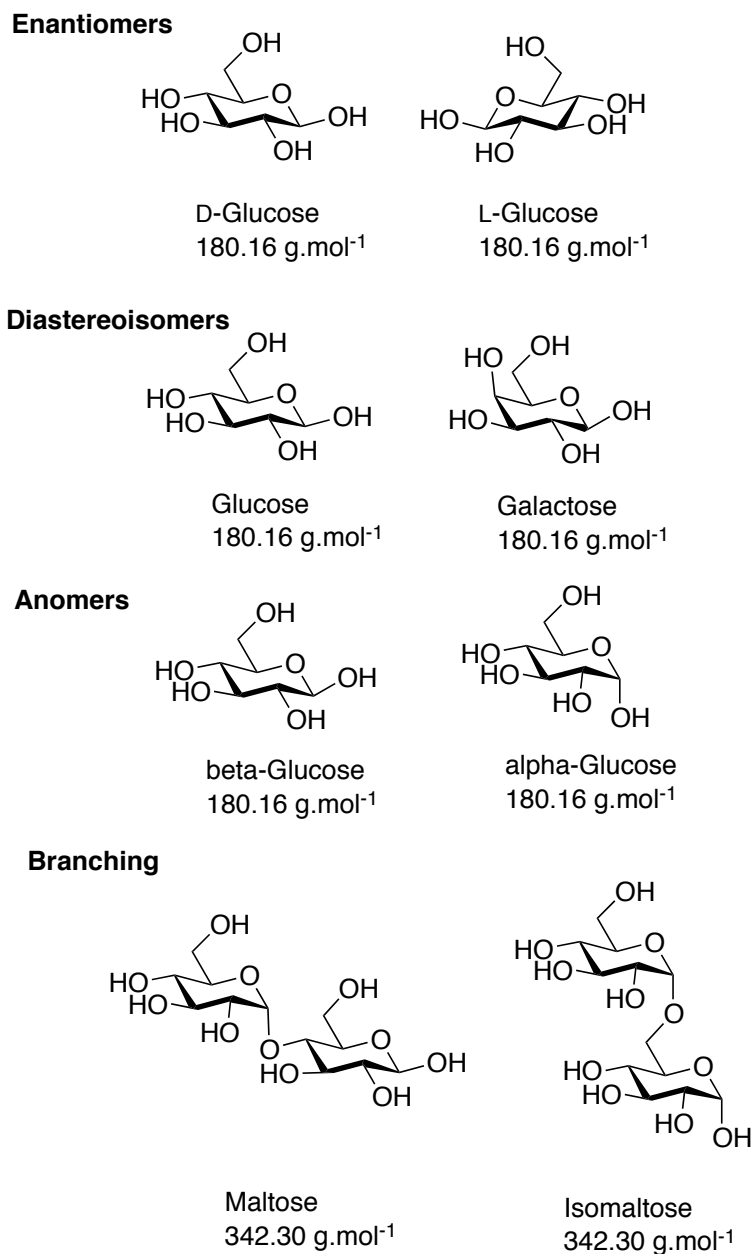
Figure 1.2: Isomerisation complexity of carbohydrates.

Due to the presence of multiple functional groups (most commonly hydroxyl groups), carbohydrates are capable of forming many different combinatorial structures, including branching, from relatively small number of sugar units.[18] Mammalian glycans rely on a group of ten common monosaccharide units (Figure 1.3).[9] These monosaccharides assemble into linear and branched polymer structures, which are made more complex by the possible stereochemical linkages between the

units (α or β), resulting in a high degree of potential complexity.[16] These ten mammalian building blocks can give rise to a tremendous number of possible glycans compared to linear macromolecules like nucleic acids or proteins.[9] Therefore information density in carbohydrates is huge, far greater than with DNA and proteins where DNA has four nucleotide building blocks and proteins have 20 amino acid building blocks. Theoretical calculations on the number of different hexamers of amino acids have yielded 46,656 structure whereas for mammalian glycans, which have a limited monosaccharide pool, the number of possible hexasaccharides structures has been calculated to be greater than 10^{12}.[8, 19] These structures are not all possible, due to only certain linkages and branching patterns being accessible, but the current list of known *N*-linked glycans contains more than 2000 structures and this list is constantly growing.[8]
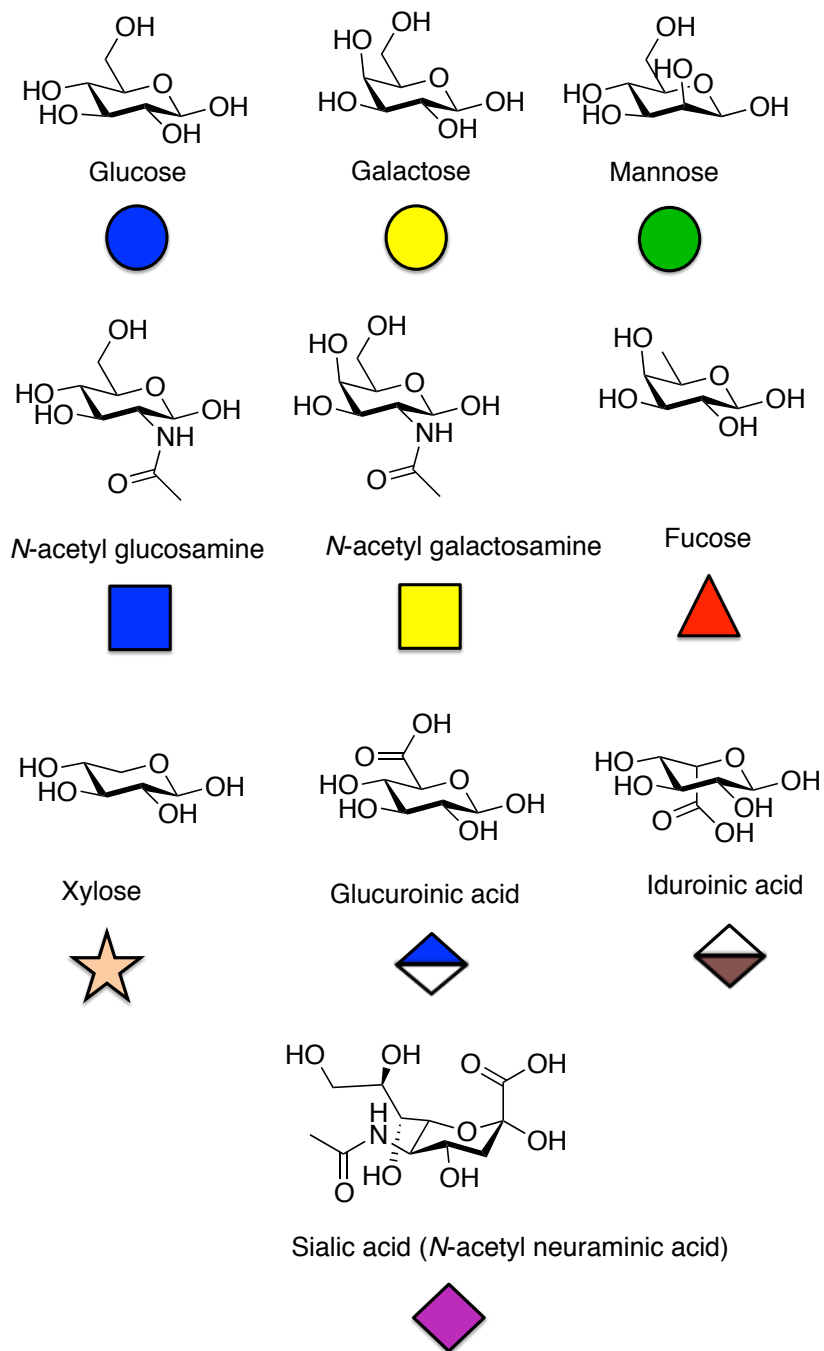
Figure 1.3: The ten mammalian monosaccharides. Symbols are the CFG[20] nomenclature.

Due to their high information density, protein-carbohydrate interactions are employed in nature to mediate many critical biological recognition processes, such as those involved in cell signalling, fertilisation, and inflammation, as well as the adhesion of viruses, bacteria and toxins (Figure 1.4).[21] Proteins that interact with

carbohydrates non-covalently occur widely in nature. Prominent examples are carbohydrate-specific enzymes, anti-carbohydrate antibodies, and lectins.[22]
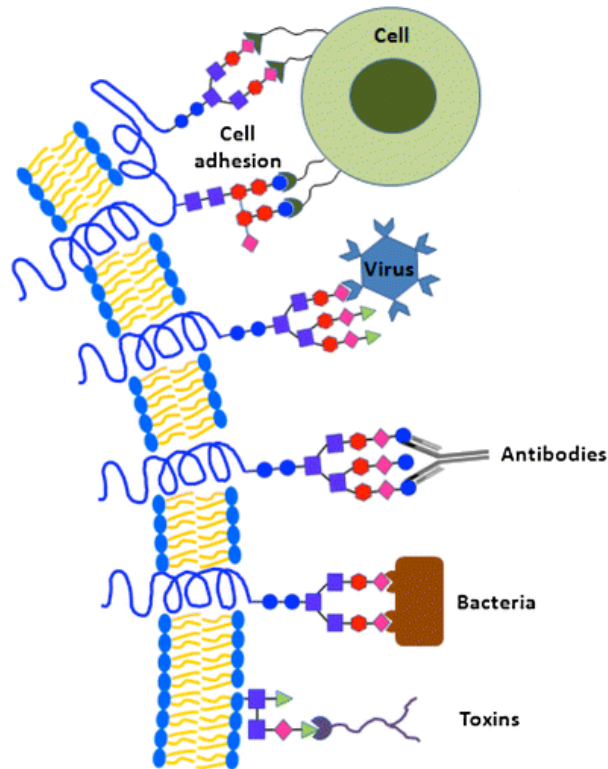
Figure 1.4: Protein-carbohydrate interactions, figure adapted from reference 23.

The proteins responsible for deciphering this information are known as lectins. They specifically (and noncovalently) bind carbohydrates based on their branching pattern, stereochemistry, and chemical functionality.[24, 25] Carbohydrate-binding sites are often shallow depressions on the surface of the protein. In all cases the combining site appears to be pre-formed, since few conformational changes occur upon binding. Lectins are found in plants, animals and on bacteria.

1.2.1 Plant lectins

Legume lectins represent the largest and most thoroughly studied family of lectins. Around 100 members have been characterised, almost all isolated from the seeds of the plants in which they are present. Concanavalin A (Con A), the lectin from the jack beans, is the prototype member of the family. The relative abundance of this protein in jack bean, the ease of its preparation and the large number of saccharides with which it can interact, have led to numerous studies on Con A. Con A is a dimer at low pH (<5.5) and a tetramer at high pH (>7). Each subunit contains a binding site that binds specifically to α-mannosyl and α-glucosyl residues. In all legume lectins, irrespective of their specificity, four invariant amino acid residues participate in the ligand binding: an aspartic acid, an asparagine, a glycine and an aromatic amino acid or leucine.[24] For peanut agglutinin (PNA), the lectin from *Arachis hypogaea,* which recognises the T-antigen (Galβ1-3GalNAc) these amino acids are Asp83, Gly104, Asn127 and Tyr125. (Figure 1.5).
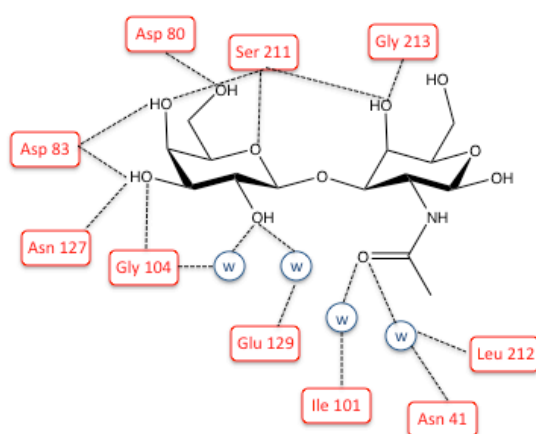
Figure 1.5: Schematic of the peanut agglutinin carbohydrate-binding site coordinating Galβ1-3GalNAc, figure adapted from reference 24.

Cations such as Ca^{2+} and Mn^{2+} are situated in close proximity to the carbohydrate-binding pocket, they are not always directly involved in carbohydrate binding, but help the positioning of the amino acid residues interacting with the carbohydrate. The aspartic acid and asparagine residues participate in coordinating Ca^{2+}. The carbohydrate is complexed to the protein by forming coordination bonds with a conserved Ca^{2+} as well as by hydrogen bonding with the acid and amide side chains that coordinate the Ca^{2+}.[26, 27] Water molecules also mediate the binding between the carbohydrate and the binding site.

1.2.1.1 Plant toxins

Several plant lectins are also toxins. Ricin is a toxic lectin that presents a potential security threat. It is a lethal, type 2 ribosome-inactivating protein found in the castor bean plant *Ricinus communis*. It is an A-B toxin whereby its B-chain adheres to terminal galactose residues on mammalian cell surfaces, facilitating the delivery of the toxic A-chain into the cytosol of the cell. The A-chain catalyses the hydrolytic cleavage of a single base from eukaryotic ribosomal RNA, leading to a shutdown in protein synthesis and ultimately cell death.[28] Ricin is several thousand times more toxic to man than cyanide, with the median lethal dose (LD_{50}) for an adult estimated to be around 22 $\mu g.kg^{-1}$ of body weight (> 1.8 mg for an average adult). *Ricinus communis* agglutinin (RCA_{120}) is a non-toxic surrogate for ricin. It is also found in the *Ricinus communis* plant, has an 80 % homology with ricin and also binds to galactose residues in the same manner and can be used as a ricin substitute for research purposes.

1.2.2 Bacterial toxins

Protein toxins constitute an important part of the virulence factors that mediate the harmful effects of several species of pathogenic bacteria.[29, 30] Bacterial toxins have an impressive variety of mechanisms of action: they can act on receptors at the cell surface, disrupt the plasma membrane, or enzymatically modify intracellular targets. The latter type are know as A-B toxins, with the binding (B) moiety mediating receptor binding and toxin translocation, and the active (A) subunit containing an enzymatic domain, which disrupts cellular homeostasis. Examples of these include, the shiga-like toxins, cholera toxin and heat-labile enterotoxin.

Enterohemorrhagic *E. coli* is a pathogen transmitted through food and water that causes severe gastroenteritis. It produces the shiga-like toxin (SLT) as its main virulence factor. SLTs are released by the bacteria in the lumen of the gastrointestinal tract, causing diarrhea. SLTs are AB_5-type toxins that interact with the globotriaosylceramide Gb_3 on the cell surface, where it is endocytosed.[29] SLTs bind only weakly to individual Gb_3 oligosaccharides, up to 15 copies of the Gb_3 ligand can simultaneously bind an SLT B pentamer.[31]

Cholera is still a life-threatening disease in many parts of the world. It is a diarrheal disease caused by *Vibrio cholerae* (*V. cholerae*), a bacteria transmitted by contaminated food and water. Cholera is endemic in many regions of the world and it is estimated that it is attributable to 120,000 deaths each year. The cholera toxin (CTx) secreted by *V. cholerae* is the causative agent of the cholera symptoms and is a multimeric AB_5 lectin-like complex. (Figure 1.6).[32]
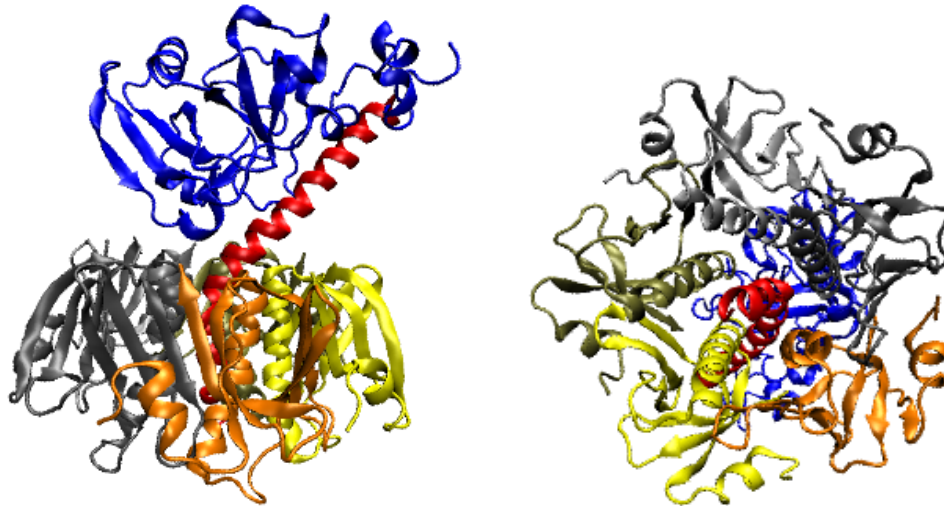
Figure 1.6: Structure of the cholera toxin (PDB entry 1xtc). The toxic A-subunit is shown in blue (left) and the five B subunits (right).

The five B-subunits bind GM1 gangliosides (Galβ1-3GalNAcβ1- 4(Neu5Acα2-3)-Gal-β1-4Glc ceramide) present on the surface of the intestinal epithelium cells.[33] The complex of CTx and GM1 is one of the highest affinity protein-carbohydrate interactions known.[34] Following initial adhesion of the B-pentamer, the toxins enter the cells by endocytosis. They are then transported through the cell to the endoplasmic reticulum where the toxic A-subunit is released into the cytosol to have its cytotoxic effect. CTx ADP-ribosylates the Gs_α protein, which leads to a rise in cAMP concentration in the cell and a complex series of events that result in release of water into the intestine.[29, 35]

Heat labile enterotoxin (LT) also recognises the GM1 ganglioside and shares 80 % homology with CTx. It acts similarly to CTx by raising cAMP levels through ADP-ribosylation of the Gs_α protein leading to the activation of adenylate cyclase.

1.2.3 Bacterial surface lectins

Another virulence factor, in addition to toxins secreted by bacteria, is surface lectins. Adhesion of pathogenic organisms to host tissues is the prerequisite for the initiation of the majority of infectious diseases.[36] The proteins that mediate adhesion are called adhesins. Adhesins are often part of bacterial appendages called pili or fimbriae, although adhesins have been identified on the cell surface. Urinary tract infections in humans are strongly associated with *E. coli* producing type 1, P, S and F1C fimbriae. The type 1 fimbriae are the most studied; an example of this is the FimH adhesin. Type 1 fimbriae, or pili, are the most abundant surface structure both in pathogenic and non-pathogenic gram-negative bacteria. The FimH adhesins are mannose-specific and found at the tip of the fimbriae. Fimbriae are uniformly distributed on *Enterobacteriaceae,* commonly between 100 and 400 per cell. Their length varies between 1-2 μm and their width is approximately 7 nm and made up of largely repeating immunoglobulin-like FimA subunits that are helically arranged.[37] Type 1 fimbriae are expressed by a large number of *E. coli* strains, and are found in more that 95 % of *E. coli* isolates from intestinal and extra-intestinal infections such as urinary ones.[36, 38] Whilst type 1 fimbriated *E. coli* are involved in lower urinary tract infections, *E. coli* presenting P-fimbriae cause bladder infections resulting in acute pyelonephritis. P-fimbriae are terminated by PapG, a tip-associated adhesin that recognises the Galα(1-4)Gal (galabiose) moiety.[39]

Pulmonary pathogens such as *Pseudomonas aeruginosa*, *Streptococcus pneumoniae* and *Klebsiella pneumoniae* are opportunistic pathogens associated with chronic airway infections, typically affecting cystic fibrosis patients, and require GalNAcβ(1-4)Gal as a minimal binding sequence. The GalNAcβ(1-4)Gal sequence was shown to be present in lung tissue in higher abundance in cystic fibrosis-affected

lung epithelia. This strain also synthesises two lectins, LecA and LecB, which bind galactose and fucose respectively. Both are tetrameric, known virulence factors under quorum sensing control, and while non-classical adhesins, these lectins do appear to mediate adhesion.

1.3 Multivalency in protein-carbohydrate interactions

Despite their role in signalling, the actual binding affinity of a monosaccharide to its target lectin is typically very weak ($K_d = 10^{-3}$-10^{-6} M) compared to antibody antigen interaction, which are typically $< 10^{-9}$ M. This is circumvented in nature by the presentation of multiple copies of the target carbohydrate on the cell surfaces which gives rise to an increase in affinity greater than that of the linear sum of the individual sugars, this is known as the `cluster glycoside effect'.[18, 40, 41]

In 1983, Lee *et al*.[40] synthesised a series of oligosaccharides, resembling natural *N*-acetyllactosamine type glycans and tested them for their ability to inhibit the binding to the mammalian hepatic lectin on rabbit hepatocytes. A dramatic hierarchy of inhibitory potency over several orders of magnitude in the order, tetraantennary > triantennary >> biantennary >> monoantennary. An inhibitory potency of ~1 mM was noted for the monoantennary oligosaccharides, whereas ~1 nM was noted for the triantennary oligosaccharides, even though the absolute galactose concentration increased only 3-fold. It was found that the number of galactose residues per cluster and their branching mode are major determinants of binding affinity of ligands to the hepatic lectin on the surface of hepatocytes.

Multivalent assemblies provide a distinct advantage over monovalent ligands by enhancing binding strength through multiple interactions with their corresponding

target.[42] There are a number of mechanisms of action of multivalent ligand binding, that are inaccessible to monovalent compounds, that contribute to their potency, such as; chelation, subsite binding, clustering and statistical rebinding. (Figure 1.7).
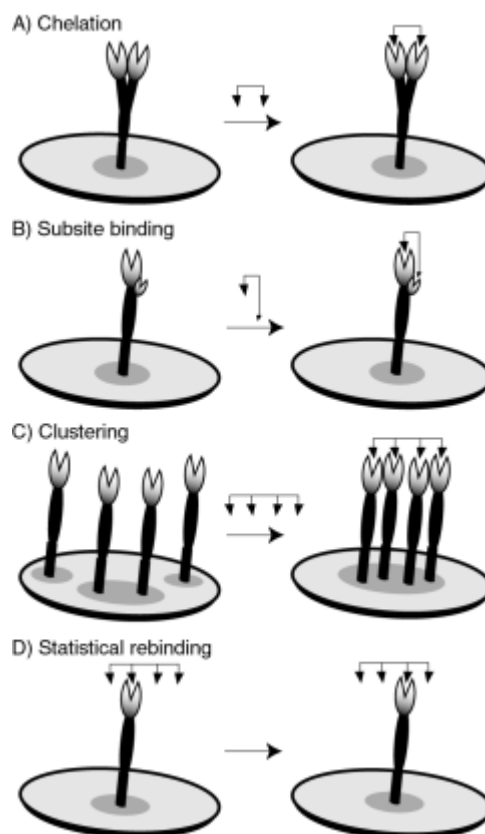
Figure 1.7: Multivalent ligand binding mechanisms, figure adapted from reference 43.

The chelate effect is observed when carbohydrates can bridge multiple binding sites on a single oligomeric receptor. The cost for translational entropy is paid with the first protein-ligand interaction and subsequent binding interactions proceed without additional translational entropy penalties. Similarly, some carbohydrate binding proteins possess binding subsites in proximity to their primary binding site, these can be occupied by multivalent ligands. Even with receptors that are not oligomeric, multivalent ligands can bind to multiple receptors on the cell surface. This clustering process is facilitated in the fluid lipid bilayer by the two-

dimensional diffusion of receptors. Additionally, in statistical rebinding, the effective local concentration of ligand near the receptor is increased, producing an overall gain in binding affinity.[43] Collectively, these modes of multivalent binding prevent the disassociation of ligand upon individual unbinding events.[42]

1.4 Anti-adhesion therapy

Antibiotics have long been the preferred treatment for bacterial diseases. However, there are several advantages in targeting the virulence factors rather than the bacteria themselves.[29] The development of such resistance is inherent to antibiotics that kill pathogens and provide selection pressure. It is widely accepted that alternative approaches against bacterial pathogens should be explored. Strategies that do not kill the pathogens yet interfere with their pathogenicity may provide the much needed alternative. One such strategy is anti-adhesion therapy (Figure 1.8).[44]
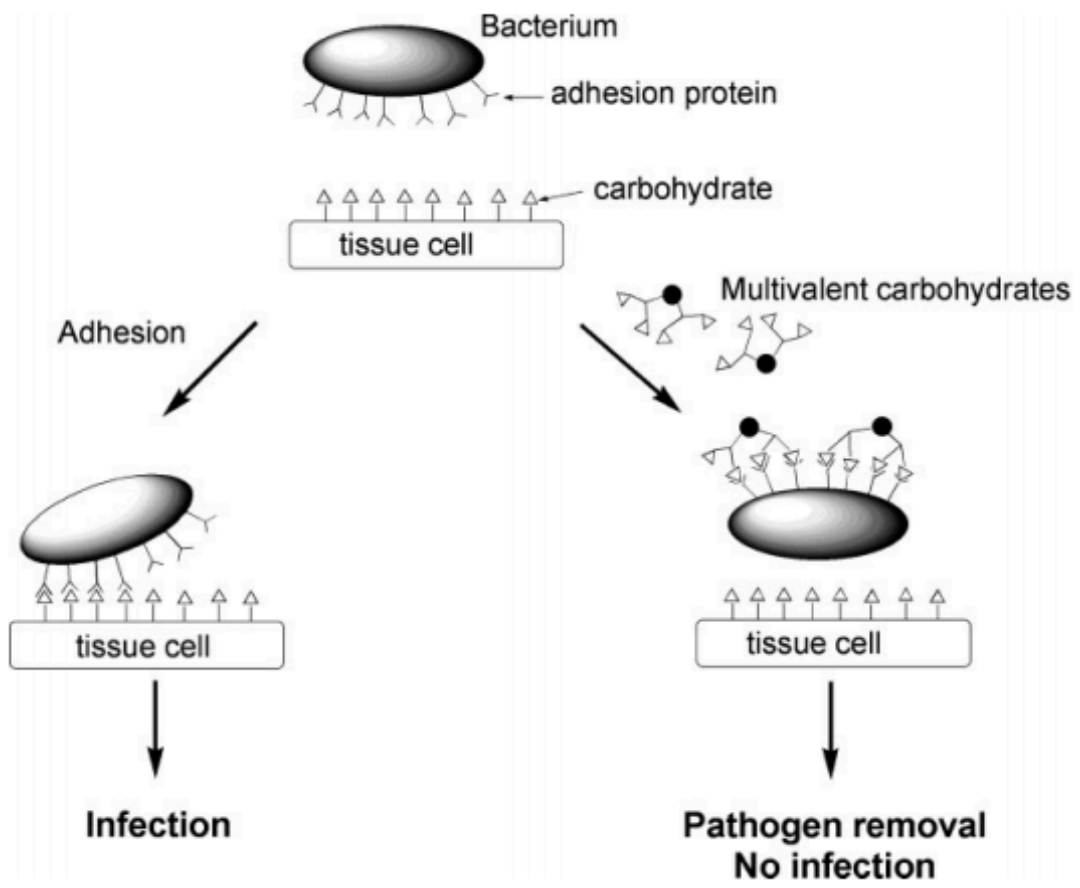
Figure 1.8: Concept of anti-adhesion therapy figure adapted from reference 44.

As protein–carbohydrate interactions are an essential prerequisite for cell entry and toxin activity, the development of inhibitors for these interactions has attracted much interest over recent years.[31] Inhibition of these lectins, by suitable carbohydrate or their analogues, for the prevention and treatment of microbial diseases is the aim of anti-adhesion therapy. Carbohydrates are ideal for this purpose as they are unlikely to be toxic or immunogenic.

Anti-adhesion therapy has many potential advantages; since anti-adhesive agents do not act by killing or arresting growth of the pathogens, it is very likely that strains resistant to such agents will emerge at a markedly lower rate than those that

are resistant to antibiotics, and their spread in the environment will be minimal.[36] Toxins can also continue to cause symptoms even after bacteria have been cleared from the host. Additionally, non-antibiotic treatments circumvent the disruption of the normal microbiota that is typically associated with antibiotic treatments.[29]

In general it is very challenging to make low molecular weight inhibitors of carbohydrate-binding proteins as the binding sites are typically shallow and highly solvated. Monovalent receptor-binding approaches focus on strong binding interactions and are based on the design and synthesis of ligands that closely mimic the natural ligand action at the cell surface.[28, 45, 46] An excellent example of monovalent inhibitor specificity was described by Thépaut et al..[47] In their work they designed inhibitors of DC-SIGN. DC-SIGN is a carbohydrate-binding protein involved in HIV transmission, langerin is a related lectin with selectivity for the same binding partner gp120 but exhibits an opposing role in blocking HIV transmission. Therefore, it is important to inhibit DC-SIGN, without blocking langerin. NMR, X-ray crystallography and surface plasmon resonance (SPR) studies were used to determine the binding mode of monovalent inhibitors that showed selectivity for DC-SIGN over langerin.

Due to the challenges that lie in making low molecular weight, monovalent inhibitors, researchers have instead focussed their attention on making multivalent inhibitors that can engage multiple carbohydrate binding sites simultaneously. Chemists have overcome the low binding affinities of monovalent glycosides by successfully conjugating synthetic oligosaccharides to a number of multivalent scaffolds.[48] The design, synthesis and testing of glycoconjugates for the inhibition of bacteria and toxins has been extensively reviewed.[10, 24, 31, 36, 44, 49-53]

1.5 Potent inhibition using multivalency

1.5.1 Multivalency for specific targeting of lectins

Rational design of multivalent inhibitors to specifically interact with lectins is important in order to interact with multi-binding site proteins. Pentavalent ligands designed to interact with all five binding site of an AB_5 toxin have been explored. Structural information about the spatial arrangement of the target binding sites is taken into account when designing ligands ideal for maximising the interaction with the receptor.

The modular synthesis of multivalent ligands of LT, an AB_5 toxin similar to that of CTx, from *E. coli* was reported by Fan and co-workers.[54] In this study, pentavalent ligands of β-amidated D-galactose attached to a semi-rigid core by flexible linkers to interact with the 5 binding sites of the pentamer were synthesised. Different lengths of the linker were tested and the inhibitory activity determined by an enzyme-linked immunosorbent assay (ELISA). All pentavalent ligands led to significant affinity gains over the monovalent ones; the best showing an IC_{50} 10^5-fold lower than galactose, approaching the affinity of the natural ligand GM1. It was also found that the pentavalent ligands formed a 1:1 complex with the toxin and no large-scale aggregates were observed. Higher affinity inhibitors were produced by incorporating *m*-nitrophenyl-α-galactose as a ligand group and improving the linker solubility. The resulting compound had an IC_{50} of 6 nM, which was about 3 times more potent than the GM1 oligosaccharide.

Arguably one of the most elegant examples of inhibitory activity using structurally relevant arrangement of multivalent ligands was reported by Kitov *et al.*[55] A decavalent inhibitor was developed, nicknamed STARFISH, whose structure

was complementary to the AB_5 structure of SLT-I and SLT-II. STARFISH exhibited more than a 10^6-fold increase in inhibition over the native Gb_3 trisaccharide. STARFISH was designed to achieve high affinity by simultaneously binding all of the five peripheral bridged dimers to the sites 1 and 2 of the B-pentamer. However, crystallographic studies of the formed complex revealed a different binding mode. One STARFISH molecule was found to bind to two B-subunit monomers from separate toxin molecules (Figure 1.9).
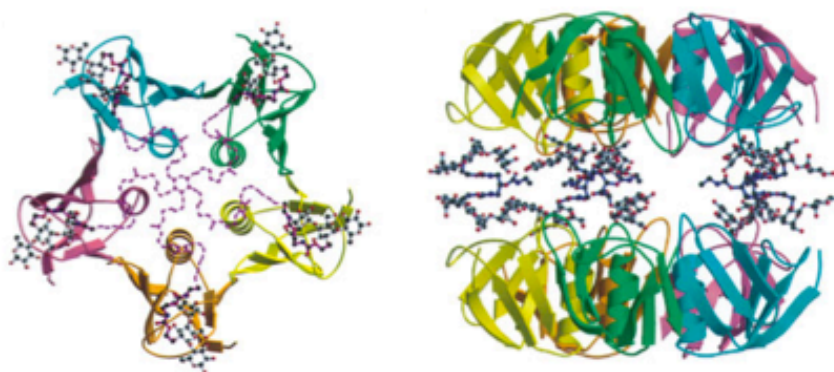
Figure 1.9: STARFISH synthesised by Kitov *et al*. bound to SLT-I, figure adapted from reference 55.

Two further examples of pentavalent inhibitors were reported by Zuilhof *et al*. both presenting GM1 oligosaccharide (GM1os) ligands with flexible polyethylene glycol (PEG) linkers on scaffolds with 5-fold symmetry, corannulene[56] and calix-[5]-arene.[57] Both showed IC_{50} values of 5 nM and 405 pM respectively, determined by an ELISA-type assay.

The synthesis of large multivalent scaffolds is very challenging; therefore Branson *et al*.[58] developed a highly potent pentavalent inhibitor for CTx based on an inactive mutant of the B subunit of CTx (CTxB), modified with GM1os ligands. They were designed to match exactly to the size for the target CTx protein. This was found to be a highly potent inhibitor by enzyme-linked lectin assay (ELLA), 104

pM, which is the most potent pentavalent ligand reported to date. A 1:1 complex between the inhibitor and the target CTxB was observed as determined by dynamic light scattering (DLS) and analytical ultracentrifugation.

1.5.2 Glycodendrimer inhibitors

Dendrimers are perfectly branched, monodisperse synthetic macromolecules that generally feature symmetrical spherical architectures, that, in principle, combine the advantages of homogenous small molecular inhibitors with the dimensions and high valencies of glycopolymers (see section 1.5.4).[59] Dendrimers contain a relatively high density of functionalisable termini that are typically positioned on the exterior of the structure. However, they can be highly challenging to synthesise.

Thompson and Schengrund[60] designed glycodendrimer inhibitors to prevent toxins such as CTx and LT. Polypropyleneimine (PI) and polyamidoamine (PAMAM) cores were used presenting GM1os carbohydrate moieties. The multivalent glycodendrimers were capable of inhibiting binding at 1000-fold lower concentration than the monovalent GM1 ganglioside.

The Pieters group synthesised a set of dendrimers, prepared by a convergent approach, with a variety of carbohydrate end groups as CTxB inhibitors. Their first scaffolds were prepared with two, four and eight arms with terminal lactose moieties.[61] It was found that the multivalent dendrimers gave an increase in inhibition, with the octavalent ligand having the strongest binding with a K_d of 33 μM as measured by a fluorescence titration assay. Increasing the linker lengths, improved the reach of their ligands as determined by SPR.[62] Pieters and co-workers also synthesised an octameric galabiose derivative anchored to a PAMAM

dendrimer core (Figure 1.10),[63] which showed a 256-fold improvement over the monovalent galabiose.
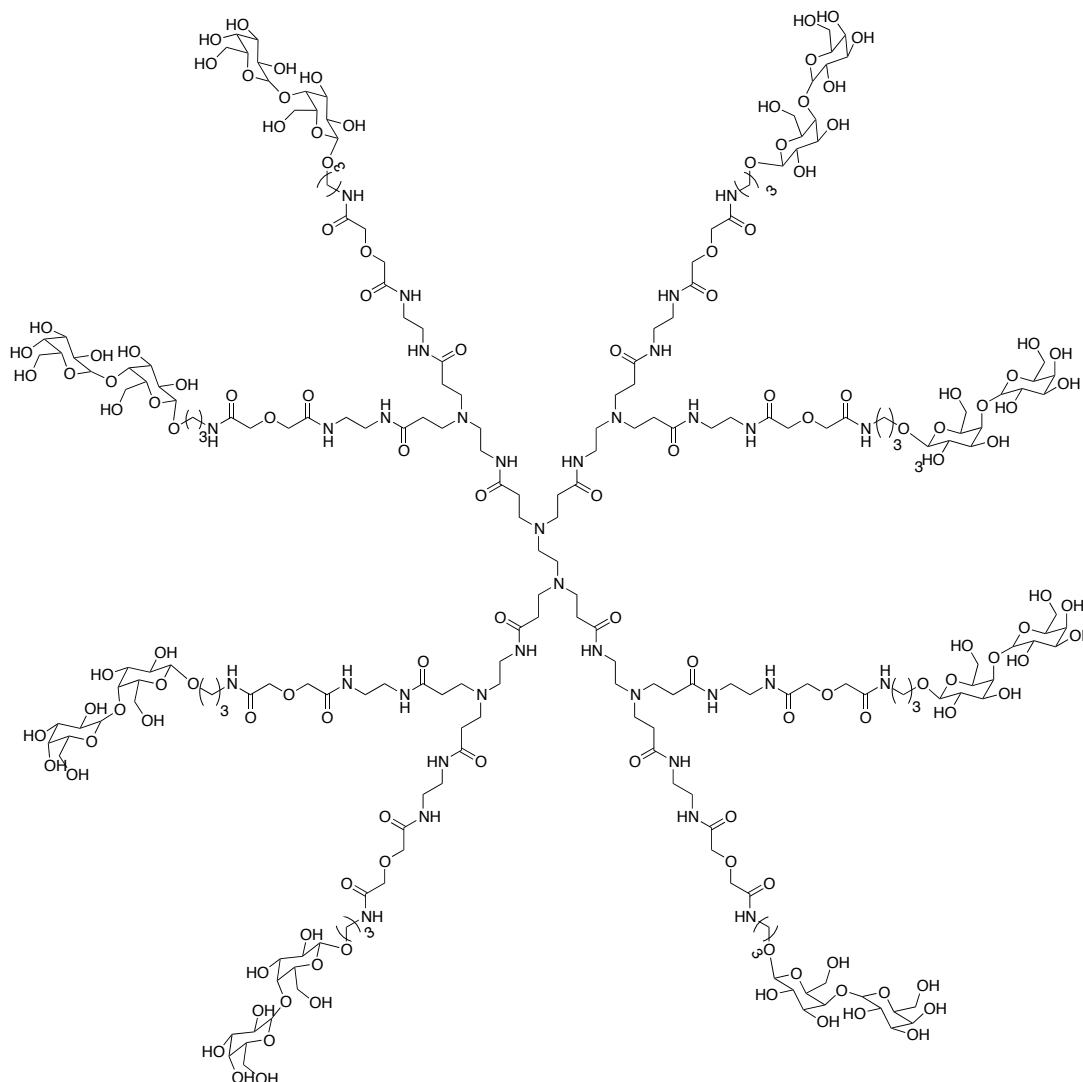
Figure 1.10: (Galabiose)$_8$ glycodendrimer based on a PAMAM core as a multivalent inhibitor of PapG adhesins of *E. coli*. Figure adapted from reference 63.

While most dendrimers are made up of organic polymer building bocks, peptide dendrimers are assembled from amino acids using diamino acids such as lysine as branching points. These peptides arms can then be capped with carbohydrate derivatives.[64] It has been shown that galactosylated and fucosylated

dendrimers are potent inhibitors of *P. aeruginosa* biofilm formation by inhibition of LecA and Lec B proteins.[65, 66]

1.5.3 Glycopeptide inhibitors

Glycopeptide materials can be used to study and manipulate interactions between saccharides and their receptors. They provide advantages such as manipulation of the backbone conformation and functional group location.[48] The Kiick group has extensively investigated the effect of carbohydrate density, the specific distance between carbohydrates on a polypeptide chain, spacer length from the polypeptide backbone and secondary structure of the peptide. Galactosylated peptides were prepared as inhibitors for CTxB. Interestingly, it was found that as the density of ligands increases, the inhibitory effect decreases in terms of absolute peptide amount.[67] It was also concluded that the best inhibition was achieved when the spacing between ligands on the polymer chain was matched to the distance between binding pockets of the toxin; this distance being 35 Å for CTxB. It was proposed that when the density was sufficiently high that spacing between carbohydrates was smaller than the distance between binding sites, steric hindrance created by unbound ligands decreased overall binding. Inhibition was greater when the spacer matched the natural ligand length of GM1 (16 Å). A longer ligand could therefore fully penetrate the binding site as opposed to a reduced accessibility when a shorter spacer is used. Kiick and co-workers also found that random coil backbones were better suited than those with restricted α-helical conformations, as flexibility of the polymers allows higher accessibility of the ligand groups.[68, 69, 70]

Fan and co-workers synthesised cycloglycopeptides with five galactosamines as inhibitors of CTx.[71] The effect of ring size and linker was investigated.

Interestingly, a 100,000-fold increase in inhibitory activity over monovalent galactose was noted for cyclopeptides containing short flexible linkers.

Wittmann et al.[72] presented the first example of a split-and-mix approach to the synthesis of a library of glycoclusters presenting two to six GlcNAc residues on a cyclopeptide scaffold made of alternating L- and D-amino acids with variable side chains. This library of GlcNAc glycopeptides were screened for their binding affinity to the GlcNAc specific wheat germ agglutinin (WGA) lectin. Penta- and hexavalent glycopeptides were found to have over 600-fold stronger binding than free GlcNAc as determined by an ELLA.

Lindhorst and co-workers[73] developed effective inhibitors of type 1 fimbriated bacteria based on α-D-mannopyrannoside functional glycopeptides. The conformational properties, as well as the spatial arrangement of the pendant mannosyl residues were investigated. Inhibitory potency was determined by the glycopeptides ability to prevent GFP-tagged FimH expressing bacteria from binding to a mannan-functional 96-well microtitre plate. Greater inhibitory potency was observed for glycopeptides exhibiting a phenylmannoside and when a greater distance between carbohydrate moieties is used.

1.5.4 Glycopolymers

Multivalent inhibitors can engage multiple carbohydrate binding sites simultaneously. Synthetic glycopolymers with pendant and/or terminal carbohydrates are being increasingly explored as biomaterials for medicinal applications.[51, 74] The vast chemical versatility polymer platforms provide for generating multivalent architecture gives them huge possible potential as potent anti-

adhesion therapies. In contrast to dendrimers, glycopolymers have a degree of dispersity, however, they are easy to synthesise and polymerisations are easily scalable.

Synthetic glycopolymers mimic the function of the cell-surface saccharides and efficiently interact with proteins, cells and pathogens based on the multivalent effect. The relative ease of synthesis and variability of structure and length make them ideal for use as scaffolds for multivalent presentation. Polymers can easily span large distances, which provides a distinct advantage over many other scaffolds for targeting lectins. Modern polymer chemistry is providing new opportunities for the synthesis of tailored, biologically active polymeric (or oligomeric) ligands.[75] The multivalent ligands derived from polymers are typically composed of a central backbone that presents multiple copies of a carbohydrate. Ligands of this type can be produced by using a variety of synthetic methods. Polymers are generally assembled in a single step by methods such as radical, ionic, or ring-opening metathesis polymerisation (ROMP) of carbohydrate bearing monomers. Certain polymerisation reactions are more tolerant of biologically active functionality than others; the types of epitopes to be incorporated will determine the most effective synthetic strategy.

Roy and co-workers[76] reported a new method of synthesising acrylamide monomers that contained carbohydrate residues. 4-nitrophenol was reacted with glycosyl bromide, which gave 4-nitrophenol-β-glycoside with total anomeric stereocontrol, this was easily converted to an acrylamide-based monomer by reaction with the appropriate amine. These monomers were polymerised using free radical polymerisation using acrylamide as a co-monomer. These copolymers proved to bind lectin effectively as determined by an ELLA.

Living polymerisation reactions, in which the rates of chain termination are low, are powerful methods for generating well-defined multivalent ligands. Polymers of narrow dispersity can be generated when the polymerisations have fast initiation and slow propagation rates. The architecture of glycopolymers is vital to their application due to factors such as; orientation of the carbohydrate, scaffold shape, flexibility, size and valency, which can influence biological activity and their interaction with lectins. It is therefore necessary to consider appropriate synthetic approaches to these. Controlled polymerisation techniques (Figure 1.11) such as reversible addition fragmentation chain transfer (RAFT) polymerisation, atom transfer radical polymerisation (ATRP), Nitroxide-mediated polymerisation (NMP), ROMP, together with click chemistries have been widely used in the synthesis of glycopolymers.
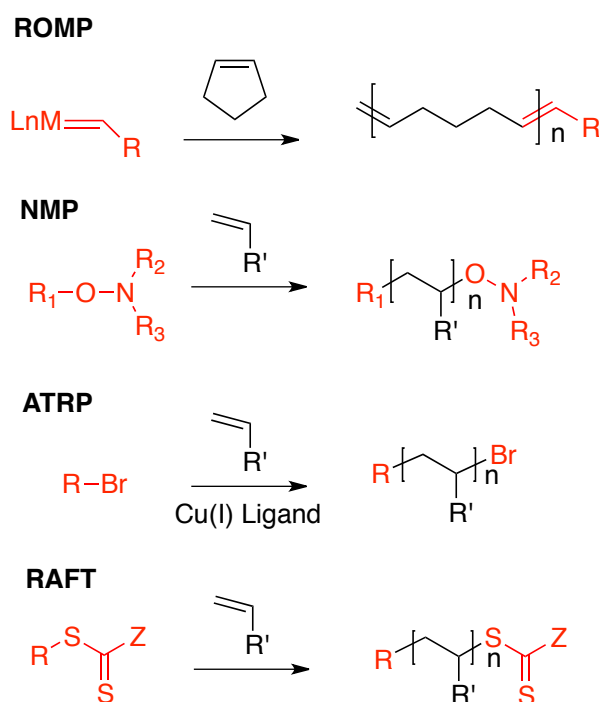
Figure 1.11: Mediating agents and general reaction scheme of controlled polymerisation techniques.

Linear glycopolymers of targeted molecular weights and dispersities (Đ) can be prepared directly from the controlled polymerisation of glyco-monomers.[77] ROMP provides the benefits of living polymerisation and can thus produce well-defined polymers of various architectures, however, the limitations are that there are only a small number of monomer types available, they are not easily functionalised and the transition metal catalyst can be expensive to remove. Fraser and Grubbs synthesised several carbohydrate functional norbornene derivatives with a series of protected glucose functionalities attached *via* an amide linkage.[78] Kiessling and co-workers,[79, 80] synthesised 7-oxanorbenene derivatives carrying one or two saccharide moieties attached *via* *C*-glycoside or *O*-glycoside linkages. They studied the dependence of Con A binding on the length of the glycopolymers. A plateau in the heamagglutinin inhibition was noted with polymers of degree of polymerisation (DP) > 50.[81]

Nitroxide-mediated polymerisation has the desirable attribute that the products contain no inorganic residues and it only requires a single compound, unlike RAFT and ATRP. The most commonly used nitroxide is TEMPO, which is relatively inexpensive, however, it is not suited to all systems. Synthesis of specific nitroxides can be challenging and time consuming. Nitroxide polymerisations are generally carried out in bulk or at high concentration, which can lead to heat transfer problems and issues with product extraction. There are very few examples in the literature of glycopolymers synthesised by NMP. Ohno *et al*.[82] reported the synthesis of the first glycopolymers by NMP in 1998. The polymerisation of a non-protected carbohydrate monomer was controlled and gave relatively narrow dispersity polymers, however did not proceed to high conversion due to retardative transfer to

the hydroxyl groups, determined due to polymerisation of the acetylated monomer reaching 90 % conversion.

Copper-mediated living radical polymerisation (CMLRP) is a versatile technique; it is tolerant to a wide variety of monomers, almost all functionalities and can be performed in any solvent and at any temperature. It produces polymers with good control over molecular weight and low dispersities, however residual copper often resides after polymerisation and can be an issue for biological applications. Narain and Armes[83, 84] reported the first synthesis of glycopolymers by CMLRP using unprotected carbohydrate-containing monomers. Low dispersity polymers were obtained, under mild conditions.

RAFT is a versatile controlled radical polymerisation (CRP) technique, applicable to a wide range of monomers, functionalities and conditions and can be carried out in aqueous media. Lowe *et al.*[85] presented the first example of the direct polymerisation of a carbohydrate containing monomer (2-methylacryloxyethyl glucoside) *via* RAFT, without the need for protecting groups. Albertin *et al.* used a chemoenzymatic route to the synthesis of 6-*O*-vinyladipoyl-D-glucopyranose monomer[86] and synthesised narrow dispersity glycopolymers using RAFT in aqueous media.[87, 88]

Whilst the direct polymerisation of carbohydrate functional monomers by CRP techniques is useful, there still remains the challenge of obtaining well-defined libraries of polymers with sequential modifications and identical DPs, particularly for exploring protein-carbohydrate interactions in which valency plays such an important role in the activity of multivalent assemblies. To address this, the concept of post-polymerisation modification is frequently employed, whereby a reactive

polymeric precursor is directly functionalised ensuring all members of the library have identical DPs.[89]

1.5.4.1 Post polymerisation modification

Post-polymerisation modification gives access to functional polymers that may be difficult to access by direct polymerisation. Polymers made by a post-polymerisation modification, whereby a single batch of a precursor polymer results in all derivative polymers having the same dispersity and DP leads to functional polymers that can be more directly compared. Polymer scaffolds can be tailored to be compatible with a wide range of chemical conjugation strategies. Libraries of polymers with similar molecular weights and molecular weight distributions can facilitate identification of structure-property relationships.[89] Reactive polymers are often synthesised directly from monomers containing functionalities that are inert to the polymerisation conditions but that can be used post-polymerisation to introduce additional functionality (Figure 1.12). Highly efficient functionalisation strategies are essential for this, examples of these reactive precursor scaffolds are active esters and 'click'-functionalities.
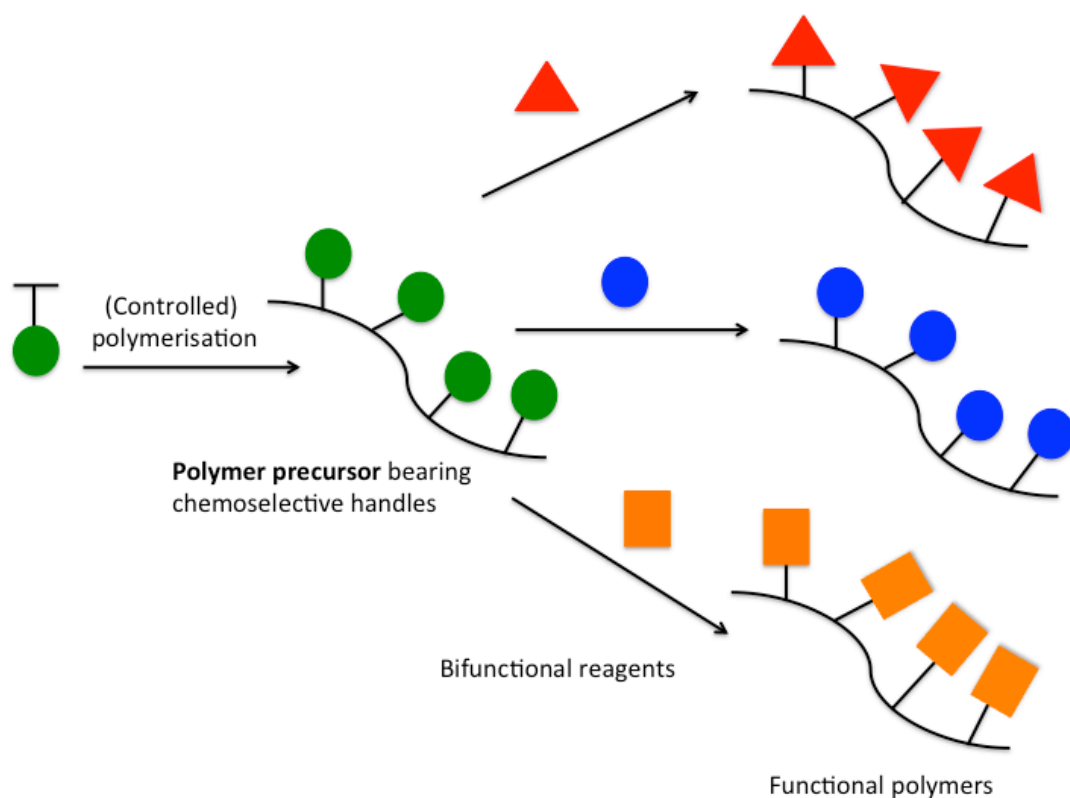
Figure 1.12: Concept of post-polymerisation modification.

Advantages of active ester-type monomers are their easy accessibility, and the use of amines as functionalisation moieties that are commercially available. Activated esters of *N*-hydroxysuccinimide, pentafluorophenol (PFP) and 4-nitrophenol have been exploited for the introduction of functionality to polymers with nucleophilic groups such as amines and alcohols. Polymeric active esters can be obtained from a variety of monomers using controlled radical polymerisations.[89] Amides are reacted with active esters because of their good nucleophilicity compared to other functional groups such as alcohols.

Whitesides and co-workers[90, 91] synthesised sialic acid containing glycopolymeric inhibitors of influenza virus X-31 using a poly(*N*-acrylyloxy succinimide (pNAS) reactive scaffold. Using heamagglutination and ELISA assays,

the inhibitory activity of theses polymers were found to be between 10^3 and 10^6 times greater than the α-methyl-sialoside.

The Théato group has shown the potential of PFP ester groups.[92, 93] Gibson *et al.*[94] used RAFT polymerisation to synthesis poly(pentafluorophenyl methacrylate) (pPFMA) as reactive scaffold towards many functionalities including glycopolymers for determining structure-activity relationships from the same starting scaffold and therefore the same chain length distribution.

The post-modification techniques described above have proven to be successful, but still suffer from very low atom efficiency (either due to displacement reactions or protecting group removal) as well as side reactions and competitive hydrolysis which can impede this approach. Azlactones are an interesting alternative; they are lactone-based functional groups that undergo ring-opening reactions in the presence of nucleophiles such as primary amines, alcohols, or thiols. They react rapidly at room temperature with primary amines, making it a useful approach for the rapid synthesis of side-chain functionalised poly(acrylamide)s.[95, 96] Despite this, until now, azlactones have not been used to synthesise glycopolymers (See Chapter 3).

Sharpless[97] introduced the concept of 'click' chemistry which describe highly efficient coupling reactions that proceed to quantitative conversion without any side products and are conducted in benign media. Cu(I)-mediated Huisgen 1,3-dipolar cycloaddition reaction has been extensively used for post-polymerisation modification because it gave high yielding conversion under mild condition in aqueous or organic media. The radical addition of thiols to vinyl groups is another highly efficient, widely used post polymerisation technique.[98, 99] Alkyne/azide and

thiolated carbohydrates have been synthesised to afford 'clickable' carbohydrate units (Figure 1.13).[100, 101]
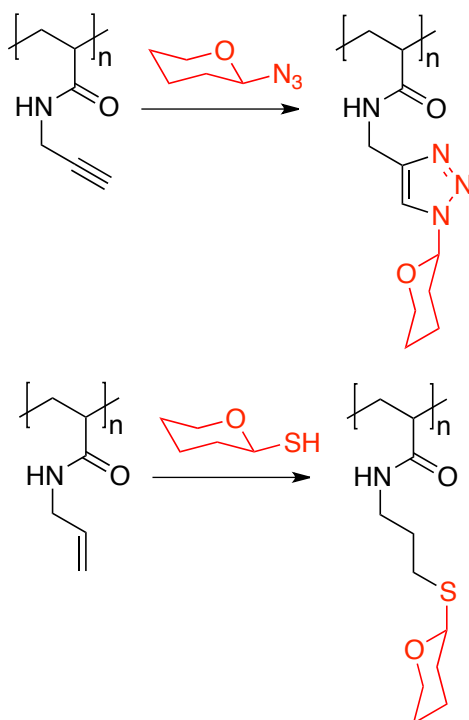
Figure 1.13: Schematic of glycopolymers from 'clickable' scaffolds.

A key challenge associated with the synthesis of 'clickable' scaffolds is that the pendant functionality, typically alkenes and alkynes, are incompatible with controlled radical polymerisations and require protection/deprotection chemistry which itself must be 100 % efficient.[102] Haddleton and co-workers prepared hetero-neoglycopolymers by 'co-clicking' two different sugar azides by copper catalysed alkyne-azide cycloaddition (CuAAC) on to a propargyl-functionalised polymer. The poly(propargyl) scaffold was obtained by CMLRP of trimethylsilyl-protected propargyl methacrylate precursors.

1.5.5 Glycopolymer inhibitors

Glycopolymers provide a simple route to high affinity, multivalent inhibitors of carbohydrate proteins. Haddleton *et al*. synthesised a small library of heteroglycopolymers bearing variable relative proportions of mannose (αMan) and galactose (βGal) motifs, prepared as detailed above.[102] Multichannel SPR was used to investigate the binding affinity of this library of glycopolymers with recombinant human DC-SIGN tetramers. 100 % αMan polymers have sub-nanomolar affinity (4.96 x 10^{-10} M). The presentation of mannose in clustered polymeric form was essential for high-affinity binding, as the equivalent mass of free D-mannose gave no binding signal. No significant binding was observed with the βGal-polymer, highlighting the specificity of the binding site for terminal mannose residue and as expected, βGal density correlated negatively with the binding affinity to DC-SIGN. A competition assay showed that an IC_{50} value of 37 nM was observed for DC-SIGN towards gp120 (Figure 1.14).[103]
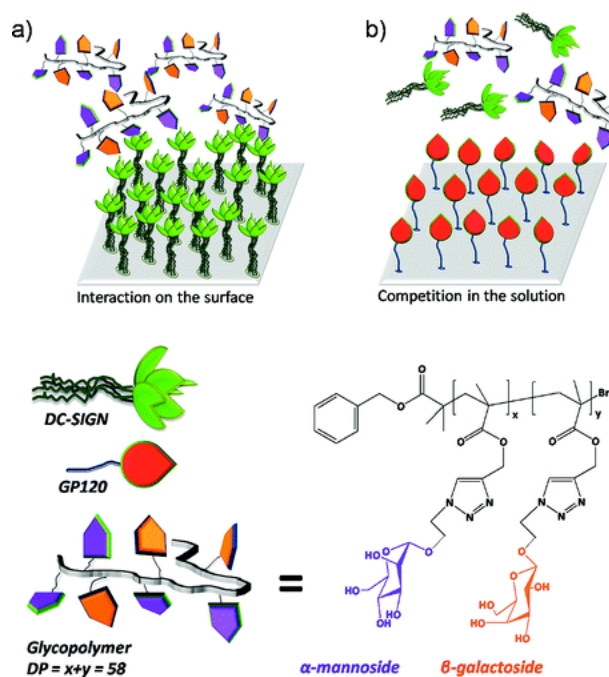
Figure 1.14: Mannose and galactose functional polymers that competitively interact with DC-SIGN. Figure adapted from reference 103.

The procedure for the post-polymerisation modification of alkyne- bearing polymer scaffolds with glycosyl azides was optimised by Gibson and co-workers.[104] This involved a one-pot synthesis of glycosyl azides, in aqueous solution, without the need for protecting groups and in multi-gram scale. Through an optimisation study, it was determined that the ideal ligand for alkyne-azide 'click' reaction was tris[(1-benzyl-1H-1,2,3-triazol-4-yl)methyl]amine (TBTA).

In addition to the terminal βGal residue, the neuraminic acid moiety (NeuNAc) is important for affinity and selectivity of GM1 towards CTx[34] and therefore a target for precision polymers. Bundle and co-workers have reported a novel approach to generate libraries of CTx inhibitors. The synthesis and inhibitory activities of a series of heterobifunctional ligands conjugated to two polymer carriers (polyacrylamide and dextran) were described (Figure 1.15).[105] Since multivalent presentations of βGal residues been have demonstrated to exhibit exceptional high activity towards CTxB, all the conjugates contained an invariable βGal fragment and variable non-galactose fragment incorporated by CuAAC reaction. The inhibitory potencies of the heterobifunctional neoglycopolymers were assessed by an ELISA. Conjugation of a second fragment resulted in nanomolar inhibitors of CTx, far greater than galactose alone. High potencies resulted from aromatic secondary binding groups with electron withdrawing groups such as fluorine. The length of the linker is sufficient for both βGal and the secondary binder to reach their respective positions in the GM1 binding site on the surface of CTx.
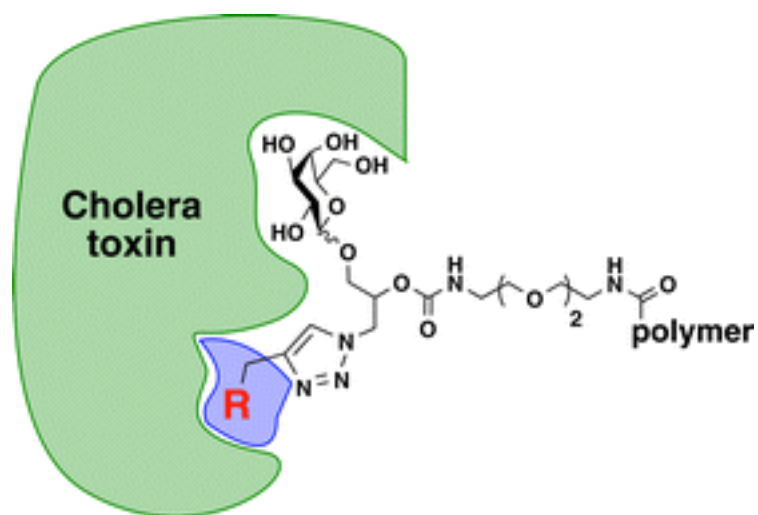
Figure 1.15: Synthetic rationale of heterobifuntional glycopolymers synthesised by Bundle and co-workers. Figure adapted from reference 105.

Singha *et al.*[106] introduced the concept of tandem post-polymerisation modification as a versatile route to synthesise well-defined highly functional polymers. A poly(pentafluorophenyl methacrylate) (pPFMA) scaffold was functionalised with allylamine to achieve pendant alkene functionality that would not be achievable by direct polymerisation. This was further modified using thiol-ene 'click' chemistry to introduce biofunctionality. To date, this methodology has not been used to explore glyco-functionality (See Chapter 2).

1.6 Detection of bacteria and lectins

The problem of antibiotic resistant bacteria is being exacerbated by the lack of rapid point-of-care diagnostics tools for detection of the bacterial species responsible for an infection. Detection and quantification of bacteria is important in clinical, environmental, and public health sectors. In clinical diagnostics, conventional plating and culturing is generally used to identify causative bacterial pathogens,[2] an effective and accurate method, however, it is time-consuming (more than 24 hours).

While several high-tech methods, including PCR, have been used to detect specific microorganisms, these are complex and require expensive, sophisticated equipment. Therefore, a facile and rapid detection method for the identification of the most prevalent pathogens would be of great value for providing effective therapeutics. If used as a point-of-care diagnostic tool they could not only increase the therapeutic efficacy but also go towards reducing the occurrence of drug-resistant bacteria arising due to the inappropriate administration of antibiotics.

The nature of carbohydrates can differ considerably between diseased and normal cells. Unique glycan markers of diseased cells can be exploited for early diagnosis, prevention and treatment of illnesses.[10] Surface glycans appear to be modulated depending on the physiological status, such as during developmental processes and oncological transformations.[18] The glycans on proteins have emerged as important biomarkers in the diagnosis of diseases such as cancer and play a significant role in how pathogenic viruses gain entry into cells.

In recent years, advancements in carbohydrate synthesis, analysis and glycoarray technology have facilitated the development of chemical approaches to 'glycomics' that provide a better understanding of the biological processes involving complex carbohydrates.[14, 107, 108] For instance databases such as the Consortium for Functional Glycomics (CFG)[20] are large research initiatives that provide resources and bioinformatics tools for the scientific community and sources of reference and information on the glycan-binding proteins.

Proper design of the synthetic multivalent systems used in molecular recognition studies is critical. Control of clustering, selection of adequate spacers and scaffolds, stability of the whole construction, and solubility in biological media are important to achieve high affinity and specificity.

1.6.1 Glycopolymers for bacteria and lectin detection

Polymer-based detection methods for cells have the advantage of simulating multiple interactions through the display of many ligands on a single polymer. The Seeberger group developed a fluorescent detection method for bacteria based on a water-soluble fluorescent-conjugated glycopolymer.[109] Carbohydrate-functionalised poly(*p*-phenylene ethynylene) (PPE), synthesised using a post-polymerisation modification method, were used to detect *E. coli* by exploiting the interaction between FimH and mannosides. Incubation of the polymers with FimH expressing *E. coli* showed that the glycopolymers binds to the bacteria and yield brightly fluorescent cell clusters due to multivalent interactions between the mannosylated polymer and the FimH on bacterial pili, as determined by microscopy. The presence of the bacteria was detected in less than 15 min, but requires an isolation step. Similarly, Phillips *et al*.[110] synthesised water-soluble carbohydrate functionalised PPE for detection of Con A and type 1 fimbriated *E. coli*. They found that when the carbohydrate moiety was placed further away from the conjugated backbone, or there is an increase in carbohydrate density, there was an increased propensity to induce aggregation of *E. coli*.

Pasparakis *et al*.[111] synthesised thermoresponsive glycopolymers that could control the reversible aggregation of a specific bacterial strain, with a view to developing a reusable cell-sensing material. Aggregation of fluorescently labelled FimH expressing *E. coli* was observed. TOP10 was used as a control strain that does not express the FimH adhesin, no aggregation behaviour was noted with this strain. Pasparakis *et al*. also synthesised glycopolymers vesicles that presented glucose as a first step towards artificial cell mimics.[112]

1.5.2 Glyconanoparticles

Glyconanoparticles are rapidly emerging as biosensors, in imaging, and in therapeutics.[113] They can be coupled with multiple carbohydrate moieties, which provides an increased potential for the enhancement of biomolecular interactions. Thus, glyconanoparticles constitute a good biomimetic model of carbohydrate presentation at the cell surface, and are excellent tools for glycobiology.

1.5.2.1 Gold nanoparticles

Gold nanoparticles (AuNPs) exhibit characteristic optical properties that are dependant on surface plasmon resonance, which arises due to the collective oscillation of the conduction electrons. The maximum wavelength and shape of the local surface plasmon resonance (LSPR) are determined by the particle size and shape. AuNPs have extremely high extinction coefficients, which are three to five orders of magnitude greater than those of traditional molecular dyes.

Monodisperse AuNPs between 10 nm and 80 nm appear red in colour, when the interparticle is greater than that of the particle diameter. As the interparticle distance decreases to less than that of the particle diameter, coupling and dipole-dipole interactions between the plasmons of neighbouring particles result in a broadening and a shift to longer wavelengths of the surface plasmon absorption band, resulting in the AuNPs appearing blue (Figure 1.16). It is this colourimetric aggregation that is exploited for the use in bioassays. This colourimetric change can be detected spectrophotometrically and visually.[114]
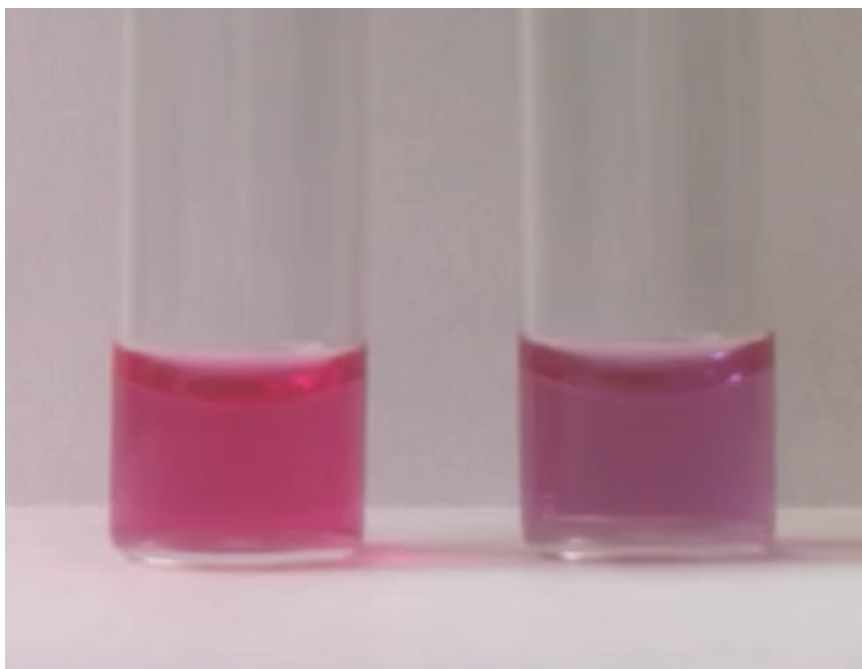
Figure 1.16: Red/pink to blue/purple colour change of AuNPs.

Colourimetric assays for investigating biomolecular interactions using AuNPs functionalised with biomolecules such as proteins,[115, 116] peptides,[117] antibodies,[118-123] and DNA[124, 125] have been developed. The detection of bacterial DNA using AuNPs originated in the pioneering work of Mirkin *et al.*[124] who demonstrated that as little as 10 fmol of an oligonucleotide analyte could be detected by exploiting the aggregation phenomenon of AuNPs.

Carbohydrate-functionalised AuNPs (glycoAuNPs) are emerging as an important tool for colourimetric bioassay of protein-carbohydrate interactions. They present a multivalent array of carbohydrates and provide a glycocalyx-like surface. They mimic carbohydrate presentation at the cell surface and can be used to study protein-carbohydrate interaction and to interfere with carbohydrate mediated biological processes. GlycoAuNPs are advantageous as they can also allow direct visualisation without the need for laborious protein labelling steps. GlycoAuNPs are typically prepared by treating pre-synthesised AuNPs with thiol-ending

glycoconjugates in order to displace the protecting shell ligands, typically citrates or thiols, on the gold surface by insertion of other ligands.

1.6.3 Glyconanoparticles for bacteria and lectin detection.

The influence of linkers (lengths, aliphatic/hydrophilic), density, and gold core size on AuNPs-lectin interactions has been studied by several groups. The influence of carbohydrate density on the aggregation of bivalent *Ricinus communis* agglutinin (RCA$_{120}$) was investigated by Otsuka *et al.*[126] on 9 nm AuNPs bearing lactose. It was found that more than 20 % lactose was required for aggregation to occur.

The influence of carbohydrate linker and core size (6 and 20 nm) on mannose-AuNP aggregation induced by Con A was studied by Lin *et al.*[127] The 20 nm AuNPs showed the highest affinity as determined by SPR. Lin *et al*. also synthesised mannose-functionalised particles (6 nm) to specifically bind to FimH adhesin of bacterial type 1 pili and not to a strain of *E. coli* that do not express FimH, as observed by transmission electron microscopy (TEM) (Figure 1.17).[128] Due to the small core size of the particles colourimetric aggregation of the particles was not investigated in this work (See Chapter 7).
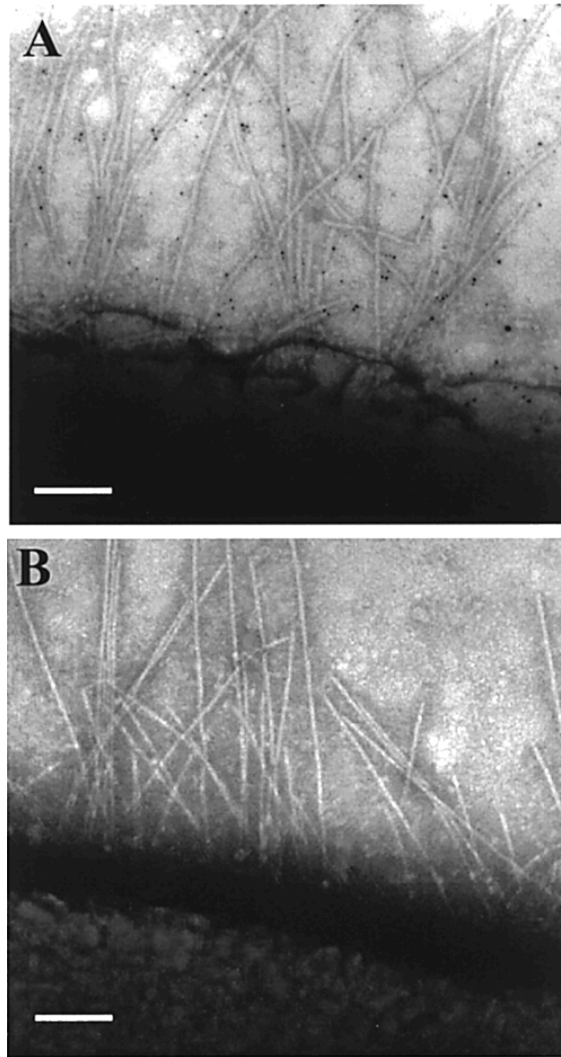
Figure 1.17: TEM of glycoAuNPs interacting with FimH expressing fimbriae on *E. coli* (A) and no interaction observed with a mutant that does not express FimH (B). Figure adapted from reference 128.

Schofield *et al.*[129] developed a colourimetric bioassay based on the aggregation of carbohydrate-stabilised gold nanoparticles for the detection of RCA_{120} − a ricin surrogate. AuNPs were stabilised with either a thiolated galactose derivative (9-mercapto-3,6-diaoxaoctyl-β-D-galactoside) and a thiolated triethylene glycol derivative as a dilutant to investigate the effect of carbohydrate surface coverage. Interestingly, it was found that a 70 % coverage of galactose was optimum for RCA_{120} detection, they also noted that a short linker between the particle and the pendant galactose gave greater aggregation, however, the longer chain gave a more

stable sensing systems. The same was carried out for Con A, it was found that 100 % carbohydrate coverage was optimum for this protein.

The preparation of thiolated carbohydrate derivatives requires multiple modification steps that can be difficult and time consuming. Chuang et al.[130] used a simple and versatile method for the preparation of glycoAuNPs using underivatised carbohydrates on hydrazide functionalised particles, utilising microwave irradiation. The strength of the interaction between Con A and maltose, mannose, glucose, lactose and Man5 functionalised particles was determined.

GlycoAuNPs are typically synthesised by the preparation of AuNPs, such as by the citrate reduction method of Turkevich et al.[131] followed by the introduction of carbohydrate functionality by Au-S ligand exchange. Watanabe et al.[132] developed a simple one-pot synthesis of thioglucose stabilised AuNPs. A diameter of 40-50 nm was considered to be optimum for the colourimetric bioassay of Con A. The ligands must be immobilised with a short linker in order to ensure aggregated particles are in the closest proximity to each other to maximise coupling between the particles.

Marín et al.[133] synthesised glycoAuNPs presenting a trivalent α2-6-thio-linked sialic acid that can detect strains of human influenza within 30 min using a simple colourimetric assay. It was found that a ratio of 25:75 trivalent ligand to PEG ligand was optimum for the detection of human influenza virus X31. The trivalent ligand provided significantly superior results to a monovalent α-thio-linked sialic acid. Impressively, these particles also showed specificity for human influenza virus over avian influenza virus.

Jayawardena et al.[134] employed glycoAuNPs to differentiate between plant lectins. Various carbohydrates were conjugated on AuNPs using a previously developed photocoupling chemistry.[135] The changes in LSPR upon lectin binding

were recorded and the data were subjected to the statistical analysis method of linear discriminant analysis (LDA). The glycoAuNPs successfully differentiated all the lectins.

1.7 Summary

Multivalent presentation of carbohydrate moieties is critical for high affinity inhibition of protein-carbohydrate interactions. Important considerations for designing multivalent architectures to target carbohydrate-binding proteins include: the multivalent scaffold used, ligand valency and density, linker length between the pendant carbohydrate moiety and the multivalent scaffold, the three-dimensional spatial arrangement of the carbohydrate ligands and ability to complement the binding site of the target protein. Excellent affinity gains can be achieved by designing multivalent inhibitors that interact with the target based on the structural arrangement of the binding sites and engineering an inhibitor that interacts with its target. However, multivalent scaffolds that exactly complement the binding site arrangements can be highly challenging to synthesise. Glycopolymers provide a simple alternative to these and show good affinity for the target lectin. However, most of the currently synthesised polymeric multivalent ligands show a 'random' multivalency, which rarely allows an affinity enhancement higher than 1000-fold. Therefore, there is a real need for high affinity glycopolymeric inhibitors that show good affinity but also high selectivity for the target lectin.

GlycoAuNPs have shown promise as tools for understanding and detecting protein-carbohydrate interactions. However, it appears that the core size and ligand density needs to be tuned to the target. Also little regard for their stability in biological, saline-rich media has been paid, which is important for applications in

biological media. GlycoAuNPs have been shown to interact with bacteria in response to carbohydrate-binding proteins expressed on their fimbriae however, the colourimetric detection of bacteria using glycoAuNPs has not yet been explored. Therefore the development of fast, saline stable, target specific glycoAuNPs is important.

1.8 Aims and thesis summary

Considering the above, this thesis aimed to achieve two main targets: firstly the development of high affinity glycopolymeric inhibitors of CTx, that also showed specificity for the target over other carbohydrate binding proteins with similar specificities. The second aim was the development of a colourimetric detection method for lectins and type 1 fimbriated bacteria based on glycoAuNPs.

This thesis is split into two sections: Inhibition and Detection. **Section 1** concerns glycopolymeric inhibitors of lectins and bacterial toxins and comparing and developing techniques for determining their inhibitory activity. **Chapter 2** describes the development of galactose-functionalised polymers synthesised using a newly developed tandem post-polymerisation modification method as inhibitors of CTx. The role of linker length between the pendant galactose and the polymer scaffold and the density of the galactose on the polymer scaffold were investigated on their inhibitory activity and lectin specificity for CTx. **Chapter 3** develops a route to these glycopolymeric inhibitors that used a more efficient one-pot method opposed to the two step, PFP/alkyne azide method used in the previous chapter. This provides the first example of the use of a poly(azlactone) reactive scaffold for the synthesis of glycopolymers. This versatile method was probed in depth and the inhibitory activities of the resulting polymers were determined by a fluorescent-linked sorbent

assay (FLSA) on the inhibition of Con A and CTx. **Chapter 4** shows the development of glycopolymers to target CTx more specifically by introducing a secondary unit along with the pendant saccharide to target the neuramimic acid site of CTx. The post-polymerisation method uses a poly(glycidyl methacrylate) precursor that can be ring opened using sodium azide resulting in a polymer with pendant azide and alcohol functionality. A galactose moiety can be installed using CuAAC chemistry and a variable functional group was installed using the pendant alcohol group. The inhibitory potency and specificity for CTx over another galactose specific lectin, PNA was determined using FLSA. **Chapter 5** probes the methods used for assessing carbohydrate-protein interactions and poses the question: which method is best for determining inhibitory activity? QCM-d and FLSA were used to determine the inhibitory activity of mannose functional polymers towards Con A. **Chapter 6** looks at an alternative method to assessing protein-carbohydrate interactions. Citrate stabilised AuNPs were employed as a developing agent for carbohydrate-binding proteins bound to 96-well microtitre plates. Due to the high extinction coefficient of AuNPs, the extent of a protein-carbohydrate interaction could be determined by a simple combination of a mobile phone camera and open source image software leading to a low technology/low cost method to analysing protein-carbohydrate interactions.

Section 2 concerns the development, optimisation and application of glycoAuNPs for the detection and discrimination of bacteria and lectins. **Chapter 7** proves the concept that glycoAuNPs can be used to discriminate between bacterial phenotypes of *E. coli*. However, there are limitations to this in the saline stability of these particles and methods to counteract this lead to particles with slower and limited readout potentials. Due to the delicate balance between saline stability and

speed of colourimetric readout, the development of an optimised method for the rapid, saline stable, and selective detection of lectins is described in **Chapter 8**. This optimised method is then improved upon in **Chapter 9** using a more versatile conjugation chemistry that can be used with any reducing sugar therefore removing the need for derivatisation. Finally, lectin discrimination was carried using a statistical method, linear discriminate analysis.

1.9 References

1.   C. Nathan, *Nature*, 2004, **431**, 899-902.

2.   B. S. Reisner and G. L. Woods, *J. Clin. Microbiol.*, 1999, **37**, 2024-2026.

3.   A. Opar, *Na. Rev. Drug Discov.*, 2007, **6**, 943-944.

4.   M. A. Fischbach and C. T. Walsh, *Science*, 2009, **325**, 1089-1093.

5.   R. A. Weinstein, *Emerg. Infect. Dis.*, 2001, **7**, 188-192.

6.   H. C. Neu, *Science*, 1992, **257**, 1064-1073.

7.   K. M. G. O'Connell, J. T. Hodgkinson, H. F. Sore, M. Welch, G. P. C. Salmond and D. R. Spring, *Angew. Chem. Int. Ed.*, 2013, **52**, 10706-10733.

8.   K. T. Pilobello and L. K. Mahal, *Curr. Opin. Chem. Biol.*, 2007, **11**, 300-305.

9.   A. Adibekian, P. Stallforth, M.-L. Hecht, D. B. Werz, P. Gagneux and P. H. Seeberger, *Chem. Sci.*, 2011, **2**, 337-344.

10.   M. C. Galan, D. Benito-Alifonso and G. M. Watt, *Org. Biomol. Chem.*, 2011, **9**, 3598-3610.

11.   A. Varki, *Essentials of glycobiology*, 1999, xvii+653p-xvii+653p.

12.   J. A. Prescher and C. R. Bertozzi, *Cell*, 2006, **126**, 851-854.

13.   J. Hirabayashi, M. Yamada, A. Kuno and H. Tateno, *Chem. Soc. Rev.*, 2013, **42**, 4443-4458.

14.   J. Hirabayashi, *Glycoconjugate J.*, 2004, **21**, 35-40.

15.   J. E. Turnbull and R. A. Field, *Nat. Chem. Biol.*, 2007, **3**, 74-77.

16.   R. A. Dwek, *Chem. Rev.*, 1996, **96**, 683-720.

17.   M. S. M. Timmer, B. L. Stocker and P. H. Seeberger, *Curr. Opin. Chem. Biol.*, 2007, **11**, 59-65.

18.   Y. C. Lee and R. T. Lee, *Acc. Chem. Res.*, 1995, **28**, 321-327.

19.   N. V. Bovin and H. J. Gabius, *Chem. Soc. Rev.*, 1995, **24**, 413-&.

20.   CFG, www.functionalglycomics.org

21.   C. R. Bertozzi and L. L. Kiessling, *Science*, 2001, **291**, 2357-2364.

22.   H. Lis and N. Sharon, *Chem. Rev.*, 1998, **98**, 637-674.

23.   X. Zeng, C. A. S. Andrade, M. D. L. Oliveira and X.-L. Sun, *Anal. Bioanal. Chem.*, 2012, **402**, 3161-3176.

24.   M. Ambrosi, N. R. Cameron and B. G. Davis, *Org. Bio. Chem.*, 2005, **3**, 1593-1608.

25.   H. Feinberg, D. A. Mitchell, K. Drickamer and W. I. Weis, *Science*, 2001, **294**, 2163-2166.

26.   K. Drickamer, *Curr. Opin. Struct. Biol.*, 1999, **9**, 585-590.

27.   W. I. Weis and K. Drickamer, *Annu. Rev. Biochem.*, 1996, **65**, 441-473.

28.   M. Fais, R. Karamanska, S. Allman, S. A. Fairhurst, P. Innocenti, A. J. Fairbanks, T. J. Donohoe, B. G. Davis, D. A. Russell and R. A. Field, *Chem. Sci.*, 2011, **2**, 1952-1959.

29.   M. E. Ivarsson, J.-C. Leroux and B. Castagner, *Angew. Chem. Int. Ed.*, 2012, **51**, 4024-4045.

30.   T. Beddoe, A. W. Paton, J. Le Nours, J. Rossjohn and J. C. Paton, *Trends Biochem. Sci.*, 2010, **35**, 411-418.

31. T. R. Branson and W. B. Turnbull, *Chem. Soc. Rev.*, 2013, **42**, 4613-4622.

32. D. Vanden Broeck, C. Horvath and M. J. S. De Wolf, *Int. J. Biochem.Cell Biol.*, 2007, **39**, 1771-1775.

33. E. A. Merritt, S. Sarfaty, F. Vandenakker, C. Lhoir, J. A. Martial and W. G. J. Hol, *Protein Sci.*, 1994, **3**, 166-175.

34. W. B. Turnbull, B. L. Precious and S. W. Homans, *J. Am. Chem. Soc.*, 2004, **126**, 1047-1054.

35. L. de Haan and T. R. Hirst, *Mol. Membr. Biol.*, 2004, **21**, 77-92.

36. N. Sharon, *Biochim. Biophys. Acta*, 2006, **1760**, 527-537.

37. S. D. Knight and J. Bouckaert, *Glycoscience and Microbial Adhesion*, 2009, **288**, 67-107.

38. M. Hartmann and T. K. Lindhorst, *Eur. J. Org. Chem.*, 2011, 3583-3609.

39. K. W. Dodson, J. S. Pinkner, T. Rose, G. Magnusson, S. J. Hultgren and G. Waksman, *Cell*, 2001, **105**, 733-743.

40. Y. C. Lee, R. R. Townsend, M. R. Hardy, J. Lonngren, J. Arnarp, M. Haraldsson and H. Lonn, *J. Biol. Chem.*, 1983, **258**, 199-202.

41. J. J. Lundquist and E. J. Toone, *Chem. Rev.*, 2002, **102**, 555-578.

42. P. M. Levine, T. P. Carberry, J. M. Holub and K. Kirshenbaum, *Med. Chem. Comm.*, 2013, **4**, 493-509.

43. L. L. Kiessling, J. E. Gestwicki and L. E. Strong, *Curr. Opin. Chem. Biol.*, 2000, **4**, 696-703.

44. R. J. Pieters, *Org. Biomol. Chem.*, 2009, **7**, 2013-2025.

45. A. Bernardi and P. Cheshev, *Chem. Eur. J.*, 2008, **14**, 7434-7441.

46. A. Bernardi, A. Checchia, P. Brocca, S. Sonnino and F. Zuccotto, *J. Am. Chem. Soc.*, 1999, **121**, 2032-2036.

47. M. Thepaut, C. Guzzi, I. Sutkeviciute, S. Sattin, R. Ribeiro-Viana, N. Varga, E. Chabrol, J. Rojo, A. Bernardi, J. Angulo, P. M. Nieto and F. Fieschi, *J. Am. Chem. Soc.*, 2013, **135**, 2518-2529.

48. M. C. Galan, P. Dumy and O. Renaudet, *Chem. Soc. Rev.*, 2013, **42**, 4599-4612.

49. J. L. Jimenez Blanco, C. Ortiz Mellet and J. M. Garcia Fernandez, *Chem. Soc. Rev.*, 2013, **42**, 4518-4531.

50. A. Bernardi, J. Jimenez-Barbero, A. Casnati, C. De Castro, T. Darbre, F. Fieschi, J. Finne, H. Funken, K.-E. Jaeger, M. Lahmann, T. K. Lindhorst, M. Marradi, P. Messner, A. Molinaro, P. V. Murphy, C. Nativi, S. Oscarson, S. Penades, F. Peri, R. J. Pieters, O. Renaudet, J.-L. Reymond, B. Richichi, J. Rojo, F. Sansone, C. Schaeffer, W. B. Turnbull, T. Velasco-Torrijos, S. Vidal, S. Vincent, T. Wennekes, H. Zuilhof and A. Imberty, *Chem. Soc. Rev.*, 2013, **42**, 4709-4727.

51. S. G. Spain and N. R. Cameron, *Polym. Chem.*, 2011, **2**, 60-68.

52. V. Wittmann and R. J. Pieters, *Chem. Soc. Rev.*, 2013, **42**, 4492-4503.

53. N. P. Pera and R. J. Pieters, *Med. Chem. Comm.*, 2014, **5**, 1027-1035.

54. E. K. Fan, Z. S. Zhang, W. E. Minke, Z. Hou, C. Verlinde and W. G. J. Hol, *J. Am. Chem. Soc.*, 2000, **122**, 2663-2664.

55. P. I. Kitov, J. M. Sadowska, G. Mulvey, G. D. Armstrong, H. Ling, N. S. Pannu, R. J. Read and D. R. Bundle, *Nature*, 2000, **403**, 669-672.

56. J. Garcia-Hartjes, S. Bernardi, C. A. G. M. Weijers, T. Wennekes, M. Gilbert, F. Sansone, A. Casnati and H. Zuilhof, *Org. Biomol. Chem.*, 2013, **11**, 4340-4349.

57.   M. Mattarella, J. Garcia-Hartjes, T. Wennekes, H. Zuilhof and J. S. Siegel, *Org. Biomol. Chem.*, 2013, **11**, 4333-4339.

58.   T. R. Branson, T. E. McAllister, J. Garcia-Hartjes, M. A. Fascione, J. F. Ross, S. L. Warriner, T. Wennekes, H. Zuilhof and W. B. Turnbull, *Angew. Chem. Int. Ed.*, 2014, **53**, 8323-8327.

59.   W. B. Turnbull and J. F. Stoddart, *Rev. Mol. Biotechnol.*, 2002, **90**, 231-255.

60.   J. P. Thompson and C. L. Schengrund, *Glycoconjugate J.*, 1997, **14**, 837-845.

61.   I. Vrasidas, N. J. de Mol, R. M. J. Liskamp and R. J. Pieters, *Eur. J. Org. Chem.*, 2001, 4685-4692.

62.   D. Arosio, I. Vrasidas, P. Valentini, R. M. J. Liskamp, R. J. Pieters and A. Bernardi, *Org. Biomol. Chem.*, 2004, **2**, 2113-2124.

63.   H. M. Branderhorst, R. Kooij, A. Salminen, L. H. Jongeneel, C. J. Arnusch, R. M. J. Liskamp, J. Finne and R. J. Pieters, *Org. Biomol. Chem.*, 2008, **6**, 1425-1434.

64.   J.-L. Reymond, M. Bergmann and T. Darbre, *Chem. Soc. Rev.*, 2013, **42**, 4814-4822.

65.   R. U. Kadam, M. Bergmann, M. Hurley, D. Garg, M. Cacciarini, M. A. Swiderska, C. Nativi, M. Sattler, A. R. Smyth, P. Williams, M. Camara, A. Stocker, T. Darbre and J.-L. Reymond, *Angew. Chem. Int. Ed.*, 2011, **50**, 10631-10635.

66.   E. M. V. Johansson, S. A. Crusz, E. Kolomiets, L. Buts, R. U. Kadam, M. Cacciarini, K.-M. Bartels, S. P. Diggle, M. Camara, P. Williams, R. Loris, C. Nativi, F. Rosenau, K.-E. Jaeger, T. Darbre and J.-L. Reymond, *Chem. Biol.*, 2008, **15**, 1249-1257.

67.   B. D. Polizzotti and K. L. Kiick, *Biomacromolecules*, 2006, **7**, 483-490.

68.   S. Liu and K. L. Kiick, *Macromolecules*, 2008, **41**, 764-772.

69.   B. D. Polizzotti, R. Maheshwari, J. Vinkenborg and K. L. Kiick, *Macromolecules*, 2007, **40**, 7103-7110.

70.   R. Maheshwari, E. A. Levenson and K. L. Kiick, *Macromol. Biosci.*, 2010, **10**, 68-81.

71.   Z. S. Zhang, J. Y. Liu, C. Verlinde, W. G. J. Hol and E. K. Fan, *Journal of Organic Chemistry*, 2004, **69**, 7737-7740.

72.   V. Wittmann and S. Seeberger, *Angew. Chem. Int. Ed.*, 2004, **43**, 900-903.

73.   A. Schierholt, M. Hartmann and T. K. Lindhorst, *Carbohydr. Res.*, 2011, **346**, 1519-1526.

74.   Y. Miura, D. Koketsu and K. Kobayashi, *Polym. Adv. Technol.*, 2007, **18**, 647-651.

75.   L. L. Kiessling, J. E. Gestwicki and L. E. Strong, *Angew. Chem. Int. Ed.*, 2006, **45**, 2348-2368.

76.   M. G. Baek and R. Roy, *Macromolecular Bioscience*, 2001, **1**, 305-311.

77.   V. Ladmiral, E. Melia and D. M. Haddleton, *Eur. Polym. J.*, 2004, **40**, 431-449.

78.   C. Fraser and R. H. Grubbs, *Macromolecules*, 1995, **28**, 7248-7255.

79.   K. H. Mortell, R. V. Weatherman and L. L. Kiessling, *J. Am. Chem. Soc.*, 1996, **118**, 2297-2298.

80.   K. H. Mortell, M. Gingras and L. L. Kiessling, *J. Am. Chem. Soc.*, 1994, **116**, 12053-12054.

81.   M. Kanai, K. H. Mortell and L. L. Kiessling, *J. Am. Chem. Soc.*, 1997, **119**, 9931-9932.

82. K. Ohno, Y. Tsujii, T. Miyamoto, T. Fukuda, M. Goto, K. Kobayashi and T. Akaike, *Macromolecules*, 1998, **31**, 1064-1069.

83. R. Narain and S. P. Armes, *Macromolecules*, 2003, **36**, 4675-4678.

84. R. Narain and S. P. Armes, *Chem. Commun.*, 2002, 2776-2777.

85. A. B. Lowe, B. S. Sumerlin and C. L. McCormick, *Polymer*, 2003, **44**, 6761-6765.

86. L. Albertin, C. Kohlert, M. Stenzel, L. J. R. Foster and T. P. Davis, *Biomacromolecules*, 2004, **5**, 255-260.

87. L. Albertin, M. H. Stenzel, C. Barner-Kowollik, L. J. R. Foster and T. P. Davis, *Macromolecules*, 2005, **38**, 9075-9084.

88. L. Albertin, M. Stenzel, C. Barner-Kowollik, L. J. R. Foster and T. P. Davis, *Macromolecules*, 2004, **37**, 7530-7537.

89. M. A. Gauthier, M. I. Gibson and H.-A. Klok, *Angew. Chem. Int. Ed.*, 2009, **48**, 48-58.

90. M. Mammen, G. Dahmann and G. M. Whitesides, *J. Med. Chem.*, 1995, **38**, 4179-4190.

91. G. B. Sigal, M. Mammen, G. Dahmann and G. M. Whitesides, *J. Am. Chem. Soc.*, 1996, **118**, 3789-3800.

92. M. Eberhardt, R. Mruk, R. Zentel and P. Theato, *Eur. Polym. J.*, 2005, **41**, 1569-1575.

93. P. Theato, *J. Polym. Sci. A Polym. Chem.*, 2008, **46**, 6677-6687.

94. M. I. Gibson, E. Froehlich and H.-A. Klok, *J. Polym. Sci. A Polym. Chem.*, 2009, **47**, 4332-4345.

95. M. E. Buck and D. M. Lynn, *Polym. Chem.*, 2012, **3**, 66-80.

96.   S. M. Heilmann, J. K. Rasmussen and L. R. Krepski, *J. Polym. Sci. A Polym. Chem.*, 2001, **39**, 3655-3677.

97.   H. C. Kolb, M. G. Finn and K. B. Sharpless, *Angew. Chem. Int. Ed.*, 2001, **40**, 2004-2021.

98.   M. J. Kade, D. J. Burke and C. J. Hawker, *J. Polym. Sci. A Polym. Chem.*, 2010, **48**, 743-750.

99.   S. Slavin, J. Burns, D. M. Haddleton and C. R. Becer, *Eur. Polym. J.*, 2011, **47**, 435-446.

100.   A. Dondoni and A. Marra, *Chemical Society Reviews*, 2012, **41**, 573-586.

101.   A. Dondoni, *Chemistry-an Asian Journal*, 2007, **2**, 700-708.

102.   V. Ladmiral, G. Mantovani, G. J. Clarkson, S. Cauet, J. L. Irwin and D. M. Haddleton, *J. Am. Chem. Soc.*, 2006, **128**, 4823-4830.

103.   C. R. Becer, M. I. Gibson, J. Geng, R. Ilyas, R. Wallis, D. A. Mitchell and D. M. Haddleton, *J. Am. Chem. Soc.*, 2010, **132**, 15130-15132.

104.   N. Vinson, Y. Gou, C. R. Becer, D. M. Haddleton and M. I. Gibson, *Polym. Chem.*, 2011, **2**, 107-113.

105.   T. Huu-Anh, P. I. Kitov, E. Paszkiewicz, J. M. Sadowska and D. R. Bundle, *Org. Biomol. Chem.*, 2011, **9**, 3658-3671.

106.   N. K. Singha, M. I. Gibson, B. P. Koiry, M. Danial and H.-A. Klok, *Biomacromolecules*, 2011, **12**, 2908-2913.

107.   P. H. Seeberger and D. B. Werz, *Nature*, 2007, **446**, 1046-1051.

108.   S. Park, J. C. Gildersleeve, O. Blixt and I. Shin, *Chem. Soc. Rev.*, 2013, **42**, 4310-4326.

109.   M. D. Disney, J. Zheng, T. M. Swager and P. H. Seeberger, *J. Am. Chem. Soc.*, 2004, **126**, 13343-13346.

110. R. L. Phillips, I.-B. Kim, B. E. Carson, B. Tidbeck, Y. Bai, T. L. Lowary, L. M. Tollbert and U. H. F. Bunz, *Macromolecules*, 2008, **41**, 7316-7320.

111. G. Pasparakis, A. Cockayne and C. Alexander, *J. Am. Chem. Soc.*, 2007, **129**, 11014 - 11015.

112. G. Pasparakis and C. Alexander, *Angew. Chem. Int. Ed.*, 2010, **49**, 241-241.

113. M. Marradi, F. Chiodo, I. Garcia and S. Penades, *Chem. Soc. Rev.*, 2013, **42**, 4728-4745.

114. L. Dykman and N. Khlebtsov, *Chem. Soc. Rev.*, 2012, **41**, 2256-2282.

115. J. E. Ghadiali and M. M. Stevens, *Adv. Mater.*, 2008, **20**, 4359-4363.

116. G. J. Nusz, S. M. Marinakos, A. C. Curry, A. Dahlin, F. Hook, A. Wax and A. Chilkoti, *Anal. Chem.*, 2008, **80**, 984-989.

117. A. Laromaine, L. L. Koh, M. Murugesan, R. V. Ulijn and M. M. Stevens, *J. Am. Chem. Soc.*, 2007, **129**, 4156-4157.

118. A. K. Singh, D. Senapati, S. G. Wang, J. Griffin, A. Neely, P. Candice, K. M. Naylor, B. Varisli, J. R. Kalluri and P. C. Ray, *ACS Nano*, 2009, **3**, 1906-1912.

119. K. M. Mayer, S. Lee, H. Liao, B. C. Rostro, A. Fuentes, P. T. Scully, C. L. Nehl and J. H. Hafner, *ACS Nano*, 2008, **2**, 687-692.

120. S. H. Huang, *Sensor. Actuat. B Chem.*, 2007, **127**, 335-340.

121. A. J. Haes, L. Chang, W. L. Klein and R. P. Van Duyne, *J. Am. Chem. Soc.*, 2005, **127**, 2264-2271.

122. P. Englebienne, *Analyst*, 1998, **123**, 1599-1603.

123. N. Ohtake, K. Niikura, T. Suzuki, K. Nagakawa, H. Sawa and K. Ijiro, *Bioconjugate Chem.*, 2008, **19**, 507-515.

124.   R. Elghanian, J. J. Storhoff, R. C. Mucic, R. L. Letsinger and C. A. Mirkin, *Science*, 1997, **277**, 1078-1081.

125.   P. V. Baptista, M. Koziol-Montewka, J. Paluch-Oles, G. Doria and R. Franco, *Clin. Chem.*, 2006, **52**, 1433-1434.

126.   H. Otsuka, Y. Akiyama, Y. Nagasaki and K. Kataoka, *J. Am. Chem. Soc.*, 2001, **123**, 8226-8230.

127.   C. C. Lin, Y. C. Yeh, C. Y. Yang, G. F. Chen, Y. C. Chen, Y. C. Wu and C. C. Chen, *Chem. Commun.*, 2003, 2920-2921.

128.   C. C. Lin, Y. C. Yeh, C. Y. Yang, C. L. Chen, G. F. Chen, C. C. Chen and Y. C. Wu, *J. Am. Chem. Soc.*, 2002, **124**, 3508-3509.

129.   C. L. Schofield, B. Mukhopadhyay, S. M. Hardy, M. B. McDonnell, R. A. Field and D. A. Russell, *Analyst*, 2008, **133**, 626-634.

130.   Y. J. Chuang, X. C. Zhou, Z. W. Pan and C. Turchi, *Biochem. Biophys. Res. Co.*, 2009, **389**, 22-27.

131.   J. Turkevich, P. C. Stevenson and J. Hillier, ed. P. C. Stevenson, Discuss Faraday Soc, 1951, vol. 11, pp. 55-75.

132.   S. Watanabe, K. Yoshida, K. Shinkawa, D. Kumagawa and H. Seguchi, *Colloid. Surface. B*, 2010, **81**, 570-577.

133.   M. J. Marin, A. Rashid, M. Rejzek, S. A. Fairhurst, S. A. Wharton, S. R. Martin, J. W. McCauley, T. Wileman, R. A. Field and D. A. Russell, *Org. Biomol. Chem.*, 2013, **11**, 7101-7107.

134.   H. S. N. Jayawardena, X. Wang and M. Yan, *Anal. Chem.*, 2013, **85**, 10277-10281.

135.   X. Wang, O. Ramstrom and M. Yan, *J. Mater. Chem.*, 2009, **19**, 8944-8949.

Section 1: Inhibition

Chapter 2

Probing bacterial-toxin inhibition with synthetic glycopolymers prepared by tandem post-polymerisation modification: role of linker length and carbohydrate density

S-J. Richards, M. W. Jones, M. Hunaban, D. M. Haddleton, M. I. Gibson, *Angew. Chem. Int. Ed.*, **2012**, *51*, 7932-7936

This chapter contains the paper on inhibiting cholera toxin using synthetic glycopolymers synthesised using a newly developed tandem post-polymerisation method. This work aimed to produce polymeric inhibitors that had not only good affinity but also specificity for the target toxin.

Mathew Jones synthesised the poly(pentafluorophenol methacrylate) scaffold polymers and the longer alkyne linker. I carried out the post-polymerisation modifications of the polymers to produce glycopolymeric inhibitors of the cholera toxin. I also tested the inhibitory activity of the polymers using a fluorescence-linked sorbent assay. Mark Hunabun was an MChem student I supervised and he modified the polymers with different carbohydrate densities and I carried out the inhibition testing of these polymers. I was responsible for the preparation of the manuscript.

2.1 Abstract

A tandem post-polymerisation modification strategy was used to systematically probe the multivalent inhibition of a bacterial toxin as a function of linker length, carbohydrate density, and glycopolymer chain length. Guided by structural-biology information, the binding-pocket depth of the toxin was probed and used as a means to specifically improve inhibition of the toxin by the glycopolymer.

2.2 Introduction

Carbohydrate-protein interactions mediate many critical biological recognition processes, such as those involved in cell signalling, fertilisation, and inflammation, as well as the adhesion of viruses and bacterial toxins.[1] The proteins responsible for deciphering this information are termed lectins, which specifically (and noncovalently) bind carbohydrates based on their branching pattern, stereochemistry, and chemical functionality.[2, 3] The protein–saccharide interactions are usually weak, but are amplified by clustered saccharides, resulting in a binding constant that is greater than the simple sum of the total number of ligands. This observation is referred to as the 'cluster glycoside' effect.[4] Considering this information, glycopolymers are attractive materials to interact with lectins and have been shown to display binding affinities several orders of magnitude greater than a single carbohydrate molecule.[2, 5-9] One of the most attractive applications of glycopolymers is to interfere with the binding of lectins from a pathogen to the host organism and therefore prevent infection from occurring; this is known as anti-adhesion therapy.[10-14]

Anti-adhesion therapy is not limited to polymeric glycoconjugates, and many high-affinity, small-molecule inhibitors of lectin binding are known.[15] The increased

57

affinity of these small-molecule inhibitors is often because of favourable interactions within the sugar-binding pocket, obtained by structural biology studies.[15, 16] Despite the wealth of structural information available, this design approach has rarely been applied to the design of polymeric inhibitors.[13] The cholera toxin (CTx), secreted by *Vibrio cholerae*, which is the causative agent of cholera, is a multimeric AB_5 lectin-like complex. The five B subunits bind GM1 gangliosides (Galβ1-3GalNAcβ1-4(Neu5Acα2-3)-Gal-β1-4Glc ceramide) present on the surface of the intestinal epithelium cells, initiating a series of events that results in the cholera symptoms. Multivalent, glycosylated STARFISH dendrimers successfully protected cells from similar toxins.[17] Polizzotti and Kiick have demonstrated that galactose-functionalised poly(L-glutamic acid) (PLG) is an effective inhibitor of CTx.[18] Interestingly, lowering the density of the galactose residues on the PLG backbone from approximately 50 % to 10 % gave a dramatic increase in activity. The inhibitory activity was further enhanced when the spacing between PLG and galactose was increased, making the binding site more accessible, and was also related to the depth of the CTx galactose binding pocket, which was estimated as being 16 Å. Others have speculated that longer linkers could enhance binding affinity, but these studies were not systematic or relied on a simple turbidimetry-based assay. The thermodynamics of this process have been evaluated in detail by Kane.[19]

A challenge associated with studying multivalent interactions is the synthesis of libraries of glycopolymers with precise control over the chain length, carbohydrate density, and nature of the linker. Direct polymerisation of two glycosylated monomers is unlikely to lead to polymers with identical degrees of polymerisation, which considering the importance of valency in carbohydrate-lectin interactions, is a major challenge.[20] The synthesis of glycopolymers by post-

polymerisation modification has attracted much interest, especially with the development of "click"-type reactions.[21-23] Haddleton *et al.* have synthesised several classes of glycopolymers through cycloaddition of glycosyl azides with poly(propargylmethacrylate) scaffolds[5, 24] and used these to inhibit the binding of gp120 (derived from HIV) to DC-SIGN (one of its targets in humans)[25] The direct polymerisation of alkyne (or alkene) monomers by radical methods is generally not possible because of competing side reactions, due to competing reactivity of the alkynyl/vinyl bonds leading to loss of polymerisation control and polymer branching.[22] Also, the incorporation of co-monomers has the problem of obtaining identical length polymers. To address this, Shigha *et al.* introduced tandem post-polymerisation modification to introduce incompatible functionality and control functional group density.[26] Using poly(pentafluorophenyl methacrylate) as the template scaffold, allylamine was introduced as a reactive, orthogonal "handle" and the remaining ester groups reacted with 2-hydroxypropylamine to give a water-soluble backbone. This powerful method allows precise control over of a wide range of chemical space.

Herein, we use tandem post-polymerisation modification to obtain glycopolymers with precisely controlled chain length, carbohydrate density, and crucially, defined backbone–carbohydrate linker lengths. This series of polymers was used to study the multivalent interactions between CTx and peanut agglutinin (PNA) another 'galactose specific' lectin, to probe the impact of modulating the binding site complementarity on the inhibitory activity of the glycopolymers. This unique combination of structural biology with materials science gives insights into the cluster glycoside effect and will allow design of active inhibitors.

2.3 Results and Discussion

The tandem post-polymerisation modification strategy is outlined in Scheme 2.1. This approach is advantageous because it allows us to explore a large area of chemical space (through side-chain modification) while ensuring that the average degree of polymerisation (DP) is identical within each series.
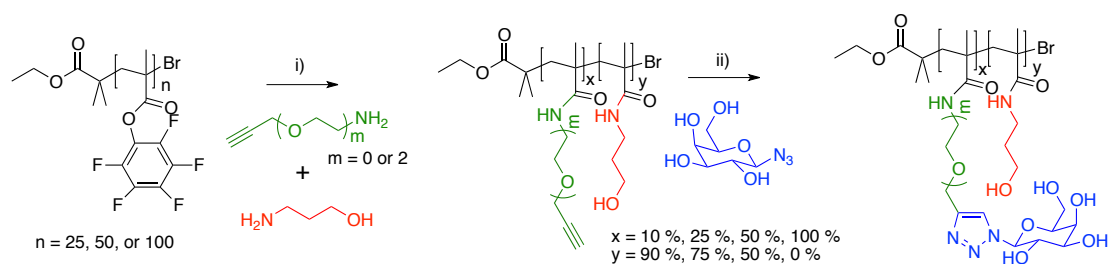
Scheme 2.1: Synthesis of glycopolymer libraries. i) amine (variable amounts)/triethylamine (TEA; 1 equiv.)/dimethylformamide (DMF), 5 h.; ii) GalN$_3$ (1.5 equiv)/CuBr/TBTA, DMSO

Two different amino-functional alkynes were selected as the polymer-carbohydrate spacers. Propargylamine (**Alkyne 1**) acts as a short linker and a diethylene glycol group acts as a longer spacer (**Alkyne 2**). The reactive polymeric precursor, poly(pentafluorophenyl methacrylate), pPFMA, was synthesised by copper-mediated controlled-radical polymerisation to give a series of polymers with varying DPs, Table 2.1. As previously reported,[27] size exclusion chromatographic (SEC) analysis of pPFMA gave values of M_n in disagreement with the theoretical M_n, due to elution volumes being different to the calibration standard, it being a non-ideal solvent or interactions with the column. pPFMA reacts readily with sterically unhindered amines, such as those used here.[27]

Table 2.1. pPFMA precursor polymers.

Polymer	[M]:[I][a]	Conversion[b] (%)	$M_{n(theo)}$[c]	$M_{n, (SEC)}$[d]	M_w/M_n[d]	DP[e]
P1	25	71	4500	7800	1.19	18
P2	50	65	8200	8800	1.20	33
P3	100	70	17640	11400	1.16	70

[a] Feed ratio of monomer to initiator. [b] Determined by ^{1}H NMR. [c] Theoretical M_n, calculated from feed ratio and conversion. [d] Determined by SEC in THF using polystyrene standards. [e] Theoretical number-average degree of polymerisation.

Homopolymers were synthesised by addition of a three-fold molar excess of **Alkyne 1** or **2**, as well as several copolymers (see below for rationale) by addition of 10, 25, and 50 mol % of **Alkyne 2**, followed by a three molar excess of 3-aminopropanol. Conversion of the pentafluorophenyl (PFP) groups into amides was confirmed by IR spectroscopy as the desired amide product (1675 cm^{-1}) and PFP ester (1786 cm^{-1}) have unique vibrational frequencies. In all cases, a small amount (< 5 %) of carboxylic acid units can be seen at 1730cm^{-1}, Figure 2.1. Fluorine NMR spectroscopy is often used to determine conversion of PFP groups, but does not discriminate between functionalisation and hydrolysis, and therefore can give false positive results.
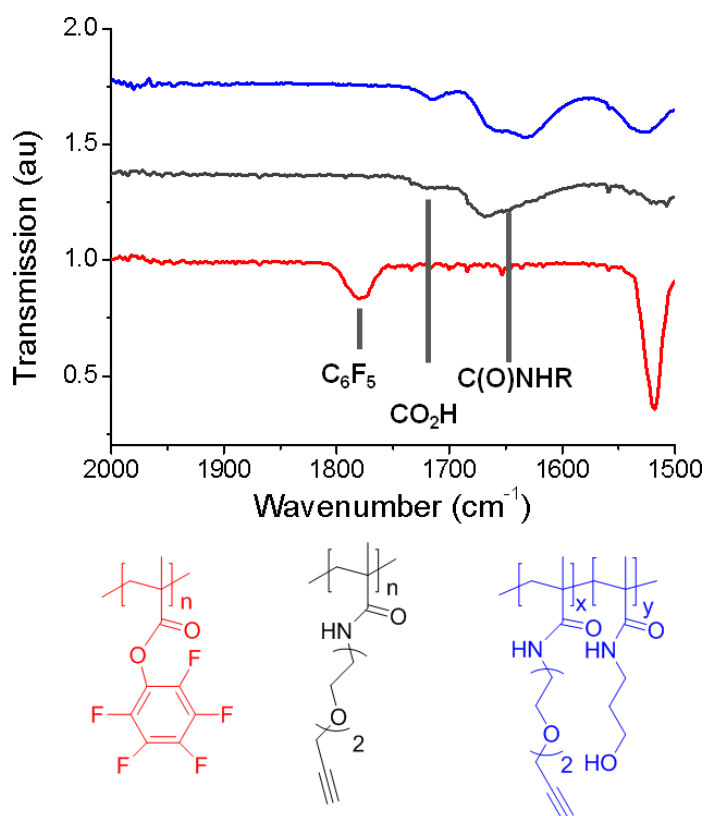
Figure 2.1: Infrared spectra showing conversion of the PFP groups (1786 cm^{-1}) into amides (1675 cm^{-1}). Carboxylic acid impurities are also indicated. Copolymer (blue line) has two distinct amide peaks.

The alkyne functional (co)polymers were subsequently functionalised with 1-azido-β-D-galactose (GalN$_3$) (synthesis procedure of GalN$_3$ can be found in appendix 1) using the CuI/tris(benzyltriazolylmethyl)amine (TBTA) catalyst system, in dimethyl sulfoxide (DMSO)[5] to yield homogenous glycopolymers, with no detectable alkyne or azide groups by NMR or IR spectroscopy. Over the course of the tandem post-polymerisation functionalisation, there was no evidence of fractionation, and all the polymers obtained were well defined with dispersities (Đ) below 1.3 (SEC data are included in Appendix 1). Table 2.2 summarises the diverse glycopolymer library that was synthesised and used for biological evaluation, below.

Table 2.2: Glycopolymers obtained by tandem modification.

Polymer	DP[a]	Linker[b]	Density[c]	M_n (g.mol^{-1})[d]	M_w/M_n[d]
GP1	18	Alkyne 1	100	5100	1.29
GP2	33	Alkyne 1	100	5340	1.27
GP3	70	Alkyne 1	100	6000	1.26
GP4	18	Alkyne 2	100	7250	1.32
GP5	33	Alkyne 2	100	10000	1.28
GP6	70	Alkyne 2	100	11900	1.27
GP7	33	Alkyne 2	50	10800	1.23
GP8	33	Alkyne 2	25	10700	1.21
GP9	33	Alkyne 2	10	10500	1.2

[a] Theoretical number-average degree of polymerisation. [b] Alkyne used to modify pPFMA scaffold. [c] Percentage of repeat units functionalised with a galactose unit. [d] Determined by SEC in DMF.

The aim of this investigation was to probe the effect of carbohydrate-binding site accessibility on the measured affinity between multivalent glycopolymers and their target lectins. The B subunit domain of CTx (CTxB) was chosen because it is nontoxic, and a report by Polizzotti and Kiick showed that longer linkers resulted in increased inhibitory activity of CTx.[18] Peanut agglutinin (PNA) was used as a control as it also binds β-galactose, but its binding sites are surface exposed.[28, 29] It is critical to include this second lectin, because it allows us to separate the effect of binding-site accessibility from increased side chain flexibility; the latter has been suggested to alter the binding of glycopolymers by allowing access to a larger number of possible conformations and leading to increased clustering. A recent study found that longer polymer–carbohydrate linkers showed increased affinity for the lectin, but the valency of each structure was not identical and there was no consideration of the depth of the lectin binding site.[30] Figure 2.2 shows schematic depictions of the galactose-binding domains of CTx and PNA in comparison to the two-linker systems used herein, which were selected to mimic these distances.
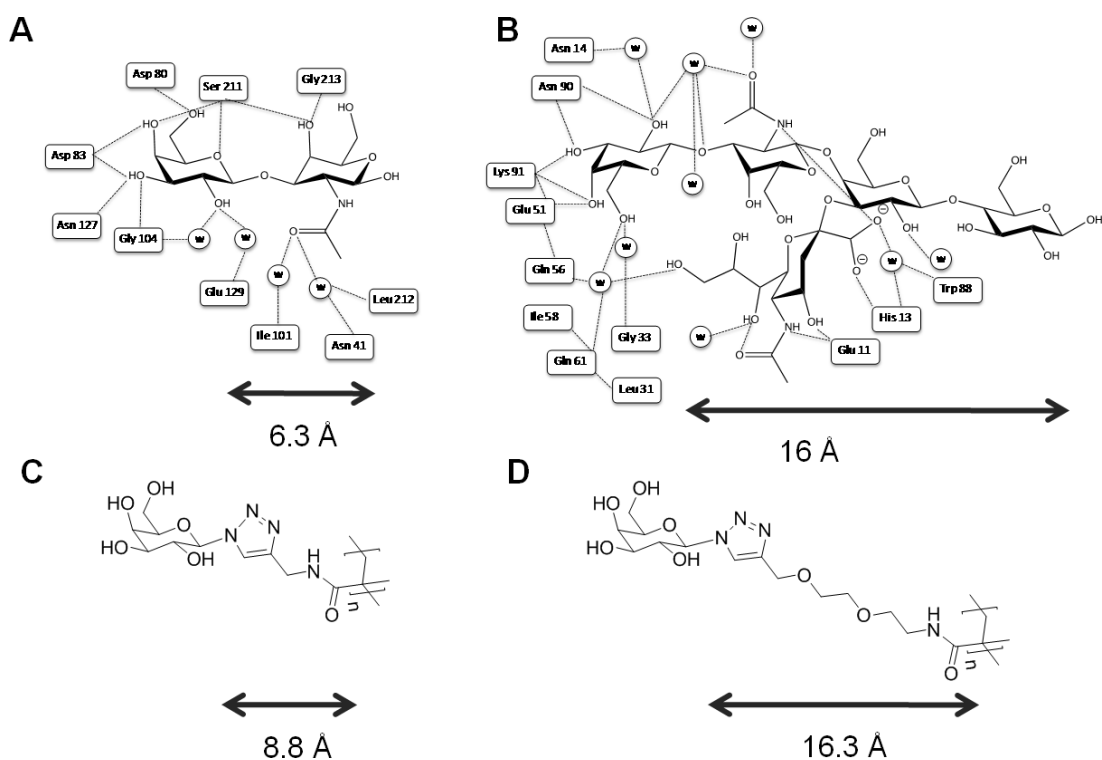
Figure 2.2: Binding sites of PNA (A) and CTx (B). W = water ligand. C, D) Polymer side-chain linkers. Arrows indicate the distance from the terminal β-Gal residue to the far end of the native ligand. Distances for the protein-binding site of CTx are taken from literature values.[18]

Fluorescence-linked sorbent assays were used to measure the inhibitory activity of the polymers. Briefly, microtitre plates were functionalised with GM1 ganglioside, which binds strongly to both lectins.[31] Fluorescein-labelled lectins (0.5 µM) were then incubated with a dilution series of the polymers for 30 minutes at 37 °C, and the unbound lectins were washed away. The total fluorescence was measured and inhibitory curves constructed. Data is presented as the minimum concentration required to inhibit 50 % binding of the lectin (MIC_{50}), Figure 2.3.
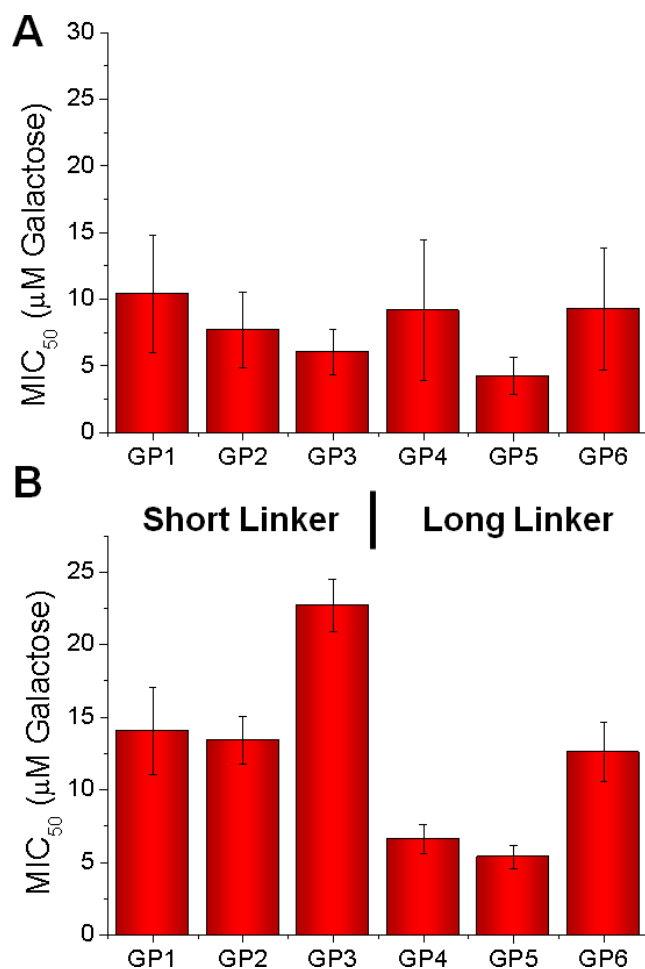
Figure 2.3: Inhibitory activity of glycopolymers GP1-GP6 with A) PNA and B) CTx. MIC_{50} values are expressed as total galactose concentration.

For PNA (Figure 2.3A), there was a very weak effect of polymer chain length on inhibitory activity, but the differences were not statistically significant. The inhibitory activity of all the polymers is greatly increased relative to monovalent galactose (*circa* 100-fold). Although there are many reports of longer polymers having increased association constants with lectins, we recently demonstrated that this does not necessarily translate into improved inhibitory activity, in agreement with the data presented herein (See Chapter 5).[32] Our previous work also showed that above a certain chain length, no improved inhibition (based on carbohydrate

concentration) was measured, as seen with the current results. For CTx inhibition (Figure 2.3B), there was a similarly weak dependence on polymer chain length, and no statistically significant differences were recorded. However, there was a significant decrease in the MIC_{50} values upon increasing the length of the linker. This result agrees with the hypothesis that the longer linker better mimics the native ligand, GM1. The use of a hydrophilic ethylene glycol linker allows us to rule out any hydrophobic interactions in the binding pocket. These carefully chosen conditions and the use of a control lectin (PNA) ensure that binding-pocket depth is the only parameter contributing to increased activity. Control experiments with an α-manno-polymer showed no inhibition in the concentration range tested (less than 100 μM carbohydrate), highlighting the specificity of the interaction.

Previous research has shown that a decrease in galactose density on the polymer backbone is accompanied by an increase in CTx inhibition.[18, 33] However, rigid α-helical polypeptide scaffolds were used, which cannot easily be reconfigured, and they also had a net-negative charge, which might promote electrostatic interactions. **P2** was functionalised with 10, 25, or 50 mol % of the longer linker (because of its higher binding affinity) followed by an excess of 3-aminopropanol to give variable density, and uncharged glycopolymers (**GP7–9**). Inhibition data are shown in Figure 2.4.
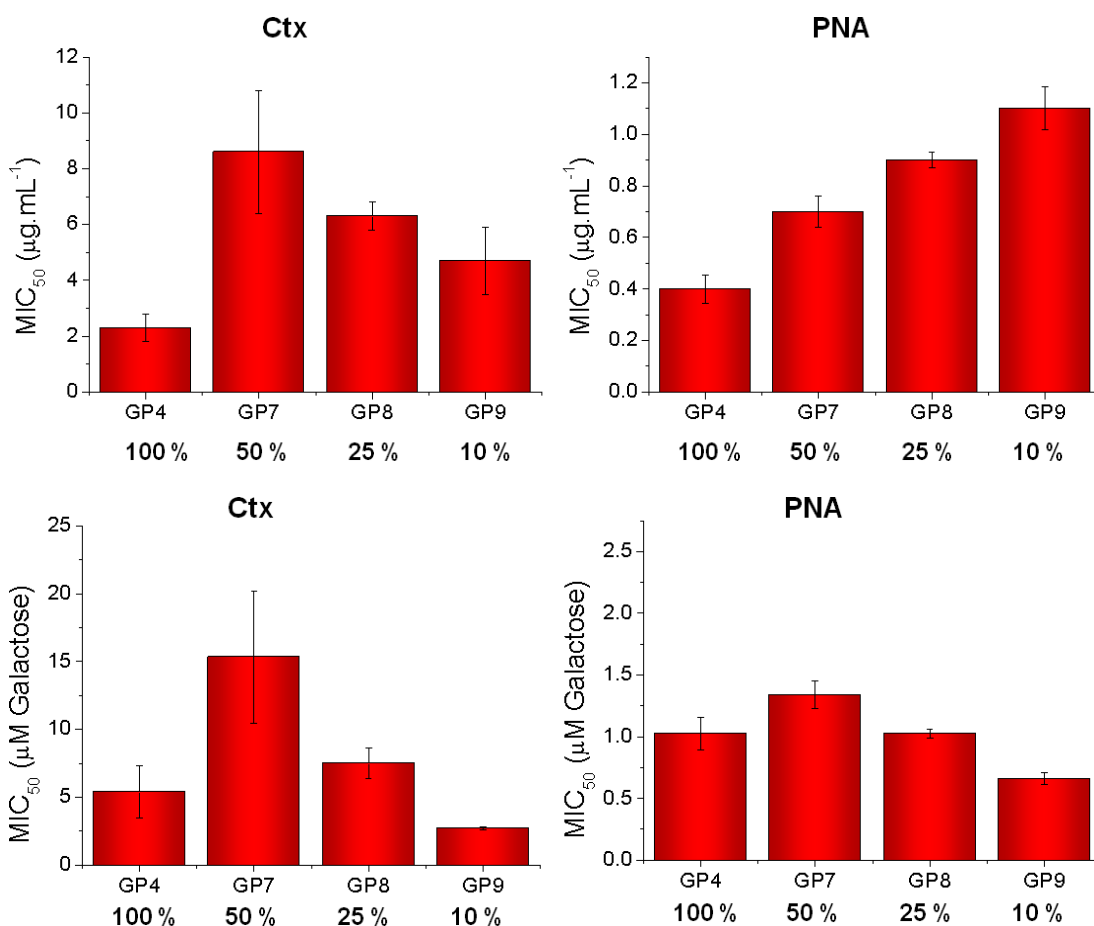
Figure 2.4: Inhibitory activity of variable density glycopolymers expressed in terms of A) polymer mass concentration and B) galactose concentration. Percentages on the x-axis indicate the percentage of repeat units on the polymer chain that have a galactose moiety.

Figure 2.4A shows inhibition data in terms of polymer mass concentration. For PNA, decreasing the saccharide density gives a concurrent increase in MIC_{50} (*i.e.* less activity), which can be interpreted as lower galactose densities leading to a relative decrease in binding affinity/inhibitory activity. For CTx, the 50 % functionalised polymer was the least active. However, this analysis is oversimplified, and it is necessary to consider the data in terms of relative activity per saccharide unit (Figure 2.4B). In this manner, the 10 % and 100 % functionalised polymers are the most active on a per-carbohydrate basis for both lectins, suggesting several features of the macromolecules contribute to inhibitory activity. The control

experiments with PNA, also showed a clear decrease in affinity as the galactose density decreased, implying that spanning of multiple sites is not the most important feature for inhibition. This result agrees with our previous findings using the Con A/mannose pairing that indicated the spanning of multiple sites contributed to higher association constants, but not to increased inhibition (Chapter 5).[32] A second component of this result could be steric hindrance of adjacent galactose residues; crowding may reduce rebinding of galactose into the deep binding pocket of CTx resulting in lower inhibitory activity for 50 % polymers compared to the 10 % functionalised polymers. These data fit with the hypothesis that the binding site in CTx limits accessibility, relative to the shallow binding site on PNA, for which the polymers with the highest valency showed highest inhibitory activity. The high activity (on a per-sugar basis) of the 100 % versus 50 % functionalised polymers would seem to contradict the above hypothesis. However, in this case the density of the 100 % functionalised polymers might be sufficiently high to overcome the limitations of steric crowding and benefit from a higher rate of statistical rebinding, or slower rate of dissociation.

2.4 Conclusion

In summary, a series of glycopolymers with varying saccharide density, linker length, and chain length were synthesised by tandem post-polymerisation modification. Longer linkers were shown to result in increased inhibition of CTxB, which is attributed to the depth of the binding pocket. Comparison with PNA, which has a shallower binding pocket, revealed no difference in inhibitory activity as a function of linker length. The tandem post-polymerisation modification strategy also allowed the effect of carbohydrate density to be studied. A nonlinear relationship

was measured, in which the highest and lowest density polymers tested (100 % and 10 %) were most active, on a per-sugar basis, highlighting the complexity of these interactions. These measurements demonstrate that in the design of biomimetic macromolecules for anti-adhesion or other therapeutic applications, structural biological information must be considered, in conjunction with using the relevant assays. Furthermore, the best polymer structure for a particular lectin is not necessarily the optimum structure for other lectins, even those with the same carbohydrate specificity.

2.5 Experimental

2.5.1 Materials

Tris-(benzyltriazolylmethyl)amine (TBTA) and pentafluorophenyl methacrylate (PFMA) was synthesised according to literature procedures.[27] *N,N,N',N',N''*-pentamethyldiethylenetriamine (PMDETA) was purchased from Sigma Aldrich, degassed and stored in an ampoule under a N_2 atmosphere. 1,2,3,4,6-Pentaacetyl galactose, hydrogen bromide (33 %) in acetic acid, sodium azide, pentafluorophenol and methacryloyl chloride were all obtained from Sigma-Aldrich and used as supplied. Pentaflurophenyl methacrylate was synthesised according to previously published procedures.[27] Peanut agglutinin and the B-sub unit of the cholera toxin were obtained from Sigma Aldrich and made into 0.1 mg.mL^{-1} solutions in HEPES buffer immediately before use. The HEPES buffer used, unless indicated, contained the following: 0.10 M HEPES, 0.15 M NaCl, 1 mM $MgCl_2$, 1 mM $CaCl_2$ and 1 mM $MnCl_2$, pH 7.4. Ultrahigh quality water with a resistance of 18.2 MΩ.cm (at 25 °C) was obtained from a Millipore Milli-Q gradient machine fitted with a 0.22 μm filter.

2.5.2 Physical and analytical methods

NMR spectra were recorded on Bruker DPX-300 and DPX-400 spectrometers for ^{1}H NMR (400 MHz) and ^{13}C NMR (125 MHz). Chemical shifts are reported in ppm relative to the deuterated solvent resonances and spectra analysed with WIN-NMR software. SEC (THF) was performed on a Varian 390-LC MDS system equipped with a PL-AS RT/MT autosampler, a PL-gel 3 μm (50 × 7.5 mm) guard column, two PL-gel 5 μm (300 × 7.5 mm) mixed-D columns equipped with a differential refractive index and a Shimadzu SPD-M20A diode array detector, using THF as the eluent with a flow rate of 1.0 mL min^{-1}. Narrow molecular weight PMMA standards (200 - 1.0 × 10^{6} g mol^{-1}) were used for calibration using a second order polynomial fit. GPC (DMF) was performed on a Varian 390-LC MDS system equipped with a PL-AS RT/MT autosampler, a PL-gel 3 μm (50 × 7.5 mm) guard column, two PL-gel 5 μm (300 × 7.5 mm) mixed-D columns equipped with a differential refractive index, using DMF (with 1 mg mL^{-1} LiBr) as the eluent with a flow rate of 1.0 mL min^{-1} at 50 °C. Narrow molecular weight PMMA standards (200 - 1.0 × 10^{6} g mol^{-1}) were used for calibration using a second order polynomial fit. SEC (aqueous) was performed on a Varian 390-LC MDS system equipped with a PL-AS RT/MT autosampler, a PL-aquagel-OH 8 μm (50 × 7.5 mm) guard column, a PLaquagel-OH column set consisting of two 8 μm (300 × 7.5 mm) columns equipped with a differential refractive index detector using phosphate buffer (pH 8.2) as the eluent at a flow rate of 1.0 mL min^{-1}. Narrow molecular weight PEO standards (100 - 1.26 × 10^{6} g mol^{-1}) were used for calibration using a second order polynomial fit. Infrared absorption spectra were recorded on a Bruker VECTOR-22 FTIR spectrometer using a Golden Gate diamond attenuated total reflection cell. Mass spectra were recorded

using a Micromass Autospec apparatus. Polymer-carbohydrate linker lengths were determined by assuming bond angle of 109.4° and bond lengths of 0.154 nm.

2.5.3 Synthetic procedures

Poly(pentafluorophenylmethacrylate), pPFMA: Ethyl 2-bromoisobutyrate (0.247 g, 1.27 mmol), pentafluorophenyl methacrylate (8.00 g, 31.7 mmol), Cu(I)Br (0.182 g, 1.27 mmol), mesitylene (1.14 g, 9.51 mmol) and toluene (16 mL) were added to an oven dried Schlenk tube and subjected to four freeze pump thaw cycles. PDMETA (0.40 mL, 1.9 mmol) was added to the solution via degassed syringe and the Schlenk tube immersed in and oil bath at 60 °C. Samples were taken periodically via degassed syringe for analysis by ^{1}H NMR and GPC. After 7 hours, the polymerisation was quenched by exposing the solution to air and bubbling for a further 4 hours. The solution was the diluted with toluene (200 mL) and passed through a column of neutral alumina to remove solids. The remaining solution was concentrated under reduced pressure and the final product isolated by precipitation into petroleum ether as an off-white solid.

M_n = 7800 g.mol^{-1}, PDi = 1.22 (THF SEC).; ^{1}H NMR (400 MHz, CDCl$_3$) δ$_{ppm}$: 1.53 (3H, CH$_3$), 2.53 (2H, CH$_2$); ^{13}C NMR (100 MHz, ^{1}H decoupled, CDCl$_3$) δ$_{ppm}$: 25.6 (CH$_3$), 45.36 (CH$_2$), 124.1 (C-O), 136.1 – 141.7 (C-F), 172.0 (C=O); IR (neat) $\tilde{v}$ = 3150 (C-H), 1786 (C=O active ester) cm^{-1}.

2-(2-(Prop-2-ynyloxy)ethoxy)ethanamine:

Tert-butyl 2-(2-(prop-2-ynyloxy)ethoxy)ethylcarbamate (1.58 g, 6.49 mmol) was dissolved in 50 mL of dichloromethane and TFA added (5 mL). The solution was

allowed to stir at room temperature for 24 h and the solvents removed under reduced pressure to yield the product as a viscous oil (0.874 g, 94 % yield).

^{1}H NMR (300 MHz, CDCl$_3$) δ = 4.18 (d, J = 2.3 Hz, 2H), 3.72 (t, J = 4.7 Hz, 2H), 3.70 - 3.66 (m, 4H), 3.15 (t, J = 4.7 Hz, 2H), 2.47 (t, J = 2.4 Hz, 1H); ^{13}C NMR (125 MHz, CDCl$_3$) δ = 79.3, 75.2, 70.2, 69.0, 66.8, 58.4, 39.6; IR (neat) ṽ = 3251, 2110, 1590, 1444, 1092 cm^{-1}; HRMS (ES+) calcd for C$_7$H$_{13}$NO$_2$ [M+ Na]$^+$ 166.0838, observed 166.084.

Synthesis of 1-Azido-1-deoxy-β-D-galactopyranoside

2,3,4,6,-tetra-*O*-acetyl-α-D-galactopyranosyl bromide: 1,2,3,4,6-Pentaacetyl galactose (40 g, 102.4 mmol) was dissolved in DCM (240 mL) To this, hydrogen bromide (33% in acetic acid, 200 mL) was added. The reaction mixture was stirred at room temperature and after 3 hours, T.L.C. (ethyl acetate/petroleum ether 1:2) indicated the formation of product (R$_f$ > 0.5) with complete consumption of the starting material (R$_f$ 0.5). The reaction mixture was partitioned between DCM (200 mL) and H$_2$O (200 mL) and the aqueous phase was re-extracted with DCM (2 x 100 mL). The combined organics were washed with a saturated sodium carbonate solution and the organic phase dried over magnesium sulphate, filtered and concentrated under vacuum to afford the product as a yellow oil (40.7 g, 99.3 mmol, 97 %).

^{1}H NMR (400 MHz, CDCl$_3$) δ = 1.95, 2.00, 2.05, 2.15 (4s, 4 × COCH$_3$), 4.05 (dd, 1H, J = 6.3 Hz, CH$_2$), 4.15 (dd, 1H, J = 6.5 Hz, CH$_2$), 4.45 (dd, 1H, J = 6.7 Hz, CH), 5.00 (dd, 1H, J_1 = 10.5 Hz J_2 = 4 Hz, CH), 5.35 (dd, 1H, J_1 = 10.7 Hz J_2 = 3.4 Hz, CH), 5.50 (dd, 1H, J_1 = 11.3 Hz J_2 = 3.5 Hz, CH) 6.65 (d, 1H J = 4 Hz, CH); ^{13}C NMR (125 MHz, CDCl$_3$) δ = 20.6, 20.6, 20.7, 20.8 (4s, 4 × COCH$_3$), 60.8 (s, 1C,

CH$_2$ C-6), 67.0 (s, 1C, CH, C-4), 67.8 (s, 1C, CH, C-2), 68.0 (s, 1C, CH, C-3), 71.1 (s, 1C, CH, C-5), 88.2 (s, 1C CH, C-1), 169.8, 169.9, 170.1, 170.3 (4s, 4 × COCH$_3$).

2,3,4,6,-tetra-*O*-acetyl-β-D-galactopyranosyl azide: To 2,3,4,6,-tetra-*O*-acetyl-α-D-galactopyranosyl bromide (20.18 g, 49.2 mmol, 1 eq.), Bu$_4$NHSO$_4$ (16.7 g, 49.2 mmol, 1 eq.), NaN$_3$ (16.0 g, 246 mmol, 5 eq.) in DCM (200 mL) and saturated aqueous NaHCO$_3$ (200 mL) was added. The biphasic solution was allowed to stir vigorously at room temperature for 16 hours. T.L.C. (1:2 ethyl acetate : petroleum ether) of the solution showed complete consumption of the starting material and the reaction mixture was extracted with ethyl acetate and the organic phase was washed successively with NaHCO$_3$. The organic layer was dried over anhydrous MgSO$_4$, filtered and the solvent removed to afford 2,3,4,6-tetra-*O*-acetyl-β-D-galactopyranosyl azide as a white powder (12.78 g, 34.5 mmol, 70%).

^{1}H NMR (400 MHz, CDCl$_3$) δ = 2.00, 2.05, 2.10, 2.20 (4s 4 × COCH$_3$), 4.00 (m, 1H, CH), 4.10-4.25 (m, 2H, CH$_2$ and CH), 4.60 (d, 1H, *J* = 8.8 Hz, CH, H-1), 5.05 (dd, 1H, *J* = 3.3 Hz CH), 5.15 (dd, 1H, *J* = 8.5 Hz CH) 5.45 (dd, 1H *J$_1$* = 1.4 Hz *J$_2$* = 3.4 Hz, CH); ^{13}C NMR (125 MHz, CDCl$_3$) δ = 20.52, 20.61, 20.67, (4s, 4 × COCH$_3$), 61.23, (s, 1C, CH$_2$, C-6), 66.86 (s, 1C, CH, C-4), 68.06 (1C, CH, C-2), 70.73 (s, 1C, CH, C-3), 72.87 (s, 1C, CH, C-5), 88.30, (s, 1C, CH, C-1), 169.37, 169.99, 190.12, 120.37 (4s, 4 × COCH$_3$).

1-Azido-1-deoxy-β-D-galactopyranoside: To a solution of 2,3,4,6-tetra-O-acetyl-β-D-galactopyranosyl azide (12.78g, 34.5 mmol) in methanol (120 mL), sodium methoxide (3 mL) was added. The resulting mixture was stirred at room temperature overnight. This solution was neutralised with Amberlite IR-120H$^+$ and the ion

exchange resin removed by filtration. The solvent was evaporated under vacuum to afford a yellow oil which crystallised to the product (6.18 g, 30.1 mmol, 88 %).

^{1}H NMR (400 MHz, CDCl$_3$) δ = 3.35 (1H, dd, CH, J_1 = 9.8 Hz J_2 = 3.4 Hz, H-2), 3.50 (1H, dd, CH, J_1 = 9.9 Hz J_2 = 3.4 Hz, H-3), 3.60 - 3.70 (3H, m, CH$_2$ and CH, H$_{6a}$, H$_{6b}$, H-5), 3.80 (1H, d, CH, J = 3.3 Hz H-4), 4.50 (1H, d, CH, J = 8.5, H-1);

^{13}C NMR (125 MHz, CDCl$_3$) δ = 60.94, (s, 1C, CH$_2$, C-6), 68.51 (s, 1C, CH, C-4), 70.32 (s, 1C, CH, C-2), 72.65 (s, 1C, CH, C-3), 77.20 (s, 1C, CH, C-5), 90.54, (s, 1C, CH, C-1).

Functionalisation of pPFMA with amino-functional alkynes:

Poly(pentafluorophenyl methacrylate) (100 mg, 0.39 mmol PFP), alkyne linker (propargyl amine or 2-[2-(prop-2-ynyloxy)ethoxy]ethanamine (varying amounts)), and TEA (80 mg, 0.79 mmol) in DMF (5 mL) were stirred at 50 °C for 16 h. After this time, a three molar excess (relative to PFP groups) of 3-aminopropanol was added, when copolymers were desired, and stirred for a further 16 h at 50 °C. The solution was twice precipitated into diethyl ether, then centrifuged and dried under vacuum to afford the alkynyl-functionalised polymers.

Alkyne 1: ^{1}H NMR (400 MHz, MeOD): δ = 1.2 (CH$_3$ backbone), 1.8 (CH$_2$ backbone), 3.2 (C≡CH), 4.4 ppm (s, NH-CH$_2$) ; IR : ṽ =1650 cm^{-1} (amide C=O).

Alkyne 2: ^{1}H NMR (400 MHz, MeOD): δ = 1.2 (CH$_3$ backbone), 1.8 (CH$_2$ backbone), 3.1 (CH$_2$), 3.2 (C≡CH), 3.5 (CH$_2$), 3.7 (CH$_2$), 4.2 ppm (s, NH-CH$_2$); IR: ṽ = 1720 cm^{-1} (CO$_2$H), 1650 cm^{-1} (amide C=O).

Copper-catalysed [3+2] cycloaddition of GalN$_3$ with alkyne-functionalised polymers: Alkynyl functionalised polymer (20 mg, 0.18 mmol), 1-azido-β-D-galactose (80 mg, 0.36 mmol), TEA (10 mg, 0.072 mmol), and CuBr (2 mg, 0.014

mmol) dissolved in [D_6]-DMSO (4 mL) were charged in an ampoule and deoxygenated through three freeze–pump–thaw cycles before being placed under nitrogen. TBTA (8 mg, 0.015 mmol) was added and the reaction was degassed and left under nitrogen for 48 h. The glycopolymer was purified by dialysis against water using 1000 Da MWCO tubing and freeze-dried. **GP1**: ^{1}H NMR (400 MHz, MeOD): δ = 1.2 (CH_3 backbone), 1.8 (CH_2 backbone), 4.4 (s, NH-CH_2), 3.4–3.5 (2 H, H-2 + H-3), 3.60–3.80 (3 H, CH_2 and CH, H-6a, H-6b, H-5, H-4), 4.7 ppm (1H, H-1); IR $\tilde{v}$ = 3100–3300 cm^{-1} (OH), 3050 cm^{-1} (C-H), 1650 cm^{-1} (amide C=O); SEC (DMF): M_n = 5100 g.mol^{-1}, M_w / M_n = 1.29.

2.5.4 Inhibitory assays

Fluorescence-linked sorbent assay for inhibitory activity: 96-Well microtitre plates were incubated for 16 hr with 180 μL of 100 mg.mL^{-1} GM-1 ganglioside dissolved in phosphate-buffered saline (PBS), per well. Unattached GM-1 was removed by washing extensively with PBS. Polymer solutions were made up as serial dilutions in HEPES from 100 μg.mL^{-1}. 20 μL of 0.3 mg.mL^{-1} PNA-FITC in HEPES was added to 80 μL of each polymer solution to result in 0.5 μM PNA-FITC. 100 μL of the polymer PNA-FITC solutions were added to the GM-1 surfaces and incubated at 37 °C for 30 mins. Fluorescence was then measured at excitation/emission wavelengths of 485/528 nm. All experiments were carried out in triplicate. Percentage inhibition was compared to relative to controls of pure PNA-FITC (with no polymer). Identical procedures were used using the cholera toxin B-subunit, with a final concentration of 0.5 μM used. Non-linear regression analysis was carried out in Origin.

2.6 References

1. C. R. Bertozzi and L. L. Kiessling, *Science*, 2001, **291**, 2357-2364.

2. M. Ambrosi, N. R. Cameron and B. G. Davis, *Org. Bio. Chem.*, 2005, **3**, 1593-1608.

3. H. Feinberg, D. A. Mitchell, K. Drickamer and W. I. Weis, *Science*, 2001, **294**, 2163-2166.

4. Y. C. Lee, R. R. Townsend, M. R. Hardy, J. Lonngren, J. Arnarp, M. Haraldsson and H. Lonn, *J. Biol. Chem.*, 1983, **258**, 199-202.

5. N. Vinson, Y. Gou, C. R. Becer, D. M. Haddleton and M. I. Gibson, *Polym. Chem.*, 2011, **2**, 107-113.

6. S. G. Spain, M. I. Gibson and N. R. Cameron, *J. Polym. Sci. A Polym. Chem.*, 2007, **45**, 2059-2072.

7. J. J. Lundquist and E. J. Toone, *Chem. Rev.*, 2002, **102**, 555-578.

8. C. W. Cairo, J. E. Gestwicki, M. Kanai and L. L. Kiessling, *J. Am. Chem. Soc.*, 2002, **124**, 1615-1619.

9. M. I. Gibson, C. A. Barker, S. G. Spain, L. Albertin and N. R. Cameron, *Biomacromolecules*, 2009, **10**, 328-333.

10. R. J. Pieters, *Org. Biomol. Chem.*, 2009, **7**, 2013-2025.

11. G. Mulvey, P. I. Kitov, P. Marcato, D. R. Bundle and G. D. Armstrong, *Biochimie*, 2001, **83**, 841-847.

12. R. M. Hyland, T. P. Griener, G. L. Mulvey, P. I. Kitov, O. P. Srivastava, P. Marcato and G. D. Armstrong, *J. Med. Microbiol.*, 2006, **55**, 669-675.

13. A. Imberty, Y. M. Chabre and R. Roy, *Chem. Eur. J.*, 2008, **14**, 7490-7499.

14. S. G. Spain and N. R. Cameron, *Polym. Chem.*, 2011, **2**, 60-68.

15. M. Fais, R. Karamanska, S. Allman, S. A. Fairhurst, P. Innocenti, A. J. Fairbanks, T. J. Donohoe, B. G. Davis, D. A. Russell and R. A. Field, *Chem. Sci.*, 2011, **2**, 1952-1959.

16. A. Bernardi and P. Cheshev, *Chem. Eur. J.*, 2008, **14**, 7434-7441.

17. P. I. Kitov, J. M. Sadowska, G. Mulvey, G. D. Armstrong, H. Ling, N. S. Pannu, R. J. Read and D. R. Bundle, *Nature*, 2000, **403**, 669-672.

18. B. D. Polizzotti and K. L. Kiick, *Biomacromolecules*, 2006, **7**, 483-490.

19. R. S. Kane, *Langmuir*, 2010, **26**, 8636-8640.

20. M. G. Baek and R. Roy, *Macromol. Biosci.*, 2001, **1**, 305-311.

21. M. Mammen, G. Dahmann and G. M. Whitesides, *J. Med. Chem.*, 1995, **38**, 4179-4190.

22. M. A. Gauthier, M. I. Gibson and H.-A. Klok, *Angew. Chem. Int. Ed.*, 2009, **48**, 48-58.

23. S. Slavin, J. Burns, D. M. Haddleton and C. R. Becer, *Eur. Polym. J.*, 2011, **47**, 435-446.

24. V. Ladmiral, G. Mantovani, G. J. Clarkson, S. Cauet, J. L. Irwin and D. M. Haddleton, *J. Am. Chem. Soc.*, 2006, **128**, 4823-4830.

25. C. R. Becer, M. I. Gibson, J. Geng, R. Ilyas, R. Wallis, D. A. Mitchell and D. M. Haddleton, *J. Am. Chem. Soc.*, 2010, **132**, 15130-15132.

26. N. K. Singha, M. I. Gibson, B. P. Koiry, M. Danial and H.-A. Klok, *Biomacromolecules*, 2011, **12**, 2908-2913.

27. M. I. Gibson, E. Froehlich and H.-A. Klok, *J. Polym. Sci. A Polym. Chem.*, 2009, **47**, 4332-4345.

28. E. A. Merritt, S. Sarfaty, F. Vandenakker, C. Lhoir, J. A. Martial and W. G. J. Hol, *Protein Sci.*, 1994, **3**, 166-175.

29. R. Ravishankar, M. Ravindran, K. Suguna, A. Surolia and M. Vijayan, *Curr. Sci.*, 1997, **72**, 855-861.

30. J. Kumar, L. McDowall, G. Chen and M. H. Stenzel, *Polym. Chem.*, 2011, **2**, 1879-1886.

31. D. A. Sack, S. Huda, P. K. B. Neogi, R. R. Daniel and W. M. Spira, *J. Clin. Microbiol.*, 1980, **11**, 35-40.

32. Y. Gou, S.-J. Richards, D. M. Haddleton and M. I. Gibson, *Polym. Chem.*, 2012, **3**, 1634-1640.

33. B. D. Polizzotti, R. Maheshwari, J. Vinkenborg and K. L. Kiick, *Macromolecules*, 2007, **40**, 7103-7110.

Chapter 3

Poly(azlactone)s: versatile scaffolds for tandem post-polymerisation modification and glycopolymer synthesis

M. W. Jones, **S-J. Richards**, D. M. Haddleton, M. I. Gibson, *Polym. Chem.* **2013**, *4*, 717

This chapter contains the paper that built on the findings from Chapter 2, in which was found that a longer linker is required for effective inhibition of the cholera toxin due to its relatively deep binding site. In this chapter a poly(azlactone) scaffold is used which leads to a linker of the correct length being formed in a one-pot reaction. This is a simpler method for the one-step synthesis of glycopolymer inhibitors compared to the two-step system used previously. The versatility of this technique is outlined in this chapter and the inhibitory activity against Con A and CTx were assessed using a fluorescent-linked sorbent assay.

Mathew Jones synthesised the polymers and I tested them for their inhibitory activity. I also helped with the manuscript preparation.

3.1 Abstract

The synthesis of polymers with latent reactivity suitable for 'click' type modifications in a tandem post-polymerisation modification process starting with poly(azlactone) precursors is investigated. Poly(azlactones), obtained by copper(I) mediated radical polymerisation, were functionalised in a one-pot process with amines bearing functional groups which are incompatible with controlled radical polymerisation: alkynes, alkenes, furfuryl and phenol. The reaction is quantitative and 100 % atom efficient presenting an efficient route to clickable scaffolds without the need for protecting group chemistry. Additionally, the poly(azlactones) were exploited to obtain synthetic glycopolymers. The ring opening procedure introduces a 5-atom spacer between glycan and backbone, which provides improved access to carbohydrate-binding proteins with deep binding pockets, such as the cholera toxin, for anti-adhesion applications.

3.2 Introduction

There are two conceptual methodologies for obtaining side-chain functionalised polymers. The first is direct polymerisation of functional monomers, which has been enabled by the advent of modern, tolerant, controlled polymerisation processes such as ring opening metathesis polymerisation (ROMP) and controlled radical polymerisation. Whilst this methodology is useful, there still remains the challenge of obtaining well-defined libraries of polymers with sequential modifications and identical degrees of polymerisation (DPs), particularly for exploring biological interactions, and even the most tolerant polymerisation methodologies also have some incompatibilities. To address this, the concept of post-polymerisation modification is frequently employed, whereby a reactive polymeric precursor is

directly functionalised ensuring all members of the library have identical DPs.[1] Highly efficient functionalisation strategies are essential for this, with those based on 'click' reactions proving to be the most useful. A key challenge associated with the synthesis of 'clickable' scaffolds is that the latent functionality (typically alkenes and alkynes) are incompatible with controlled radical polymerisations and require protection/deprotection chemistry which itself must be 100 % efficient.[2] To circumvent this, Singha *et al.* introduced the concept of tandem post-polymerisation modification whereby poly(pentafluorophenyl methacrylate), with an activated ester side-chain is first modified by allyl (or propargyl) amine with high efficiency, generating a reactive scaffold with variable side chain density.[3] This has been exploited to generate polypeptide hybrid materials and also to probe the affinity of multivalent galactosides for the toxin secreted by *Vibrio cholerae* (See Chapter 2).[4] Advantages of active ester-type monomers are their easy accessibility, and the use of amines as functionalisation moieties that are commercially available. Activated esters of *N*-hydroxysuccinimide,[5] pentafluorophenol,[6, 7] and 4-nitrophenol have been exploited for the introduction of functionality to polymers with nucleophilic groups such as amines and alcohols.[6, 8] Synthetic glycopolymers, with side-chain carbohydrate moieties have been prepared by post-polymerisation modification by both 'click' and active ester type reactions.[2, 8, 9] This allows for the side chain composition to be varied while ensuring identical DPs, which is required when studying multivalent glycosides due to the cluster glycoside effect: multivalent presentation of carbohydrates results in an increase in avidity greater than the linear sum of the individual carbohydrates. In order to understand carbohydrate–protein interactions it is therefore important to control every aspect of the macromolecular architecture[8, 10, 11] with the aim of obtaining highly active anti-adhesion therapies.[12]

The post-modification techniques described above have proven to be successful, but still suffer from very low atom efficiency (either due to displacement reactions or protecting group removal) as well as side reactions and competitive hydrolysis which can impede this approach.[7, 13] Alkenyl azlactones[14] such as 2-vinyl-4,4-dimethylazlactone (VDMA) (1) are particularly interesting as an alternative to activated esters due to the electrophilic nature of the ring, which readily undergoes ring opening in the presence of nucleophiles such as primary amines, alcohols and thiols.[15, 16] Early reports of VDMA-based polymers were centered on their synthesis *via* free radical polymerisation although advances in controlled radical polymerisation (CRP) techniques such as nitroxide-mediated polymerisation (NMP),[17] atom transfer polymerisation (ATRP)[18, 19] and reversible-addition–fragmentation chain transfer (RAFT)[20] polymerisation have enabled the synthesis of well-defined polymers with predetermined molecular weights. The first report of the controlled polymerisation (NMP) of VDMA was by Tully *et al.*,[21] with high conversions and narrow molecular weight distributions achieved in homo- and co-polymerisations with a number of co-monomers. ATRP of VDMA was first described by Fontaine *et al.*,[22] and used to prepare well-defined pVDMA solid supports which proved effective primary amine scavengers from solution. The polymerisation of VDMA by RAFT has been investigated by Kilbey *et al.*[23] and Fontaine *et al.*[24] with these polymers readily crosslinked with diamines to yield stable nanoparticles.[25] The reactivity of azlactones has been widely explored by Lynn and Buck for a wide range of applications.[26] Exploiting the "spring-loaded" reactivity of pVDMA has enabled the ready synthesis of thin films using a layer-by-layer assembly approach[27, 28] in order to synthesise hollow microcapsules,[29] super hydrophobic surfaces[30] and to modify hair and cellulose.[31] The pVDMA scaffold

also presents a robust platform for the introduction of multiple amino functionalities to the same polymer on a one- pot system.[32, 33] A recent report by Fournier *et al.* describes the modification of azlactone-functional styrenic copolymers synthesised by RAFT. A range of commercially available functional amines were employed to introduce diverse functionality to the polymer chains.[34] RAFT has also been employed by Fontaine *et al.* as a route to end-functional polymers where an azlactone functional RAFT agent was employed for the chain end modification of polymers with functional amines.[35]

The aim of this current work was to probe the use of pVDMA scaffolds as reactive precursors for direct and tandem post-polymerisation modification as an alternative to traditional scaffolds. In particular, these scaffolds are investigated for the preparation of synthetic glycopolymers as novel anti-adhesion therapies against pathogenic toxins.

3.3 Results and Discussion

The introduction of both alkyne- and alkene-functionalities to polymer backbones is highly desirable for subsequent functionalisation but the intrinsic reactivity of these functionalities towards radicals can hamper their direct utilisation under CRP conditions. A key aim of this work is using pVDMA as the reactive scaffold for tandem post-polymerisation modification procedures in a one-pot system.[1] The 100 % atom efficiency observed upon nucleophilic ring opening of the azlactone was also particularly desirable, since traditional approaches to these reactive scaffolds usually involve protecting groups or the loss of bulky groups in the case of activated esters. In order to quantify the efficiency of ring opening, our initial approach involved analysis of the ring opening of the azlactone ring using functional primary

amines. VDMA (1) was synthesised as described by Fontaine *et al.*[25] and used in a number of preliminary reactions with propargyl and allyl amine.

Equimolar quantities of propargylamine and allylamine were added to a solution of VDMA in toluene and stirred at ambient temperature overnight (Scheme 3.1). In both cases, precipitation of white crystalline solids was observed, and following isolation by filtration, analysis by ^{1}H and ^{13}C NMR, FT-IR and mass spectrometry confirmed the presence of the desired product in quantitative yield, with no observable side reactions (characterisation data is included in Appendix 2).
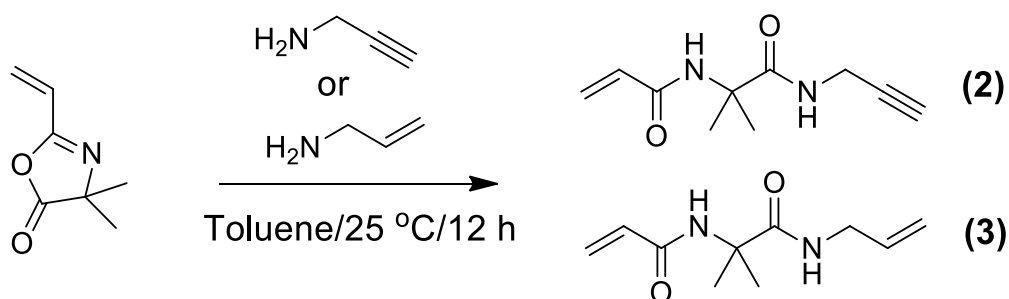
Scheme 3.1: Ring opening of VDMA with primary amines, propargyl amine and allyl amine at ambient temperature and in the absence of a catalyst.

Encouraged by the successful monomer functionalisation, pVDMA was obtained by polymerisation at 25 °C using the optimised conditions described by Fontaine *et al.*[22] Conversion was monitored by ^{1}H NMR and upon reaching 80 % conversion (140 minutes) the polymerisation was quenched by bubbling with air for 10 minutes. Pseudo-living characteristics were observed throughout the polymerisation, with a linear increase in molecular weight against conversion, 1st order kinetics and relatively narrow molecular weight distributions indicating a controlled radical polymerisation process, Figure 3.1 (Scheme 3.2).
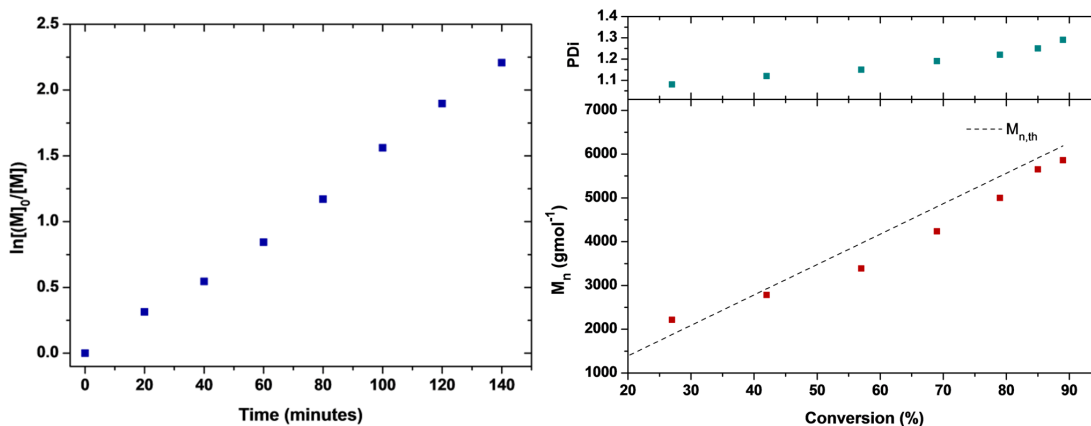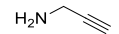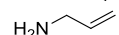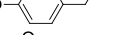
Figure 3.1: Kinetic and SEC analysis of the polymerisation of VDMA (left). Kinetic measurements determined by ^{1}H NMR by monitoring conversion of vinyl groups (right).
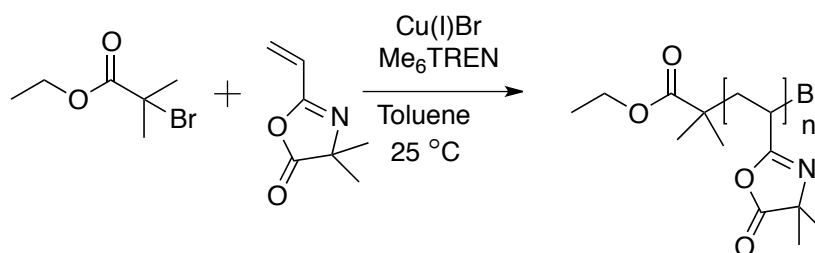
Scheme 3.2: Polymerisation of VDMA (1) by ATRP.

There was some increase in M_w/M_n at high conversions we do not believe this was due to chain transfer or crosslinking due to evidence shown in Figure 3.1. The observed values for M_n were greater than expected from the monomer : initiator feed ratio indicating non-quantitative initiator efficiency, or that the SEC solvent was non-ideal (Table 3.1).

Table 3.1: Initial polymer and those obtained by post-polymerisation modification.

Polymer	Conversion (%)	$M_{n(Theo)}$ (g.mol^{-1})	$M_{n(SEC)}$[e] (g.mol^{-1})	M_w/M_n[e]
pVDMA	89[a]	6280[c]	3500	1.32
Post Modifications				
+ H_2N—propargyl	> 95[b]	8760[d]	12500	1.20
+ H_2N—allyl	> 95[b]	8850[d]	12800	1.15
+ HO—C$_6$H$_4$—CH$_2$CH$_2$—NH$_2$	> 95[b]	12500[d]	11700	1.28
+ furfurylamine (furan—CH$_2$NH$_2$)	> 95[b]	10660[d]	10200	1.35

[a] Conversion of monomer into polymer, determined by ^{1}H NMR; [b] Conversion of VDMA units into ring-opened form. Estimated by ^{1}H NMR and IR; [c] Determined from the [monomer]:[initiator] feed ratio and conversion; [d] Determined from the theoretical molecular weight of the precursor pVDMA and the degree of incorporation of amine side chains; [e] Determined by SEC in DMF against PMMA standards.

The direct one-pot functionalisation of the synthesised pVDMA was investigated with a range of commercially available amines bearing functional groups not compatible with CRP techniques. Allylamine and propargylamine, were investigated for the synthesis of poly(alkyne) and poly(alkene) homo-polymers derived from the same pre-scaffold. These functionalities are desired for further post-polymerisation modification *via* 'thiol–ene' and 'alkyne–azide' click-type reactions. The amines were added to the crude polymer solution (1.5 eq. of amine relative to azlactone), along with DMSO in order to fully solubilise the obtained polymers and left to stir overnight at room temperature, in the absence of any added catalysts (Table 3.1). Each solution was then diluted and twice precipitated into ethyl acetate to yield white solids. ^{1}H NMR analysis of the obtained polymers revealed complete consumption of the signals corresponding to pVDMA, with the appearance of broad signals derived from both alkene and alkyne functionalities in each case. SEC analysis (Figure 3.2) of the obtained polymers showed the expected increase in

molecular weight following ring opening. Infrared (IR) spectroscopy (Figure 3.3) also confirmed complete functionalisation of the pre-scaffold, with no trace of the azlactone cyclic ester and a strong signal from the two amide groups generated upon ring opening. (Additional characterisation in Appendix 2).
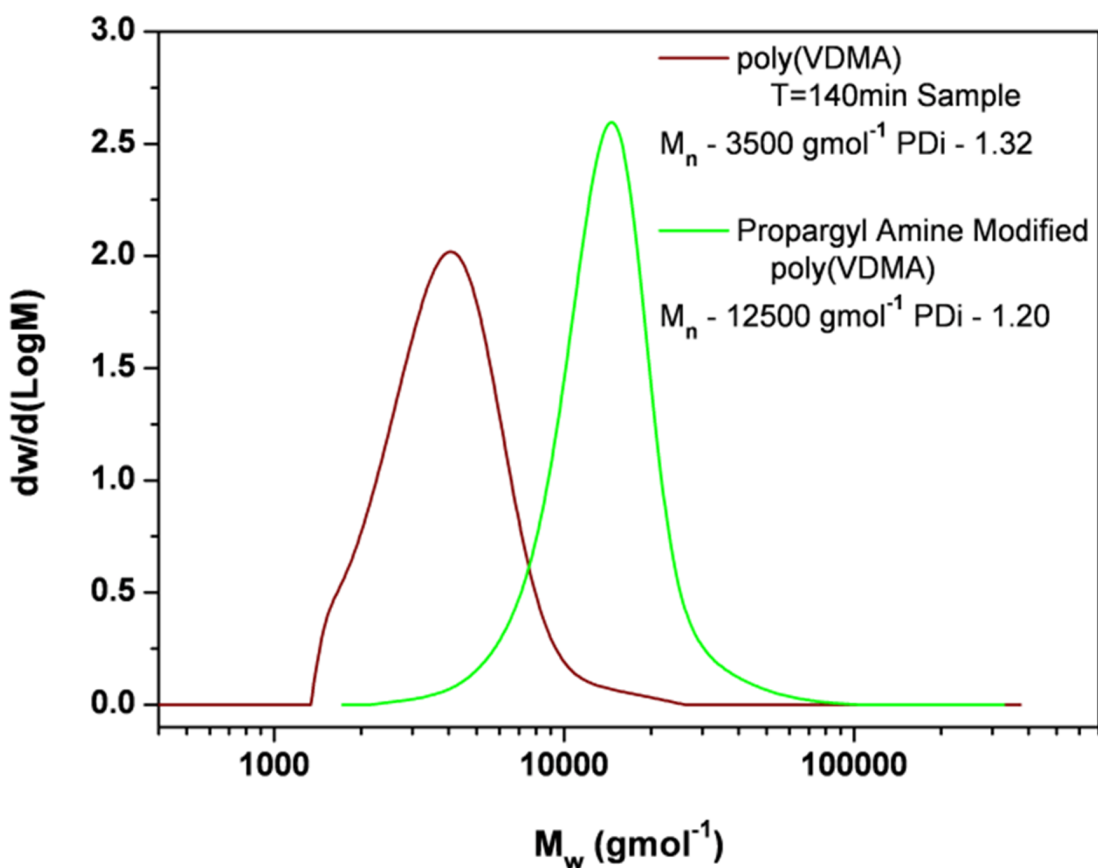
Figure 3.2: SEC analysis of pVDMA before (red) and after (green) modification with propargylamine.
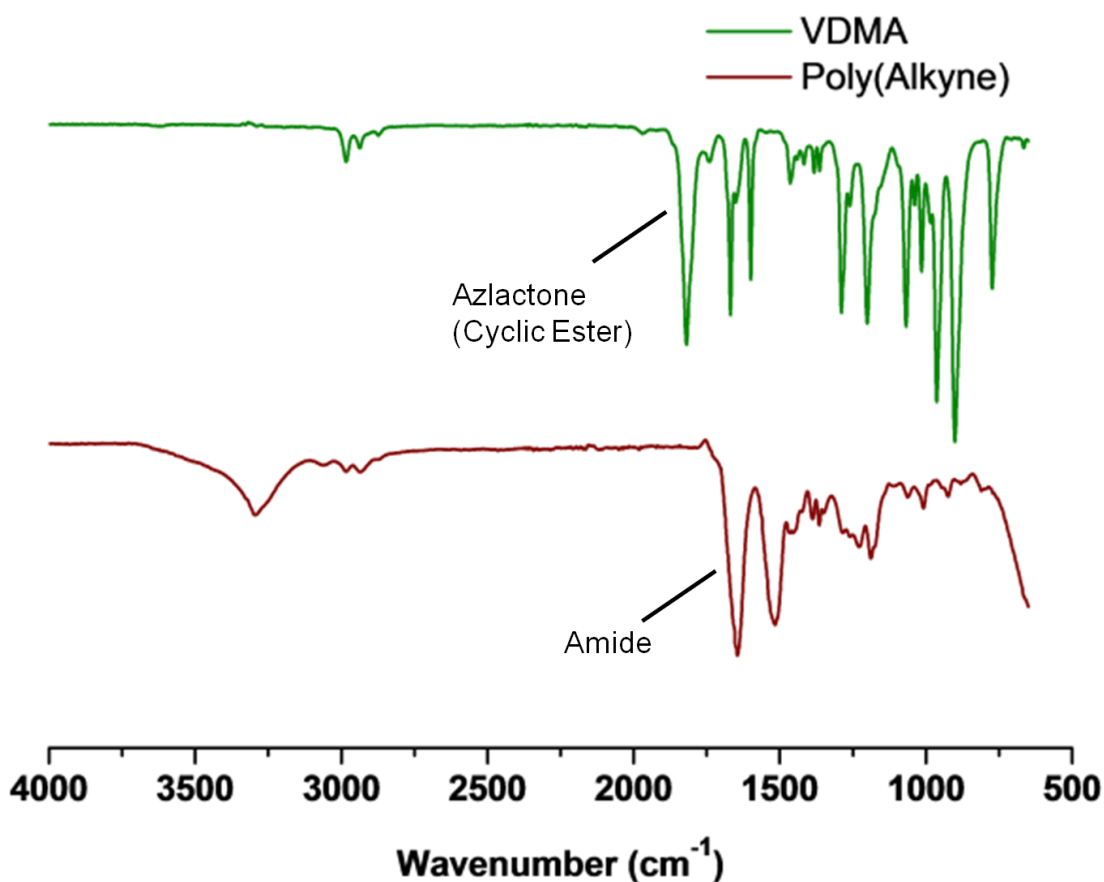
Figure 3.3: Infrared analysis of post-polymerisation modification of pVDMA (green) and after addition of propargylamine (red).

Following the successful synthesis of alkene- and alkyne- functional homopolymers, this one-pot approach was used to introduce additional functionality that is often not compatible with radical polymerisation (Table 3.1). Phenols are commonly used as radical polymerisation inhibitors although they have been shown to enhance the rate of ATRP[36] and SET-LRP.[37] The direct synthesis of poly(phenols) can however be problematic and they are usually synthesised by deprotection of masked phenolic functionalities such as acetoxystyrene following polymerisation.[38,39] As above, pVDMA was obtained and upon reaching 80 % conversion, the polymerisation was quenched and a solution of tyramine in DMSO added. Following isolation complete disappearance of the original signal for the azlactone ring was observed by IR spectroscopy, with the formation of the new amide signal,

confirming quantitative ring opening. SEC analysis of the purified polymer revealed the expected mass increase upon modification of the pre-polymer with formation of a well-defined product. ^{1}H NMR also supported the formation of the desired polymers (Appendix 2).

We were also interested in the introduction of other functionalities, namely furan groups, since these are commonly employed in Diels–Alder reactions and may yield materials with reversible crosslinking capabilities.[40] As previously, the quenched crude polymerisation solution of pVDMA was added to furfurylamine in DMSO and allowed to stir at room temperature overnight. Following isolation, IR analysis of the resulting polymer showed, as expected, complete disappearance of the original ester derived from pVDMA, as well as formation of the newly generated amide groups. SEC analysis showed the expected mass increase upon modification of the scaffold, with a well-defined polymer observed. The above results demonstrate that pVDMA is an excellent scaffold for tandem-post-polymerisation modification as an alternative to either active ester precursor polymers, or the direct polymerisation of protected alkyne/alkenes.

3.3.1 Glycopolymer Synthesis and Inhibitory Activity

Encouraged by the quantitative conversion observed using relatively unhindered amines, the pVDMA scaffold was subsequently investigated for the one-pot synthesis of glycopolymers. Synthetic glycopolymers have been demonstrated to be useful in anti-adhesion therapies, but in order to fully understand the cluster glycoside effect sequentially modified glycopolymers with identical valencies (DPs) are required.[4, 41, 42] Additionally, we have demonstrated that increasing the separation between polymer backbone and carbohydrate can specifically increase the inhibitory

activity of β-D-galactose functional polymers against the cholera toxin (CTx), owing to its deep carbohydrate binding pocket,[43] while not affecting its avidity for other galactose-binding lectins.[4] Upon ring opening of a VDMA unit, a longer spacer is generated (5 atoms) compared to direct substitution of an activated ester which only gives 2 carbon atoms,[7] and therefore pVDMA offers a practical route to obtain these potent multivalent inhibitors. To probe this, VDMA was polymerised using identical conditions as described above, and upon quenching the solution was split into three portions. To each of the portions, solutions of 2-deoxy, 2-amino- gluco-/manno-/galacto-pyranoside hydrochloride salts in DMSO with triethylamine were added and the mixtures allowed to stir at room temperature for 16 hours. Each solution was subsequently diluted with 1 : 1 H_2O–methanol and dialysed against the same mixture for 3 days. Removal of the solvent by lyophilisation yielded each product as a white powder, Figure 3.4 (Scheme 3.3).
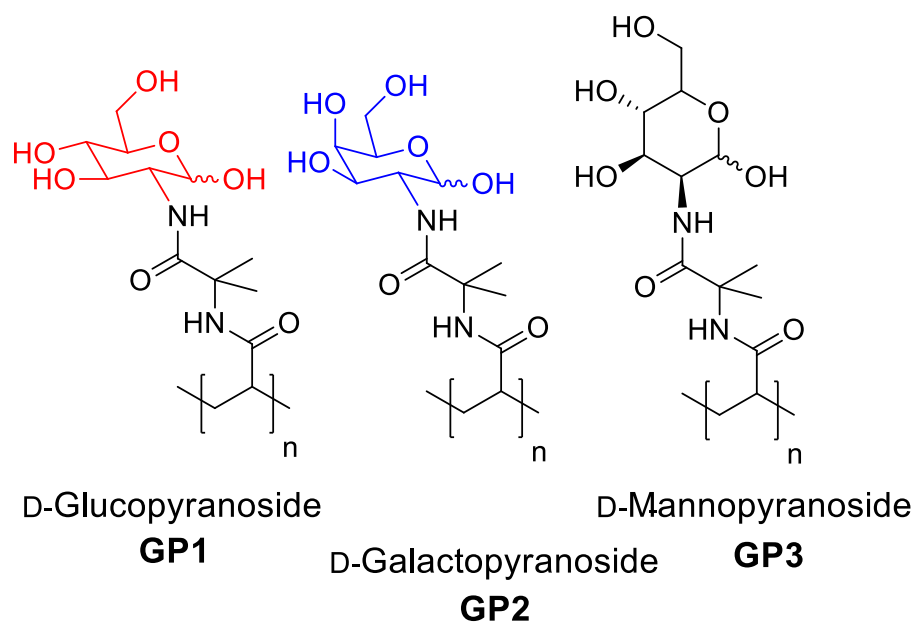
Scheme 3.3: Glycopolymers obtained by post-polymerisation modification of pVDMA with 2-aminoglycosides.
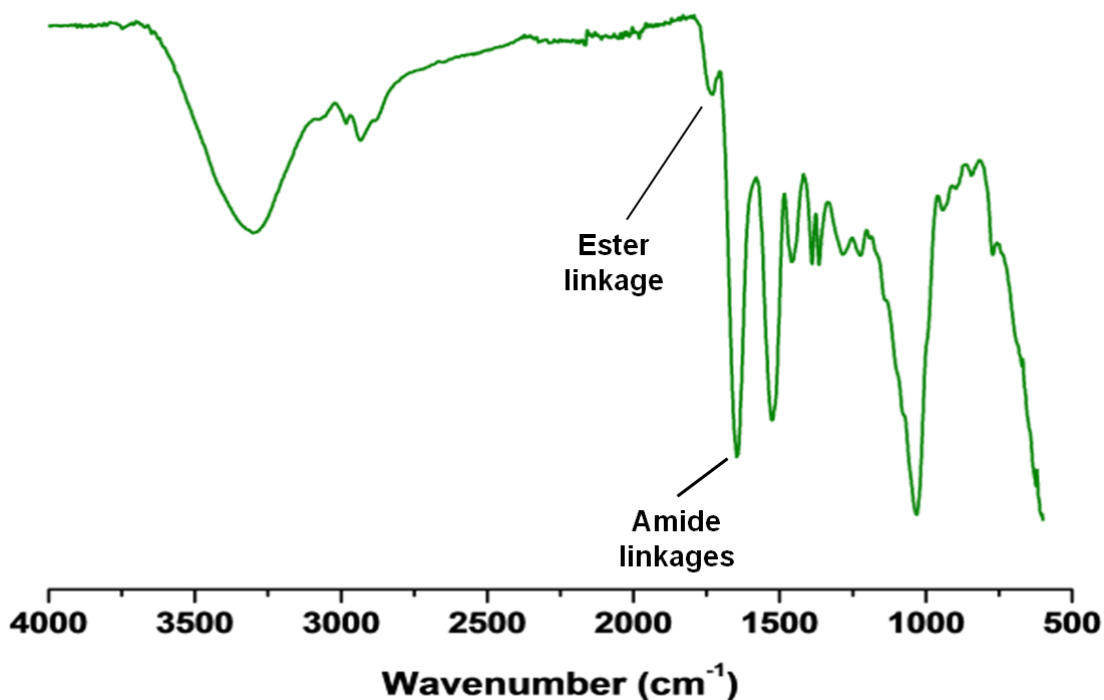
Figure 3.4: Infrared spectrum of 2-deoxy, 2-amino-mannopyranoside modified pVDMA. Assignments of carbonyl vibrations as described in the main text are indicated.

Aqueous SEC indicated well defined polymers were obtained in each case, with monomodal distributions. This would seem to rule out crosslinking side-reactions, but pVDMA is known to react with alcohols. Analysis of the glycopolymers by IR revealed complete disappearance of the signal corresponding to the original azlactone ring, with the expected appearance of the amide signals derived from ring opening with the amino functionality of the saccharides (Figure 3.4). In each case however, a smaller carboxyl signal was also observed (ca. 1730 cm^{-1}), and was postulated to be either a product of ring hydrolysis or ester formation following ring opening with the sugar hydroxyl groups. In order to identify the secondary signals, pVDMA was subjected to ring opening in the presence of sodium hydroxide as well as ring opening by methanol in the presence of DBU as a catalyst. Following ring opening at 50 °C overnight, the solutions were dialysed against water

for 3 days and lyophilised. IR analysis of the obtained polymers confirmed that alcohol ring opening of the azlactone ring was the source of the second carbonylic signal, due to the similarity of the signal obtained to that from ring opening with methanol (Appendix 2). The ring opening of azlactone rings with alcohols is well established[44] but since monomodal, relatively well defined polymers were obtained, intermolecular crosslinking of chains is expected to be minimal and the ester signals are expected to be derived from intramolecular reactions with adjacent sugar moieties.

With this panel of glycopolymers obtained, their biological activity was assessed using fluorescence-linked inhibitory assays. Inhibitory assays are predictive of the ability of the glycopolymers to function as anti-adhesives, as opposed to the extremely limited turbidimetry methodologies that give limited information[45] and require large quantities of lectins (not typically possible for medically relevant proteins). Briefly, the surface of microtitre plates was functionalised with an appropriate carbohydrate and the corresponding fluorescently labelled lectin was added with various concentrations of the glycopolymers. The minimum concentration required to inhibit 50 % of the lectin binding (MIC_{50}) was determined by fluorescent measurements. Concanavalin A (Con A) which binds gluco- and manno-pyranoside terminal carbohydrates and the B-subunit of CTx (CTxB), which binds β-D-galactopyranoside residues were used in these assays. An example inhibitory curve for Con A by the glucose-functional polymer and CTx by galactose-functional polymer are shown in Figure 3.5, and the values obtained in Table 3.2.
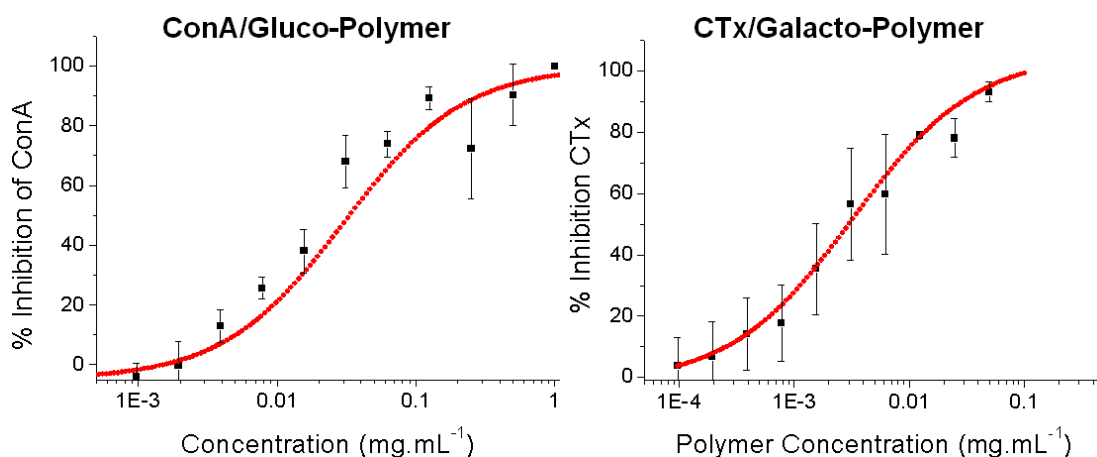
Figure 3.5: Inhibition of Con A binding to mannan-functional surface by glucose-containing glycopolymer (left) and of cholera toxin (CTx) to GM1 by galactose-containing glycopolymer (right). Values shown are average of 3 measurements. Red line is line of best fit.

Table 3.2: Inhibitory potency of synthetic glycopolymers.

Polymer[a]	Lectin	MIC_{50} (μg.mL^{-1})[b]
Galactose (**GP2**)	Cholera Toxin B subunit	3.2 ± 0.3
Glucose (**GP1**)	Concanavalin A	19.7 ± 0.37
Mannose (**GP3**)	Concanavalin A	$0.51 + 0.07$

[a] Refers to the side chain functionality of the polymer. [b] Minimum concentration of polymer required to inhibit 50 % of the lectin from binding to a surface-immobilised carbohydrate.

All the polymers tested had sub 20 μg mL^{-1} MIC_{50} values indicating their high affinity due to the cluster glycoside effect. The mannose-functional polymer was 40 times more potent than the glucose polymer indicating Con A's preference for manno- versus gluco-units. The galactose functional polymer displayed significant activity against the CTx comparable to other polymers we have used,[4] but was obtained in a far simpler fashion. Such inhibitors may find application as non-antibiotic prophylactic treatments.[12] Mismatched glycopolymer lectin pairs (*i.e.* with the wrong carbohydrate) displayed no appreciable inhibition in the concentration ranges tested.

3.4 Conclusions

In summary, we have demonstrated the use of poly(azlactone)s as versatile scaffolds for both direct, and tandem, post-polymerisation modification. In particular, the 100 % atom efficiency and the ability to conduct polymerisation and functionalisation in a one-pot, two-step process is highlighted. Vinyl, alkyne, phenol and furanyl side chain polymers were obtained in quantitative yield, which is not possible by direct radical polymerisation of the functional monomers.

Secondly, a series of synthetic glycopolymers with 5-atom spacers between carbohydrate and backbone were obtained by direct post-polymerisation modification of the poly(azlactone) scaffold. The glycopolymers inhibitory activity was measured to demonstrate they retained their lectin-specificity. Due to the increased linker length, poly(galactose) functional polymers were demonstrated to be particularly active against CTx, and hence the polymers' potential as prophylactic anti-adhesion therapies has been demonstrated.

3.5 Experimental

3.5.1 Materials

2-Aminoisobutyric acid, acryloyl chloride, sodium hydroxide, ethyl chloroformate, copper(I) bromide, ethyl-2-bromoisobutyrate, propargyl amine, allylamine, tyramine, furfuryl amine, glucosamine hydrochloride, mannosamine hydrochloride, galactosamine hydrochloride, triethylamine and diazabicyclo[5.4.0]undec-7-ene (DBU) were all purchased from Sigma Aldrich and used as received. Me_6TREN was synthesised as described by Percec et al.[46]

3.5.2 Physical and analytical methods

^{1}H and ^{13}C NMR spectra were recorded on Bruker DPX-300 and DPX-400 spectrometers using deuterated solvents obtained from Sigma Aldrich. Chloroform SEC was performed on a Varian 390-LC MDS system equipped with a PL-AS RT/MT auto- sampler, a PL-gel 3 mm (50 x 7.5 mm) guard column, two PL-gel 5 mm (300 x 7.5 mm) mixed-D columns equipped with a differential refractive index detector, using CHCl3 as the eluent with a flow rate of 1.0 mL min^{-1}. Narrow molecular weight PMMA standards (200–1.0 106 g.mol^{-1}) were used for calibration using a second order polynomial fit. DMF SEC was performed on a Varian 390-LC MDS system equipped with a PL-AS RT/MT autosampler, a PL-gel 3 mm (50 x 7.5 mm) guard column, two PL-gel 5 mm (300 x 7.5 mm) mixed-D columns using DMF with 0.1% LiBr at 50 °C as the eluent at a flow rate of 1.0 mL min^{-1}. The SEC system was equipped with ultraviolet (UV) (set at 280 nm) and differential refractive index (DRI) detectors. Narrow molecular weight PMMA standards (200–1.0 x 106 g.mol^{-1}) were used for calibration using a second order polynomial fit. Infrared absorption spectra were recorded on a Bruker VECTOR-22 FTIR spectrometer using a Golden Gate diamond attenuated total reflection cell.

3.5.3 Synthetic procedures

VDMA (**1**) was synthesised according to a procedure by Fontaine *et al.*[47]

_N_-(2-methyl-1-oxo-1-(prop-2-ynylamino)propan-2-yl)acrylamide: 2-Vinyl-4,4-dimethyl azlactone (VDMA) (30 mg, 216 μmol) and propargyl amine (11.9 mg, 216 μmol) were dissolved in 3 mL of toluene and left to stir overnight at room temperature. Precipitation of a white crystalline solid was observed and the product

was isolated upon removal of the solvent under reduced pressure (41.8 mg, quantitative yield).

^{1}H NMR (400.03 MHz, CDCl$_3$, 298 K) δ = 7.02 (br s, 1H, NH), 6.39 (br s, 1H, NH), 6.28 (dd, 1H, J = 16.6, 1.5 Hz, CH), 6.13 (dd, 1H, J = 17.1, 10.4 Hz, CH), 5.66 (dd, 1H, J = 10.4, 1.5 Hz, CH), 4.03 (dd, 2H, J = 2.5 Hz, CH$_2$), 2.21 (t, 1H, J = 2.5 Hz), 1.61 (s, 6H). ^{13}C NMR (100.59 MHz, CDCl$_3$, 298 K) δ = 174.2, 165.6, 131.0, 127.2, 79.5, 71.6, 57.5, 29.6, 25.2.). IR (solid) ν = 3263, 2437, 2391, 1650, 1607, 1544, 1438, 1218, 959 cm^{-1}. HRMS (ES+) calculated for C$_{10}$H$_{14}$N$_2$O$_2$ [M + Na]$^+$ 217.0947, observed 217.0953.

N-(1-(allylamino)-2-methyl-1-oxopropan-2-yl)acrylamide: 2-Vinyl-4,4-dimethyl azlactone (VMDA) (30 mg, 216 μmol) and allyllamine (12.3 mg, 216 μmol) were dissolved in 3 mL of toluene and left to stir overnight at room temperature. Precipitation of a white crystalline solid was observed and the product was isolated upon removal of the solvent under reduced pressure (42.3 mg, quantitative yield).

^{1}H NMR (400.03 MHz, CDCl$_3$, 298 K) δ = 6.79 (br s, 1H, NH), 6.55 (br s, 1H, NH), 6.26 (dd, 1H, J = 16.6, 1.5 Hz, CH), 6.12 (dd, 1H, J = 16.6, 10.4 Hz, CH), 5.81 (tq, 1H, J = 10.5, 5.0 Hz, CH), 5.63 (dd, 1H, J = 10.4, 1.5 Hz, CH), 5.13 (qdd, 1H, J = 23.1, 17.1, 1.5 Hz, CH), 3.87 (tt, 2H, J = 5.5, 1.5 Hz, CH$_2$), 1.61 (s, 6H). ^{13}C NMR (100.59 MHz, CDCl$_3$, 298 K) δ = 174.4, 165.4, 134.0, 131.2, 126.9, 116.1, 57.5, 42.1, 25.3. IR (solid) ν = 3276, 3060, 2979, 2928, 1655, 1620, 1536, 1251 cm^{-1}. HRMS (ES+) calcd for C$_{10}$H$_{16}$N$_2$O$_2$ [M + Na]$^+$ 219.1104, observed 219.1109.

Synthesis of pVDMA by ATRP: VDMA (3.00 g, 21.6 mmol), ethyl 2-bromoisobutyrate (0.0841 g, 0.43 mmol), Cu(I)Br (0.0619 g, 0.43 mmol), mesitylene (0.518 g, 4.31 mmol) and toluene (6 mL) were added to an oven dried Schlenk tube and subjected to four freeze-pump-thaw cycles and left under a blanket of nitrogen. Me$_6$TREN was added to the Schlenk tube *via* a degassed syringe and the brown solution immersed in an oil bath at 30 °C. Samples were taken periodically for analysis by ^{1}H NMR and SEC and after 140 minutes (89 % monomer conversion) the polymerisation was quenched by exposing the solution to air. SEC analysis (Quenched at 140 min) – M$_n$ = 5900 gmol^{-1}, Đ =1.32. The solution was immediately employed for the ring opening of various amines to yield the desired functionalised polymers.

Propargyl Amine Modification of pVDMA: 4.5 mL of the crude pVDMA solution (containing 10.8 mmol of azlactone functionality) was added to a round bottomed flask and diluted with 5 mL of DMSO. Propargylamine (0.891 g, 16.2 mmol) was added to the polymer solution in 10 mL of DMSO and the solution allowed to stir at room temperature overnight. The solution was added dropwise into ethyl acetate, with precipitation of the polymer. The solid was collected by centrifugation and isolated as a crystalline solid. Infra-red analysis of the obtained polymer showed complete disappearance of the signals corresponding to the azlactone ring, along with the appearance of a strong signal corresponding to the two amide moieties generated upon ring opening. SEC analysis revealed a clear mass increase upon ring opening with propargyl amine, and a well-defined final polymer observed. SEC Analysis (DMF) – M$_n$ = 12,500 gmol^{-1}, Đ = 1.20.

Allyl Amine Modification of pVDMA: 4.5 mL of the crude pVDMA solution (containing 10.8 mmol of azlactone functionality) was added to a round-bottomed flask and diluted with 5 mL of DMSO. Allylamine (0.92 g, 16.2 mmol) was added to the polymer solution in 10 mL of DMSO and the solution allowed to stir at room temperature overnight. The solution was added dropwise into ethyl acetate, with precipitation of the polymer. The solid was collected by centrifugation and isolated as a crystalline solid. Infra-red analysis of the obtained polymer showed complete disappearance of the signals corresponding to the azlactone ring, along with the appearance of a strong signal corresponding to the two amide moieties generated upon ring opening. SEC analysis revealed a clear mass increase upon ring opening with allylamine, and a well-defined final polymer observed. SEC Analysis (DMF) – M_n = 12,800 gmol^{-1}, Đ = 1.15.

Tyramine Modification of pVDMA: 4.5 mL of the crude pVDMA solution (containing 10.8 mmol of azlactone functionality) was added to a round-bottomed flask and diluted with 5 mL of DMSO. Tyramine (2.218 g, 16.2 mmol) was added to the polymer solution in 10 mL of DMSO and the solution allowed to stir at room temperature overnight. The solution was added dropwise into ethyl acetate, with precipitation of the polymer. The solid was collected by centrifugation and isolated as a crystalline solid. Infra-red analysis of the obtained polymer showed complete disappearance of the signals corresponding to the azlactone ring, along with the appearance of a strong signal corresponding to the two amide moieties generated upon ring opening. SEC analysis revealed a clear mass increase upon ring opening with tyramine, and a well-defined final polymer observed. A strong UV absorbance (280 nm) was also observed for the functionalised polymer, further evidence of

incorporation of the aromatic group to the polymer backbone. SEC Analysis (DMF) – M_n = 11,700 gmol^{-1}, Đ = 1.28.

Furfuryl amine modification of pVDMA: 4.5 mL of the crude pVDMA solution (containing 10.8 mmol of azlactone functionality) was added to a round-bottomed flask and diluted with 5 mL of DMSO. Furfurylamine (1.570 g, 16.2 mmol) was added to the polymer solution in 10 mL of DMSO and the solution allowed to stir at room temperature overnight. The solution was added dropwise into ethyl acetate, with precipitation of the polymer. The solid was collected by centrifugation and isolated as a crystalline solid. Infra-red analysis of the obtained polymer showed complete disappearance of the signals corresponding to the azlactone ring, along with the appearance of a strong signal corresponding to the two amide moieties generated upon ring opening. SEC analysis revealed a clear mass increase upon ring opening with furfurylamine, and a well-defined final polymer observed. SEC Analysis (DMF) – M_n = 10,200 gmol^{-1}, Đ = 1.35.

Glucosamine modified pVDMA: 4.5 mL of the crude pVDMA solution (containing 10.8 mmol of azlactone functionality) was added to a round-bottomed flask and diluted with 5 mL of DMSO. Glucosamine hydrochloride (3.49 g, 16.2 mmol) was added to the polymer solution in 10 mL of DMSO, along with triethylamine (1.63 g, 16.2 mmol) and the solution allowed to stir at room temperature overnight. Volatiles were then removed and the crude polymer solution diluted with water and dialysed against water (MWCO 1000 Da) for 3 days to remove low molecular weight species. The water was removed by lyophilisation to yield the product as a white fluffy powder. Infra-red analysis of the obtained polymer showed complete disappearance

of the signals corresponding to the azlactone ring, along with the appearance of a strong signal corresponding to the two amide moieties generated upon ring opening. SEC analysis revealed a clear mass increase upon ring opening with glucosamine. SEC Analysis (Aqueous) – M_n 11,900 gmol^{-1}, PDi 1.40.

3.5.4 Inhibitory assays

Concanavalin A (Con A): Microtitre plates were incubated for 16 h with 180 μL of 100 μg.mL^{-1} mannan dissolved in phosphate-buffered saline (PBS) per well. Unattached mannan was removed by washing extensively with PBS. Polymer solutions were made up as serial dilutions in 10 mM HEPES buffer with 0.5 mM CaCl$_2$, 0.5 mM MgCl$_2$ and 0.5 mM MnCl$_2$ from 1 mg.mL^{-1}. 20 μL of 12.5 μg.mL^{-1} Con A–FITC in HEPES was added to 100 mL of each polymer solution to result in 2 μg mL^{-1} ConA– FITC. 100 μL of the polymer ConA–FITC solutions were added to the mannosylated surfaces and incubated at 37 °C for 30 min. Fluorescence was then measured at excitation/emission wavelengths of 485/528 nm. All experiments were carried out in triplicate.

Cholera toxin B sub unit (CTxB): 96-Well microtitre plates were incubated for 16 h with 180 μL of 100 μg.mL^{-1} GM1 ganglioside dissolved in phosphate-buffered saline (PBS), per well. Unattached GM1 was removed by washing extensively with PBS. Polymer solutions were made up as serial dilutions in PBS from 1 mg mL^{-1}. 20 μL of 12.5 μg.mL^{-1} CTxB–FITC in PBS was added to 100 μL of each polymer solution to result in 2 μg.mL^{-1} CTxB– FITC. 100 μL of the polymer CTxB–FITC solutions were added to the GM1 surfaces and incubated at 37 °C for 30 min.

Fluorescence was then measured at excitation/emission wavelengths of 485/528 nm. All experiments were carried out in triplicate.

3.6 References

1. M. A. Gauthier, M. I. Gibson and H.-A. Klok, *Angew. Chem. Int. Ed.*, 2009, **48**, 48-58.

2. V. Ladmiral, G. Mantovani, G. J. Clarkson, S. Cauet, J. L. Irwin and D. M. Haddleton, *J. Am. Chem. Soc.*, 2006, **128**, 4823-4830.

3. N. K. Singha, M. I. Gibson, B. P. Koiry, M. Danial and H.-A. Klok, *Biomacromolecules*, 2011, **12**, 2908-2913.

4. S.-J. Richards, M. W. Jones, M. Hunaban, D. M. Haddleton and M. I. Gibson, *Angew. Chem. Int. Ed.*, 2012, **51**, 7812-7816.

5. E. Pedone, X. W. Li, N. Koseva, O. Alpar and S. Brocchini, *J. Mater. Chem.*, 2003, **13**, 2825-2837.

6. P. Theato, *J. Polym. Sci. A Polym. Chem.*, 2008, **46**, 6677-6687.

7. M. I. Gibson, E. Froehlich and H.-A. Klok, *J. Polym. Sci. A Polym. Chem.*, 2009, **47**, 4332-4345.

8. M. Mammen, G. Dahmann and G. M. Whitesides, *J. Med. Chem.*, 1995, **38**, 4179-4190.

9. G. Chen, S. Amajjahe and M. H. Stenzel, *Chem. Commun.*, 2009, 1198-1200.

10. S. G. Spain, M. I. Gibson and N. R. Cameron, *J. Polym. Sci. A Polym. Chem.*, 2007, **45**, 2059-2072.

11. Y. M. Chabre, D. Giguere, B. Blanchard, J. Rodrigue, S. Rocheleau, M. Neault, S. Rauthu, A. Papadopoulos, A. A. Arnold, A. Imberty and R. Roy, *Chem. Eur. J.*, 2011, **17**, 6545-6562.

12. N. Sharon, *Biochim. Biophys. Acta*, 2006, **1760**, 527-537.

13. S. R. A. Devenish, J. B. Hill, J. W. Blunt, J. C. Morris and M. H. G. Munro, *Tetrahedron Lett.*, 2006, **47**, 2875-2878.

14. S. M. Heilmann, J. K. Rasmussen and L. R. Krepski, *J. Polym. Sci. A Polym. Chem.*, 2001, **39**, 3655-3677.

15. S. M. Heilmann, D. M. Moren, L. R. Krepski, S. V. Pathre, J. K. Rasmussen and J. Stevens, *Tetrahedron*, 1998, **54**, 12151-12160.

16. J. M. Messman, B. S. Lokitz, J. M. Pickel and S. M. Kilbey, II, *Macromolecules*, 2009, **42**, 3933-3941.

17. M. K. Georges, R. P. N. Veregin, P. M. Kazmaier and G. K. Hamer, *Macromolecules*, 1993, **26**, 2987-2988.

18. M. Kato, M. Kamigaito, M. Sawamoto and T. Higashimura, *Macromolecules*, 1995, **28**, 1721-1723.

19. J. S. Wang and K. Matyjaszewski, *J. Am. Chem. Soc.*, 1995, **117**, 5614-5615.

20. J. Chiefari, Y. K. Chong, F. Ercole, J. Krstina, J. Jeffery, T. P. T. Le, R. T. A. Mayadunne, G. F. Meijs, C. L. Moad, G. Moad, E. Rizzardo and S. H. Thang, *Macromolecules*, 1998, **31**, 5559-5562.

21. D. C. Tully, M. J. Roberts, B. H. Geierstanger and R. B. Grubbs, *Macromolecules*, 2003, **36**, 4302-4308.

22. D. Fournier, S. Pascual and L. Fontaine, *Macromolecules*, 2004, **37**, 330-335.

23. B. S. Lokitz, J. M. Messman, J. P. Hinestrosa, J. Alonzo, R. Verduzco, R. H. Brown, M. Osa, J. F. Ankner and S. M. Kilbey, II, *Macromolecules*, 2009, **42**, 9018-9026.

24. S. Pascual, T. Blin, P. J. Saikia, M. Thomas, P. Gosselin and L. Fontaine, *J. Polym. Sci A Polym. Chem.*, 2010, **48**, 5053-5062.

25.   M. E. Levere, H. Hien The, S. Pascual and L. Fontaine, *Polym. Chem.*, 2011, **2**, 2878-2887.

26.   M. E. Buck and D. M. Lynn, *Polym. Chem.*, 2012, **3**, 66-80.

27.   M. E. Buck, J. Zhang and D. M. Lynn, *Adv. Mater.*, 2007, **19**, 3951-3955.

28.   M. E. Buck and D. M. Lynn, *Adv. Mater.*, 2010, **22**, 994-998.

29.   E. M. Saurer, R. M. Flessner, M. E. Buck and D. M. Lynn, *J. Mater. Chem.*, 2011, **21**, 1736-1745.

30.   M. E. Buck, S. C. Schwartz and D. M. Lynn, *Chem. Mater.*, 2010, **22**, 6319-6327.

31.   M. E. Buck and D. M. Lynn, *Acs Appl. Mater. Interfaces*, 2010, **2**, 1421-1429.

32.   M. I. Kinsinger, M. E. Buck, F. Campos, D. M. Lynn and N. L. Abbott, *Langmuir*, 2008, **24**, 13231-13236.

33.   M. I. Kinsinger, M. E. Buck, N. L. Abbott and D. M. Lynn, *Langmuir*, 2010, **26**, 10234-10242.

34.   A. Laquievre, N. S. Allaway, J. Lyskawa, P. Woisel, J.-M. Lefebvre and D. Fournier, *Macromol. Rapid Commun.*, 2012, **33**, 848-855.

35.   H. Hien The, F. Leroux, S. Pascual, V. Montembault and L. Fontaine, *Macromol. Rapid Commun.*, 2012, **33**, 1753-1758.

36.   D. M. Haddleton, A. J. Clark, M. C. Crossman, D. J. Duncalf, A. M. Heming, S. R. Morsley and A. J. Shooter, *Chem. Commun.*, 1997, 1173-1174.

37.   P. M. Wright, G. Mantovani and D. M. Haddleton, *J. Polym. Sci, A Polym. Chem.*, 2008, **46**, 7376-7385.

38.   J. M. J. Frechet, T. G. Tessier, C. G. Willson and H. Ito, *Macromolecules*, 1985, **18**, 317-321.

39. G. G. Barclay, C. J. Hawker, H. Ito, A. Orellana, P. R. L. Malenfant and R. F. Sinta, *Macromolecules*, 1998, **31**, 1024-1031.

40. A. P. Bapat, J. G. Ray, D. A. Savin, E. A. Hoff, D. L. Patton and B. S. Sumerlin, *Polym. Chem.*, 2012, **3**, 3112-3120.

41. C. R. Becer, M. I. Gibson, J. Geng, R. Ilyas, R. Wallis, D. A. Mitchell and D. M. Haddleton, *J. Am. Chem. Soc.*, 2010, **132**, 15130-15132.

42. S. G. Spain and N. R. Cameron, *Polym. Chem.*, 2011, **2**, 60-68.

43. B. D. Polizzotti and K. L. Kiick, *Biomacromolecules*, 2006, **7**, 483-490.

44. B. Sun, X. Liu, M. E. Buck and D. M. Lynn, *Chem. Comm.*, 2010, **46**, 2016-2018.

45. Y. Gou, S.-J. Richards, D. M. Haddleton and M. I. Gibson, *Polym. Chem.*, 2012, **3**, 1634-1640.

46. J. Voepel, U. Edlund, A.-C. Albertsson and V. Percec, *Biomacromolecules*, 2011, **12**, 253-259.

47. H. The Hien, M. Levere, J.-C. Soutif, V. Montembault, S. Pascual and L. Fontaine, *Polym. Chem.*, 2011, **2**, 1258-1260.

Chapter 4

Glycopolymers with secondary binding motifs mimic glycan branching and display bacterial lectin selectivity in addition to affinity

M. W. Jones, L. Otten, **S-J. Richards**, R. Lowery, D. J. Phillips, D. M. Haddleton, M. I. Gibson, *Chem. Sci.*, **2014**, *5*, 1611-1616

This chapter further builds on the first two chapters and aimed to develop more potent polymeric inhibitors of the cholera toxin that also display good specificity for their target. A new versatile post-polymerisation modification technique was developed to identify potent glycopolymer inhibitors of the cholera toxin that along with a galactose moiety, also contain a variable side groups with the view to creating favourable interactions with the binding site of the cholera toxin.

Mathew Jones and Daniel Phillips made the glycopolymers. Lucienne Otten, Richard Lowery and I did the inhibitor testing. Richard was a project student under the supervision of Lucienne and me. Lucienne and I performed crude protein docking experiments. Daniel, Lucienne and I helped prepare the manuscript.

4.1 Abstract

The application of synthetic glycopolymers to anti-adhesive therapies has so far been limited by their lack of lectin specificity. Here we employ a macromolecular engineering approach to mimic glycan architecture. A new, three-step tandem post-polymerisation methodology was developed which afforded precise control over both chain length and carbohydrate-polymer backbone linker distance. This route also allowed a secondary binding (branched) motif to be introduced onto the linker, increasing specificity and affinity towards bacterial toxins without the need for extensive carbohydrate or organic chemistry. Sequential variation of this motif was found to dramatically alter both the affinity and the specificity of the glycopolymers towards two lectins, cholera toxin and peanut agglutinin, by up to 20-fold either *via* direct binding, or increased steric constraints. Using this method, a glycopolymer that showed increased specificity towards cholera toxin was identified.

4.2 Introduction

Protein-carbohydrate interactions dictate the outcomes of a large and varied number of cellular recognition processes, controlling immune responses, tumour metastasis, gamete fertilisation and many more.[1] The structure, function or even identity of many glycans remains unknown. It is estimated that 50 % of human proteins are glycosylated and there remains significant analytical challenges associated with the isolation and characterisation of complex glycans.[2] Proteins which recognise and process the signals associated with carbohydrates are termed lectins: carbohydrate binding proteins which are neither antibodies nor enzymes and they are widely distributed in nature.[3] Despite their role in normal physiology, lectins/glycans can also act as a potential site for infection, which can be exploited by pathogenic

organisms to interface with their host. For example, pathogenic *Escherichia coli, E. coli,* expresses the FimH adhesin, which can bind mannose residues in the urinary tract, influenza has sialic acid binding lectin (heamagglutinins) for adhesion to erythrocytes and *Vibrio cholerae* secretes a toxin that binds to intestinal epithelial cells.[1, 4-6] Conversely, HIV expresses high-mannose structures on its envelope that enables it to bind to DC-SIGN lectin on the surface of dendritic cells in the human immune system.[7] With the widespread emergence of antibiotic resistance, new interventions to prevent and detect infectious disease are urgently required.[8, 9] Anti-adhesion therapy, which seeks to use compounds that have higher affinity than the pathogen for the target binding site, thus preventing the adhesion step and hence reducing the infectivity, has emerged as a promising potential treatment.[4, 10-14] As this process does not involve killing the pathogen, there should be no evolutionary stress, hence reducing resistance development and could be administered prophylactically.

The binding affinity of a monosaccharide to its target lectin is typically very weak ($K_d = 10^{-3} - 10^{-6}$ M), limiting their use in anti-adhesion therapy. The sugars' weak affinity is overcome in nature by the presentation of multiple copies on cell surfaces which gives rise to an increase in affinity which is greater than the linear sum of the individual sugars, the so-called cluster glycoside effect.[15-19] Lee *et al.* first demonstrated that multivalent *N*-acetyllactosamine with one to four carbohydrates showed progressively increasing binding affinities, over several orders of magnitude, towards rabbit hepatocytes.[15] Kiessling and co-workers have elegantly shown that polymer architecture (linear, branched, dendritic) has profound effects on lectin binding affinity, with particular focus on their ability to cluster receptors.[20] Ambrosi *et al.* found that galacto-functional polymers have a 100-fold increase in binding

affinity compared to free galactose.[21] STARFISH-based monodisperse glycodendrimers were shown by Kitov *et al.* to neutralise Shiga-like toxins, with a measured affinity over 10^6-fold greater than the monovalent carbohydrate.[22] Exploitation of the high affinity of glycopolymer-lectin interactions also has applications in biosensing.[23, 24]

Advances in controlled (radical) polymerisation methods[11, 25, 26] together with the development of highly efficient and orthogonal 'click'[27] reactions has facilitated the synthesis of glycopolymers by pre- and post-polymerisation modification thus widening the chemical and architecture diversity of glycopolymers.[25, 28] Despite the interest in developing synthetic glycopolymers with high affinity for their respective lectins, there has been significantly less focus placed on their *specificity*.[6] What is often not studied is the relative affinity of the glycopolymer for various lectins with similar specificities, which is essential to avoid unwanted therapeutic side effects or to enable precise diagnostics. An important target for multivalent anti-adhesion therapies/diagnostics is the cholera toxin (CTx), secreted by *Vibrio cholerae*, the causative agent of cholera infection that is estimated to cause over 100,000 deaths per year, and infects more than 3 million people. β-galactose functional inhibitors have been shown to have high affinity to CTx, but there is a need to avoid unwanted interactions with other mammalian lectins, such as the galectins, which also bind β-galactose and could lead to immune responses such as cytokine production.[29] Lectin targets for which selective anti-adhesive therapies have been studied include DC-SIGN/langerin in HIV therapy, or BmbL/DC-SIGN to treat *Burkholderia ambifaria*.[30-33] The relative affinity of a series of bivalent galactosides towards chicken galectins has also been studied.[34] Moreover, selectivity presents a challenge when identifying biological warfare agents based on lectins such as ricin.[35]

Oligosaccharide-mimetic agents have also been developed with high specificity based on tuning their 3-D structure to fit the lectin binding site but without the need for total oligosaccharide synthesis.[36]

Examples of synthetic polymers that have demonstrated lectin selectivity are rare, despite the obvious benefits of their multivalent nature.[37] We have demonstrated that galactose-functional polymers can be engineered to have increased selectivity for CTx B-subunit (CTxB) (See Chapter 2).[38] This was achieved by modulating the distance between backbone and carbohydrate to match the relatively deep cleft of the CTx binding domain, compared to other galactose-binding lectins with shallower domains.[39] Selectivity is required here to discriminate between other pathogenic lectins (or bacteria) that bind galactose including ricin[35] or indeed dietary lectins which can reduce the inhibitor's potency as this would need to function in the intestinal tract.

In this work, we present a macromolecular engineering approach to introduce specificity into glycopolymers, inspired by glycan branching and guided by structural biology information. In particular, we were motivated to achieve selectivity without resorting to multi-step total glycan synthesis, which is non-trivial. Using a new, three-step, tandem post-polymerisation process, secondary motifs are introduced on to the polymer side chain, to increase specificity and affinity towards bacterial toxins.

4.3 Results and Discussion

As the first step, microarray data were extracted from the Consortium for Functional Glycomics (CFG) database to enable a short bioinformatics study to probe lectin affinity and specificity.[40] The relative affinity of CTx and a model galactose-binding

non-pathogenic lectin, peanut agglutinin (PNA), to several oligosaccharides was measured and the most relevant results are shown in Figure 4.1A (full analysis in Appendix 3). PNA was found to bind the disaccharide Gal-β-GalNAc 100-fold more than CTx. However, changing this to a branched oligosaccharide (GM1), which retains the Gal-β-GalNAc unit but also introduces a neuraminic acid branch results in the CTx affinity increasing approximately 100-fold, but with no change in PNA affinity. The increased binding affinity of CTx to the branched saccharide is attributable to allosteric interactions of the neuraminic acid with a secondary binding pocket within CTx, which is not present in PNA[41] We therefore reasoned that if a secondary motif could be installed on the linker between galactose and backbone on a polymer it would be possible to attenuate the binding affinity of the polymer to CTx as shown by Bundle and co-workers,[42] but also selectivity towards the CTx over PNA. Figure 4.1B shows the crystal structure of CTx binding to the branched glycan unit from GM1 showing both the primary and secondary binding pockets, which is simplified in Figure 4.1C using standard glycan notation. Figure 4.1D shows the proposed polymer, with a sufficiently long linker to penetrate the cleft in CTx and a secondary motif to target the allosteric neuraminic acid site.
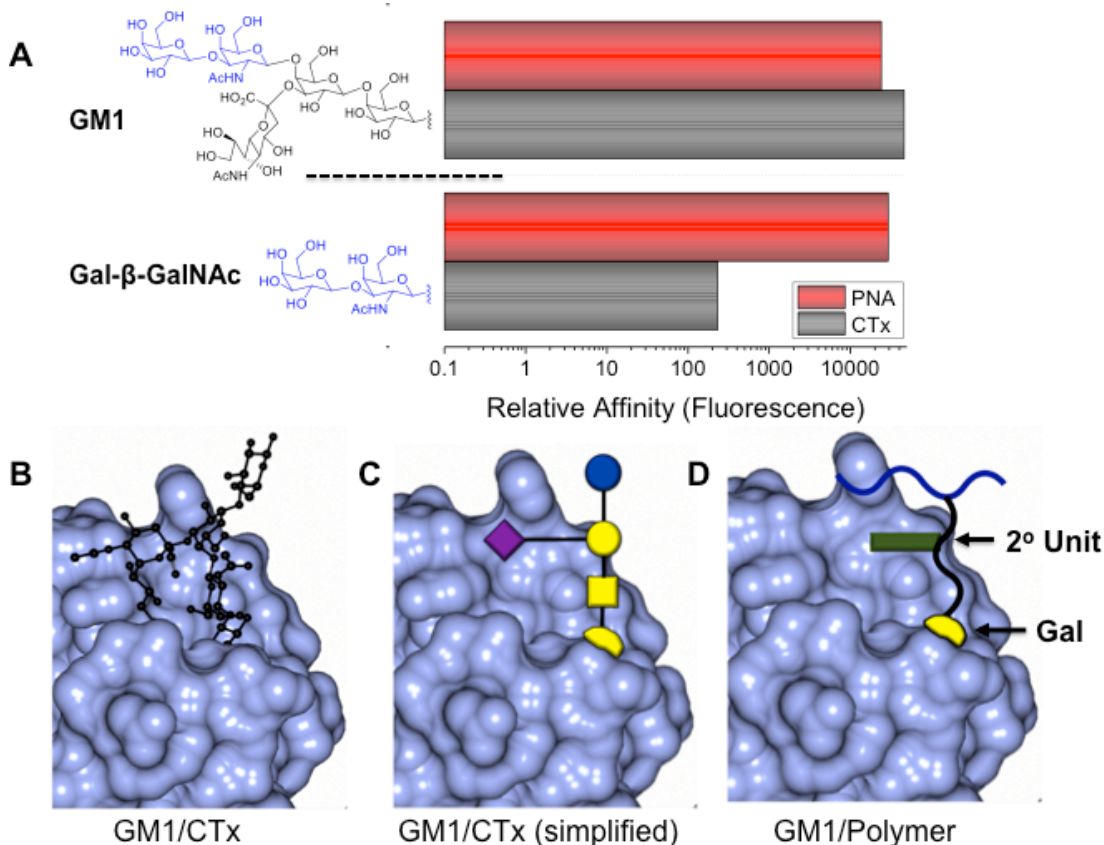
Figure 4.1: A) Glycan microarray analysis showing relative affinity of CTx and PNA to two related glycans. B) Crystal structure of CTx binding to the oligosaccharide portion of GM1. C) CTx crystal structure with glycan drawn in standard ball/stick notation. (Appendix 3 for key). D) Synthetic polymer design concept with idealised polymer shown (schematic, not simulation).

To enable installation of branched motifs in a semi-combinatorial manner, we have developed a new synthetic methodology based on three tandem post-polymerisation modifications.[19, 43] This introduces large chemical diversity that is not normally found on glycans, but ensures chain length (and hence valency) homogeneity across all samples overcoming a common challenge in functional polymers, Figure 4.2.
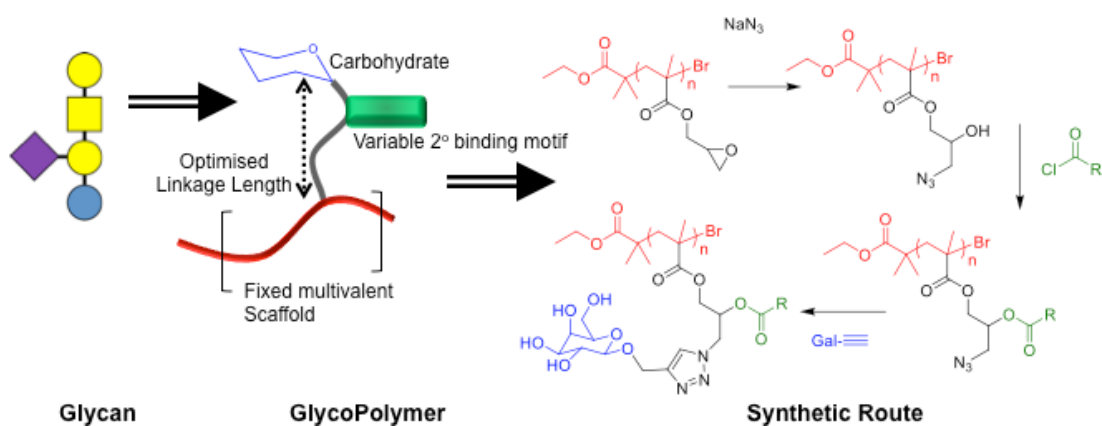
Figure 4.2: Glycopolymer design principle and the newly developed synthetic route. Glycan structure is shown in standard notation (Appendix 3).

The synthetic method fulfilled the following criteria: i) sufficient separation between backbone and carbohydrate to enable penetration into the CTx binding site; ii) an azide group for subsequent glycosylation with β-D-propargyl galactose; iii) esterification of the hydroxyl group, generated during epoxide ring-opening. Poly(glycidyl methacrylate) was synthesised by Cu(I)-mediated polymerisation to produce a well-defined polymer with a degree of polymerisation (DP) ~ 100 and M_w/M_n = 1.2. This molecular weight was targeted as our previous results have shown that above DP of ~30, no further increase in avidity towards CTx was observed.[38] The polymer was produced by controlled radical polymerisation to ensure a lack of low molecular weight tail that would confuse the interpretation of the activity measurements (*vide infra*). Installation of the azide was achieved by addition of sodium azide in DMF at 50 °C, which simultaneously, and quantitatively, installed the necessary orthogonal handle and produced a secondary alcohol as confirmed by infrared spectroscopy (IR), Figure 4.3. In the second step a range of acyl chlorides were reacted with the alcohol to install secondary motifs as confirmed by the disappearance of the OH stretch at 3400 cm^{-1} and the addition of a second carbonyl stretching frequency. The acyl chlorides were chosen based on evidence that aromatic groups can bind the sialic acid site.[42] In the final modification reaction,

112
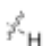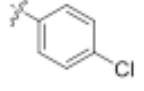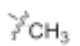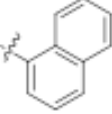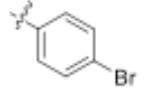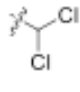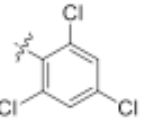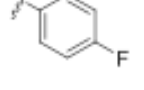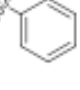
β-D-propargyl galactose was installed by Cu(I)-catalysed cycloaddition, which could

be monitored by the reduction in the azide vibration at 2100 cm^{-1}.
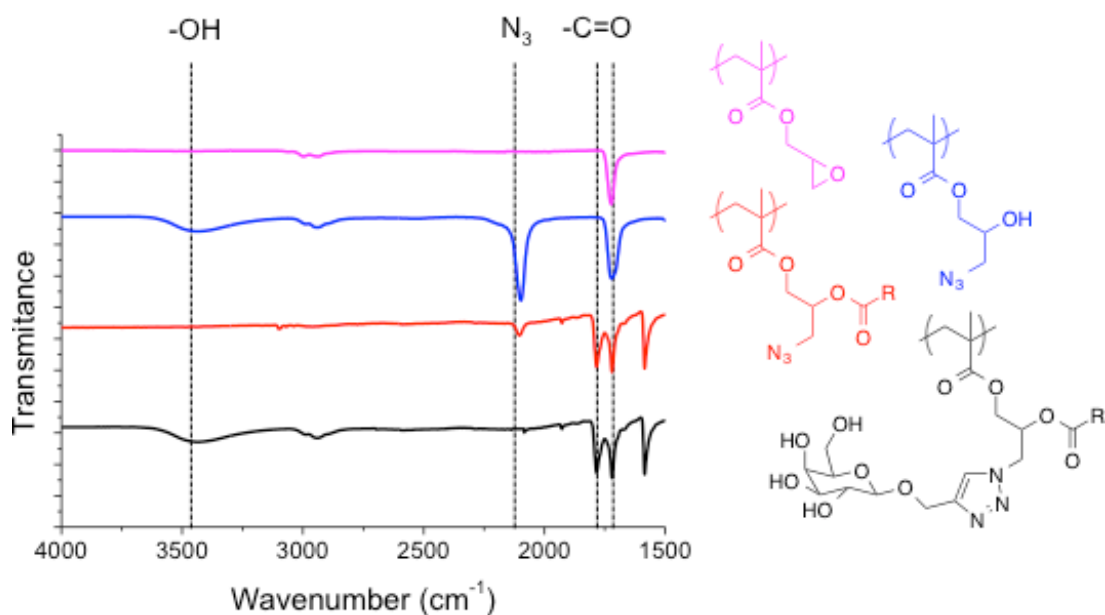
Figure 4.3: Infrared analysis of the three-stage, glycan mimetic, tandem post-polymerisation strategy used here. IR analysis was of purified product.

Table 4.1 summarises the polymer library obtained, the side chains installed and the

calculated log$P$ values of a single repeat unit of the polymer (*vide infra*). Log$P$

values are included as an estimate of the relative hydrophobicity of the binding units.

Table 4.1: Side chains installed on to the polymers and Log*P* values[a].

Code	Structure	LogP	Code	Structure	LogP	Code	Structure	LogP
P1	H	-1.57 ± 0.61	P5	Cl (phenyl)	1.3 ± 0.7	P9	CH$_3$	- 0.17 ± 0.6
P2	naphthyl	1.96 ± 0.68	P6	Br (phenyl)	1.48 ± 0.75	P10	CHCl$_2$	-0.36 ± 0.82
P3	trichlorophenyl	1.70 ± 0.7	P7	F (phenyl)	0.81 ± 0.75	P11	phenyl	0.73 ± 0.68
P4	alkyl chain	3.08 ± 0.6	P8	C(CH$_3$)$_2$Br	0.22 ± 0.63			

[a] Log*P* values are based on a single repeat unit of the polymer, with the methyl capping at each chain end.

With this panel of sequentially modified glycopolymers in hand, a fluorescence-liked sorbent assay was used to evaluate the affinity of the polymers towards each of the lectins.[44-46] Briefly, the glycopolymers were incubated at various concentrations with fluorescently labelled lectins. The solutions were then added to galactose-functionalised microtitre plates. The concentration of polymer required to inhibit 50 % of binding to the plates was reported as the MIC$_{50}$ value. Upon initial testing it was found that several members of the library were insufficiently soluble in buffer to be used in the assays. It was possible to solubilise the polymers in 5 % (v/v) aq. DMSO, but we found this compromised the CTx-assay giving false positive results and hence only the polymers which could be directly dissolved into buffer were tested. The less soluble polymers are still shown in Table 4.1 to highlight the synthetic diversity achieved by this approach. As predicted, addition of the secondary motifs had a dramatic influence on the inhibitory potential of the glycopolymers against both of the lectins, Figure 4.4.
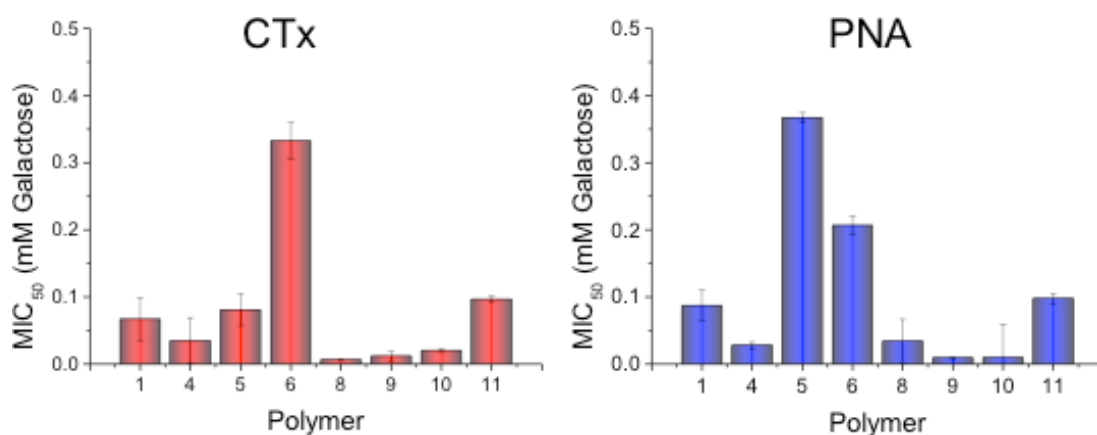
Figure 4.4: Inhibition of lectin binding by synthetic glycopolymers. Values shown are the average of at least 3 measurements, and errors are the standard deviation.

Figure 4.4 reveals some general trends between molecular structure and lectin affinity. Three of the secondary units, **P8**, **P9** and **P10** gave rise to large 10-fold decreases in the MIC_{50} towards both lectins, compared to **P1**. Whilst these groups were relatively diverse, the common theme was that they did not contain an aromatic group, but **P8** and **P10** did contain halogenated alkanes. **P8** and **P10** side chains are significantly larger than in **P9** which suggests that their affinity modulation was not entirely due to steric constraints and may indicate that branching at the side chain increases affinity to CTx. Polymers **P11**, **P5** and **P6**, led to either no changes, or significantly increased the MIC_{50} values. Due to the size and rigidity of these functional groups, steric constraints might be crucial, preventing access of the polymer to both lectins, or limiting conformational flexibility. Polymer **P4**, which had a linear, but flexible, hexamethylene group gave modest improvements (lower MIC_{50}) in binding to both lectins. Our observations are in contrast to those of Bundle and coworkers who have observed that pendant aromatic units can enhance the binding to CTx *via* interactions with the neuraminic acid binding pocket, but they used polymers with a very low density of carbohydrate side chains and different length side chains on polydisperse scaffolds, making comparisons difficult.[42] Here

we have densely packed side-chains that impose additional steric restraints. The high affinity of CTx to GM1 in nature is attributable to the intrinsic rigidity of GM1, which has also been found to be important in small-molecule GM1 mimics and is probably contributing here.[47, 48] Comparison of the observed inhibitory values against the calculated partition coefficient did not reveal any obvious trend suggesting simple hydrophobic/hydrophilic interactions are not responsible (Appendix 3).

As indicated in the introduction, the key aim of this study was to use glycan-mimetic branching to introduce *specificity*/*selectivity* as well as *affinity* into synthetic glycopolymers. Analysis of the data in Figure 4.4 revealed that **P1** and **P5** (chlorobenzyl) showed the most dramatic differences in terms of relative affinities for each lectin. Figure 4.5 shows the relative affinity (shown as $1/MIC_{50}$ for convenience), for **P1** and **P5** against the two lectins.
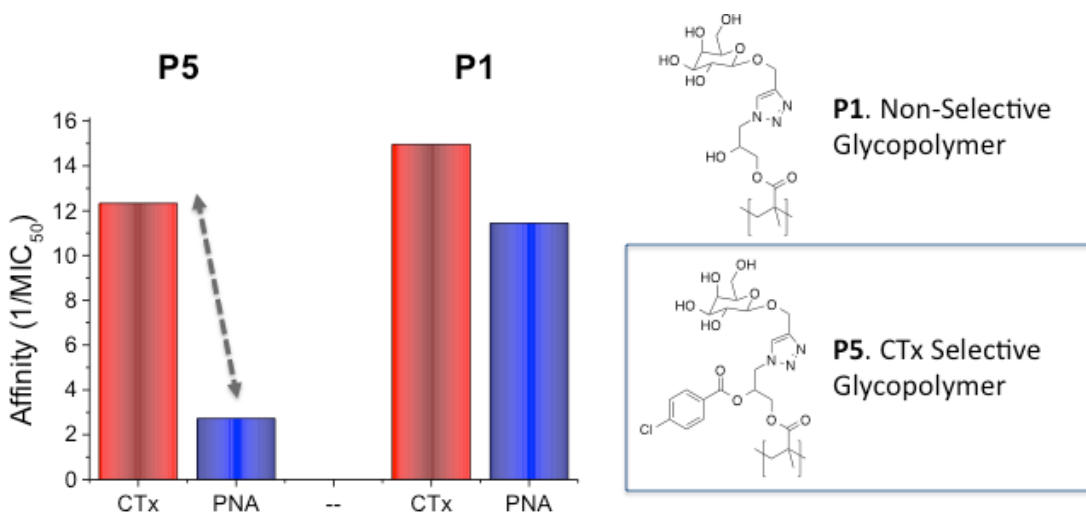
Figure 4.5: Relative affinity ($1/MIC_{50}$) of **P1** and **P5** for CTx and PNA.

P1 shows similar affinity for both PNA and CTx indicating that it cannot discriminate/select between two different galactose-binding lectins. However, addition of 4-chlorobenzyl unit (**P5**) leads to dramatic differentiation in response to

PNA and CTx, with a significant decrease in affinity towards PNA, but essentially no change in affinity to CTx. This demonstrates that **P5** displays lectin selectivity, using biomimetic macromolecular engineering, but without multistep carbohydrate chemistry. The exact mechanism of binding which leads to selectivity cannot be rationalised at this stage, but the additional bulk of the chlorobenzyl group may prevent access to the PNA binding site, but still be of correct dimensions to fit the neuraminic acid site in CTx. Furthermore, the influence of substituting the chloro- for a bromo- group (**P5** – **P6**) cannot be explained. **P6** has vastly increased MIC_{50} values towards CTx relative to **P5**, but less effect on PNA binding. The additional steric bulk of a bromide might simply be too large for a good fit into the binding cleft in CTx. **P1/P5** also displayed similar affinities for $RCA_{120,}$ another galactose-binding lectin indicating that the structural motifs added here only affect the target lectins (Appendix 3). This supports our hypothesis that the secondary motif is causing an obstruction to the binding site of PNA giving us the specificity CTx, which can accommodate it in its binding site, and hence the polymers have decreased affinity to both of these lectins. These observations rule out non-specific hydrophobic association between polymer/lectins as this would be expected to give enhancements to all test lectins.

4.4 Conclusions

We have demonstrated a new bio-inspired approach to mimicking glycan architecture by using macromolecular engineering, guided by structural biology, and without the need for multi-step oligosaccharide synthesis. Bioinformatics revealed that the addition of branched side chains to galacto-terminal carbohydrates could increase binding affinity to their corresponding lectins, relative to simple monosaccharides. To mimic this branched structure a new, three-step, tandem post-

polymerisation methodology was developed. This enabled precise control over not only chain length, but also carbohydrate-polymer backbone linker distance and the introduction of secondary branched motifs onto the linker. Sequential variation of this motif was found to dramatically (up to 20-fold) alter both the affinity and the selectivity of the glycopolymers towards two lectins; CTx and PNA. Using this method, a glycopolymer was identified which showed increased specificity towards CTx. Glycopolymers with high selectivity may feature in the development of sensitive and precise sensors or anti-adhesive therapies, which has so far limited the application of synthetic glycopolymers. These results show that combining structural biology tools with macromolecular chemistry enables the creation of synthetic glycans which can mimic, or outperform their natural counterparts and will find applications in anti-adhesive therapy and biomolecular sensors.

4.5 Experimental

4.5.1 Materials

Dichloromethane, diethyl ether, tetrahydrofuran, dichloromethane, triethylamine and dimethyl sulfoxide were all purchased from Fisher Scientific at laboratory reagent grade. Ethyl 2-bromoisobutyrate (99.0 %), glycidyl methacrylate (≥ 97.0 %), copper (I) bromide (98.0 %), anisole (≥ 99.0 %), benzoyl chloride (99.0 %), 1-naphthoyl chloride (97.0%), 2,4,6-trichlorobenzoyl chloride (97.0 %), decanoyl chloride (98.0 %), 4-chlorobenzoyl chloride (99.0 %), 4-bromobenzoyl chloride (98.0 %), 4-fluorobenzoyl chloride (98.0 %), α-bromoisobutyryl bromide (98.0 %), acetyl chloride (98.0 %), dichloroacetyl chloride (98.0 %), and 2,2'-bipyridyl (≥99.0 %) were all purchased from Sigma-Aldrich. *N*-ethyl-2-pyridylmethanimine[1] and β-D-1-propargyl galactose[2] were synthesised using previously reported methods. Fluorescein isothiocyanate (FITC) labelled peanut agglutinin (PNA) from *Arachis*

hypogaea was purchased from Vector Laboratories. Galactocerebrosides (GCS), FITC labelled cholera toxin subunit B (CTxB), calcium chloride ($CaCl_2$), Sodium chloride (NaCl), manganese (II) chloride, HEPES powder, and Tris buffer were all purchased from Sigma-Aldrich, UK. 96-well high binding microtitre plates were purchased from Greiner Bio-one. Tris buffer containing 0.1 mmol $CaCl_2$ and 0.5 mmol NaCl (pH 8, TBS) was prepared in 250 mL of 119illiQ water (with a resistance >19 mOhms), and 10 mmol HEPES buffer containing 0.15M NaCl, 0.1mM $CaCl_2$ and 0.01mM Mn^{2+} (pH 7.5, HEPES) was prepared in 250 mL of 119illiQ water (with a resistance >19 MΩ.cm).

4.5.2 Physical and analytical methods

NMR spectra were recorded on Bruker DPX-300 and DPX-400 spectrometers for ^{1}H NMR (400 MHz) and ^{13}C NMR (125 MHz). Chemical shifts are reported in ppm relative to the deuterated solvent resonances and spectra analysed with WIN-NMR software. GPC (DMF) was performed on a Varian 390-LC MDS system equipped with a PL-AS RT/MT autosampler, a PL-gel 3 μm (50 × 7.5 mm) guard column, two PL-gel 5 μm (300 × 7.5 mm) mixed-D columns equipped with a differential refractive index, using DMF (with 1 mg.mL^{-1} LiBr) as the eluent with a flow rate of 1.0 mL.min^{-1} at 50 °C. Narrow molecular weight PMMA standards (200 - 1.0 × 10^6 g.mol^{-1}) were used for calibration using a second order polynomial fit. SEC (aqueous) was performed on a Varian 390-LC MDS system equipped with a PL-AS RT/MT autosampler, a PL-aquagel-OH 8 μm (50 × 7.5 mm) guard column, a PLaquagel-OH column set consisting of two 8 μm (300 × 7.5 mm) columns equipped with a differential refractive index detector using phosphate buffer (pH 8.2) as the eluent at a flow rate of 1.0 mL.min^{-1}. Narrow molecular weight PEO standards (100 - 1.26 × 10^6 g.mol^{-1}) were used for calibration using a second order

polynomial fit. Infrared absorption spectra were recorded on a Bruker VECTOR-22 FTIR spectrometer using a Golden Gate diamond attenuated total reflection cell. Mass spectra were recorded using a Micromass Autospec apparatus. Partition coeffecients (LogP) were estimated using ACD labs software 4.5.3 Synthetic procedures

Synthesis of poly(glycidyl methacrylate): To an oven dried Schlenk tube, ethyl 2-bromoisobutyrate (0.55 g, 2.81 mmol), glycidyl methacrylate (40 g, 281 mmol), copper (I) bromide (0.40 g, 2.81 mmol) and anisole (80 mL) were added. The tube was sealed and subjected to four freeze-pump-thaw cycles and left under a blanket of nitrogen. *N*-Ethyl-2-pyridylmethanimine (1.25 mL, 8.44 mmol) was added to the solution *via* a degassed syringe and the Schlenk tube immersed in an oil bath at 50 °C. Samples were taken hourly and analysed by ^{1}H NMR and GPC. After 6 hours, the reaction was quenched by immersing the flask in liquid nitrogen. The solution was then bubbled with air for 12 hours, passed through a short column of neutral alumina and the solvent removed under vacuum. The resulting crude mixture was redissolved in dichloromethane, precipitated three times into diethyl ether and dried under vacuum to yield the product as a white solid. Conversion (NMR): 84.2 %; M_n (theoretical): 12000 g.mol^{-1}; M_n (SEC) = 22900 g.mol^{-1}; M_w/M_n (SEC) = 1.20.

Synthesis of poly(2-hydroxy-3-azidopropyl methacrylate): Poly(glycidyl methacrylate) (1) (7.34 g, 0.051 mmol of polymer repeat unit) was dissolved in DMF (250 mL). Sodium azide (10.07 g, 0.155 mmol) and ammonium chloride (8.29 g, 0.155 mmol) were added to the solution and the mixture stirred for 24 hours. After this time, the mixture was poured into water and the solid collected by filtration. The

polymer was washed several times with water and dried to leave an off-white solid. M_n (SEC) = 26000 g.mol^{-1}, M_w/M_n = 1.8.

Example Acylation Reaction using Benzoyl chloride: Poly(2-hydroxy-3-azidopropyl methacrylate) (200 mg, 8.73 μmol) was dissolved in anhydrous THF (50 mL), along with triethylamine (0.45 mL, 3.24 mmol – 3 eq. for each polymer repeat unit). Benzoyl chloride (0.46 g, 3.24 mmol - 3 eq. for each polymer repeat unit) was dissolved in 50 mL of anhydrous DCM and added dropwise to the solution over a period of 30 minutes. Following complete addition, the solution was left to stir at room temperature for 24 hours. A further portion of triethylamine (0.45 mL, 3.24 mmol) and benzoyl chloride (0.46 g, 3.24 mmol) were added to the solution and allowed to stir for a further 24 hours. The solution was then diluted with 100 mL of DCM and quenched with 100 mL of water. The organic layer was washed with water (2 × 50 mL), dried over anhydrous MgSO$_4$, filtered and the solvent removed. The crude polymer solution was then redissolved in 50 mL of THF and twice precipitated into a 1:1 mixture of diethyl ether/petroleum ether. The solids were isolated by centrifugation and dried under vacuum to yield the product as a off-white powder.

Example 1,3-Dipolar Cycloaddition Reaction of Benzoyl Chloride-Modified Polymer with Galactose Alkyne: Polymer (100 mg, 345.67 μmol), Cu(I)Br (4.9 mg, 34.16 μmol) and galactose alkyne (226 mg, 1.04 mmol) was dissolved in DMSO (8 mL) in a Schlenk tube. This solution was degassed by a minimum of 3 freeze-pump-thaw cycles and frozen with liquid nitrogen. The Schlenk tube was then opened, 2,2'-bipyridyl (10.8 mg, 69.15 μmol) was added and the tube re-sealed. The frozen solution was evacuated three times, back-filled with dry nitrogen and left to defrost. After stirring at ambient conditions for 4 days, the solution was diluted with

distilled water and dialysed against water for 3 days. The resulting suspension was centrifuged and the supernatant was lyophilised to leave an off-white powder.

4.5.4 Inhibitory assays

Example fluorescence-linked sorbent assay for inhibitory activity against cholera toxin B subunit (CTxB): 96-well microtitre plates were incubated for 16 h with 150 μL of 100 μg.mL^{-1} galactocerebroside (GCS) (in 95% ethanol, 5% water and heated to 45 °C). Unbound GCS was removed by washing extensively with water. Polymer solutions were made up as serial dilutions (up to 10 dilutions per sample from either 1 mg.mL^{-1} or 0.1 mg.mL^{-1} in water). 10 μL of 100 μg.mL^{-1} CTx-FITC in 10 mM Tris with 0.1 mM CaCl$_2$ and 0.5 mM NaCl (pH 8) was added to 90 μL of polymer solution to a final concentration of 11 μg.mL^{-1}. 100 μL of the PNA/polymer solutions were then added to GCS coated wells and incubated at 37 °C for 30 mins. After this the wells were extensively washed with water and fluorescence was measured at excitation/emission wavelengths of 485/528 nm. All experiments were carried out in triplicate. Percentage inhibition was compared to relative to controls of pure CTx-FITC (with no polymer).

4.6 References

1. C. R. Bertozzi and L. L. Kiessling, *Science*, 2001, **291**, 2357-2364.

2. K. Marino, J. Bones, J. J. Kattla and P. M. Rudd, *Nat. Chem. Biol.*, 2010, **6**, 713-723.

3. M. Ambrosi, N. R. Cameron and B. G. Davis, *Org. Bio. Chem.*, 2005, **3**, 1593-1608.

4. T. R. Branson and W. B. Turnbull, *Chem. Soc. Rev.*, 2013, **42**, 4613-4622.

5.   T. Beddoe, A. W. Paton, J. Le Nours, J. Rossjohn and J. C. Paton, *Trends Biochem. Sci.*, 2010, **35**, 411-418.

6.   R. R. Dinglasan and M. Jacobs-Lorena, *Infect. Immun.*, 2005, **73**, 7797-7807.

7.   A. T. Haase, *Nature*, 2010, **464**, 217-223.

8.   S. B. Levy and B. Marshall, *Nat. Med.*, 2004, **10**, S122-S129.

9.   C. Dye, *Lancet*, 2006, **367**, 938-940.

10.   R. J. Pieters, *Org. Biomol. Chem.*, 2009, **7**, 2013-2025.

11.   S. G. Spain and N. R. Cameron, *Polym. Chem.*, 2011, **2**, 60-68.

12.   G. Mulvey, P. I. Kitov, P. Marcato, D. R. Bundle and G. D. Armstrong, *Biochimie*, 2001, **83**, 841-847.

13.   D. A. Rasko and V. Sperandio, *Nat. Rev. Drug. Disc.*, 2010, **9**, 117-128.

14.   K. I. P. J. Hidari, T. Murata, K. Yoshida, Y. Takahashi, Y.-h. Minamijima, Y. Miwa, S. Adachi, M. Ogata, T. Usui, Y. Suzuki and T. Suzuki, *Glycobiology*, 2008, **18**, 779-788.

15.   Y. C. Lee, R. R. Townsend, M. R. Hardy, J. Lonngren, J. Arnarp, M. Haraldsson and H. Lonn, *J. Biol. Chem.*, 1983, **258**, 199-202.

16.   J. J. Lundquist and E. J. Toone, *Chem. Rev.*, 2002, **102**, 555-578.

17.   C. R. Becer, M. I. Gibson, J. Geng, R. Ilyas, R. Wallis, D. A. Mitchell and D. M. Haddleton, *J. Am. Chem. Soc.*, 2010, **132**, 15130-15132.

18.   N. Vinson, Y. Gou, C. R. Becer, D. M. Haddleton and M. I. Gibson, *Polym. Chem.*, 2011, **2**, 107-113.

19.   M. W. Jones, S. J. Richards, D. M. Haddleton and M. I. Gibson, *Polym. Chem.*, 2013, **4**, 717-723.

20.   J. E. Gestwicki, C. W. Cairo, L. E. Strong, K. A. Oetjen and L. L. Kiessling, *J. Am. Chem. Soc.*, 2002, **124**, 14922-14933.

21.   M. Ambrosi, N. R. Cameron, B. G. Davis and S. Stolnik, *Org. Biomol. Chem.*, 2005, **3**, 1476-1480.

22.   P. I. Kitov, J. M. Sadowska, G. Mulvey, G. D. Armstrong, H. Ling, N. S. Pannu, R. J. Read and D. R. Bundle, *Nature*, 2000, **403**, 669-672.

23.   Z. Shen, M. Huang, C. Xiao, Y. Zhang, X. Zeng and P. G. Wang, *Anal. Chem.*, 2007, **79**, 2312-2319.

24.   L. Otten, S.-J. Richards, E. Fullam, G. S. Besra and M. I. Gibson, *J. Mater. Chem. B*, 2013, **1**, 2665-2672.

25.   S. G. Spain, M. I. Gibson and N. R. Cameron, *J. Polym. Sci. A Polym. Chem.*, 2007, **45**, 2059-2072.

26.   S. R. S. Ting, G. Chen and M. H. Stenzel, *Polym. Chem.*, 2010, **1**, 1392-1412.

27.   H. C. Kolb, M. G. Finn and K. B. Sharpless, *Angew. Chem. Int. Ed.*, 2001, **40**, 2004-2021.

28.   M. A. Gauthier, M. I. Gibson and H.-A. Klok, *Angew. Chem. Int. Ed.*, 2009, **48**, 48-58.

29.   A. R. Young and E. N. Meeusen, *Glycoconjugate J.*, 2002, **19**, 601-606.

30.   L. de Witte, A. Nabatov, M. Pion, D. Fluitsma, M. A. W. P. de Jong, T. de Gruijl, V. Piguet, Y. van Kooyk and T. B. H. Geijtenbeek, *Nat. Med.*, 2007, **13**, 367-371.

31.   M. Andreini, D. Doknic, I. Sutkeviciute, J. J. Reina, J. Duan, E. Chabrol, M. Thepaut, E. Moroni, F. Doro, L. Belvisi, J. Weiser, J. Rojo, F. Fieschi and A. Bernardi, *Org. Biomol. Chem.*, 2011, **9**, 5778-5786.

32. M. Thepaut, C. Guzzi, I. Sutkeviciute, S. Sattin, R. Ribeiro-Viana, N. Varga, E. Chabrol, J. Rojo, A. Bernardi, J. Angulo, P. M. Nieto and F. Fieschi, *J. Am. Chem. Soc.*, 2013, **135**, 2518-2529.

33. B. Richichi, A. Imberty, E. Gillon, R. Bosco, I. Sutkeviciute, F. Fieschi and C. Nativi, *Org. Biomol. Chem.*, 2013, **11**, 4086-4094.

34. S. Andre, D. V. Jarikote, D. Yan, L. Vincenz, G.-N. Wang, H. Kaltner, P. V. Murphy and H.-J. Gabius, *Bioorg. Med. Chem. Lett.*, 2012, **22**, 313-318.

35. M. Fais, R. Karamanska, S. Allman, S. A. Fairhurst, P. Innocenti, A. J. Fairbanks, T. J. Donohoe, B. G. Davis, D. A. Russell and R. A. Field, *Chem. Sci.*, 2011, **2**, 1952-1959.

36. A. Bernardi and P. Cheshev, *Chem. Eur. J.*, 2008, **14**, 7434-7441.

37. K. C. A. Garber, K. Wangkanont, E. E. Carlson and L. L. Kiessling, *Chem. Commun.*, 2010, **46**, 6747-6749.

38. S.-J. Richards, M. W. Jones, M. Hunaban, D. M. Haddleton and M. I. Gibson, *Angew. Chem. Int. Ed.*, 2012, **51**, 7812-7816.

39. B. D. Polizzotti, R. Maheshwari, J. Vinkenborg and K. L. Kiick, *Macromolecules*, 2007, **40**, 7103-7110.

40. CFG, http://www.functionalglycomics.org.

41. W. B. Turnbull, B. L. Precious and S. W. Homans, *J. Am. Chem. Soc.*, 2004, **126**, 1047-1054.

42. T. Huu-Anh, P. I. Kitov, E. Paszkiewicz, J. M. Sadowska and D. R. Bundle, *Org. Biomol. Chem.*, 2011, **9**, 3658-3671.

43. N. K. Singha, M. I. Gibson, B. P. Koiry, M. Danial and H.-A. Klok, *Biomacromolecules*, 2011, **12**, 2908-2913.

44.   L. Otten, S.-J. Richards, E. Fullam, G. S. Besra and M. I. Gibson, *Journal of Materials Chemistry B*, 2013, **1**, 2665-2672.

45.   S.-J. Richards, M. W. Jones, M. Hunaban, D. M. Haddleton and M. I. Gibson, *Angew. Chem. Int. Ed.*, 2012, **51**, 7812-7816.

46.   D. A. Sack, S. Huda, P. K. B. Neogi, R. R. Daniel and W. M. Spira, *J. Clin. Microbiol.*, 1980, **11**, 35-40.

47.   A. Bernardi, D. Arosio, D. Potenza, I. Sanchez-Medina, S. Mari, F. J. Canada and J. Jimenez-Barbero, *Chem. Eur. J.*, 2004, **10**, 4395-4406.

48.   A. Bernardi, L. Carrettoni, A. G. Ciponte, D. Monti and S. Sonnino, *Bioorg. Med. Chem. Lett.*, 2000, **10**, 2197-2200.

Chapter 5

Investigation of glycopolymer–lectin interactions using QCM-d: comparison of surface binding with inhibitory activity

Y. Gou, **S-J. Richards**, D. M. Haddleton, M. I. Gibson, *Polym. Chem.*, **2012**, *3*, 1634-1640

This chapter consists of a paper where the main focus was the determination of inhibitor efficacy. Two techniques were used to determine the activity of glycopolymers for the inhibition of Concanavalin A, quartz crystal microbalance with dissipation monitoring (QCM-d) and a fluorescent-linked sorbent assay (FLSA). These results were also related to another paper I contributed to – Y. Gou, J. Geng, **S-J. Richards**, J. Burns, J., C. R. Becer, D. M. Haddleton, *J. Polym. Sci., Part A: Polym. Chem.* **2013**, *51*, 2588–2597.

Yanzi Gou synthesised the polymers and carried out the QCM-d work. I tested the polymers using a FLSA and analysed the data. I helped in the preparation of the manuscript.

5.1 Abstract

Glycopolymers offer many opportunities for interfacing synthetic materials with biological systems. However, the nature of the interactions between glycopolymers and their biological targets, lectins, and the structural features necessary to obtain high-affinity materials are not fully understood. Here, the enhancement in binding affinity of multivalent glycopolymers to their corresponding lectins is investigated by quartz-crystal microbalance with dissipation monitoring. This technique allows the conformation of the adsorbed polymers to be probed and the direct observation of spanning of multiple binding sites on lectin-functional surfaces. The measured affinity was compared to the anti-adhesion activity of the polymers in solution, and it is shown that increased association constants did not directly correlate with inhibitory activity.

5.2 Introduction

Carbohydrates control many critical recognition events in biological systems, which are mediated by a class of carbohydrate binding proteins termed lectins.[1] Although these interactions are highly specific, determined by the number, branching pattern and stereochemistry of the carbohydrates, the observed sugar-protein association constants are actually quite weak. This is overcome in nature through the presentation of multiple copies of identical carbohydrates on cell surfaces, which due to the 'cluster glycoside effect',[2] results in an enhancement in the binding affinity greater than the simple linear sum of the individual carbohydrates. The exact mechanism for this binding enhancement is still unknown but is thought to arise from several complementary components: receptor clustering; chelation of multiple binding sites and statistical rebinding of carbohydrate ligands.[3-5] In order to probe

128

these phenomena and to develop new bioactive constructs capable of interfacing with biological signalling processes, synthetic glycopolymers have emerged as useful tools. By presenting tens or hundreds of copies of carbohydrates on a polymer backbone a significant increase in binding affinity compared to free sugars is observed. For example Lee *et al.* demonstrated that a tetravalent lactoside bound its lectin 100-fold stronger than the free sugar.[6] Haddleton and co-workers have demonstrated that poly(mannosylated) glycopolymers can bind to DC-SIGN (Dendritic Cell-Specific Intercellular adhesion molecule-3-Grabbing Non-integrin) with nanomolar affinities.[7] Many pathogenic species exploit carbohydrate binding as a first stage of infection: for example *Mycobacteria* (tuberculosis) and HIV both bind to DC-SIGN[8] and cholera toxin binds to galactose residues in the intestine.[9] Therefore, high-affinity multivalent constructs that can out-compete the pathogenic adhesion process can be used to *prevent* infection without actually killing the pathogen, which will help reduce evolutionary resistance. This process is termed anti-adhesion therapy, and has been reviewed extensively.[10-13] There are many examples of glycopolymers in the literature, with most studies focused on their preparation by traditional,[14] controlled polymerisation[15-18] or post-polymerisation modification[19-21] techniques, followed by simple lectin precipitation assays.[22] Cameron *et al.* have reported ITC (isothermal titration calorimetry) studies between galactosylated glycopolymers and the lectins peanut agglutinin[23] and *ricinus communis* agglutinin.[24] These studies indicated that entropic and enthalpic contributes, respectively, were important for the multivalent enhancement observed. Brewer and co-workers have undertaken detailed studies of the complex binding mechanisms of multivalent systems, using thermodynamic data. This suggests that the total affinity can be described by a series of micro-equilibria between each

binding event allowing the lectin to "bind and slide" across a carbohydrate surface.[25, 26] This results in a decreased dissociation rate constant (k_{off}) and hence an increase in overall affinity despite the weak and reversible, carbohydrate-lectin interactions. The complexity of these interactions is highlighted by studies showing that modification of carbohydrate density and linker length can improve the inhibition of cholera toxin[27] or the incorporation of a secondary sugar can improve inhibition of shiga-like toxins.[28] Rigidity also plays an important role.[29] In this work, we make use of quartz-crystal microbalance with dissipation monitoring (QCM-d) in conjunction with inhibitory assays to probe the actual mechanism of the multivalent enhancement and compare the relative activity in solution and solid-state assays. By using this technique, we reveal dramatic differences in the binding modes of glycopolymers as a function of their chain length. We provide fresh insight into the complementarity of different biophysical assays that must be tuned to their desired application, to avoid false interpretation of results.

5.3 Results and Discussion

To probe multivalent interactions we used the α-D-mannose/Concanavalin A (Con A) pairing. The rationale for using this lectin was based on there being a good understanding of its tertiary structure and its ready availability, allowing us to access traditional clustering (precipitation) assays in addition to the biophysical assays. To access a panel of α-D-mannosylated glycopolymers a post-polymerisation modification approach was used, which we have previously optimised.[20] Briefly, poly(propargylmethacrylate) was obtained by either cobalt catalysed catalytic chain transfer (CCT) or copper-mediated living radical polymerisation (CMLRP) according to published procedures Scheme 5.1 and Table 5.1.[20, 30] CCT is

particularly useful to obtain oligomers, which are challenging to access by conventional controlled radical polymerisation techniques.
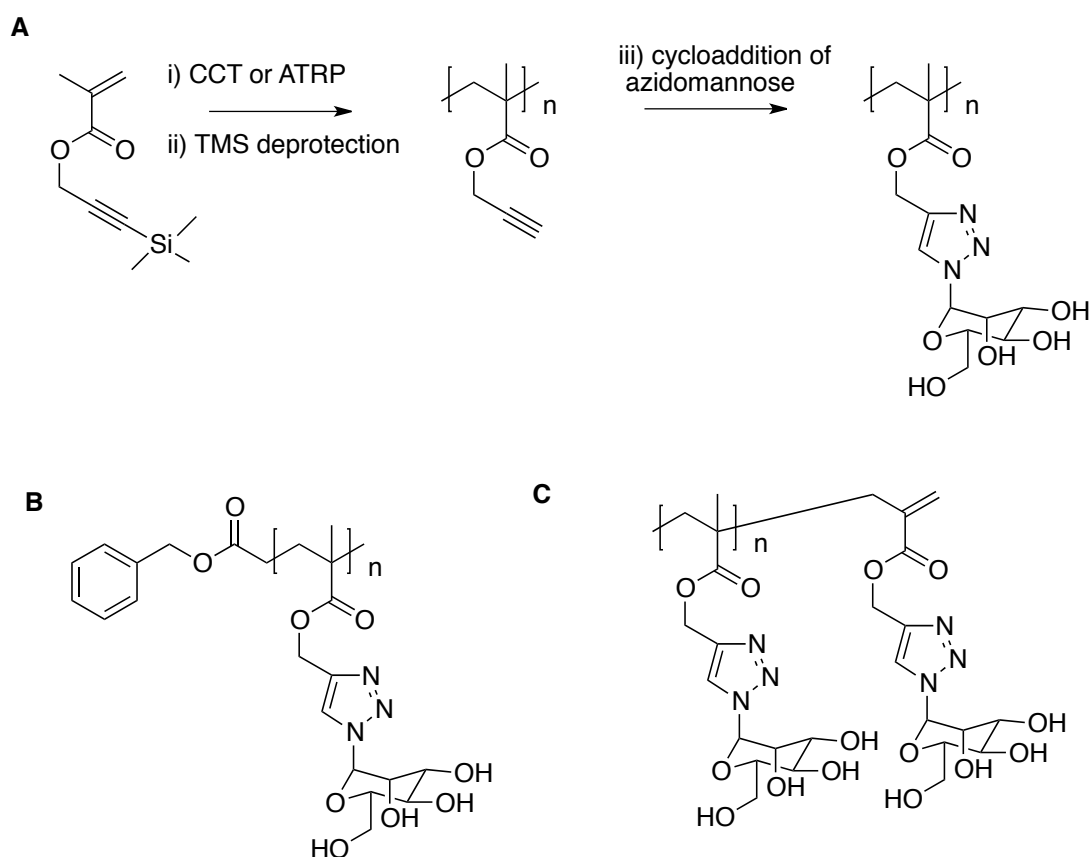
Scheme 5.1: General Synthetic Route A); structure of polymers, including end-groups obtained by CM-LRP (B) and CCT (C).

Table 5.1: α-D-mannose glycopolymers used in this study.

Polymer	Method	$M_{n(SEC)}$[a] (g.mol^{-1})	M_w/M_n[a]	$DP_{(NMR)}$[b]	l[c] (nm)
P1	CCT	4900	1.10	8	2.01
P2	CCT	11200	1.21	23	5.77
P3	CM LRP	14000	1.38	42	10.4

[a] Determined by size exclusion chromatography in DMF against PEG standards. [b] Determined by ^{1}H NMR end group analysis. [c] Approximated fully extended chain length assuming dihedral angle of 109.5 ° and C-C bond length of 0.154 nm.

Three distinct assays were selected to probe the multivalent interactions: QCM-d, fluorescence-linked sorbent assay (FLSA) and lectin precipitation/turbidimetry. Con A was immobilised onto a carboxylated quartz chip

using standard coupling protocols.[31] Figure 5.1A shows the frequency shift (Δf) observed when solutions of **P2** were flowed over the chip, giving a clear dose-dependent response, and Figure 5.1B summarises the equilibrium Δf for all polymers as function of concentration. Control experiments (at 2 mg.mL^{-1}) using β-D-galactosylated polymers gave frequency shifts below 2 Hz ruling out non-specific surface absorption.
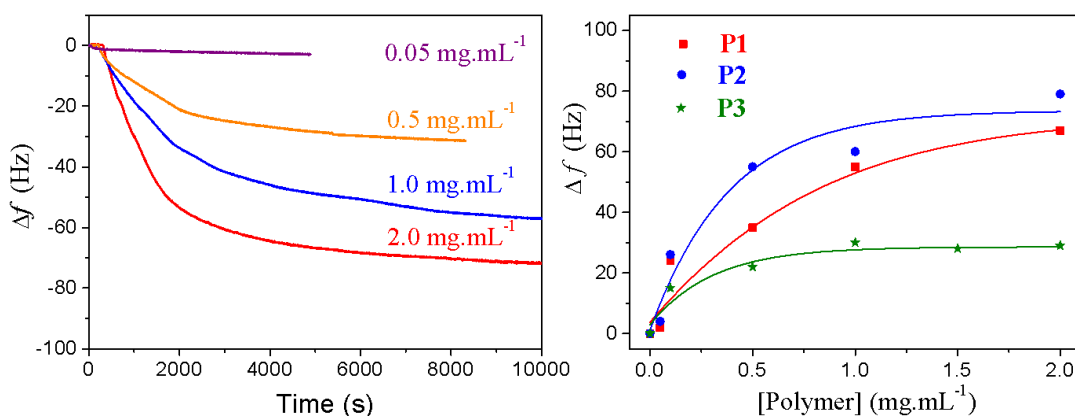
Figure 5.1: QCM of Con A functional chips and polymer. A) Frequency shift as a function of **P2** concentration. B) Equilibrium frequency shifts (Δf_{max}) for **P1-P3** as a function of concentration.

In the standard interpretation of QCM (or SPR) analysis, increased mass of glycoside binding to the lectin surface is interpreted as being due to a higher binding affinity between the sugar-protein pairing and it is used a screening method for new inhibitors.[32] The general trend with glycopolymers is that longer polymers display greater binding affinity and therefore would be expected to give larger values of Δf.[11, 24, 33] Considering this, it was surprising to find that **P1** and **P2** gave larger frequency shifts than **P3**, although careful consideration showed that **P3** reached equilibrium at far lower concentrations. The association constants of the glycopolymers were estimated using a Langmuir-type isotherm (which only gives an estimate of K_a, due to the complex micro-equilibria involved in multivalent

interactions[24-26, 33]) and compared to the total frequency shift, Table 5.2. Clearly, the total mass of **P3** absorbed onto the lectin surface was significantly less than **P1** and **P2**, but the association constant was significantly larger.

Table 5.2. Results of the protein binding assays.

	QCM			FLSA	Turbidity/Clustering		
	K_a[a] $(M^{-1}_{mannose})$	K_a[a] $(M^{-1}_{polymer})$	Δf_{max}[b] (Hz)	MIC_{50}[c] (mM)	k_i[d] $(AU.min^{-1})$	ConA: Polymer[e]	MIC_{50}[f] (mM mannose)
P1	3.83×10^4	3.07×10^5	67	0.09 ± 0.0046	n/a	n/a	n/a
P2	5.56×10^4	1.28×10^5	79	0.012 ± 0.0023	1.31	7 (3.28)	73.48
P3	1.51×10^5	6.33×10^6	28	0.017 ± 0.0034	3.75	10 (4.2)	71.48

[a] Association constant determined by QCM. [b] Maximum frequency shift observed at saturation. [c] MIC_{50} value (correct to total mannose concentration) for polymers to inhibit binding of Con A (0.5 μM) to mannosylated surface. [d] Rate of clustering of Con A/polymer in solution. [e] Quantitative precipitation assay. Number of Con A's precipitated per polymer. Number in parentheses is ratio of mannose residues per Con A tetramer precipitated). [f] MIC_{50} value for the concentration of mannose required to reverse solution aggregation of polymer/Con A mixtures. QCM = quartz crystal microbalance, FLSA = fluorescence-linked sorbent assay.

In Table 5.2, the association constant is expressed in terms of moles of polymer chains, and also concentration of carbohydrate, which is essential to avoid over-estimation of the multivalent enhancement for longer polymers (which have lower concentration of chains at equal concentration of sugars compared to short polymers). Corrected to affinity per sugar, **P1** and **P2** have very similar association constants, but **P3** is approximately double, indicating that chain length is important, but only above a certain length (*vide infra*). The huge discrepancies between these observations raise the simple questions: which polymer has the highest affinity for the lectin, and why is there such a difference?

To probe into this further, solid-phase inhibitory assays were undertaken using fluorescently labelled Con A and a mannosylated surface. Fluorescein-labelled Con A was incubated with a dilution series of the polymers on a mannosylated 96-well plate for 30 mins at 37 °C, the plates were washed and the total fluorescence

measured. This allowed construction of the inhibitory curves and determination of the minimum concentration to inhibit 50 % binding of the lectin (MIC$_{50}$), Figure 5.2.
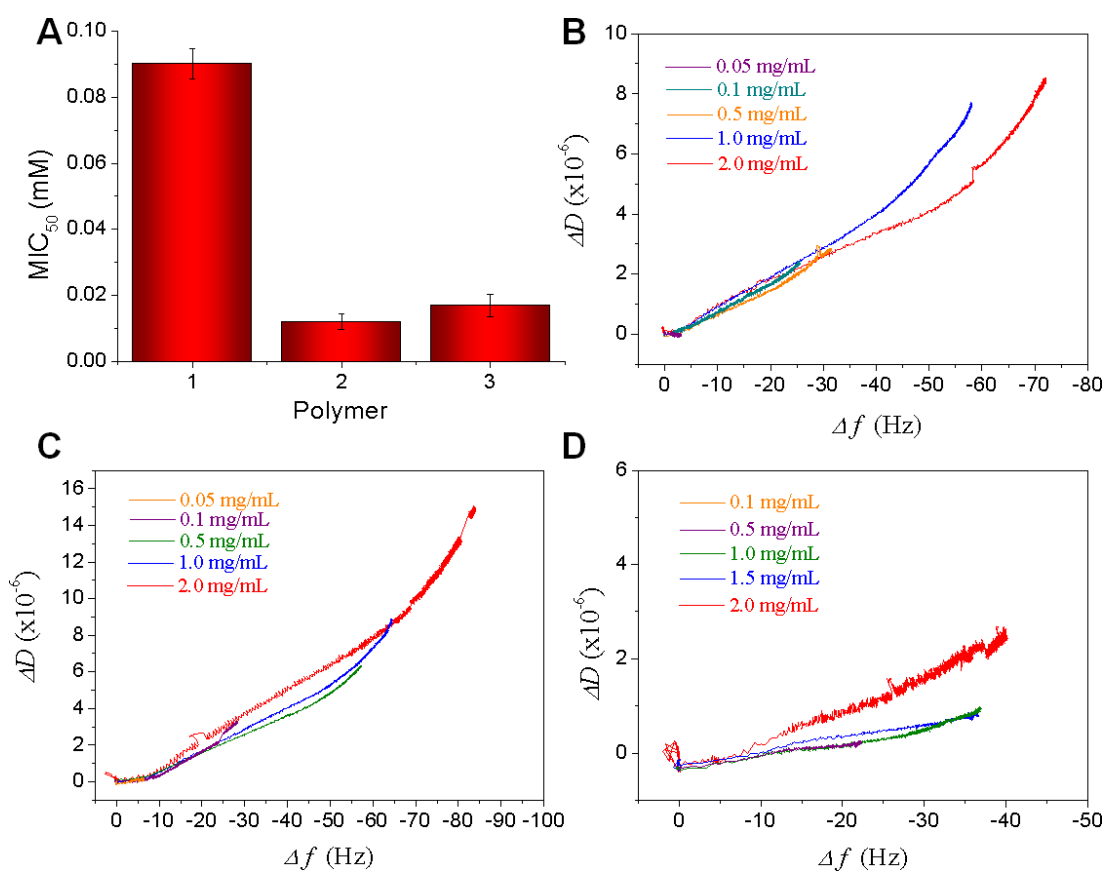
Figure 5.2: A) Solid phase inhibitory assay of Con A onto a mannosylated surface. [Con A] = 0.5µM, normalised to total mannose concentration. B-D) Frequency (Δf) verses dissipation plots (ΔD) function of polymer concentration. B) **P1**; C) **P2**; D) **P3**.

The inhibitory assay is representative of a "real" application of anti-adhesion therapies at cell surfaces and probes the *activity* of the inhibitors rather than their actual binding *affinities*.

P2 and **P3** were approximately 10x more efficacious at inhibiting the Con A compared to **P1**, which is in agreement with previous inhibitory studies.[18] This is in contrast to the QCM studies though, which suggest that **P3** has far high binding affinity than **P2**, but is capable of absorbing far less mass onto the immobilised lectin. It also suggests that binding affinity/surface absorption may not be predictive of MIC$_{50}$ and hence therapeutic potential. Classic turbidometric cluster assays

indicated **P3** had a faster clustering rate than **P2** and that it was capable of precipitating more Con A per mannose residue, with the absolute value in agreement with previous studies, even though the number of Con A per chain appears large, considering the relative size of the species in solution.[34] Interestingly, the concentrating of free mannose required to break these clusters was identical for **P2** and **P3** indicating that the rate of clustering is less important than the strength of the clusters in determining inhibitory activity. Toone *et al.* have previously discussed the discrepancies between different assays and cautioned against using single assays.[2, 35] It has been shown by ITC and haemagglutinin assays, using multivalent mannosides, that binding affinity and agglutination capacity are not predictive of each other.[16] In an attempt to shed light on these apparently contradictory observations and to gain a deeper mechanistic insight, the QCM experiments were repeated with parallel dissipation monitoring. Dissipation monitoring probes the viscoelasticity of the formed films on a surface. Large changes in dissipation (ΔD) indicate a flexible film, compared to smaller increases in D, which suggest a rigid, non-flexible coating. ΔD vs ΔF plots for **P1** and **P2** show that the dissipation signal increases in a non-linear fashion at concentrations above 1 mg.mL^{-1}, which is interpreted as the formation of a viscoelastic film. Conversely, **P3** shows a linear response with very low increases in D as F increases which is indicative of a flat, rigid film.

This difference in film structure as a function of polymer chain length indicates a significant difference in the polymers' conformation at the lectin surface. A discussion of these observations follows, which does not include consideration of the micro-equilibrium between bound and free carbohydrate, but rather the average conformation assumed by the polymer, which generates the signal in QCM-d.
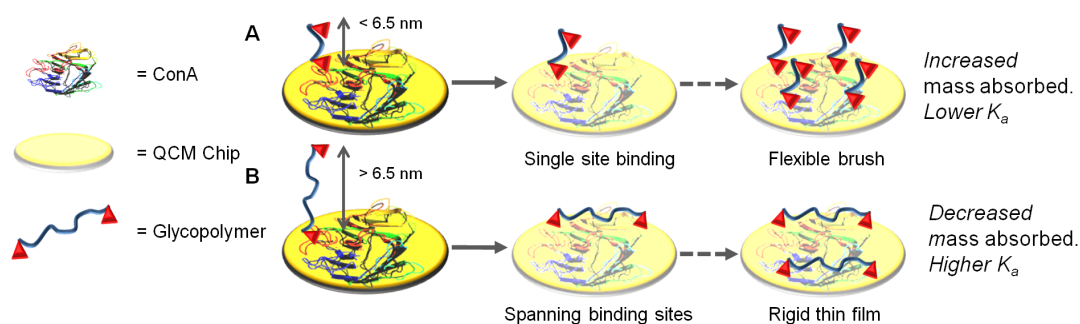
Scheme 5.2: Proposed binding mechanism of low A) and high B) molecular weight polymers onto the Con A surface. This model ignores the competition from carbohydrates on the already bound polymer chain and only represents the extreme cases when the polymer is fully extended.

Scheme 5.2A shows the case of a short (< 6.5 nm) polymers (**P1**/**P2**) which can only bind a single site on Con A, which are separated by ~ 6.5 nm.[18] As the concentration is increased, polymers from solution can either displace this binding, or bind to another vacant site (along with competition from carbohydrates on the already bound polymer). As polymer concentration increases more Con A binding sites are filled and hence a significant mass increase is observed by QCM, and the polymers adopt a brush like conformation, in agreement with the dissipation observations; agreeing with the near-identical association constants for **P1**/**P2** on a per sugar basis (Table 2). In Scheme 2B, a large (> 6.5nm) polymer (**P3**) is used. Following an initial binding event, there are two options (ignoring competition from carbohydrates on the already bound polymer): either another polymer from solution can bind to the Con A, or the already bound polymer can span to another, vacant site (bind and slide). If further polymers from solution were binding (*i.e.* competing) to vacant sites then as polymer concentration increases a larger mass increase would be expected, which would be more than seen for small (< 6.5 nm) polymers, and the dissipation signal would indicate a flexible brush like film. As this is not observed, then the mechanism must be that the already bound polymer preferentially spans multiple binding sites, which gives an increase in avidity, preventing polymers in solution

136

from displacing it (Scheme 5.2). This will result in a lower total mass of polymer compared to the short polymers and a thin, rigid, film as demonstrated by QCM-d. It should be noted that these rearrangements are only possible due to the reversible nature of the lectin-carbohydrate interactions. A previous report by Munoz *et al*. showed that different generations of mannosylated dendrimers which were too small to span multiple binding sites did not have significantly higher affinity constants towards Con A under conditions where lectin-lectin crosslinking was not possible.[33] Conversely, they showed that in inhibitory assays, increased dendrimer size led to increased potency. Similar results were observed in the present study, with **P2/P3** having equal inhibitory activity, but **P3** having a greater K_a, and the ability to span multiple binding sites. Therefore, taking into account the evidence presented in this report, and by Munoz *et al*. it would seem that in the design of inhibitors for lectin binding, that lectin-lectin crosslinking, or reduced dissociation rate constants (not obtained here) are more important than spanning binding sites (although this may play a role) on a single lectin. This can also help to explain why low valency inhibitors can display high inhibitory potency despite limited cross-linking potential.[2]

5.4 Conclusions

We have probed the mechanism of how multivalent polymeric glycoconjugates span multiple binding sites with the use of QCM-d. Glycoconjugates that are sufficiently large to span binding sites in solid phase assays-show a large K_a this did not translate to increased inhibitory potential in solution-phase assays. Furthermore, as a result of spanning binding sites, the polymers with the highest K_a actually showed the *least* total mass binding, due to the formation of a flat film, rather than extended brush

structures that are seen for short polymers. When screening multivalent glycopolymers, single-concentration measurements will not reveal the highest affinity binders unlike with monovalent carbohydrates. This work also serves to highlight the challenges in designing efficient multivalent (glycopolymer) inhibitors of lectins. Different assays identify different 'most active' polymers. Therefore, the assays most relevant to the intended application (anti-adhesion, receptor-mediated uptake *etc.*) must be used, preferably in combination with others to fully assign the mode of action. It was only possible to obtain these insights through the use of complimentary polymerisation techniques (CCT and CMLRP) that gave access to the oligomeric glycoconjugates coupled with QCM-d which reveals additional information compared to SPR or fluorescent microarray analysis. There is no intention to imply that higher valency conjugates are not useful (as it is not true), nor less active. It is also important to highlight that the present study did not probe many of the features of multivalency, such as statistical rebinding and chain flexibility or entropic contributions, but rather attempts to link surface binding to solution inhibition. While many fundamental studies have been undertaken with discrete, low molecular weigh species, synthetic polymers are more complex due to their inherent dispersity and potential differences in local chain conformation. Future studies are focusing on applying these insights to medically relevant systems and comparisons between high and low valency inhibitors.

5.5 Experimental Section

5.5.1 Materials

Copper(I) bromide, tetrabutylammonium fluoride (TBAF) in THF (1.0 M), acetic acid, 2,2'-bipyridyl (bipyridine), 2-chloro-1,3-dimethylimidazolinium chloride (DMC), sodium azide, L-fucose, mannan, concanavalin A (Con A) and FITC-labelled Con A were purchased from Sigma-Aldrich. Triethylamine was purchased and used directly from Fisher Scientific. 3-(Trimethylsilyl)-2-propyn-1-ol, D-(+)-mannose was purchased from Alfa-Aesar. CoBF, 2-bromo-2-methyl-propionic acid benzyl ester initiator[36] and the ligand *N*-ethyl-2-pyridylmethanimine[37] were prepared as described previously. All other reagents and solvents were purchased at the highest purity available from Sigma-Aldrich and used without further purification unless stated. Ultrahigh quality water with a resistance of 18.2 MΩ cm (at 25 °C) was obtained from a Millipore Milli-Q gradient machine fitted with a 0.22 μm filter.

5.5.2 Physical and analytical methods

^{1}H and ^{13}C NMR spectra were recorded on Bruker DPX-300 and DPX-400 spectrometers using deuterated solvents obtained from Sigma-Aldrich. SEC was conducted on a Varian 390-LC system in DMF (1 g.L^{-1} LiBr) at 50 °C, equipped with refractive index and viscometry detectors, 2 x PLgel 5 μm mixed-D columns (300 x 7.5 mm), 1 x PLgel 5 μm guard column (50 x 7.5 mm) and an autosampler. Data were analysed using Cirrus 3.2 software. Molecular weight was determined relative to narrow poly(methyl methacrylate) standards. All the QCM-d experiments were performed using the Q-Sense E4 System with four sensor chambers for four parallel measurements at 25 °C The system was equipped with QE 401 Electronics Unit, QCP 401 Chamber Platform, and QFM 401 Flow Module with Ismatec IPCN

139

Pump. The quartz crystal chip was an optically polished Au coated quartz sensor (AT-cut; diameter: 14 mm; thickeness: 0.3 mm; surface roughness of electrode <3 nm; electrode layer: 10–300 nm) with fundamental resonant frequency 5 MHz. UV-vis and fluorescence measurements were undertaken on a Biotech Synergy HT and processed using the Gen5 software package or Microcal Origin.

5.5.3 Synthetic procedures

Trimethyl-silyl propargyl methacrylate: A solution of trimethylsilyl propyn-1-ol (40.0 g, 312 mmol) and triethylamine (TEA) (56.6 mL, 406 mmol) in diethyl ether (250 mL) was cooled to 0 °C. A solution of methacryloyl chloride (45 mL, 406 mmol) in diethyl ether (150 mL) was added dropwise into the mixture using a dropping funnel. The mixture was stirred at this temperature for 1 h and at ambient temperature overnight under nitrogen. The solution was passed through a basic alumina column and washed with diethyl ether. After removal of the volatiles under reduced pressure, the crude product was purified by kugelrohr distillation. 47.4 g of colourless oil was obtained as the product (yield = 77.4 %)

^{1}H NMR (400 MHz, CDCl$_3$, 298 K): δ(ppm) = 0.20 (s, 9H, Si(CH$_3$)$_3$), 1.94 (s, 3H, CH$_3$C=CH$_2$), 4.80 (s, 2H, OCH$_2$), 5.58 (s, 1H, C=CHH), 6.07 (s, 1H, C=CHH);

^{13}C NMR (100 MHz, CDCl$_3$, 298 K): δ(ppm) = 0 (3C, Si(CH$_3$)$_3$) 17.9 (1C, CH$_3$C=CH$_2$), 52.7 (1C, OCH$_2$), 91.1 (1C, C=CSi(CH$_3$)$_3$), 100.3 (1C, C≡CSi(CH$_3$)$_3$), 126.7 (1C, CH$_3$C=CH$_2$), 135.3 (1C, CH$_3$C=CH$_2$), 166.6 (1C, C=O). ESI-MS: m/z = 219.0 [M + Na]$^+$.

CCTP of TMS-protected propargyl methacrylate: In a typical polymerisation, CoBF (5.0 mg) was dissolved in MEK (10 mL), which was previously freeze–pump–thawed 3 times. AIBN (50 mg) was added to a Schlenk tube containing a magnetic stirrer, followed by addition of TMS-protected propargyl methacrylate (10 mL). The solution was freeze–pump–thawed three times and then filled with nitrogen. The CoBF solution (500 μL) was added into the Schlenk tube and the mixture was stirred at 60 °C under nitrogen overnight. At the end of the reaction, the mixture was diluted with 20 mL of MEK and bubbled with air for 2 hours. The volatiles were removed by distillation under reduced pressure and the polymer was used for deprotection (conversion = 88%; M_n = 3100 g.mol^{-1}, M_w/M_n = 1.4).

Deprotection of TMS-protected polymers: The TMS-protected polymers (2 g, 10.2 mmol TMS groups) and acetic acid (3 g, 51 mmol) were dissolved in THF (100 mL) bubbled for ten minutes and the solution was cooled to 20 °C. A 0.2 M solution of TBAF (15.3 mmol) in THF was added dropwise into the mixture. The resulting solution was stirred at this temperature for 1 hour and then warmed to ambient temperature. After stirring overnight an Amberlite IR-120 ion-exchange resin was added and stirred with the reaction mixture for 2 hours. The resin was removed by filtration and the resulting solution was concentrated under reduced pressure. The polymer was purified by precipitation in petroleum ether (boiling fraction 30–40 °C, 0.6 g, yield = 47.6%; M_n = 5400 g.mol^{-1}, M_w/M_n = 1.34).

Synthesis of α-D-Mannopyranosyl azide: D-(+)-Mannose (10 g, 55.5 mmol) 2-chloro-1,3-dimethylimidazolinium chloride (28.2 g, 0.167 mol) diisopropylethylamine (DIPEA) (96.7 mL, 0.55 mol) and sodium azide (36.1 g, 0.55

mol) were dissolved in H_2O (200 mL). After stirring for 5 h at 0 °C, the reaction mixture was concentrated under reduced pressure and ethanol (200 mL) was added. The resulting white solid was removed by filtration and the volatiles were removed under reduced pressure. The yellowish crude product was dissolved in H_2O (80 mL) again and washed with dichloromethane (3 x 100 mL), before being passed through a short column of prewashed Amberlite IR-120. The resulting aqueous solution was freeze-dried to give α-D-mannopyranosyl azide as an off-white solid.

^{1}H NMR (400 MHz, D_2O, 298 K): δ(ppm) = 3.65 (m, 1H, CHCH$_2$), 3.74 (m, 1H, CH), 3.77 (m, 2H, CH$_2$), 3.89 (m, 1H,CH), 3.94 (m, 1H, CH), 5.48 (d, J = 1.7 Hz, 1H, CH); ^{13}C NMR (100.59 MHz, D_2O, 298 K): δ(ppm) = 60.82 (CH$_2$), 66.40 (CH), 69.77 (CH), 69.84 (CH), 74.65 (CHCH$_2$), 89.74 (CHN$_3$). ESI-MS: m/z = 228.1 [M + Na]$^+$.

Alkyne–azide cycloaddition: The alkyne-functional polymer (0.1 g, 0.81 mmol alkyne groups), α-D-mannopyranosyl azide (0.305 g, 1.61 mmol), 2,2'-bipyridine (25.2 mg, 0.16 mmol) and TEA (23 mL, 0.165 mmol) were dissolved in DMSO (3 mL). The solution was freeze–pump–thawed 3 times before being cannulated over to another Schlenk tube which was previously evacuated and filled with nitrogen, containing Cu(I)Br (12 mg, 0.084 mmol). The resulting brown solution was stirred at ambient temperature for 3 days. At the end of the reaction, the solution was passed through a short neutral alumina column and washed with DMSO. The mixture was transferred to a dialysis tube and dialysed against water for 3 days, followed by freeze-drying to give the glycopolymer as a white solid (0.21 g, yield = 79% conversion = 100%; M_n = 14 000 Da, M_w/M_n = 1.38).

5.5.4 Inhibitory assays

Quartz Crystal Microbalance: Functionalisation of Au chip with concanavalin A. Au chips were cleaned in a mixture of 35% of NH_3, 33% of H_2O_2 and Milli-Q water (1 : 1 : 5, v/v) for 10 min and then rinsed with Milli-Q water and dried by a stream of nitrogen. Then the chips were immediately immersed into the solution of 10 mM 11-mercaptoundecanoic acid (MUA) in ethanol and kept over-night at ambient temperature to obtain a thiol self-assembled monolayer (SAM) on the gold surfaces. The gold chips were washed with ethanol and Milli-Q water sequentially and then immersed into a freshly prepared water solution of 0.4 M 1-[3-(dimethylamino)propyl]-3-ethyl carbodiimide (EDC) hydrochloride and 0.1 M *N*-hydroxysuccinimide (NHS) (1 : 1, v/v) to activate the carboxyl groups on the Au surface. After being washed with Milli-Q water and dried with a stream of nitrogen, the gold chips were mounted in the QCM-d cell. HBS buffer was run through the system until flat baselines of frequency and dissipation were achieved. Con A was immobilised on the surface by passing Con A buffer solution (0.1 mg mL^{-1}) over the quartz crystal chip until no further changes in frequency were observed, followed by ethanolamine hydrochloride (1 M, pH 8.5) until a stable baseline was observed, to block any residual NHS groups.

HBS buffer (10 mM HEPES, 0.15 M NaCl, pH 7.4) containing 1 mM metal ions (Ca^{2+}, Mg^{2+}, and Mn^{2+}) was pumped through the QCM-d system at a flow rate of 50 mL.min^{-1} until stable baselines of both frequency and dissipation signals were obtained. Solutions of the glycopolymers, in the same buffer, were then injected at concentrations between 0.05 and 2 mg.mL^{-1} and the experiment continued until equilibrium was reached. To estimate the association constant, a Langmuir isotherm was used, according to eqn (1), which is then rearranged to eqn (2):

143

$$\Delta f = \Delta f_{\max} \frac{K_a\,[ligand]}{1+K_a\,[ligand]} \qquad (1)$$

$$\frac{1}{\Delta f} = \frac{1}{\Delta f_{\max} K_a\,[ligand]} + \frac{1}{\Delta f_{\max}} \qquad (2)$$

where Δf is the measured frequency shift; $\Delta f_{\max}$ the frequency shift at saturation; K_a the association constant; and [ligand] the concentration of analyte. The association constant can be obtained by a linear fit to the plot of $1/\Delta f$ against $1/[\text{ligand}]$.

Fluorescence Linked Sorbent Assay: Microtitre plates were incubated for 16 h with 180 µL of 0.1 mg ml^{-1} mannan dissolved in phosphate-buffered saline (PBS) per well. Unattached mannan was removed by washing extensively with PBS. Polymer solutions were made up as serial dilutions in PBS from 0.1 mg mL^{-1}. 20 µL of 0.3 mg mL^{-1} Con A–FITC in PBS was added to 80 µL of each polymer solution to result in 0.5 µM ConA–FITC. 100 µL of the polymer Con A-FITC solutions were added to the mannosylated surfaces and incubated at 37 C for 30 min. Fluorescence was then measured at excitation/emission wavelengths of 485/528 nm. All experiments were carried out in triplicate. Percentage inhibition was compared to relative to controls of pure Con A (with no polymer).

Quantitative precipitation: The assay was followed a modified procedure.[4, 21] Con A was dissolved in the HBS buffer (0.1 M HEPES, 0.9 M NaCl, 1 mM MgCl$_2$, 1 mM CaCl$_2$ and 1 mM MnCl$_2$, pH 7.4) to make fresh stock solution and the concentration was 60 mM (assuming Con A tetramers with a molecular weight of 106 kDa). Glyco polymer solutions in HBS buffer were also prepared with a series of different concentrations. Then Con A solution and the glycopolymer solution were mixed (1 : 1, v/v) and incubated for 5 hours at 22 °C. The final concentration of

Con A was 30 µM. White precipitates were separated from solution by centrifugation at 5000 x g for 2 minutes, followed by removal of the supernatants very carefully using a pipette. Then the pellets were resuspended in cold buffer again. These washing steps were repeated twice. After removal of the supernatants, the precipitates were dissolved in a HBS buffer solution of methyl-α-D-mannopyranoside (1 mL, 1 M). With complete dissolution, the Con A content was determined by measuring the absorbance at 280 nm.

Lectin agglutination assay: This was conducted according to previously published procedures.[21] Con A was dissolved in HBS buffer (approximately 1 mg.mL^{-1}). The exact concentration of Con A was determined by measuring the absorbance at 280 nm ($A_{280} = 1.37$ x [mg.mL^{-1} Con A]). The solution was then diluted to 1 µM. After addition of 0.5 mL of glycopolymer (50 mM) into a dry polycarbonate cuvette (1 mL, 1 cm pathlength), the cuvette was placed in the UV spectrometer. By adding 0.5 mL of the diluted Con A solution into the cuvette *via* a pipette, the absorbance of the mixture was quickly recorded at 420 nm for 10 min every 0.12 s. The relative rate of interaction was determined by a linear fit of the steepest portion of the initial aggregation. Each experiment was repeated 3 times.

Reverse aggregation assay: As previously described,[4] following the turbidity measurement, the absorbance A_{420} of the solution after 2 hours at room temperature was recorded as A_{420} (t = 0). Then 0.1 mL of methyl-α-D-mannopyranoside (54 mM) in HBS buffer solution was added to the cuvette. The mixed solution was quickly placed in the spectrometer and the absorbance at 420 nm was recorded for 10 minutes. A_{420} (t = 10) was calculated as an average of the last 10 seconds of each

experiment. The percent change in absorbance was determined as (A_{420} (t = 0) - A_{420} (t = 10))/A_{420} (t = 0).

5.6 References

1.   M. Ambrosi, N. R. Cameron and B. G. Davis, *Org. Bio. Chem.*, 2005, **3**, 1593-1608.

2.   J. J. Lundquist and E. J. Toone, *Chem. Rev.*, 2002, **102**, 555-578.

3.   C. R. Bertozzi and L. L. Kiessling, *Science*, 2001, **291**, 2357-2364.

4.   C. W. Cairo, J. E. Gestwicki, M. Kanai and L. L. Kiessling, *J. Am. Chem. Soc.*, 2002, **124**, 1615-1619.

5.   L. L. Kiessling, J. E. Gestwicki and L. E. Strong, *Angew. Chem. Int. Ed.*, 2006, **45**, 2348-2368.

6.   Y. C. Lee, R. R. Townsend, M. R. Hardy, J. Lonngren, J. Arnarp, M. Haraldsson and H. Lonn, *J. Biol. Chem.*, 1983, **258**, 199-202.

7.   C. R. Becer, M. I. Gibson, J. Geng, R. Ilyas, R. Wallis, D. A. Mitchell and D. M. Haddleton, *J. Am. Chem. Soc.*, 2010, **132**, 15130-15132.

8.   H. Feinberg, D. A. Mitchell, K. Drickamer and W. I. Weis, *Science*, 2001, **294**, 2163-2166.

9.   T. Beddoe, A. W. Paton, J. Le Nours, J. Rossjohn and J. C. Paton, *Trends Biochem. Sci.*, 2010, **35**, 411-418.

10.   A. Imberty, Y. M. Chabre and R. Roy, *Chem. Eur. J.*, 2008, **14**, 7490-7499.

11.   S. G. Spain and N. R. Cameron, *Polym. Chem.*, 2011, **2**, 60-68.

12.   G. Mulvey, P. I. Kitov, P. Marcato, D. R. Bundle and G. D. Armstrong, *Biochimie*, 2001, **83**, 841-847.

13. Y. Miura, D. Koketsu and K. Kobayashi, *Polym. Adv. Technol.*, 2007, **18**, 647-651.

14. M. Ambrosi, A. S. Batsanov, N. R. Cameron, B. G. Davis, J. A. K. Howard and R. Hunter, *J. Chem. Soc., Perkin Trans. 1*, 2002, 45-52.

15. S. G. Spain, M. I. Gibson and N. R. Cameron, *J. Polym. Sci. A Polym. Chem.*, 2007, **45**, 2059-2072.

16. L. Albertin, M. H. Stenzel, C. Barner-Kowollik, L. J. R. Foster and T. P. Davis, *Macromolecules*, 2005, **38**, 9075-9084.

17. M. I. Gibson, C. A. Barker, S. G. Spain, L. Albertin and N. R. Cameron, *Biomacromolecules*, 2009, **10**, 328-333.

18. M. Kanai, K. H. Mortell and L. L. Kiessling, *J. Am. Chem. Soc.*, 1997, **119**, 9931-9932.

19. M. A. Gauthier, M. I. Gibson and H.-A. Klok, *Angew. Chem. Int. Ed.*, 2009, **48**, 48-58.

20. N. Vinson, Y. Gou, C. R. Becer, D. M. Haddleton and M. I. Gibson, *Polym. Chem.*, 2011, **2**, 107-113.

21. V. Ladmiral, G. Mantovani, G. J. Clarkson, S. Cauet, J. L. Irwin and D. M. Haddleton, *J. Am. Chem. Soc.*, 2006, **128**, 4823-4830.

22. S. R. S. Ting, G. Chen and M. H. Stenzel, *Polym. Chem.*, 2010, **1**, 1392-1412.

23. M. Ambrosi, N. R. Cameron, B. G. Davis and S. Stolnik, *Org. Biomol. Chem.*, 2005, **3**, 1476-1480.

24. S. G. Spain and N. R. Cameron, *Polym. Chem.*, 2011, **2**, 1552-1560.

25. T. K. Dam and C. F. Brewer, *Biochemistry*, 2008, **47**, 8470-8476.

26. S. M. Dimick, S. C. Powell, S. A. McMahon, D. N. Moothoo, J. H. Naismith and E. J. Toone, *J. Am. Chem. Soc.*, 1999, **121**, 10286-10296.

27. B. D. Polizzotti and K. L. Kiick, *Biomacromolecules*, 2006, **7**, 483-490.

28. A. Miyachi, H. Dohi, P. Neri, H. Mori, H. Uzawa, Y. Seto and Y. Nishida, *Biomacromolecules*, 2009, **10**, 1846-1853.

29. S. Liu and K. L. Kiick, *Macromolecules*, 2008, **41**, 764-772.

30. L. Nurmi, J. Lindqvist, R. Randev, J. Syrett and D. M. Haddleton, *Chem. Commun.*, 2009, 2727-2729.

31. Y. Gou, S. Slavin, J. Geng, L. Voorhaar, D. M. Haddleton and C. R. Becer, *ACS Macro Lett.*, 2012, **1**, 180-183.

32. M. Fais, R. Karamanska, S. Allman, S. A. Fairhurst, P. Innocenti, A. J. Fairbanks, T. J. Donohoe, B. G. Davis, D. A. Russell and R. A. Field, *Chem. Sci.*, 2011, **2**, 1952-1959.

33. E. M. Munoz, J. Correa, E. Fernandez-Megia and R. Riguera, *J. Am. Chem. Soc.*, 2009, **131**, 17765-17767.

34. J. E. Gestwicki, C. W. Cairo, L. E. Strong, K. A. Oetjen and L. L. Kiessling, *J. Am. Chem. Soc.*, 2002, **124**, 14922-14933.

35. J. B. Corbell, J. J. Lundquist and E. J. Toone, *Tetrahedron: Asymmetry*, 2000, **11**, 95-111.

36. N. J. Hovestad, G. van Koten, S. A. F. Bon and D. M. Haddleton, *Macromolecules*, 2000, **33**, 4048-4052.

37. D. M. Haddleton, M. C. Crossman, B. H. Dana, D. J. Duncalf, A. M. Heming, D. Kukulj and A. J. Shooter, *Macromolecules*, 1999, **32**, 2110-2119.

Chapter 6

Gold nanoparticle-linked analysis of carbohydrate-protein interactions, and polymeric inhibitors, using unlabelled proteins; easy measurement using a 'simple' digital camera.

L. Otten, **S.-J. Richards**, E. Fullam, G. S. Besra, M. I. Gibson, *J. Mater Chem. B.*, **2013**, *1*, 2665-2675

This chapter contains the published paper describing a novel inhibitor detection method. Here we used gold nanoparticles synthesised by the citrate reduction method to determine inhibitor efficacy by illuminating the protein concentration.

Lucienne was a project student that I supervised. Together we did all the synthesis, testing and prepared the manuscript.

6.1 Abstract

Traditional methods of measuring the affinity of lectins (or other carbohydrate-binding proteins) to their target carbohydrates rely on the use of chemically/recombinantly-modified proteins in sorbent assays, microarrays, or the use of expensive label-free methods such as surface plasmon resonance spectrometry. In this work we exploit the extremely high extinction coefficient (*i.e.* colour) of gold nanoparticles as resolving agents in sorbent assays. The anionic nanoparticles adhere strongly to immobilised proteins, but not to the carbohydrate-surfaces allowing investigation of protein binding and screening of novel multivalent inhibitors. Furthermore, the use of a simple digital camera (or mobile phone) to obtain the data is shown, providing an ultra-low cost route to the detection of native, carbohydrate-binding proteins.

6.2 Introduction

Carbohydrate-protein recognition events are responsible for a plethora of biological processes including host-pathogen interactions, immune signalling, fertilisation, cancer metastasis, blood group markers and many more. Pathogenic infection is often driven by an initial carbohydrate-protein binding event such as neuraminic acid/heamaglutinin (influenza),[1, 2] GM1 ganglioside/cholera toxin (cholera)[3] and gp120/DC-SIGN (HIV)[4], often through binding to lectins: a subset of carbohydrate-binding proteins which are neither enzymes nor antibodies. Inhibition of these binding events, to prevent infection, is termed anti-adhesion therapy and has been extensively studied for both mono- and multivalent carbohydrate derivatives.[5-9] The binding affinity of carbohydrates (and hence their potential utility) is often enhanced by the multivalent presentation of individual carbohydrates on a polymeric/dendritic

scaffold ('glycopolymer'[10]), due to the 'cluster glycoside effect',[5, 11] where the polymer binding affinity increases to an extent greater than the linear sum of the individual carbohydrates' binding affinities. The mechanisms and applications of these materials are currently under intensive investigation, but are often focused on model lectins, which are widely available and have well characterised interactions. Despite there being many carbohydrate-protein interactions being known, there still remains a huge number of carbohydrate-mediated processes (covering recognition, uptake, trafficking and binding) which are poorly characterised and hence causes a bottle-neck in the design of new therapeutics or diagnostics.[12] For example, the structure of the oligosaccharide responsible for human sperm binding was only recently elucidated despite many years of intense study.[13] In part, this is due to the challenge associated with obtaining usable quantities of complex glycans or their derivatives, compared to other biomacromolecules (DNA, proteins) that can be recombinantly expressed and/or amplified and obtained by solid-phase chemical synthesis.[14, 15] In order to evaluate carbohydrate-protein interactions; there is also a need to isolate and characterise usable quantities of the protein prior to any analysis. Standard methods for evaluating these interactions include both solution and solid phase based assays. Isothermal Titration Calorimetry (ITC) provides detailed information about the energetics of the binding interactions, but is time consuming, not high throughput and can consume a relatively large amount of material and requires specialised equipment.[16] Sometimes, direct fluorescence assays probing tryptophan/tyrosine residues can be used, but this is not always the case. A further problem of solution interactions is that many carbohydrates are normally immobilised on the surface of a cell/virus, providing an adhesion site, rather than as mobile solutes. To address this, surface plasmon resonance (SPR) is frequently

employed. SPR allows direct measurement of the binding of a biomacromolecule onto an appropriately functionalised gold surface using minimal quantities of each compound.[17, 18] However, SPR equipment is specialised, often not high-throughput, is expensive and not routinely available in all laboratories. Other surface methods such as quartz-crystal microbalance (QCM) and optical waveguide lightmode spectroscopy (OWLS) have similar problems and benefits.[19] It should be noted that immobilisation of the protein on surfaces, rather than carbohydrates is convenient but limited by the signal detection (which is essentially proportional to mass) which cannot detect small molecule binding. ELISA (enzyme-linked immunosorbent assay) and fluorescence-linked assays have found wide-spread use due to their lower equipment level requirement (microplate reader) and excellent sensitivity limits.[20, 21] A key challenge of sorbent assays is the need to use labelled proteins, rather than unmodified versions. Recombinant methods can introduce enzymatic or antigen tags which themselves can alter the function of the protein and direct chemical labelling of isolated proteins with fluorophores (such as fluorescein isothiocyanate) can provide detection, but gives rise to heterogeneous distributions of labels, which leads to well-known problems in terms of altering ligand binding affinities.[22-24] Fluorescent labels are often not photostable presenting challenges in quantitative analysis.[25] the challenges associated with carbohydrate immobilisation, or the generation of labelled carbohydrates should not be underestimated.[26]

Considering that monitoring of these interactions has huge potential in the development of novel anti-adhesion therapies or diagnostics, any technology which simplifies this process, is compatible with native proteins and relies on readily available imaging platforms could have profound benefit. Gold nanoparticles (AuNPs), which display an extremely strong coloration due to their surface plasmon

band have been shown to strongly adhere to proteins by electrostatic interactions. For example, colloidal gold has been used to stain native proteins separated by electrophoresis on gels,[27] or those on microplates[28] allowing colourimetric detection. While useful, this technique has not found widespread use, has not been optimised in terms of particle size, nor has it been used to screen for novel inhibitors of lectin binding. Other uses of AuNPs in imaging has also been reviewed extensively,[29-31] especially with regard to their aggregation-sensitive properties,[32] contrast agents in biological electron microscopy[33] and photothermal imaging.[34]

Herein we describe the use of AuNPs as resolving agents to allow quantification of protein absorption onto carbohydrate functionalised microplate surfaces and to use it as an accessible tool to probe multivalent inhibitors which are potential prophylactic antibacterial agents without the need for fluorescence detection is investigated. This visualisation should reduce the need for expensive, complicated and low throughput analytical facilities and inaccessible, labelled, protein samples. The use of a simple digital camera to probe these interactions is also studied as an ultra-low cost alternative.

6.3 Results and Discussion

The aim of this work was to use citrate-stabilised AuNPs as resolving agents for direct measurement of (unlabelled) protein binding onto carbohydrate-functional surfaces, taking advantage of their extremely strong colouration. Here it is exploited to screen novel anti-adhesion therapies without the need for labelled proteins, and to test the validity of direct 'visual' analysis of protein binding using a simple digital camera as an ultra-low cost platform.[35] The concept is outlined in Figure 6.1.
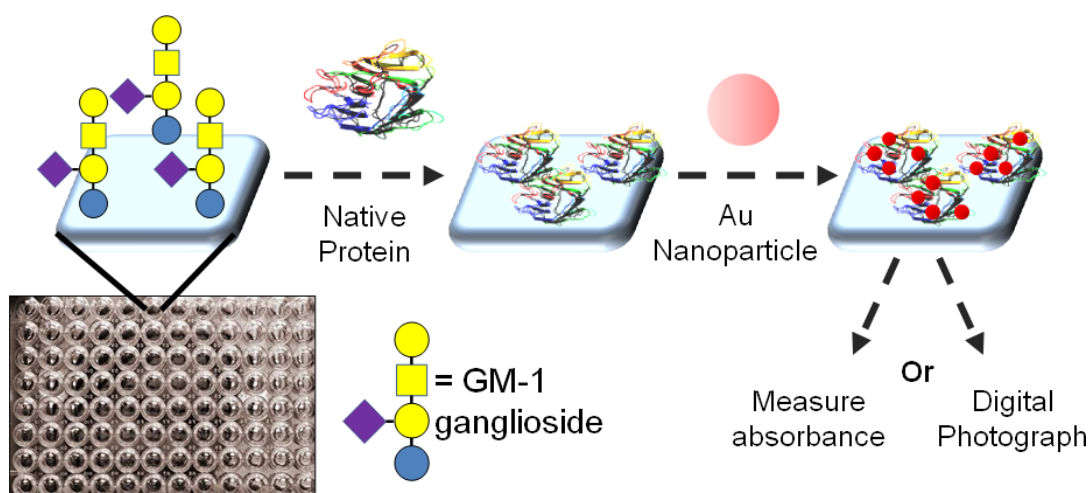
Figure 6.1: Overview of the approach used to allow direct measurement of lectin-carbohydrate binding by visualisation of surface-bound protein using AuNP on microtitre plates.

A small panel of citrate-stabilised AuNP were obtained using the standard citrate/HAuCl$_4$ reduction approach.[36, 37] This method was chosen as it is simple, scalable and gives rise to charged nanoparticles, which are essential for strong non-specific protein interactions (*vide infra*). Table 6.1 summarises the synthesis of AuNPs used in this study that characterised by UV-visible spectroscopy and dynamic light scattering (DLS) to provide an estimate of their dimensions, which were in the range of 30 – 70 nm.

Table 6.1: Citrate-stabilised AuNP used in this study.

Code	[Citrate]:[Gold][a]	λ_{spr}[b] (nm)	Particle size (UV)[c] (nm)	Particle size (DLS) (nm)	PDI[d]
AuNP1	3.5:1	526	36 nm	36	0.35
AuNP2	2.5:1	541	76 nm	76	0.58
AuNP3	1.5:1	545	70 nm	130	0.38

[a] Molar ratio of trisodium citrate to HAuCl$_4$ used in the synthesis of the nanoparticles. [b] Location of the surface plasmon peak in the UV-visible spectrum of the particles. [c] Particle size estimated by the method of Haiss *et al*.[38] [d] Polydispersity index of the particles, obtained by DLS.

The key requirement of this study is that the citrate-coated AuNP interact with proteins that have bound to carbohydrates immobilised onto the surface of

microtitre plates, providing the necessary visualisation (red colour) to determine the extent of protein binding. To test the hypothesis, two different surfaces were prepared in 96-well microtitre plates designed to promote or inhibit AuNP binding. BSA (bovine serum albumin) was directly adsorbed onto high-binding plates to provide a 'protein rich' surface and the GM1 ganglioside, which presents a carbohydrate-surface, was also immobilised. These surfaces were subsequently exposed to a 0.3 mg.mL^{-1} solution of **AuNP 1** for 30 minutes, washed with Milli-Q water, and then their UV-Vis spectra measured, Figure 6.2A. The BSA surface clearly shows absorbance at ~ 520 nm, attributable to AuNP absorbing to the protein surface, whereas the GM1 surface shows no signal. The branched oligosaccharide component of GM1 presents a highly hydrated ('non-fouling' type[39]) surface that will not interact electrostatically with the anionically charged AuNPs. The three different AuNPs listed in Table 1 were subsequently evaluated with BSA surfaces as a function of AuNP concentration to determine the optimum conditions and detection limits Figure 6.1B. Across the AuNP concentration range of 0–1 mg.mL^{-1}, the smallest nanoparticles (3.5:1 [citrate]:[Au]) gave the largest signal intensity. To maximise the signal intensity, all subsequent tests were undertaken by exposing the protein-bound surfaces to **AuNP1** at 1 mg.mL^{-1} (total Au mass).
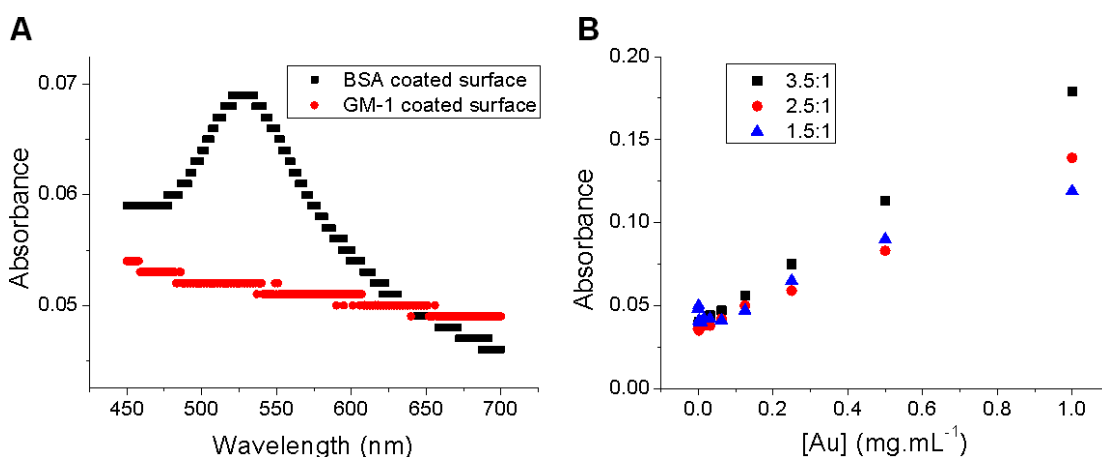
Figure 6.2: Evaluation of AuNP-surface interactions. A) UV-Visible spectra of BSA-coated surface (black trace) and GM1 coated surface (red trace) following addition of **AuNP1**. B) Absorbance intensity of the protein-bound wells at 525 nm as a function of added AuNP concentration, onto to BSA-coated microtitre plates. Legend shows ratio of [citrate]:[Au] used in preparation of the nanoparticles.

To evaluate the utility of AuNP as a reliable, scalable, accessible and economic alternative to standard SPR/QCM/ELISA type measurements of carbohydrate-protein interactions a representative panel of lectins were selected with and without, fluorescent labels to allow us to validate this approach. Mannose-functional surfaces were obtained by coating microtitre plates with mannan, and galactose-functional plates by coating with GM1. Concanavalin A (Con A) was used as a mannose-specific lectin, and peanut agglutinin (PNA) and the B-subunit of the cholera toxin (CTxB) as distinct galactose-specific lectins, Table 6.2.

Table 6.2: Coatings and lectins used in this study.

Coating	Carbohydrate-ligand	Lectin
Mannan	α-D, 1-6 linked mannose	Concanavalin A
GM1	β-D Galactose	Cholera Toxin B-subunit
GM1	β-D Galactose	Peanut Agglutinin

Figure 6.3 shows the dose-dependant binding of PNA to GM1 as a function of PNA concentration, with binding measured by fluorescence (A) or by addition of 50 μL of

1 mg.mL^{-1} **AuNP-1**. (B). Both binding curves have similar profiles and give

calculated K_d's of 72.7 nM (AuNP) and 90.9 nM (fluorescence) respectively. The

strong agreement shows that AuNPs are useful and can be used to analyse complex

interactions without the need for specialised equipment, or labelled proteins.
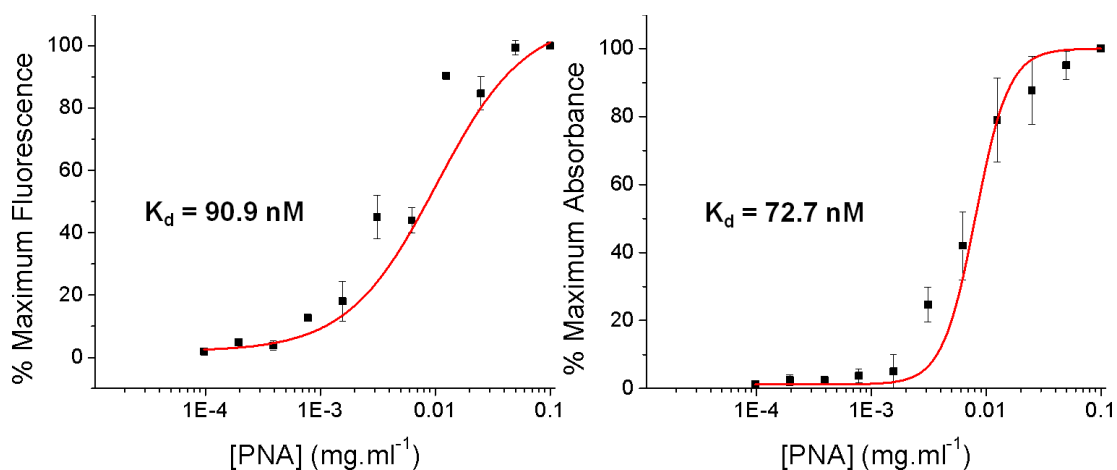
Figure 6.3: Dose-dependant binding curves of PNA onto GM1 functional surfaces. A) Fluorescence measurements (FITC - excitation/emission 485/528 nm). B) AuNP absorbance at λ_{max}. Errors bars represent $\pm$ standard deviation from a minimum of 3 repeats.

Similar results were obtained when the Con A/Mannan system were analysed

(Appendix 4). Furthermore, the AuNPs-resolved microplates were not observed to

degrade overtime. After two weeks storage, identical data was obtained in contrast to

fluorescence or enzymatic methods that suffer from photo bleaching or denaturation,

respectively. It should be noted that although the AuNPs will most likely bind each

protein to a different extent, this does not affect the measurements shown here,

which are probing equilibrium process and hence all that is required is a dose-

response curve with clear start and end points.

A more medically relevant subset of lectins for study is those secreted by

pathogenic bacteria that are key targets for prophylactic anti-adhesion therapy. The

toxin secreted by the pathogen *Vibrio cholerae* binds to GM1 on epithelial cells and is the causative agent of cholera infection. Figure 6.4. K_d values obtained for CTxB by were AuNP was 0.19 μM and by fluorescence 0.18 μM again showing exceptional agreement.
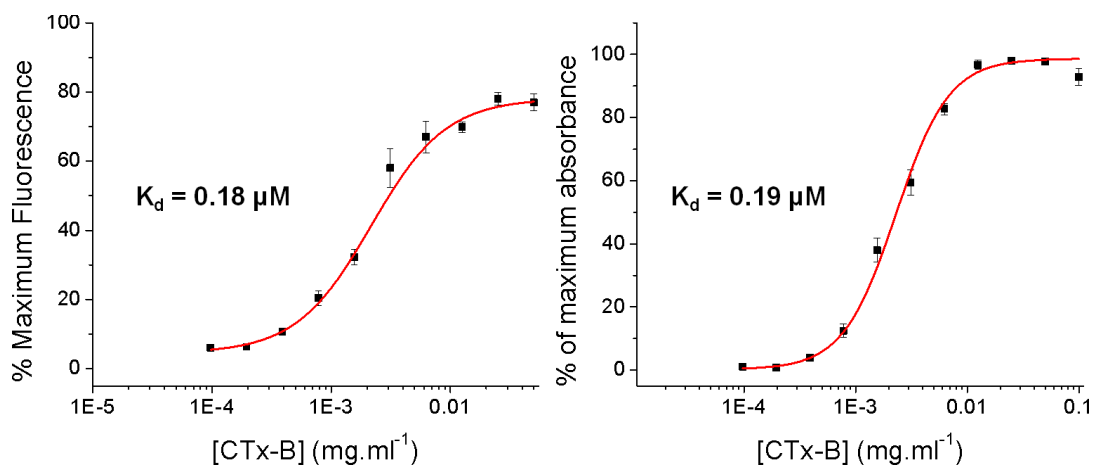

Figure 6.4: Dose-dependant binding curves of CTxB onto GM1 functional surfaces. A) Fluorescence measurements (FITC - excitation/emission 485/528 nm). B) AuNP absorbance at λ_{max}. Errors bars represent ± standard deviation from a minimum of 3 repeats.

The data presented above shows that AuNP based measurement of protein binding is comparable to fluorescence methods. We are ultimately interested in probing the inhibition of pathogenic toxins, and therefore the Au-system was applied to a competitive binding experiment. We and others have demonstrated that synthetic glycopolymers, presenting many copies of a single carbohydrate on their side chain display high binding affinities to lectins due to the cluster glycoside effect.[40, 41] Recently we demonstrated that modulation of the distance between polymer backbone and carbohydrate can improve the affinity of poly(galactoside)s for CTxB due to an improved fit to its (relatively) deep binding site (See Chapter 2). Here, three synthetic glycopolymers which were prepared by tandem post-polymerisation

modification[42] with precise control over valency and linker length were assayed for their ability to inhibit CTxB binding, Figure 6.5.
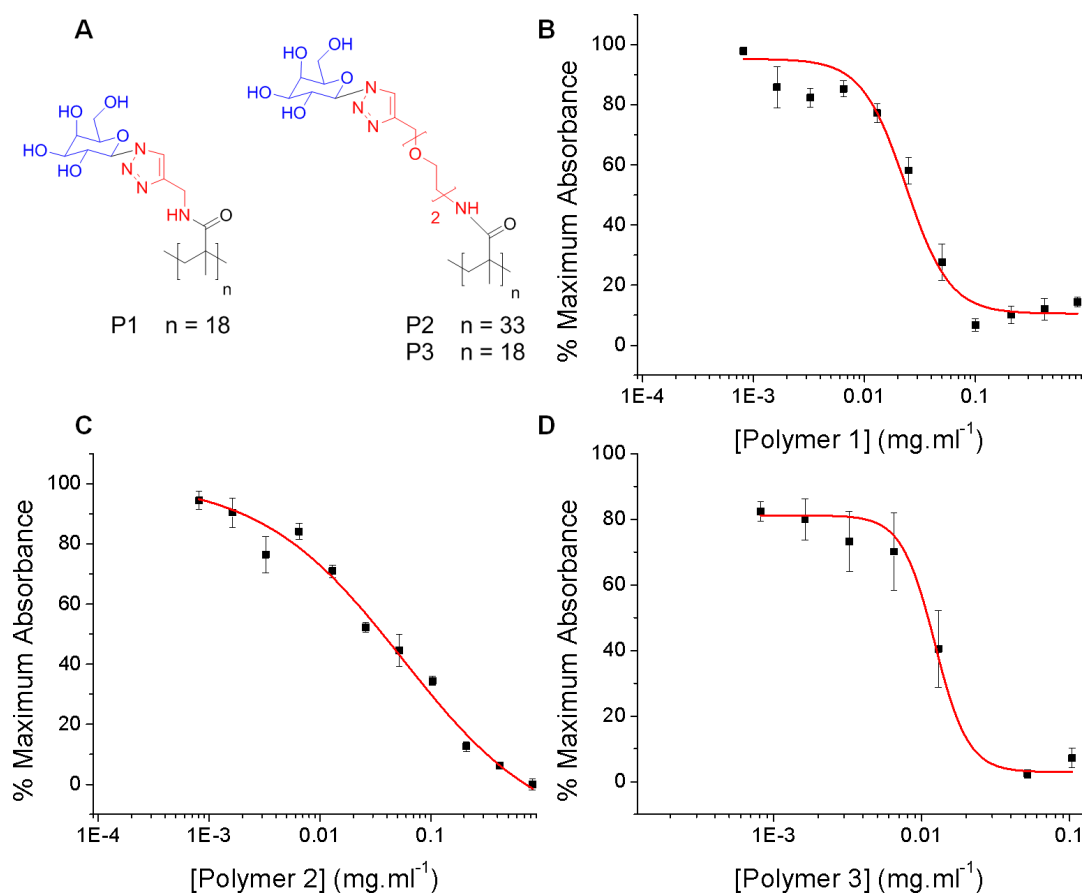
Figure 6.5: Inhibition of CTxB binding by β-D galacto-functional glycopolymers. A) Structure of glycopolymeric inhibitors. B), C), D) Inhibitory curves of Polymers **1**, **2** and **3** respectively, with CTxB, measured using AuNP method. Errors bars represent ± standard deviation from a minimum of 3 repeats.

P1 with a short linker showed the highest MIC_{50} values (lowest affinity) of 56 μg.mL^{-1} whereas the polymers with longer linkers (**P2/P3**) had approximately identical MIC_{50} values or 23 and 24 μg.mL^{-1} respectively (on a per-carbohydrate and mass–basis), which is in strong agreement with previously published observations.[41] On a per-polymer basis, **P3** was the most active, but this is biased by its higher molecular weight and hence lower molar concentration. MIC_{50} corrected to carbohydrate concentration indicates that **P3** and **P2** have identical activity and

therefore in the case of CTxB, there is no additional benefit of increasing chain length above 18 units (although further benefit by even larger polymers cannot be discounted). Compared to free galactose, all polymers were at least 100 x more active highlighting the cluster glycoside effect (Table 3). This method is therefore suitable, and amenable to high-throughput screening of lectin inhibition using unlabelled proteins.

Table 6.3: Inhibitory potency of glycopolymers against CTxB determined by gold nanoparticle method.

Polymer	DP_n[a]	Linker[b]	MIC_{50}	MIC_{50}[c] [Polymer]	MIC_{50} ([Galactose])
P1	18	Short	56 ± 2.4 $\mu g.mL^{-1}$	9.4 ± 0.4 μM	0.169 ± 0.072 mM
P2	33	Long	23 ± 18 $\mu g.mL^{-1}$	1.6 ± 1.2 μM	0.055 ± 0.43 mM
P3	18	Long	24 ± 11 $\mu g.mL^{-1}$	3.2 ± 1.46 μM	0.057 ± 0.027 mM

[a] Number average degree of polymerisation of polymer (= galactose/chain). [b] Refers to length of spacer between polymer and carbohydrate shown in Figure 5. [c] MIC_{50} adjusted in terms of concentration of polymer chains; [d] MIC_{50} adjusted in terms of total galactose concentration. The polymers used were reported in a previous study.[41] Error bars represent the standard deviation in the individual IC_{50} from each individual measurement (minimum of 3 repeats).

6.3.1 Measuring binding using digital photography

During the above-described experiments, it was observed that upon addition of AuNPs to the protein-functional plates, sufficient gold was deposited to allow visual examination of protein binding, due to the intense red colouration of AuNPs (their extinction coefficients are typically 100 – 1000 larger than fluorescence dyes). Figure 6.6A shows a photograph of a GM1 microplate following incubation with a dilution series of CTxB, revealed by addition of AuNPs. Strong red colouration can be seen at high concentrations of CTxB, with the colour decreasing in line with decreasing protein concentrations. This visual read-out is potentially useful for low-cost diagnostic applications, rapid protein-binding assays in laboratories or 3rd world applications, particularly if it can be linked to a mobile phone or digital camera

system. This would remove the need for a plate reader or similar whilst maintaining the ability to obtain quantitative data.[35] The AuNP-exposed plates were photographed using a standard digital camera (see Experimental section) and imported into image analysis software. The average pixel intensity of each well was measured and plotted against concentration of protein added, Figure 6.6B. Impressively, near identical binding curves were obtained compared to those in Figure 6.5 (CTxB by absorbance/fluorescence), with K_d values close to that obtained by either fluorescence or absorbance.
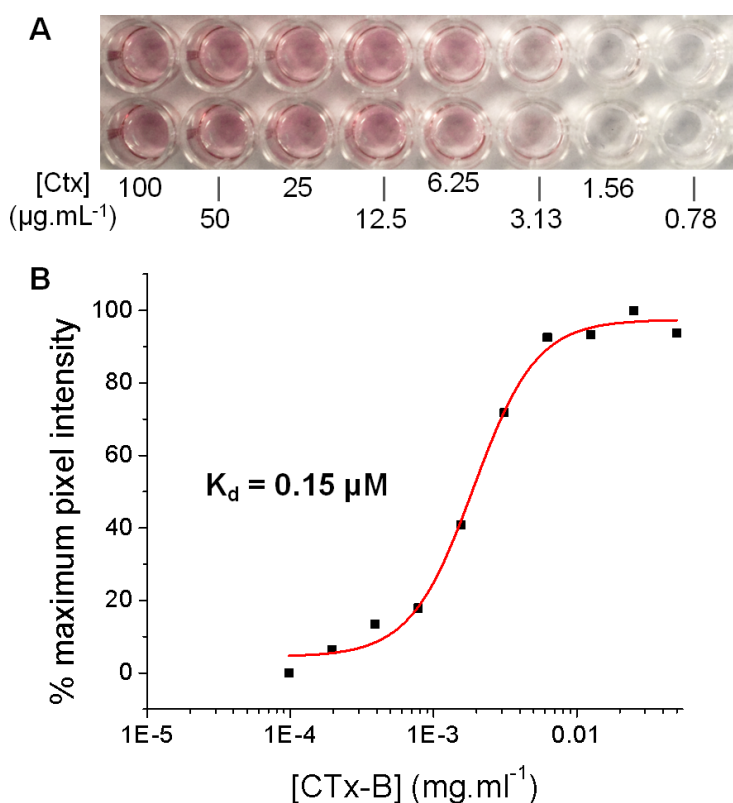
Figure 6.6: Direct optical analysis of protein binding. A) Digital photograph of GM1 functional microplates treated with a dilution series of CTxB and following developing with AuNPs for 30 minutes. B) Binding curve obtained by pixel-counting direct from digital photographs.

Figure 6.7 shows the correlation between average pixel intensity and both total fluorescence or absorbance. This analysis gave a strong positive correlation linear

fits with R^2 values above 0.98. This offers the opportunity for quantitative evaluation of lectin binding/inhibition in laboratories lacking in dedicated glycomics facilities and would be compatible with a cellular-phone based analytical system.
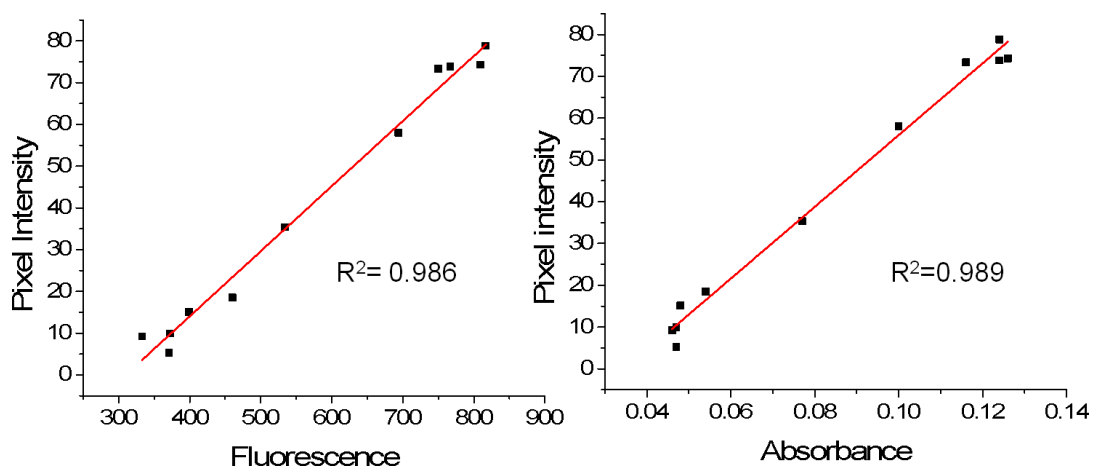
Figure 6.7: Comparison of signal intensities obtained by pixel-counting methods verses AuNP and traditional fluorescence measurements.

6.4 Conclusions

In this study, we have investigated the use of citrate-coated AuNPs as resolving agents to analyse protein binding to surfaces, as a low-cost, accurate glycomics tool. Carbohydrate-coated surfaces were incubated with their corresponding lectins and their binding isotherms were measured by direct fluorescence-linked assays and by absorbance measurements based on AuNP absorption. Strong correlation was found between the two methods; with the AuNP method having the advantage that it removes the need to use labelled proteins and can be read with a standard microplate reader, without the need for fluorescence measurements. To demonstrate the applicability of this, a series of multivalent glycopolymers were screened for their ability to inhibit the binding of CTxB, as a model of a pathogenic infection process. Finally, due to the extremely strong colouration of the AuNP resolved surfaces, it was possible to use a digital camera to simply image the microplates and use image

analysis software to extract binding isotherms, which showed strong correlation to those obtained by fluorescence or absorbance measurements. This presents the opportunity to use AuNP resolving agents for label free, low cost, high-throughput evaluation of carbohydrate-protein interactions that may have diagnostic or screening applications. In particular, it allows rapid testing of inhibitors and concentrations ranges prior to more detailed biophysical analyses (e.g. SPR/QCM).

6.5 Experimental Section

6.5.1 Materials

Concanavalin A (Con A), fluorescein isothiocyanate (FITC) labelled Con A, peanut agglutinin (PNA) from Arachis hypogaea, FITC labelled PNA, monosialotetrahexosylganglioside (GM1), bovine serum albumin (BSA), cholera toxin subunit B (CTxB), FITC labelled CTxB, mannan, preformulated phosphate buffered saline tablets (PBS), calcium chloride (CaCl$_2$), sodium chloride (NaCl), HEPES, Tris buffer, trisodium citrate dehydrate and chloroauric acid (HAuCl$_4$) where all purchased from Sigma-Aldrich, UK. 96-well high binding microtitre plates were purchased from Greiner Bio-one. Galactose-functional polymers used in this study have been previously reported and their synthesis is summarised in the Appendix 4.[43] Phosphate buffered saline (PBS) was prepared using preformulated tablets dissolved in 200 mL of Milli-Q water (with resistance >18 MΩ) cm, to give final concentration of NaCl = 0.138 M, [KCl] = 0.0027 M and pH = 7.4. 10 mmol Tris buffer containing 0.1 mmol CaCl$_2$ and 0.5 mmol NaCl (pH 8, TBS) was prepared in 250 mL of Milli-Q water (with a resistance >19 MΩ cm).

6.5.2 Physical and analytical methods

Absorbance and fluorescence measurements were made using a BioTek Synergy HT multi-detection microplate reader and Gen5 software. Dynamic light scattering was conducted using a Nano Zetasizer ZS from Malvern Instruments, UK. Scattered light was detected at 173 ° and the observed count rated recorded. Hydrodynamic radii (where appropriate) were determined using the manufacturer's software. Diameters are an average of three measurements using at least 10 scans. All protein binding curves were plotted in OriginPro (version 8.6) and the built in nonlinear curve fitting tool was used to fit a logistic curve to the data and to calculate the MIC_{50} values are defined as being the concentration of inhibitor required to reduce the binding of the lectin to the carbohydrate surface by 50 % of its maximal value. Absorbance graphs were produced by plotting the absorbance measurement at 530 nm against concentration. A linear regression analysis for the paired cholera toxin data was preformed in the open-source statistical package R (version 2.14.1). Picture of AuNP modified wells were taken using a Nikon D60 camera with automatic exposure settings from a distance of 30 cm using ambient light conditions.

6.5.3 Synthetic procedures

Functionalisation of multiwall plates: High binding 96-well plates were incubated for 16 h with 180 μL of 0.1 mg.mL^{-1} mannan, GM1 or BSA dissolved in PBS per well. After incubation, unbound mannan, GM1 or BSA was removed by washing with distilled water, after which the plates were dried and stored at 4 °C. The same procedure was also used for GM1 (0.1 mg.mL^{-1}), bovine serum albumin (BSA) (0.1 mg.mL^{-1}).

Gold nanoparticle synthesis: Sodium citrate capped gold nanoparticles were produces by chemically reducing chloroauric acid ($HAuCl_4$) with trisodium citrate dehydrate as the capping agent. An aqueous solution of trisodium citrate dehydrate (2 mL, 0.13 mmol) was added to a boiling solution of $HAuCl_4$ (35 mL, 0.35 mmol) under reflux and vigorous stirring producing a ratio of 3.5:1 (sodium citrate:$HAuCl_4$). After addition of the trisodium citrate dihydrate the solution went from pale yellow to dark blue before eventually turning deep red (about 30 minutes after addition of the trisodium citrate dihydrate). After which the solution was cooled and then stored in the dark at 4 °C. Solutions were also produced using the ratios 2.5:1 and 1.5:1 following the same procedure but using different ratios of $HAuCl_4$ to trisodium citrate dihydrate.

Lectin binding assays: 96-well microtitre plates were incubated for 16 h with 180 mL of 0.1 mg.mL^{-1} GM1 dissolved in PBS, per well. Unbound GM1 was removed by washing extensively with PBS and then water. Polymer solutions were made up as serial dilutions (up to 10 dilutions per sample in TBS from 1 mg.mL^{-1}). 20 μL of 12.5 mg.mL^{-1} CTxB in TBS was added to 100 μL of each polymer solution to result in a final concentration of 2 μg.mL^{-1} CTxB per well. 100 μL of the polymer/CTxB solutions were then added to the GM1-coated wells and incubated at 37 °C for 30 min. After this time, they were extensively washed with Milli-Q water. 50 μL of AuNP solution was then added to each well before incubation at 37 °C for 30 min. After extensive washing with Milli-Q water, absorbance in each well was measured between 450 and 700 nm in 1 nm steps. All experiments were carried out in triplicate.

Digital camera-linked assay and image analysis: Microplates were prepared as described above, and the CTxB lectin applied, washed and AuNP added following the above described procedures. A digital photograph of the AuNP- modified plates was taken from a distance of 30 cm using ambient light and the tiff image file uploaded into the open-source image processing package ImageJ (version 1.46a) where a region of interest (ROI) saturation and brightness (HSB) stack of images and the saturation image used. The ROIs drawn on the original image were added to the saturation image using the ROI manager and average pixel intensity in each region of interest was measured using an inbuilt function in ImageJ. An example image showing the colour change achieved by gold binding to protein bound to GM1 is shown in Figure 6.6.

6.6 References

1.   R. Schauer, *Glycoconjugate J.*, 2000, **17**, 485-499.

2.   G. K. Hirst, *J. Exp. Med.*, 1948, **87**, 301-314.

3.   T. R. Hirst, S. Fraser, M. Soriani, A. T. Aman, L. de Haan, A. Hearn and E. Merritt, *Int. J. Med. Microbiol.*, 2002, **291**, 531-535.

4.   T. B. H. Geijtenbeek, D. S. Kwon, R. Torensma, S. J. van Vliet, G. C. F. van Duijnhoven, J. Middel, I. Cornelissen, H. Nottet, V. N. KewalRamani, D. R. Littman, C. G. Figdor and Y. van Kooyk, *Cell*, 2000, **100**, 587-597.

5.   G. Mulvey, P. I. Kitov, P. Marcato, D. R. Bundle and G. D. Armstrong, *Biochimie*, 2001, **83**, 841-847.

6.   A. Imberty, Y. M. Chabre and R. Roy, *Chem. Eur. J.*, 2008, **14**, 7490-7499.

7.   S. G. Spain and N. R. Cameron, *Polym. Chem.*, 2011, **2**, 60-68.

8.   R. J. Pieters, *Org. Biomol. Chem.*, 2009, **7**, 2013-2025.

9. P. I. Kitov, J. M. Sadowska, G. Mulvey, G. D. Armstrong, H. Ling, N. S. Pannu, R. J. Read and D. R. Bundle, *Nature*, 2000, **403**, 669-672.

10. S. G. Spain, M. I. Gibson and N. R. Cameron, *J. Polym. Sci. A Polym. Chem.*, 2007, **45**, 2059-2072.

11. J. J. Lundquist and E. J. Toone, *Chem. Rev.*, 2002, **102**, 555-578.

12. X. Hong, M. Z. Ma, J. C. Gildersleeve, S. Chowdhury, J. J. Barchi, Jr., R. A. Mariuzza, M. B. Murphy, L. Mao and Z. Pancer, *ACS Chem. Biol.*, 2013, **8**, 152-160.

13. P.-C. Pang, P. C. N. Chiu, C.-L. Lee, L.-Y. Chang, M. Panico, H. R. Morris, S. M. Haslam, K.-H. Khoo, G. F. Clark, W. S. B. Yeung and A. Dell, *Science*, 2011, **333**, 1761-1764.

14. C. R. Bertozzi and L. L. Kiessling, *Science*, 2001, **291**, 2357-2364.

15. K. T. Pilobello and L. K. Mahal, *Curr. Opin. Chem. Biol.*, 2007, **11**, 300-305.

16. S. G. Spain and N. R. Cameron, *Polymer Chemistry*, 2011, **2**, 1552-1560.

17. E. A. Smith, W. D. Thomas, L. L. Kiessling and R. M. Corn, *J. Am. Chem. Soc.*, 2003, **125**, 6140-6148.

18. C. R. Becer, M. I. Gibson, J. Geng, R. Ilyas, R. Wallis, D. A. Mitchell and D. M. Haddleton, *J. Am. Chem. Soc.*, 2010, **132**, 15130-15132.

19. F. Hook, J. Voros, M. Rodahl, R. Kurrat, P. Boni, J. J. Ramsden, M. Textor, N. D. Spencer, P. Tengvall, J. Gold and B. Kasemo, *Colloids Surf., B*, 2002, **24**, 155-170.

20. E. Engvall and P. Perlmann, *Immunochemistry*, 1971, **8**, 871-&.

21. R. M. Lequin, *Clin. Chem.*, 2005, **51**, 2415-2418.

22. T. Kodadek, *Chem. Biol.*, 2001, **8**, 105-115.

23. Y. Fei, Y.-S. Sun, Y. Li, K. Lau, H. Yu, H. A. Chokhawala, S. Huang, J. P. Landry, X. Chen and X. Zhu, *Mol. Biosyst.*, 2011, **7**, 3343-3352.

24. Y. S. Sun, J. P. Landry, Y. Y. Fei and X. D. Zhu, *Langmuir*, 2008, **24**, 13399-13405.

25. C. Eggeling, J. Widengren, R. Rigler and C. A. M. Seidel, *Anal. Chem.*, 1998, **70**, 2651-2659.

26. K. Larsen, M. B. Thygesen, F. Guillaumie, W. G. T. Willats and K. J. Jensen, *Carbohydr. Res.*, 2006, **341**, 1209-1234.

27. R. Rohringer and D. W. Holden, *Anal. Biochem.*, 1985, **144**, 118-127.

28. C. M. Stoscheck, *Anal. Biochem.*, 1987, **160**, 301-305.

29. R. A. Sperling, P. Rivera gil, F. Zhang, M. Zanella and W. J. Parak, *Chem. Soc. Rev.*, 2008, **37**, 1896-1908.

30. H. Jans and Q. Huo, *Chem. Soc. Rev.*, 2012, **41**, 2849-2866.

31. V. W. K. Ng, R. Berti, F. Lesage and A. Kakkar, *J. Mater. Chem. B*, 2013, **1**, 9-25.

32. S. Gupta, H. Andresen and M. M. Stevens, *Chem. Commun.*, 2011, **47**, 2249-2251.

33. C. Freese, M. I. Gibson, H.-A. Klok, R. E. Unger and C. J. Kirkpatrick, *Biomacromolecules*, 2012, **13**, 1533-1543.

34. C. Pache, N. L. Bocchio, A. Bouwens, M. Villiger, C. Berclaz, J. Goulley, M. I. Gibson, C. Santschi and T. Lasser, *Opt. Express*, 2012, **20**, 21385-21399.

35. A. W. Martinez, S. T. Phillips, E. Carrilho, S. W. I. Thomas, H. Sindi and G. M. Whitesides, *Anal. Chem.*, 2008, **80**, 3699 - 3707.

36. J. Turkevich, P. C. Stevenson and J. Hillier, Discuss. Faraday Soc., 1951, **11**, 55-75.

37.   G. Frens, *Nat. Phys. Sci.*, 1973, **241**, 20-22.

38.   W. Haiss, N. T. K. Thanh, J. Aveyard and D. G. Fernig, *Anal. Chem.*, 2007, **79**, 4215-4221.

39.   J. Wang, M. I. Gibson, R. Barbey, S.-J. Xiao and H.-A. Klok, *Macromol. Rapid Commun.*, 2009, **30**, 845-850.

40.   M. W. Jones, S. J. Richards, D. M. Haddleton and M. I. Gibson, *Polym. Chem.*, 2013, **4**, 717-723.

41.   S.-J. Richards, M. W. Jones, M. Hunaban, D. M. Haddleton and M. I. Gibson, *Angew. Chem. Int. Ed.*, 2012, **51**, 7812-7816.

42.   N. K. Singha, M. I. Gibson, B. P. Koiry, M. Danial and H.-A. Klok, *Biomacromolecules*, 2011, **12**, 2908-2913.

43.   S.-J. Richards, M. W. Jones, M. Hunaban, D. M. Haddleton and M. I. Gibson, *Angew. Chem. Int. Ed.*, 2012, **51**, 7812-7816.

Section 2: Detection

Chapter 7

Discrimination between bacterial phenotypes using glyconanoparticles and the impact of polymer coating on detection readouts

S-J. Richards, E. Fullam, G. S. Besra, M. I. Gibson, *J. Mater Chem. B.*, **2014**, *2*, 1490-1498

This chapter consists of the paper describing the used of glyco-gold nanoparticles as a detection method for bacteria based on their colourimetric properties. Saline stability and speed of read-out were investigated and their effect on detector efficacy.

I carried out the particle synthesis and the lectin and bacterial testing. Elizabeth started the overnight cultures for me and assisted in the bacterial testing work. I prepared the manuscript.

7.1 Abstract

The identification and treatment of bacterial infections remains a major healthcare challenge, especially to ensure appropriate application of a limited spectrum of antibiotics. Here we describe a system capable of discriminating between different strains of *Escherichia coli* using multivalent, carbohydrate-functionalised, gold nanoparticles based upon their different expression levels of the FimH adhesin. Upon binding of the glycosylated nanoparticles to FimH positive bacteria, the nanoparticles' optical properties change enabling the identification of bacteria strain. Comparison between direct conjugation, or *via* a linker, of the carbohydrate to the nanoparticle revealed significant effects on the performance of the detection system. Using a poly(ethylene glycol) spacer increased the stability, and specificity, of the glycosylated nanoparticles but also reduced aggregation upon bacterial binding. This prevented the well-know red to blue gold colour change, meaning spectrophotometric, rather than optical, assessment methods were required. Using this method, FimH positive bacteria could be detected at approximately 1.5×10^7 colony forming units/mL.

7.2 Introduction

Due to their widespread overuse, and the emergence of resistance, antibiotics are becoming less effective and agents that were once last resort are now being used more frequently. This has lead to a looming major healthcare crisis, with few new antibiotics in the pipeline, new strategies to treat and identify bacterial infections are urgently required.[1, 2] Standard clinical methods for the detection and identification of bacterial pathogens such as *E. coli*, rely upon selective conventional culturing and plating of bacteria from a contaminated sample and conclusive results typically

require 24 hours or more. Despite being sensitive and accurate, it does not provide real-time, on-site feedback and requires sophisticated equipment and often immunoassays using fluorescence or radiolabelling.[3-5] A direct, label-free method for bioanalyte detection that is easy, sensitive even at low sample volume, high-throughput and quantifiable in real-time is critical to applications in clinical diagnostics and the real-time detection of environmental and biological toxins.[6]

Gold nanoparticles (AuNPs) have been intensively studied in bioanalytical applications due to their characteristic optical properties. They are also good alternatives to fluorescently or radiolabelled substrates used in bioassays because they are inexpensive, simple to synthesise, have high photo-stability and can be conjugated efficiently to biological molecules.[6, 7] AuNPs exhibit an intense colour in the visible region due to a local surface plasmon resonance (LSPR) that arises due to the collective oscillation of the conduction-band electrons of the gold core.[6, 8-10] These optical properties are strongly correlated with their size, shape, dispersion media and degree of aggregation making them ideal sensors. Aggregation of AuNPs leads to a dramatic colour change from red to blue/purple. This is due to electric dipole-dipole interactions and coupling between the plasmons of neighbouring particles.[6, 8-10] Triggered changes in their aggregation can be readily observed by eye and quantitative analysis only requires a UV-Vis spectrometer. It is for this reason that AuNPs are attractive for the detection of biomolecules.[8, 11] The colour changes associated with AuNP aggregation have been exploited in the development of colourimetric assays using AuNPs functionalised with biomolecules such as proteins,[7, 12] peptides,[11] antibodies,[13-18] and DNA.[19, 20] The detection of bacterial DNA using AuNPs originated in the pioneering work of Mirkin *et al.*,[20] who demonstrated that as little as 10 fmol of an oligonucleotide analyte could be detected

by exploiting the aggregation phenomenon of AuNPs. Many groups have used AuNP-based sensors in an immunoassay format, whereby disease markers can be detected using AuNPs conjugated to appropriate antibodies.[12, 14, 16, 17] The *in situ* generation of gold nanoparticles guided by enzymes has also been exploited to create ultra sensitive sensors for the detection of prostate cancer and HIV antigen p24.[21] Rotello *et al.* have developed gold nanoparticle sensors, whereby bacteria adhesion to the nanoparticles releases β-galactosidase from the surface, activating a pro-fluorescent label, providing detection of the presence of bacteria, but not the phenotype.[22]

Protein-carbohydrate interactions mediate many critical biological recognition processes, such as those involved in cell signalling, fertilisation, and inflammation, and in particular, they mediate the adhesion of viruses and bacterial toxins to their native targets.[23, 24] The proteins responsible for deciphering this information are termed lectins, which specifically (and noncovalently) bind carbohydrates.[25, 26] The protein–saccharide interactions are usually weak, but are amplified by clustered saccharides, resulting in a binding constant, which is greater than the simple sum of the total number of ligands. This observation is referred to as the 'cluster glycoside' effect.[27, 28] Considering this information, carbohydrate functionalised AuNPs (glycoAuNPs) are attractive biosensors as they are inherently multivalent and should give optical responses upon protein binding to their surface, providing the platform for new sensors.[8, 10, 29] There have been many reports of using mannose or glucose functional AuNPs to interact with Concanavalin A (Con A) as a model protein.[8-10, 29-32] Con A, however, is not an indicated target for biosensing. A more relevant target for carbohydrate-based bioanalytical platforms are outer membrane-exposed lectins on the surface of bacteria (or indeed viruses), which are

involved in cellular adhesion to the glycocalyx of mammalian cell[33, 34] One of the most important and most investigated bacterial lectins is the mannose/glucose-specific protein FimH, which is expressed on the tips of type 1 fimbriae on *E. coli*. These fimbriae are uniformly distributed on *Enterobacteriaceae*, commonly between 100 and 400 fimbriae per cell.[34] Alexander and co-workers have employed thermoresponsive glycopolymers to reversibly aggregate FimH expressing bacteria upon changing the external temperature.[35] Disney *et al*. used fluorescent glycopolymers to detect FimH positive bacteria, but this required an isolation step limiting the sensory application.[4] AuNPs have been reported to bind to fimbriae, but identification was achieved *via* electron microscopy, and did not exploit their colourimetric properties.[31] The colourimetric (red to blue) shift associated with AuNPs aggregation has been exploited for the detection of isolated lectins, and different strains of influenza[36] but not to identify bacterial phenotype.

In this work we investigate the development of a colourimetric glycoAuNP assay for the rapid, point-of-care, detection of particular bacteria phenotypes based on their surface lectin expression patterns. The role of particle structure including polymeric spacer on the sensitivity, specificity and outputted signal is investigated.

7.3 Results and Discussion

In order to obtain glycosylated nanoparticles that could selectively interact with the FimH adhesin on *E. coli*, AuNPs were synthesised using the one-pot method of Watanabe *et al.*,[8] using chemical reduction of $HAuCl_4$ using a thio-sugar as the reducing and stabilising agent. Different sized particles were obtained by tuning the molar ratio of thioglucose:Au^{3+}, Scheme 7.1. Although glucose is not the native ligand for FimH (mannose), there are several reports of multivalent glucose binding

FimH so was a suitable starting point.[35] Table 7.1 summarises the initial particles used in this study. By varying the ratio of thioglucose relative to Au^{3+} it was possible to control the diameter of the AuNPs in the range of 30 – 60 nm, as confirmed by UV-Vis and dynamic light scattering (DLS).
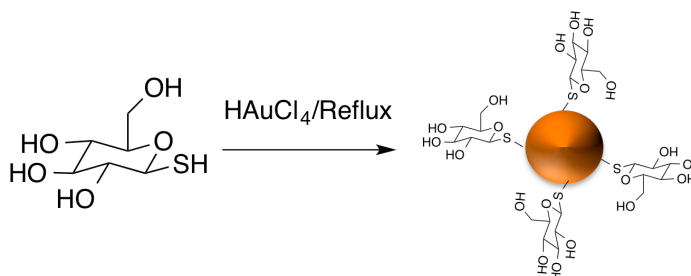

Scheme 7.1. Synthesis of AuNPs by *in situ* reduction using 1-thioglucose.

Table 7.1: AuNPs synthesised by *in situ* reduction.

Code	Molar ratio Thioglucose:Au^{3+}	Wavelength of SPR peak (nm)	Diameter[37] (nm)
AuNP1	0.55	525	32
AuNP2	0.50	530	48
AuNP3	0.45	536	60

To probe the utility of the glycoAuNPs as colourimetric readouts of the presence of lectins, Con A was selected due to its well-known affinity for glucose/mannose residues. During the initial experiments, it became clear that the glycoAuNPs could not tolerate significant quantities of salt in the buffer, so the NaCl concentration had to be reduced (see below for solutions to this – it is crucial for point-of-care diagnostics) to prevent unwanted aggregation. Addition of Con A to the AuNPs resulted in a shift in the location of the SPR peak to longer wavelengths (*i.e.* blue colouration) and a general increase in absorption at 700 nm, Figure 7.1. By plotting Abs_{700} against Con A concentration, it was possible to obtain binding isotherms that indicated larger nanoparticles had increased affinity to Con A, compared to the smaller ones. However, unravelling relative affinity/avidity in

multivalent systems is non-trivial,[38, 39] and the experiments shown here simply serve to demonstrate that the response of the AuNPs to Con A has a size dependency. To probe the underlying mechanism of this shift in the absorption behaviour of the gold, the process was monitored kinetically, by both UV-Vis and DLS, Figure 7.1C. The increase in diameter observed by DLS correlated well with Abs_{700} confirming that lectin/nanoparticle crosslinking was the macroscopic effect. This observation is crucial if a red-blue colour shift is to be obtained. If lectin adhesion does not lead to particle crosslinking the spectral changes would be more subtle and require different analysis, and is described later.
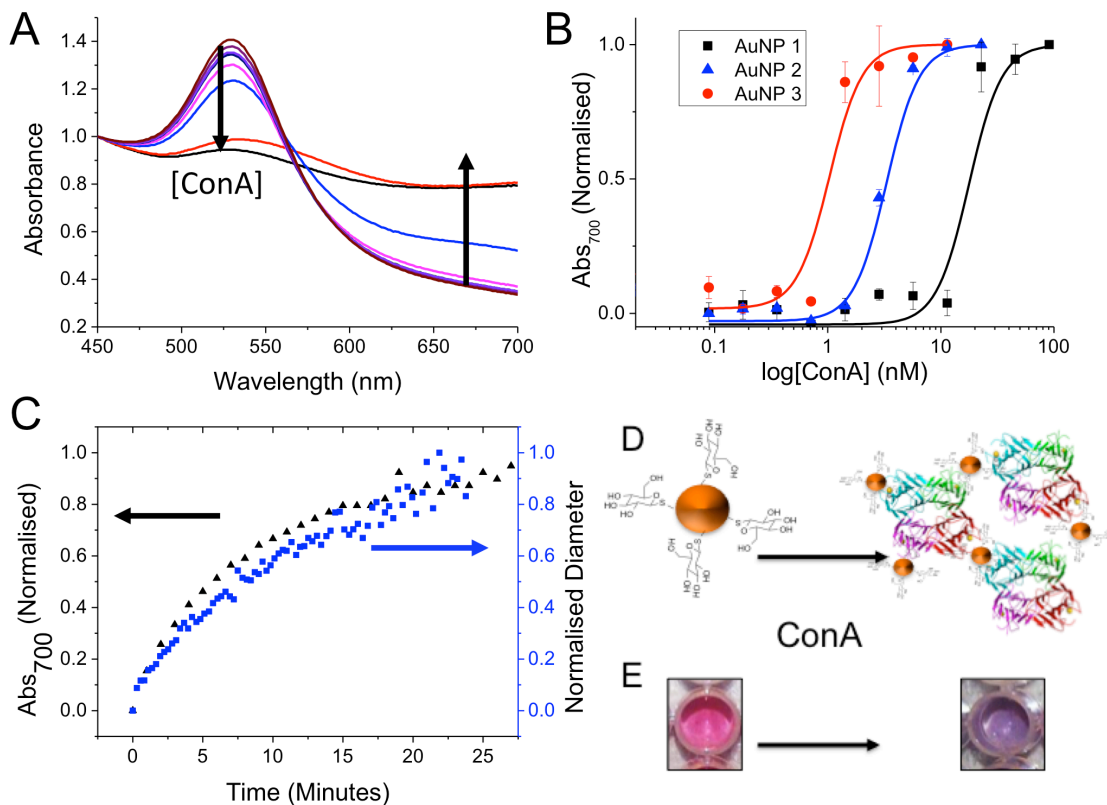
Figure 7.1: Interaction of glucose-functional AuNPs with Con A. A) UV-Vis spectrum of **AuNP2** upon addition of increasing concentrations of Con A (0.1 – 100 nM) following 30 minutes of incubation. B) Binding isotherms (at 37 °C) of AuNPs with Con A. C) Comparison of kinetics of nanoparticle responses to Con A by both UV-Vis spectroscopy and dynamic light scattering. D) Aggregation of AuNPs by Con A tetramer giving rise to colour changes (E).

Encouraged by the colour shift in response to addition of Con A, **AuNP2** was selected to interrogate two distinct strains of *E. coli*; K-12 (strain K-12 JM109) which expresses FimH, mannose-binding adhesin on its fimbriae; TOP10, which does not express FimH. The nanoparticles were incubated with a dilution series of each bacteria in a range of ODs (Optical Density – bacteria density in solution by measuring absorbance at 600 nm) from 0 to 1, for 30 minutes and their absorption spectra recorded, Figure 7.2. As can be clearly seen in Figure 7.2A, addition of **AuNP2** to K-12 resulted in a large shift in the SPR maximum to longer wavelength and an increase in absorbance at 700 nm (after correcting for the background absorbance of the bacteria), in agreement to what was observed with Con A. With

TOP10 (no FimH), the observed changes were smaller, and only occurred at higher bacteria concentrations, indicating either non-specific (fouling) interactions or unintended interactions with unknown proteins such as glucose transporters. Figure 2C shows the binding isotherm, which shows the particles responded to the K-12's at far lower concentration (100 fold) than the TOP10's, demonstrating in principle the nanoparticle's ability to discriminate. Figure 2D shows photographs of the nanoparticles with bacteria showing the very obvious colour changes from red to blue in the presence of K-12s, but not with TOP10 until very high concentrations are applied which could form the basis of a point of care diagnostic if selectivity could be improved. This limited range of selectivity is probably due to the earlier observations that the AuNPs have limited stability in complex media (and saline) and hence some aggregation will occur over time giving false-positive readouts.
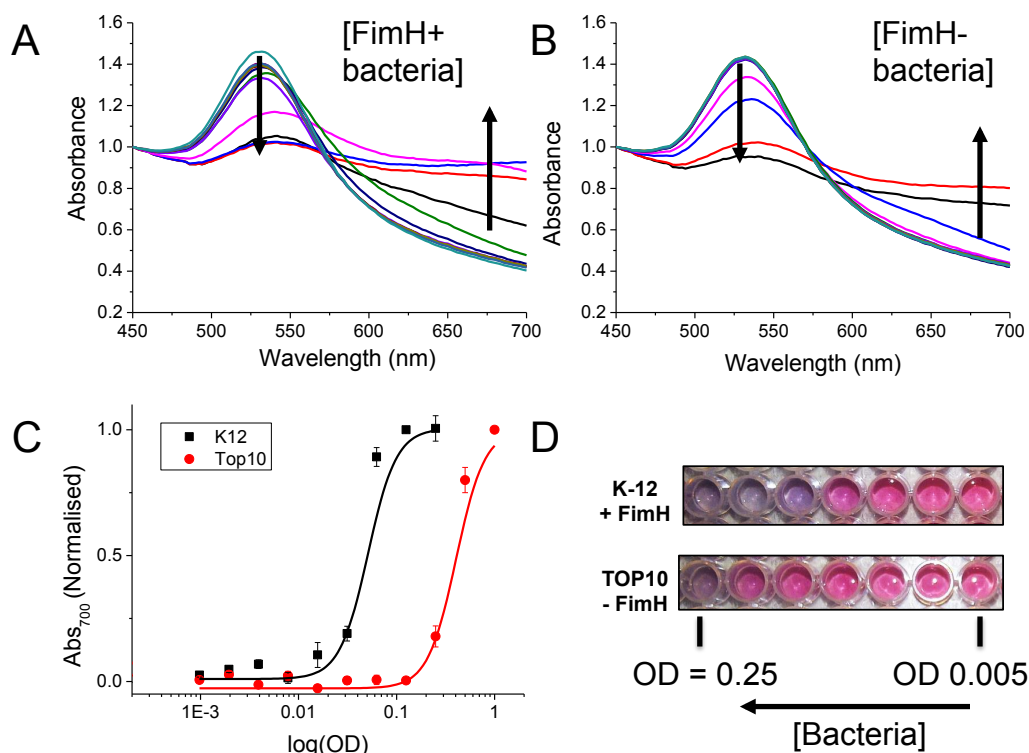
Figure 7.2: Interactions of **AuNP2** with K-12 and TOP10 bacteria. A) Absorption spectra of **AuNP2** upon addition of K-12 bacteria of OD 0.001 to 1. B) Absorption spectra of **AuNP2** upon addition of TOP10 bacteria of OD 0.001 to 1. C) Comparison of binding isotherm of glycoparticles to both bacteria at 37 °C. D) Photographs of **AuNP2** with serial dilution of bacteria and associated colour changes.

7.3.1 Improving glyconanoparticle stability and selectivity

Encouraged by the results described above, a strategy was developed to improve the selectivity and stability of the nanoparticles. To improve solution stability, it is common to immobilise hydrophilic 'non-fouling' polymers which confer both saline stability and reduce non-specific absorption of proteins onto the nanoparticle surface, most commonly with poly(ethyleneglycol) (PEG).[40] Furthermore, to improve binding to FimH, mannose was selected as the more specific ligand, compared to glucose. Installation of the mannose onto thiol-terminated PEG was achieved by cycloaddition of α-D-propargyl mannoside with the ω-terminal azide ('click'), followed by purification by dialysis, Scheme 7.2. The

mannose-functional PEG was subsequently immobilised onto pre-formed 40 nm AuNPs by a simple mixing strategy and excess polymer removed by centrifugal dialysis. Upon polymer coating an increase in hydrodynamic diameter from 40 – 55 or 57 nm was observed, along with a shift in the SPR_{max} indicating successful functionalisation, Table 7.2.
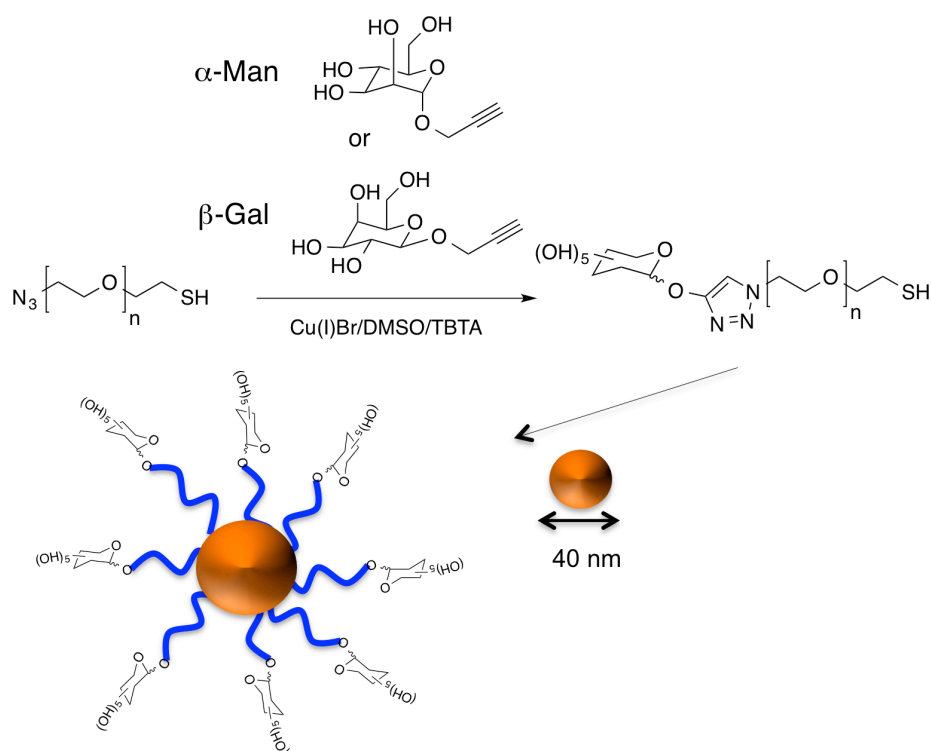
**Scheme 7.2**: Synthesis of PEGylated glyconanoparticles.

Table 7.2: Glyconanoparticles with PEG spacer.

Code	Carbohydrate	$SPR_{uncoated}$[a] (nm)	SPR_{PEG}[b] (nm)	Diameter[c] (nm)
NP-Man	α-Man	525	527	55
NP-Gal	β-Gal	525	529	57

[a] SPR maximum of 40 nm uncoated AuNPs. (b) SPR maximum of AuNPs after coating with pyranoside-PEG-SH. (c) Diameter determined by DLS.

As saline stability was a problem with the directly carbohydrate-conjugated AuNPs, resulting in false positive aggregation effects, the stabilising effect of the PEG was

assessed, Figure 7.3. The PEGylated nanoparticles were stable across all NaCl concentration ranges (up to 1 M, which is well above that required for a sensor) whereas the non-PEGylated particle aggregated even at 0.005 M NaCl. This assay ensures that any aggregation effects observed with live bacteria can be assigned to particle-bacteria interactions and not to non-specific aggregation.
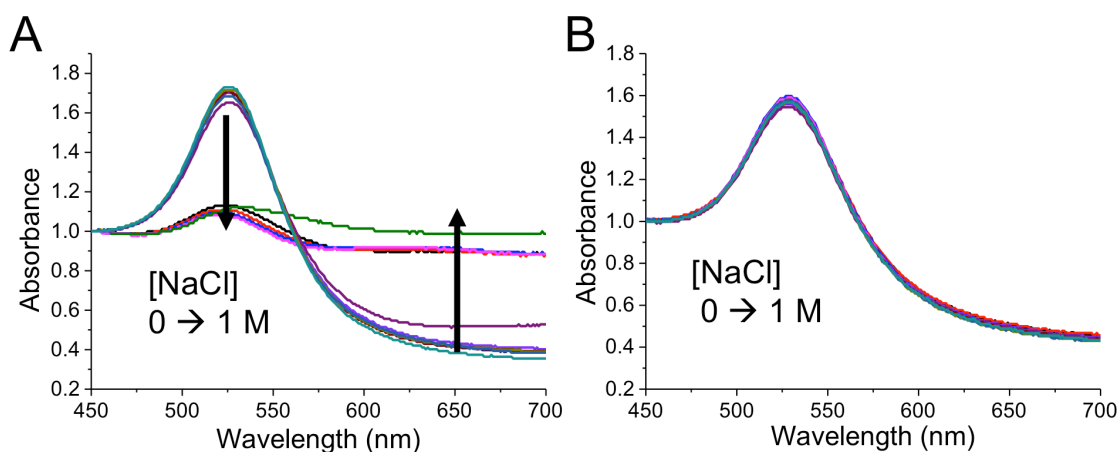
Figure 7.3: Comparison of saline stability of A) uncoated and B) PEG-coated AuNPs.

As with **AuNP 1-3**, Con A was added to the particles and their responses measured by UV-Vis. Unlike the previous examples, addition of Con A did not appear to cause a shift in the SPR maximum, but did induce a large increase at 700 nm, and a decrease in intensity of the SPR peak, Figure 7.4. Kinetic analysis (at Abs_{700}) showed the rate of change in absorbance for the PEGylated particles was significantly slower than with **AuNP2**. **AuNP2** aggregated in less than 25 minutes, but the PEGylated particles were still increasing at 700 nm even after 4.5 hours of incubation. This is interpreted as being due to the increased stability of the PEGylated particles in the buffer, which means there are no non-specific aggregation events. The increased separation between carbohydrate residues at the termini of PEG-chains (relative to directly-conjugation to gold surface) may also slow the rate of binding due to spacing effects.
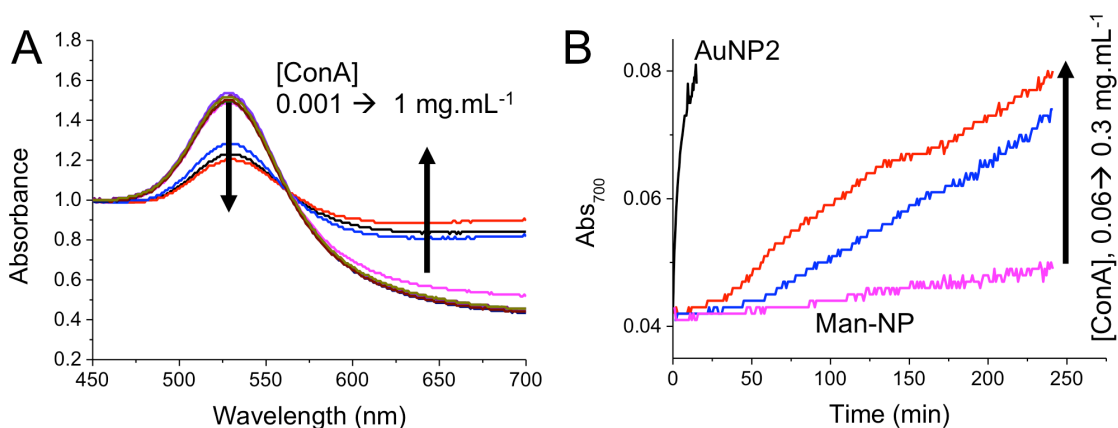
Figure 7.4: Interactions of **NP-Man** with Con A. A) Absorption spectra of particles upon addition of Con A at 37 °C for 30 minutes; B) Kinetic analysis of nanoparticle interaction with Con A, compared to non-PEGylated glycoAuNP, **AuNP2**.

To unravel the processes that occur with both types of glycoAuNP, and to aid the development of the optimum readouts for a sensor, the responses of AuNP2 and **NP-Man** are compared in Figure 7.5. The change in absorption at 700 nm (after 30 minutes) for both nanoparticles as a function of Con A concentration is almost identical, with similar inflection points. However, the changes in the SPR absorption band are in stark contrast. AuNP shows a dose–dependent shift in SPR_{max} as [Con A] increases. **NP-Man** however, does not show any shift in the SPR and hence there is no red to blue colour shift, suggesting more analysis is required if there are to be used as a diagnostic tool. DLS analysis (Appendix 5) showed no aggregation of **NP-Man** upon addition of Con A. We therefore propose that the SPR shift (red – blue) seen for **AuNP1-3** is associated with the interparticle distance decreasing, due to Con A crosslinking the particles or due to binding events leading to reduced solution stability. The change in absorption at 700 nm for **NP-Man** is not a turbidity effect (due to no increase in particle diameter for PEGylated particles) and we therefore suggest this is associated with protein binding to the AuNPs and affecting their hydration, and hence refractive index. These observations raise a question for the use

of AuNPs as biosensors, in that the commonly applied polymer coatings improve stability, but inhibit the convenient visual read-out commonly associated with nano-gold red to blue colour shift. Therefore, absorption at 700 nm will be used from this point. It should be noted that the effect of polymer coating will vary on the analyte being detected (including size of analyte: e.g. bacteria/virus), and the length of the polymer itself.[36]
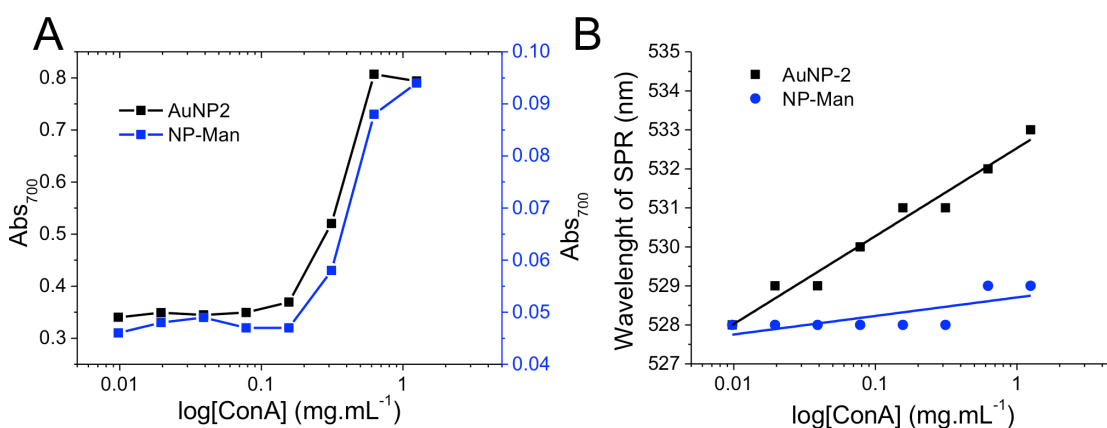

Figure 7.5: Comparison of spectral response between particles with and without PEG spacer. A) Change in absorbance at 700 nm; B) Changes in the location of the SPR absorption band as a function of lectin concentration.

Before progressing to testing with the bacteria, an additional control experiment was undertaken. Peanut agglutinin (PNA), which has preference for β-galactose was added to **NP-Man**. Pleasingly, no change was observed indicating that the polymer coating efficiently prevents non-specific interactions with proteins, and only the carbohydrate motifs are associated with recognition/output events, Figure 7.6.
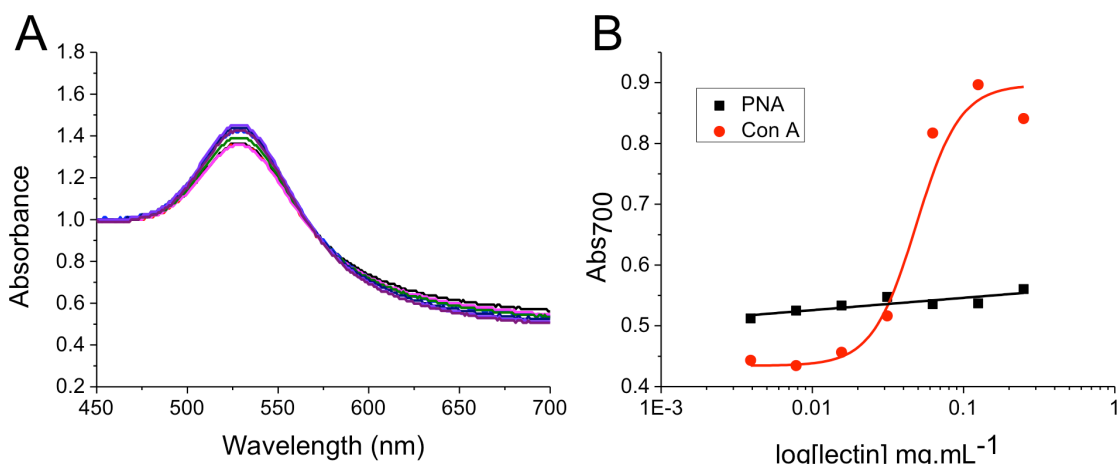
Figure 7.6: Assessment of lectin specificity of glycoAuNPs. A) UV-Vis spectra of **NP-Man** upon addition of PNA (0.001 – 1 mg.mL^{-1}); B) Comparison of change in absorbance at 700 nm of **NP-Man** upon addition of Con A (mannose binding) and PNA (galactose binding).

With the above information to hand, a series of experiments were designed to probe bacterial specificity and the optical responses of the AuNPs. To provide a negative control, galactose functional nanoparticles were also synthesised by identical synthetic methods, **NP-Gal**. **NP-Gal** should not interact with either of the bacterial strains, whereas **NP-Man** should interact with K-12 (FimH adhesin) but not TOP10, and therefore providing a rigorous panel of measurements to probe sensitivity and selectivity. Figure 7.7 shows the UV-Vis spectra of **NP-Man** with K-12 and TOP10. As was observed with the protein studies, there was no shift in the SPR maximum with either bacteria but there were decreases in the SPR intensity and increases in absorbance at 700 nm. The changes observed were far more significant, and occurred at lower bacteria concentrations in the case of K-12 compared for TOP10. The changes observed when **NP-Gal** was added to both bacterial strains was significantly less (Appendix 5).
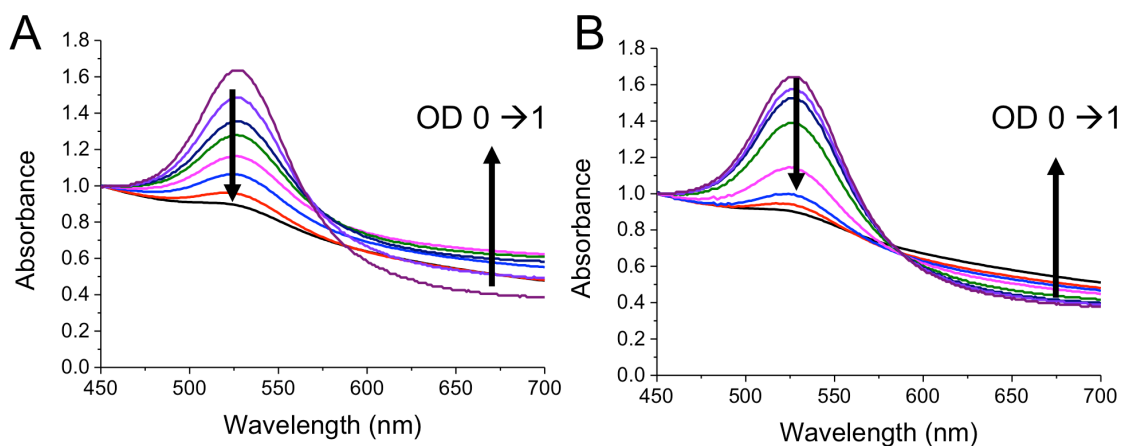
Figure 7.7. UV-visible spectra of **NP-Man** with A) K-12 and B) TOP10 bacteria.

The changes in absorbance at 700 nm for each bacterium at a variety of optical densities (proportional to bacteria concentration), with both particles is summarised in Figure 7.8. To aid visualisation, the change in Abs_{700} as a function of OD was plotted as a heat map, with the z-axis (colour) set to show large changes as blue, and small changes as red (allowing facile comparison with standard nano-gold assays). Using this visualisation, it became very obvious that only Mannose-functional particles and K-12 together gave rise to positive responses. Changing to either TOP10 or Gal functional particles did not result in positive responses. The best responses were obtained with intermediate concentration of K-12, OD = 0.03 to 0.125 where the response to K-12 was largest without any response to TOP10. Very high concentrations of K-12 (> OD 0.5) actually led to a reduction in signal from **NP-Man**. We hypothesise that this is due to the bacteria binding sites saturating the AuNP, such that there are insufficient particles to statistically bind close together, to give the desired optical outputs. Future studies will investigate this in more detail. The actual number of bacteria (colony forming units) was estimated (Appendix 5) indicated that the nanoparticle system could detect K-12 bacteria at concentrations as low as 1.5×10^7 CFU/mL. These tests shows that glycoAuNPs can discriminate

between strains of bacteria based solely upon interrogation of membrane-exposed carbohydrate-binding proteins and could form the basis of new point-of-care diagnostics.
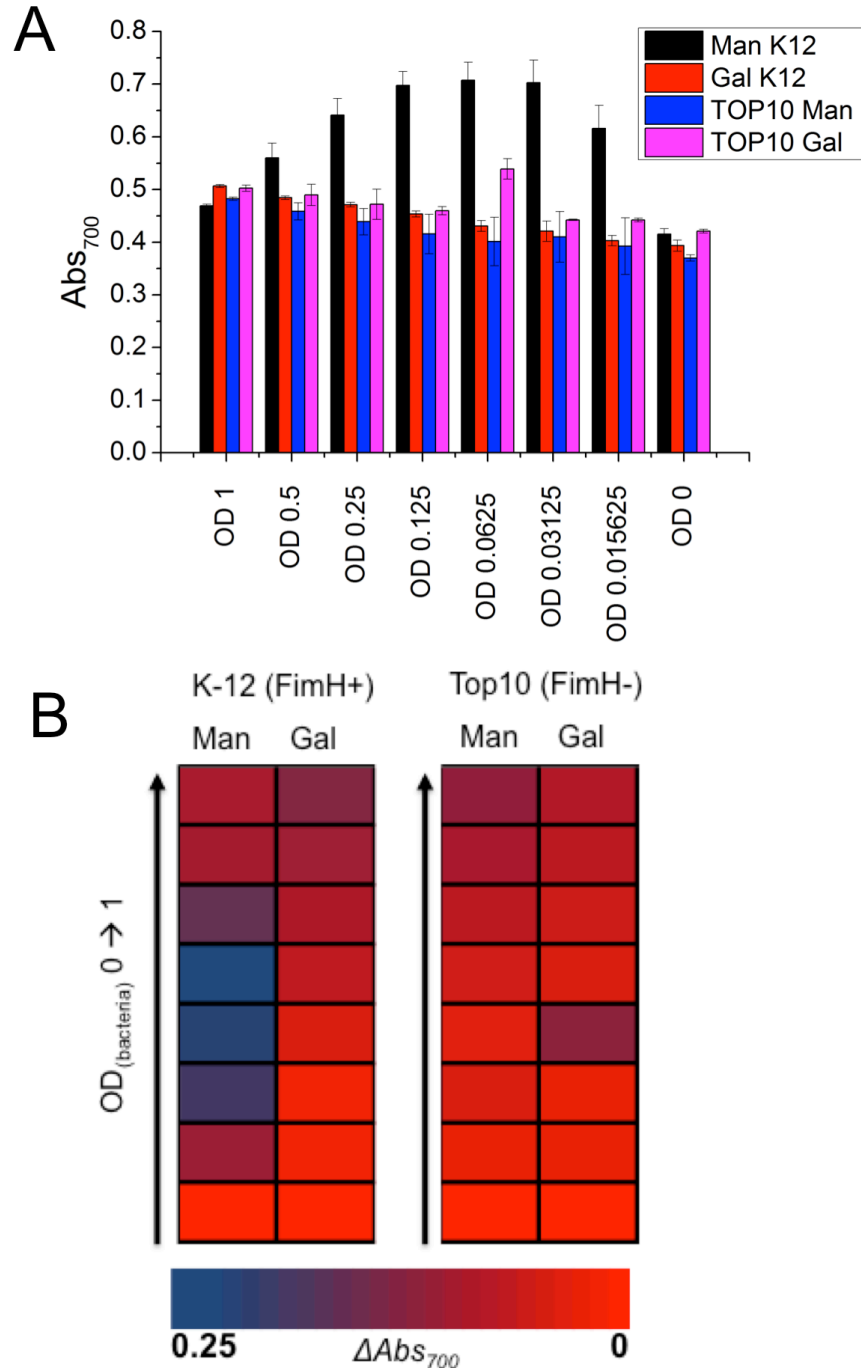
Figure 7.8. Responses of both **NP-Man** and **NP-Gal** to both K-12 and TOP10 bacteria. A) Absorbance at 700 nm for each system in response to bacteria, following subtraction of background absorbance of bacteria; B) Heat map showing change in Abs_{700} (relative to $OD_{bacteria} = 0$) for all particles. Blue colouration indicates a larger response and red indicates no response. Error bars indicate ± standard deviation from 3 experiments.

7.4 Conclusions

We have developed a sensitive and rapid colourimetric bioassay for the quantitative detection of lectins and type 1 fimbriated bacteria based upon the binding of glycoAuNPs. AuNPs with carbohydrates directly immobilised on their surface showed very rapid responses to both lectins and lectin-expressing bacteria. However, these particles also displayed low saline stability and nonspecific interactions with the bacteria limiting their discriminatory capacity. To overcome this a PEG layer was inserted between the particles and the carbohydrate. This dramatically increased the saline stability of particles whilst retaining their bio-recognition properties. An interesting side effect of the PEG layer was no red to blue colour change was observed upon lectin binding, which was hypothesised to be due to steric shielding effects of the PEG layer. Despite this, an assay was developed based on monitoring the absorbance at 700 nm with UV-Vis spectroscopy in which the mannose-functional particles specificity generated an output in the presence of K-12 bacteria and not TOP10. K-12 expressed type 1 fimbriae that bind mannose residues, but TOP10 does not. This system represents the first step in making nanoparticles that can 'read' the surface lectin composition of bacteria to enable rapid (point-of-care) phenotyping with a visual output.

7.5 Experimental Section

7.5.1 Materials

D-(+)-mannose, propargyl alcohol (99 %), copper bromide (99%), HEPES and phosphate buffered saline (PBS) were purchased from Sigma Aldrich. Triethylamine (99 %) and Hydrogen tetrachloroaurate (III) trihydrate were purchased from Acros. β-D-thioglucose sodium salt was purchased from Carbosynth. D-(+)-galactose anhydrous was purchased from MP Biomedicals. DMSO was purchased from Fisher Scientific at laboratory grade. Peanut Agglutinin and Concanavalin A were purchased from Vector Laboratories. Azido PEG thiol (N_3-(PEG)-SH, Mn = 3000 g.mol^{-1}) was purchased from NANOCS. Tris-(benzyltriazolylmethyl)amine (TBTA) was synthesised according to literature procedures.[41] Microtitre plates were purchased from Greiner Bio-one. 10 mmol HEPES buffer containing 0.15M NaCl, 0.1mM $CaCl_2$ and 0.01mM Mn^{2+} (pH 7.5, HEPES) was prepared in 200 mL of milliQ water (with a resistance >19 mOhms). 40 nm gold nanoparticles were obtained from BBI International. K12 JM109 (referred to as K12 in text) and TOP10 were both grown in LB media from frozen stocks prior to use. Bacteria were isolated by centrifugation and the resuspended to the desired optical densities in PBS.

7.5.2 Physical and analytical procedures

Absorbance measurements of the nanoparticles incubated with Con A were recorded on a BioTek SynergyTM HT multi-detection microplate reader obtained using Gen5 1.11 multiple data collection and analysis software. DLS measurement were carried out using a Malvern Instruments Zetasizer Nano-ZS. A Thermoscientific NanoDrop 2000 UV-Vis Spectrophotomer was used to measure the OD_{600} of the *E. coli* cells.

7.5.3 Synthetic procedures

Synthesis of Glucose Functionalised Gold Nanoparticles: Thioglucose-capped gold nanoparticles were synthesized according to the method of Wantanabe *et al.*[8] An aqueous 1-thioglucose solution (5.0 mL 2-20 nM) was added to a boiling solution of $HAuCl_4$ (50 mL, 0.5 mM) under reflux and vigorous stirring. On addition of the 1-thioglucose, the solution changed colour from pale yellow to ruby red almost immediately. Then the reaction was heated under reflux for a further 10 minutes. The reaction mixture was cooled and dialysed overnight against water to remove unreacted thioglucose using dialysis tubing (Spectra/Por, Cellulose ester, MWCO = 5000, Spectrum Laboratories Inc., USA).

Synthesis of Propargyl-Pyrannosides: To mannose or galactose (500 mg,) in propargyl alcohol (5 mL), 250 μL of 3 M HCl was added. Stirred overnight at room temperature. Concentrated *in vacuo*. Employed immediately for alkyne azide cycloaddition reaction.

^{1}H NMR (D$_2$O, 300 Hz) δ_{ppm} : 4.48 (1H, d, J = 7.7 Hz, CH, H^3), 4.40 (2H, t, J = 2.2 Hz, C*H$_2$*-C≡CH, H^{2a+b}), 3.84 (1H, d, J=3.4 Hz, CH, H^5), 3.68 (2H, d, J = 3.0 Hz, CH$_2$ H^{8a+b}), 3.65 (1H, d, J = 2.6, CH, H^6) 3.60 (1H, t, J = 3.9, CH, H^5), 3.45 (1H, m, CH, H^7), 2.82 (1H, t, J = 2.4, C≡C*H*, H^1)

^{13}C NMR (D$_2$O, 100 Hz) δ_{ppm}: 101.0 (CH, C^4), 76.13 (CH$_2$-C≡*C*H, C^1), 75.20 (CH$_2$-*C*≡CH, C^2), 72.65 (CH, C^8), 71.1 (CH, C^6), 70.45 (CH, C^5), 68.51 CH, C^7), 60.68(CH$_2$ C^9), 56.0(CH$_2$-C≡CH, C^3).

Copper-catalysed [3+2] cycloaddition of propargyl-pyrannosides and azide-(PEG)$_{3K}$-SH: N$_3$-(PEG)$_{3K}$-SH (20 mg, 5.9 μmol), (50 mg, 0.23 mmol), TEA (10 mg, 0.072 mmol), and CuBr (2 mg) dissolved in DMSO (4 mL) were charged in an ampoule and deoxygenated through three freeze–pump–thaw cycles before being placed under nitrogen. TBTA (8 mg, 0.14 mmol) was added and the reaction was degassed and left under nitrogen for 48 h. The polymer was purified by dialysis against water using dialysis tubing with MWCO of 1000 g.mol^{-1}.

IR ν : 3600-3200 (OH), 2890 (CH$_2$), 1105 (C-O) cm^{-1},

Preparation of Pyrannoside-(PEG)$_{3K}$ functionalised gold nanoparticles: To 5 mL of 40 nm AuNPs, pyrannoside-(PEG)$_{3K}$-SH (5 mg) was added and left for 30 mins at room temperature. The particles were then centrifuged at 6000 rpm for 15 mins and resuspended in HEPES buffer.

Size Characterisation of Glucose Functionalised Gold Nanoparticles using Absorbance Spectra: 50 μL of each glycoAuNP were loaded into a 96-well microtitre plate, 50 μL of 10 mM HEPES buffer with 0.5 mM CaCl$_2$, 0.5 mM MnCl$_2$ and 0.5 mM MgCl$_2$ was added to each and a spectrum was taken between 450 nm and 700 nm.

Concanavalin A Induced Aggregation Assays: A stock of 24 μg.mL^{-1} Con A was made up in 10 mM HEPES buffer with 0.5 mM CaCl$_2$, 0.5 mM MnCl$_2$ and 0.5 mM MgCl$_2$. 50μL serial dilutions of ConA were made up in the same buffer in a 96-well microtitre plate so that when the nanoparticles were added the resultant concentration was 12nM – 0.01 nM and a control with 0 μg.mL^{-1} of ConA. 50 μL of

the glycoAuNP was added to each concentration of Con A and incubated at 37 °C for 30 minutes with medium shaking and then an absorbance spectra between 450 nm and 700 nm was recorded. Each measurement was done in triplicate.

Concanavalin A Induced Aggregation Kinetics Studies using Absorbance Spectra: 50 μL of the nanoparticle solution was incubated with 50 μL of Con A at the K_d concentration. Readings of the absorbance at 700 nm were taken every minute for 30 seconds with medium shaking between recordings.

Concanavalin A Induced Aggregation Kinetics Studies using Dynamic Light Scattering: 300 μL of AuNP was made up in 240 μL of MilliQ water and filtered through a 0.22 μm syringe filter. 60 μL of Con A was added that would make the concentration of Con A around the K_d value. Average diameter measurements at ambient temperature were taken every 15 seconds for 30 minutes.

Bacterial Detection Assay: An adapted procedure was used of that conducted by Seeberger *et al.*[4] TOP10 (nonfimbriated) and K-12 (fimbriated) *Escherichia coli* cells were cultured overnight in LB media at 37 °C. The culture was then washed twice and resuspended in HEPES buffer with 0.5 mM $CaCl_2$, 0.5 mM $MnCl_2$ and 0.5 mM $MgCl_2$. 100 μL serial dilutions of the bugs were made up in microtitre plates and 100 μL of the gold nanoparticles were added to the cells. The suspensions were incubated at room temperature for 30 minutes. The absorbance spectra of the nanoparticle cell suspensions were taken using the cells alone as a background. Colony forming units were estimated, assuming that OD_{600nm} $1 = 10^9$ $CFU.mL^{-1}$.

7.6 References

1. D. J. Payne, M. N. Gwynn, D. J. Holmes and D. L. Pompliano, *Nat. Rev. Drug Discov.*, 2007, **6**, 29-40.

2. V. Makarov, G. Manina, K. Mikusova, U. Moellmann, O. Ryabova, B. Saint-Joanis, N. Dhar, M. R. Pasca, S. Buroni, A. P. Lucarelli, A. Milano, E. De Rossi, M. Belanova, A. Bobovska, P. Dianiskova, J. Kordulakova, C. Sala, E. Fullam, P. Schneider, J. D. McKinney, P. Brodin, T. Christophe, S. Waddell, P. Butcher, J. Albrethsen, I. Rosenkrands, R. Brosch, V. Nandi, S. Bharath, S. Gaonkar, R. K. Shandil, V. Balasubramanian, T. Balganesh, S. Tyagi, J. Grosset, G. Riccardi and S. T. Cole, *Science*, 2009, **324**, 801-804.

3. D. Pissuwan, C. H. Cortie, S. M. Valenzuela and M. B. Cortie, *Trends Biotechnol.*, 2010, **28**, 207-213.

4. M. D. Disney, J. Zheng, T. M. Swager and P. H. Seeberger, *J. Am. Chem. Soc.*, 2004, **126**, 13343-13346.

5. J. Joo, C. Yim, D. Kwon, J. Lee, H. H. Shin, H. J. Cha and S. Jeon, *Analyst*, 2012, **137**, 3609-3612.

6. K. Aslan, J. Zhang, J. R. Lakowicz and C. D. Geddes, *J. Fluoresc.*, 2004, **14**, 391-400.

7. J. E. Ghadiali and M. M. Stevens, *Adv. Mater.*, 2008, **20**, 4359-4363.

8. S. Watanabe, K. Yoshida, K. Shinkawa, D. Kumagawa and H. Seguchi, *Colloids Surf., B*, 2010, **81**, 570-577.

9. C. L. Schofield, B. Mukhopadhyay, S. M. Hardy, M. B. McDonnell, R. A. Field and D. A. Russell, *Analyst*, 2008, **133**, 626-634.

10. Y. J. Chuang, X. C. Zhou, Z. W. Pan and C. Turchi, *Biochem. Biophys. Res. Commun.*, 2009, **389**, 22-27.

11. A. Laromaine, L. L. Koh, M. Murugesan, R. V. Ulijn and M. M. Stevens, *J. Am. Chem. Soc.*, 2007, **129**, 4156-4157.

12. G. J. Nusz, S. M. Marinakos, A. C. Curry, A. Dahlin, F. Hook, A. Wax and A. Chilkoti, *Anal. Chem.*, 2008, **80**, 984-989.

13. A. K. Singh, D. Senapati, S. G. Wang, J. Griffin, A. Neely, P. Candice, K. M. Naylor, B. Varisli, J. R. Kalluri and P. C. Ray, *ACS Nano*, 2009, **3**, 1906-1912.

14. K. M. Mayer, S. Lee, H. Liao, B. C. Rostro, A. Fuentes, P. T. Scully, C. L. Nehl and J. H. Hafner, *ACS Nano*, 2008, **2**, 687-692.

15. S. H. Huang, *Sens. Actuators, B*, 2007, **127**, 335-340.

16. A. J. Haes, L. Chang, W. L. Klein and R. P. Van Duyne, *J. Am. Chem. Soc.*, 2005, **127**, 2264-2271.

17. P. Englebienne, *Analyst*, 1998, **123**, 1599-1603.

18. N. Ohtake, K. Niikura, T. Suzuki, K. Nagakawa, H. Sawa and K. Ijiro, *Bioconjugate Chem.*, 2008, **19**, 507-515.

19. P. V. Baptista, M. Koziol-Montewka, J. Paluch-Oles, G. Doria and R. Franco, *Clin. Chem.*, 2006, **52**, 1433-1434.

20. R. Elghanian, J. J. Storhoff, R. C. Mucic, R. L. Letsinger and C. A. Mirkin, *Science*, 1997, **277**, 1078-1081.

21. R. de la Rica and M. M. Stevens, *Nat. Nanotechnol.*, 2012, **7**, 821-824.

22. O. R. Miranda, X. Li, L. Garcia-Gonzalez, Z.-J. Zhu, B. Yan, U. H. F. Bunz and V. M. Rotello, *J. Am. Chem Soc.*, 2011, **133**, 9650-9653.

23. C. R. Bertozzi and L. L. Kiessling, *Science*, 2001, **291**, 2357-2364.

24. L. L. Kiessling, J. E. Gestwicki and L. E. Strong, *Angew. Chem. Int. Ed.*, 2006, **45**, 2348-2368.

25. M. Ambrosi, N. R. Cameron and B. G. Davis, *Org. Bio. Chem.*, 2005, **3**, 1593-1608.

26. H. Feinberg, D. A. Mitchell, K. Drickamer and W. I. Weis, *Science*, 2001, **294**, 2163-2166.

27. Y. C. Lee, R. R. Townsend, M. R. Hardy, J. Lonngren, J. Arnarp, M. Haraldsson and H. Lonn, *J. Biol. Chem.*, 1983, **258**, 199-202.

28. J. J. Lundquist and E. J. Toone, *Chem. Rev.*, 2002, **102**, 555-578.

29. S. Watanabe, H. Seguchi, K. Yoshida, K. Kifune, T. Tadaki and H. Shiozaki, *Tetrahedron Lett.*, 2005, **46**, 8827-8829.

30. C. S. Tsai, T. B. Yu and C. T. Chen, *Chem. Commun.*, 2005, 4273-4275.

31. C. C. Lin, Y. C. Yeh, C. Y. Yang, G. F. Chen, Y. C. Chen, Y. C. Wu and C. C. Chen, *Chem. Commun.*, 2003, 2920-2921.

32. C. C. Lin, Y. C. Yeh, C. Y. Yang, C. L. Chen, G. F. Chen, C. C. Chen and Y. C. Wu, *J. Am. Chem. Soc.*, 2002, **124**, 3508-3509.

33. J. M. De la Fuente and S. Penades, *Biochim. Biophys. Acta*, 2006, **1760**, 636-651.

34. M. Hartmann and T. K. Lindhorst, *Eur. J. Org. Chem.*, 2011, 3583-3609.

35. G. Pasparakis, A. Cockayne and C. Alexander, *J. Am. Chem. Soc.*, 2007, **129**, 11014 - 11015.

36. M. J. Marin, A. Rashid, M. Rejzek, S. A. Fairhurst, S. A. Wharton, S. R. Martin, J. W. McCauley, T. Wileman, R. A. Field and D. A. Russell, *Org. Biomol. Chem.*, 2013, **11**, 7101-7107.

37. W. Haiss, N. T. K. Thanh, J. Aveyard and D. G. Fernig, *Anal. Chem.*, 2007, **79**, 4215-4221.

38. R. J. Pieters, *Org. Biomol. Chem*, 2009, **7**, 2013-2025.

39. Y. Gou, S.-J. Richards, D. M. Haddleton and M. I. Gibson, *Polym. Chem.*, 2012, **3**, 1634-1640.

40. H. Otsuka, Y. Nagasaki and K. Kataoka, *Adv. Drug Del. Rev.*, 2003, **55**, 403-419.

41. T. R. Chan, R. Hilgraf, K. B. Sharpless and V. V. Fokin, *Org. Lett.*, 2004, **6**, 2853-2855.

Chapter 8

Optimisation of the polymer coating for glycosylated gold nanoparticle biosensors to ensure stability and rapid optical readouts

This chapter consists of the paper detailing the development of optimised polymer-gold nanoparticle composites for lectin detection. This improves on the saline stability and speed of readout issues observed in Chapter 7. Using a water soluble polymer of a range of sizes the optimum linker length was determine for stability at physiological saline concentration, but also gave a fast readout (in less than 15 minutes).

I proposed the use of RAFT polymerised water-soluble polymers as a method to improve the saline stability, by methodically probing different length linkers. I carried out all the synthesis and characterisation of the polymers and particles and the testing of the response of the differently functionalised particles to a range of lectins. I also prepared the manuscript and dealt with reviewers' comments.

8.1 Abstract

The development of new analytical tools to probe pathogenic infection processes and as point-of-care biosensors is crucial to combat the spread of infectious diseases or to detect biological warfare agents. Glycosylated gold nanoparticles that change colour due to lectin (carbohydrate-binding protein) mediated aggregation may find use as biosensors but require a polymer coating between the particle surface and sugar to ensure stability in complex media. Here, RAFT polymerisation is employed to generate glycosylated polymers to coat gold nanoparticles. Rather than being a passive component, it is shown here that the polymer coating has to be precisely tuned to achieve a balance between saline (steric) stability and speed of the readout. If the polymer is too long it can prevent or slow aggregation and hence lead to a poor readout in sensing assays. The optimised glyco nanoparticles are also demonstrated to be useful for rapid detection of a ricin surrogate.

8.2 Introduction

Protein-carbohydrate interactions mediate a multitude of important biological processes including; cell-cell signalling, inflammation and fertilisation, however, bacteria, toxins, and viruses also use the carbohydrate moieties on cell surfaces for cell adhesion as the first stage in infection. Lectins are carbohydrate-binding proteins, (other than enzymes and antibodies) which interact with carbohydrates non-covalently and reversibly with a high level of specificity.[1, 2] The binding affinity of a monosaccharide to its lectin target in typically very weak ($K_d = 10^{-3}$-10^{-6} M). This is circumvented in nature by the presentation of multiple copies of the saccharide on the cell surface, this is known as 'the cluster-glycoside effect' and hence

macromolecular structures with polyvalent presentation of carbohydrates are of interest.[3, 4]

Examples of pathogens that exploit the protein-carbohydrate interactions are the FimH adhesin found on the fimbriae of some pathogenic *Escherichia coli* (*E. coli*) that bind to mannose residues on the cell surface of the urinary tract.[5, 6] *Vibrio cholerae* secretes a carbohydrate-binding toxin that binds to the GM1 ganglioside on intestinal epithelial cells.[7-9] Ricin is a toxic lectin that presents a potential security threat. It is a lethal, type 2 ribosome-inactivating protein found in the castor bean plant *Ricinus communis*.[10] It is an A-B toxin whereby its B-chain adheres to terminal galactose residues on mammalian cell surfaces, facilitating the delivery of the toxic A-chain into the cytosol of the cell. The A-chain catalyses the hydrolytic cleavage of a single base from eukaryotic ribosomal RNA, leading to a shutdown in protein synthesis and ultimately cell death.[11] The median lethal dose (LD_{50}) of ricin for an adult is estimated to be around 22 $\mu g.Kg^{-1}$ of body weight (> 1.8 mg for an average adult). Due to its high toxicity and accessibility, its potential as a bio-warfare agent has long been recognised, with several recent incidents in the UK and the US resulting in threats to public safety, therefore its rapid detection is highly desirable.

Gold nanoparticles (AuNPs) have been extensively studied as potential biosensors due to their characteristic optical properties and ease of functionalisation with a number of biological molecules.[12-22] AuNPs exhibit an intense colour in the visible region due to local surface plasmon resonance (LSPR), which arises due to the collective oscillations of the conduction-band electrons of the gold core.[10, 23-25] These optical properties are strongly correlated with their size, shape, dispersion media and degree of aggregation. Particles larger than 10 nm and smaller than 200 nm exhibit a red colouration; upon aggregation dramatic colour change can be

observed from red to blue. This is attributed to electric dipole-dipole interactions and coupling between the plasmons of neighbouring particles.[14, 23] Carbohydrate-functionalised AuNP (glycoAuNPs) are attractive biosensors due to the inherent multivalency of the particles and lectins. The presence of lectins should lead to an optical response as a result of AuNP aggregation, providing the platform for new sensors without the need for expensive equipment and fluorescent- or radio-labelling of proteins. The colourimetric change associated with the aggregation of AuNPs using protein-carbohydrate interactions has been exploited in the detection of lectins[10, 26, 27] and different strains of influenza.[28] We have shown that mannosylated glycoAuNPs can be used to distinguish between bacteria with and without type 1 fimbriae, but that the mode of presentation of the carbohydrates and their distance from the gold surface impacts on the detection read-outs with very slow responses (aggregation) being observed with polymer coatings limiting their application as point-of-care diagnostics (See Chapter 7).[29]

Herein we employ RAFT polymerisation to generate heterotelechelic polymers that can be conjugated with a glycan at one end, and the RAFT-derived thiol at the other to immobilise onto AuNPs. By varying the chain length the crucial balance between stability in saline media and speed of colourimetric detection is probed, for the rapid detection of a series of lectins, including *Ricinus communis* Agglutinin (RCA_{120}) a surrogate for ricin.

8.3 Results and Discussion

Inspired by the glycocalyx on eukaryotic cell surfaces, which has a non-fouling membrane component (phospholipid betaines) with surface immobilised carbohydrates, telechelic polymers were designed with a conjugatable

pentafluorophenyl ester at one end and masked thiol (RAFT agent) at the other for gold immobilisation, Table 8.1. The synthetic scheme is shown in Figure 1A. Poly(*N*-hydroxyethyl acrylamide) (pHEA) was chosen for its water solubility and non-LCST behaviour (unlike PEG methacrylates for example).

Table 8.1: pHEA precursor polymers.

[M]:[CTA][a]	Conversion [%][b]	$M_{n(Theo)}$ (g.mol^{-1})[c]	$M_{n(SEC)}$ (g.mol^{-1})[d]	M_w/M_n[d]	DP[e]
10	78	1680	2800	1.14	8
15	87	2250	3500	1.19	13
20	82	2850	4100	1.16	16
25	81	3400	6200	1.10	20
50	80	6300	9400	1.14	40
75	88	9200	12500	1.20	66

[a] Feed ratio of monomer to chain transfer agent. [b] Determined by ^{1}H NMR spectroscopy. [c] Theoretical number average molecular weight, calculated from the feed ratio and percent conversion. [d] Determined by SEC in dimethylformamide (DMF) using poly(methyl methacrylate) standards. M_w = weight average molecular weight, M_n = number average molecular weight [e] Theoretical number-average degree of polymerisation.

A pentafluorophenol (PFP) trithiocarbonate RAFT agent was chosen to enable facile end-group modification with amino-glycosides[30] and to afford good control with acrylamide monomers.[31, 32] The post-polymerisation route also means that all the polymers have the same initial chain length distribution and therefore reduces the variability between particle types. Polymers with a degree of polymerisation (DP) of 10, 15, 20 25, 50 and 75 were synthesised and their molecular weight distribution was determined by size exclusion chromatograph (SEC) (Figure 8.1B) indicating low dispersites (< 1.2). The carbohydrates were introduced by reaction of the PFP end-group with 2-deoxy-2-amino mannose (ManNH$_2$) and 2-deoxy-2-amino galactose (GalNH$_2$). Infrared spectroscopy confirmed the disappearance of the C=O stretch attributable to the carbonyl of the PFP end-group (Appendix 6). An advantage of this route is that the glycosylation step also cleaves the trithiocarbonate

(RAFT) end group to generate a ω-terminal thiol group. In a subsequent step, the glycosylated, thiol-terminated polymers were incubated with 60 nm AuNPs to enable a monolayer to form. Excess polymer was removed by simple centrifugation-resuspension cycles. 60 nm AuNPs were chosen as the core, as this size range can give lower detection limits in colourimetric assays, as shown previously.[29]

A

B

C   **Incorrect Glycan**   **Correct Glycan**
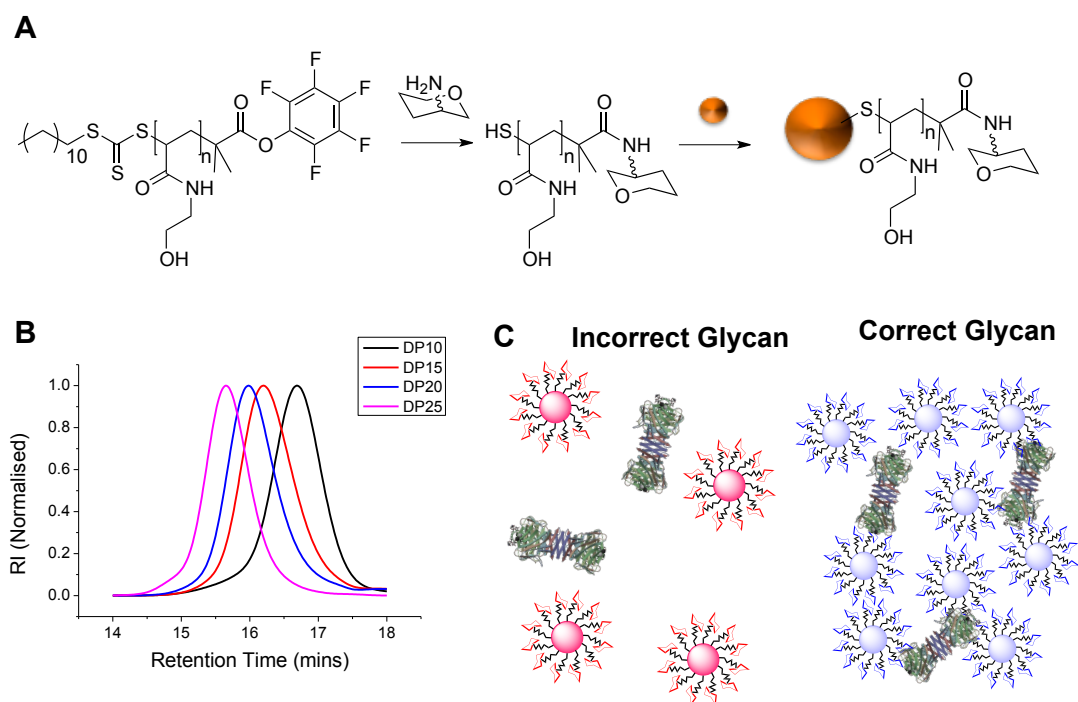
Figure 8.1: (A) Synthesis of polymer stabilised glycoAuNPs; B) SEC traces of various molecular weight pHEA polymers; C) SBA induced aggregation of AuNPs gives rise to colour changes with correct lectin glycan pairing.

The key aim of this work is to establish the ideal coating parameters to enable *rapid* and *specific* sensing of lectins. We have previously shown[29] that saline stability of AuNP sensors is crucial to avoid false positives, and therefore the polymer-coated AuNPs were evaluated by a NaCl titration starting from 1 M, Figure 8.2A. It was observed that polymers of DP 15 or less were unstable at high salt (>0.2 M which is close to physiological (0.137 M)) concentrations, making them unsuitable. Whilst longer polymers (predictably) improved saline stability, it is important to consider

the effects of having polymers that are too long; these can prevent/slow the rate of aggregation upon addition of the lectins by steric stabilisation. The kinetics of particle aggregation (red to blue colour change) triggered by the addition of Con A (preferentially binds to α-mannosides) was measured using UV/Vis spectroscopy. The change in absorbance at 700 nm (Abs_{700}) was monitored over a period of 1 hour for $ManNH_2$-pHEA-AuNPs with polymer linker lengths of DP20, DP50 and DP75. It was found that the shorter linkers resulted in faster aggregation rates (Figure 8.2B) with the DP 75 polymer having no observable changes even after 1 hour incubation. This serves to highlight the delicate balance between stability and sensing for metal nanoparticles, which are modulated by the polymer coating. Guided by these results, a panel of mixtures of DP10/DP20 polymer stabilised particles were synthesised and it was found that a mixture (1:1) of DP10/DP20 polymers affords a coated particle which is saline stable up to 1 M NaCl but retains the ultra-fast kinetics of interaction with the partner lectin (blue colouration noted < 5 mins). Figure 8.2C shows images of AuNPs with both NaCl and Con A to highlight the optimal formulation and demonstrating that macromolecular engineering is essential to obtained precise and rapid nano-biosensors.
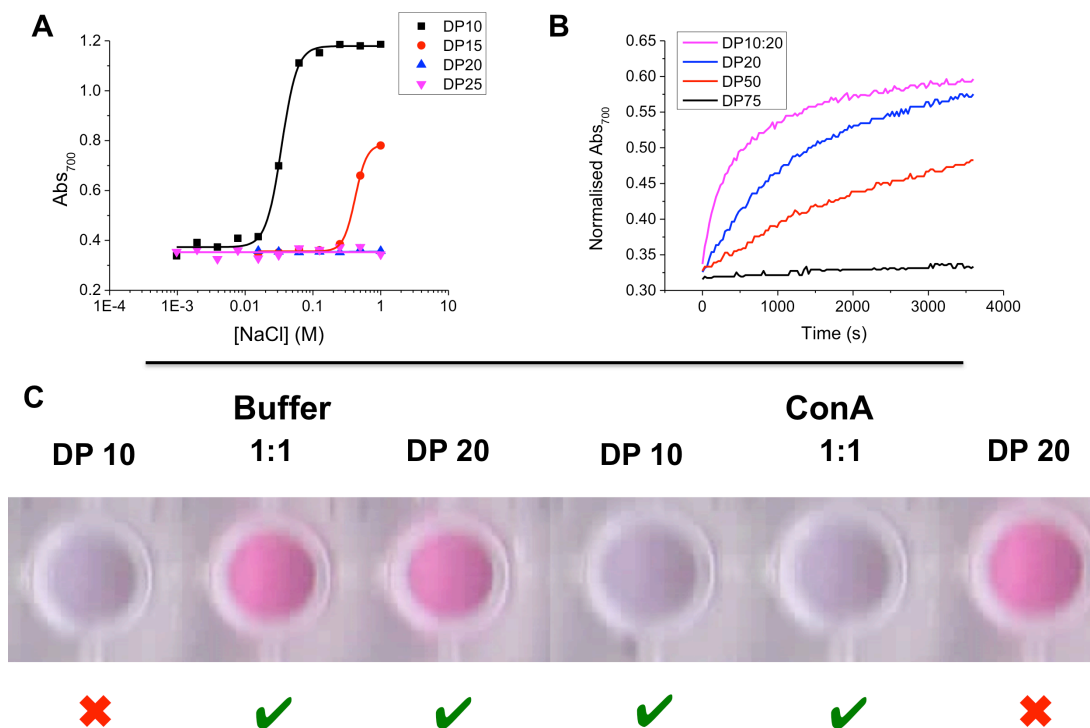
Figure 8.2: Saline stability and kinetics of Con A induced aggregation; A) NaCl titration to determine saline stability of polymer coated AuNPs; B) Kinetics of response of $ManNH_2$-terminated polymer coated AuNP to Con A by UV-Vis spectroscopy; C) Evaluation of the saline stability determined by colour remaining red in buffer and speed of colour change determined by the colour changing from red to blue in after 5 minutes.

With this optimal polymer coating composition determined, the next stage was to investigate these particles with a series of other lectins to ensure i) specificity is maintained; ii) that the coating is universally applicable. In place of $ManNH_2$, Gal NH_2 was introduced into the polymers to evaluate their binding to SBA (Soybean Agglutinin) and RCA_{120} (*Ricinus communis* Agglutinin). RCA_{120} is particularly important as it is a safe to handle relative of the biological warfare agent ricin, and obviously any new sensory systems for this could find broad applicability. Figure 8.3A shows the change in UV-Vis spectra of $GalNH_2$-pHEA-AuNPs upon addition of 0 nM - 85 nM SBA, clearly showing the shift in spectral features from red-blue and an increase in absorbance at 700 nm. The rapid kinetics of the process are shown

in Figure 8.3B highlighting that ultra-fast responses are maintained, relative to longer polymer coatings. To ensure specificity, the interaction of SBA with both GalNH$_2$ and ManNH$_2$ particles were evaluated, and shown in Figure 8.3C. The GalNH$_2$ particles show a clear dose-dependent response to the SBA with a low K$_d$ of 8 nM, whereas the ManNH$_2$ particles do not show a K$_d$ in the concentration range tested. Pleasingly, similar results were found for RCA$_{120}$, (Figure 8.3D) which shows lectin selectivity towards galactose terminal glycans. The GalNH$_2$ functional particles have a K$_d$ of 17 nM, whereas ManNH$_2$ has a far greater K$_d$ of 61 nM, which is to be expected and agrees well with microarray data.[33] Dynamic light scattering was also employed to ensure that aggregation of the particles was the cause of the colour change (rather than just surface-binding or precipitation) (Appendix 6). The size changes of the particles were monitored following addition of 85 nM SBA resulting in the GalNH$_2$ particles rapidly aggregating (as seen by UV-Vis) but the ManNH$_2$ particles showed no changes, confirming specificity of this system which should find broad applicability for large-scale screening of carbohydrate-lectin interactions and point-of-care biosensors.
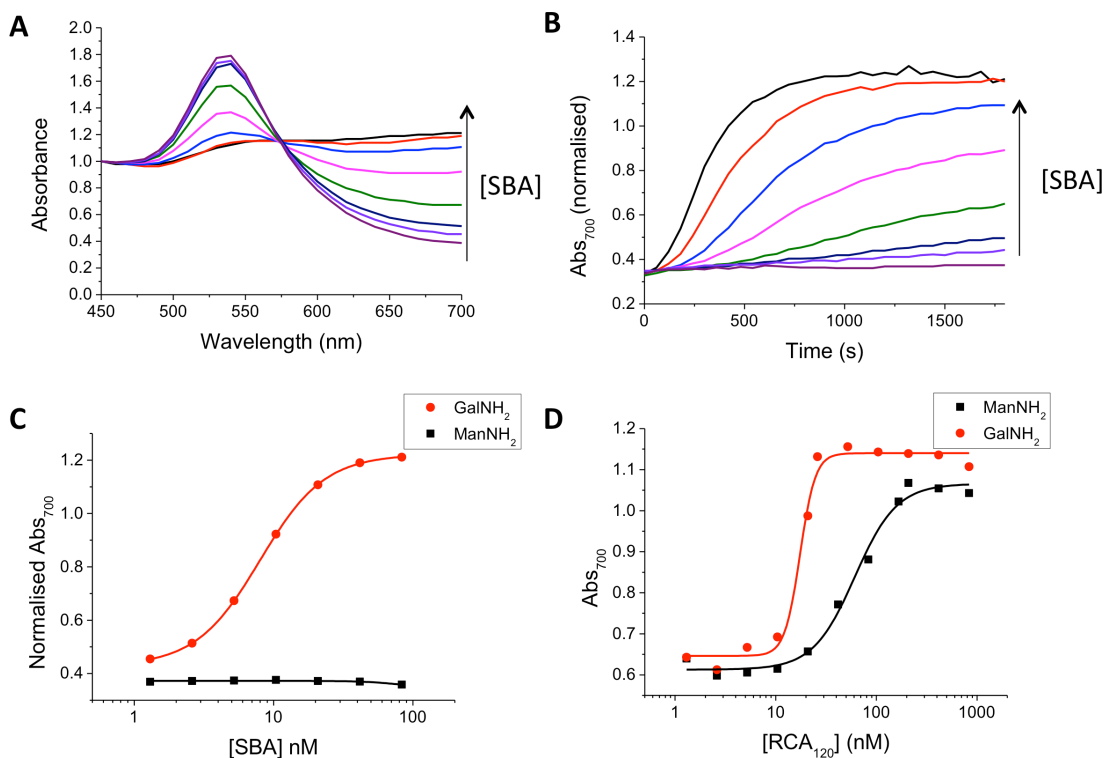
Figure 8.3: Interaction of GalNH$_2$ and ManNH$_2$ functional AuNPs with SBA. A) UV-Vis spectrum of GalNH$_2$-AuNP upon addition of increasing concentrations of SBA (0–80 nM) following 30 minutes of incubation; B) Kinetics of AuNP responses to SBA by monitoring Abs$_{700}$ over 30 mins; C) Binding isotherms (at 37 °C) of GalNH$_2$ and ManNH$_2$ AuNPs with SBA; D) Binding isotherms (at 37 °C) of GalNH$_2$ and ManNH$_2$ AuNPs with RCA$_{120}$.

8.4 Conclusions

In this work, it is shown that coating AuNPs with carbohydrate-functionalised polymers will not always result in a colourimetric assay for lectin binding due to hindrance from the polymer coating. It is crucial to ensure that the polymer is sufficiently long to endow saline stability for use in biological media, but must be balanced against the competing effect that if the polymer is too long, no aggregation events occur (in a reasonable time-scale). Using RAFT polymerisation to probe this, it was found that glycosylated poly(*N*-hydroxyethyl acylamides) with a DP above 50 were unable to generate a response to lectins, even with the correct sugar in place due to steric stabilisation. Through an optimisation study, it was found that mixtures

of DP10 and DP20 polymers gave rise to stable particles with rapid colourimetric responses. These optimised particles were then employed to study the binding interactions with three different lectins, including a surrogate for ricin – a biological warfare agent and may form the basis of new point-of-care diagnostics, especially for low-resource environments.

8.5 Experimental

8.5.1 Materials

All chemicals were used as supplied unless otherwise stated. Acetone, dichloromethane, toluene, methanol, diethyl ether were purchased from Fischer Scientific at laboratory grade. Dodecane thiol ($\geq$ 98 %), potassium phosphate tribasic ($\geq$ 98 %), carbon disulfide (99 %), *N*-Hydroxethylacrylamide (97 %), 4,4′-Azobis(4-cyanovaleric acid) (98 %), mesitylene (reagent grade), N-(3-Dimethylaminopropyl)-N′-ethylcarbodiimide hydrochloride ($\geq$ 98 %) were all purchased from Sigma-Aldrich. 2-bromo-2-methylpropionic acid (98 %), 4-(Dimethylamino)pyridine (99 %), pentafluorophenol (99 %), Triethylamine (99 %) were purchased from Acros. Clear, polystyrene, flat-bottom, half-area 96-well microtitre plates were purchased from Greiner Bio-one. 10 mmol HEPES buffer containing 0.05 M NaCl, 0.1 mM $CaCl_2$ and 0.01 mM $MnCl_2$ (pH 7.5, HEPES) was prepared in 200 mL of milliQ water (with a resistance >19 mOhms). 60 nm gold nanoparticles were obtained from BBI Solutions. Concanavalin A, *Ricinus Communis* Agglutinin and Soybean Agglutinin were purchased from Vector Labs.

8.5.2 Physical and Analytical Methods

NMR spectra were recorded on Bruker DPX-300 and DPX-400 spectrometers for ^{1}H NMR (400 MHz) and ^{13}C NMR (125 MHz). Chemical shifts are reported in ppm relative to the deuterated solvent resonances and spectra analysed with WIN-NMR software. GPC (DMF) was performed on a Varian 390-LC MDS system equipped with a PL-AS RT/MT autosampler, a PL-gel 3 μm (50 × 7.5 mm) guard column, two PL-gel 5 μm (300 × 7.5 mm) mixed-D columns equipped with a differential refractive index, using DMF (with 1 mg.mL^{-1} LiBr) as the eluent with a flow rate of 1.0 mL.min^{-1} at 50 °C. Narrow molecular weight PMMA standards (200 - 1.0 × 106 g.mol^{-1}) were used for calibration using a second order polynomial fit. Infrared absorption spectra were recorded on a Bruker VECTOR-22 FTIR spectrometer using a Golden Gate diamond attenuated total reflection cell. Absorbance measurements were recorded on a BioTek Synergy™ multidetection microplate reader using Gen5 1.11 multiple data collection and analysis software. DLS measurements were carried out using a Malvern Instruments Zetasizer Nano-ZS.

8.5.3 Synthetic procedures

Synthesis of 2-(Dodecylthiocarbonothioylthio)-2-methylpropionic acid (DMP):
Dodecane thiol (4.00 g, 19.76 mmol) was added dropwise to a stirred suspension of K$_3$PO$_4$ (4.20g, 19.76 mmol) in acetone (60 mL) over 25 minutes. CS$_2$ (4.10 g, 53.85 mmol) was added and the solution turned bright yellow. After stirring for ten minutes 2-bromo-2-methylpropionic acid (3.00 g, 17.96 mmol) was added and a precipitation of KBr was noted. After stirring for 16 hours, the KBr precipitate was removed by filtration and then the solvent was removed under *in vacuo* and the residue was extracted into DCM (2 x 200 mL) from 1 M HCl (200 mL). The organic

extracts were washed with water (200 mL) and brine (200 mL) and further dried over MgSO$_4$. The solvent was removed under reduced pressure and the residue was purified by column chromatography on silica using an eluent comprising 75:24:1 40 – 60 °C petroleum ether: diethyl ether: acetic acid to yield a bright yellow solid (4.01 g, 61 %).

^{1}H NMR (300 MHz, CDCl$_3$) δ_{ppm}: 3.26 (2H, t, J_{12-11} = 7.40 Hz, H^{12}); 1.70 (6H, s, H^{13}); 1.65 (2H, m, H^{11}); 1.36 (2H, m, H^{10}); 1.23 (16H, br. s, H$^{2-9}$); 0.86 (3H, t, J_{1-2} = 6.5 Hz, H^1); ^{13}C NMR (500 MHz, CDCl$_3$) δ_{ppm}: 220.19 (C^{13}); 177.76 (C^{16}); 54.91 (C^{14}); 36.46 (C^{12}); 31.31, 29.02, 28.95, 28.84, 28.74, 28.50, 28.36, 22.08 (C$^{2-9}$); 28.59 (C^{10}); 27.19 (C^{11}); 24.60 (C15); 13.52 (C^1); IR ν: 2921 (CH$_2$); 1714 (C=O); 1070 (S-(C=S)-S) cm^{-1}.

Synthesis of 2-(Dodecylthiocarbonothioylthio)-2-methylpropionic acid pentafluorophenyl ester (PFP-DMP): DMP (0.5 g, 1.37 mmol), N-(3-Dimethylaminopropyl)-N′-ethylcarbodiimide hydrochloride (EDC) (0.39 g, 2.05 mmol), and 4-(dimethylamino)pyridine (DMAP) (0.25 g, 2.05 mmol) in 40 mL DCM was stirred for 20 minutes under N$_2$. Pentafluorophenol (0.78 g, 4.24 mmol) in 5 mL DCM was added. The reaction was stirred overnight at room temperature. The reaction was washed successively with 3 M HCl, 1 M NaHCO$_3$ and 0.5 M NaCl. The reaction was then dried over MgSO$_4$, filtered and then concentrated *in vacuuo*.

^{1}H NMR (300 MHz, CDCl$_3$) δ_{ppm}: 3.29 (2H, t, J_{12-11} = 7.3 Hz, H^{12}); 1.84 (6H, s, H^{13}); 1.67 (2H, q, J = 7 Hz, H^{11}); 1.37 (2H, m, H^{10}); 1.23 (16H, br. s, H$^{2-9}$); 0.86 (3H, t, J_{1-2} = 6.5 Hz, H^1);^{13}C NMR (500 MHz, CDCl$_3$) δ_{ppm}: 220.19 (C^{13}); 169.77 (C^{16}); 54.91 (C^{14}); 36.46 (C^{12}); 31.31, 29.02, 28.95, 28.84, 28.74, 28.50, 28.36, 22.08 (C$^{2-9}$);

28.59 (C^{10}); 27.19 (C^{11}); 24.60 (C15); 13.52 (C^1); IR v: 2921 (CH_2); 1779 ($C_6F_5C=O$); 1070 (S-(C=S)-S) cm^{-1}.

Polymerisation of hydroxyethylacrylamide using PFP-DMP: In a typical reaction, N-Hydroxyethyl acrylamide (HEA) (0.5 g, 4.34 mmol), Pentafluorophenyl 2-(Dodecylthiocarbonothioylthio)-2-methylpropionic acid (PFP-DMP) (0.115 g, 0.22 mmol), 4,4′-Azobis(4-cyanovaleric acid) (ACVA) (0.0122 g, 0.043 mmol were dissolved in 50:50 Toluene:Methanol (4 mL). Mesitylene (150 µL) was added as an internal reference. An aliquot was taken for NMR analysis in CDCl$_3$. The solution was degassed under N$_2$ for 30 mins. The reaction was stirred at 70 °C for 90 mins. An aliquot was taken for NMR analysis in MeOD. The reaction was rapidly cooled in liquid nitrogen and precipitated into diethyl ether. The polymer was reprecipitated into diethyl ether from methanol twice to yield a yellow polymer product, which was dried under vacuum. 90 % conversion by NMR, M_n (Theoretical) = 2800 g.mol^{-1} M_n (SEC) = 4100 g.mol^{-1} M_n/M_w (SEC) = 1.14.

End group modification of PFP-pHEA using mannosamine and galactosamine: In a typical reaction, PFP-pHEA (50 mg, 0.018 mmol) and mannosamine (15 mg, 0.088 mmol) were dissolved in DMF (5 mL) with TEA (0.05 M). The reaction was stirred at 50 °C for 16 hrs. The polymer was precipitated into diethyl ether from methanol three times and dried under vacuum. IR analysis indicated loss of C=O stretch corresponding to the PFP ester.

Gold nanoparticle functionalisation using a mixture of DP10 and DP20 pHEA: 1 mg of polymer in water (100 µL) was added to 1 mL of 60 nm particles and left for 30 minutes at room temperature. The particles were centrifuged at 6000 rpm, the

supernatant with any unattached polymer was removed and the particles were resuspended in water.

Lectin induced aggregation studies by Absorbance: A stock solution of the lectin was made up (0.1 mg.mL^{-1} for Con A and 0.01 mg.mL^{-1} for SBA) in 10 nM HEPES buffer with 0.05 M NaCl, 0.1 mM CaCl$_2$ and 0.01 mM MnCl$_2$. 50 μL serial dilution was made up in the same buffer in a 96-well micro-titre plate. 50 μL of the glycoAuNP were added to each well. Absorbance at 450 nm and 700 nm was measured every minute of 30 minutes at 37 °C. After 30 minutes an absorbance spectrum was recorded from 450 nm -700 nm with 10 nm intervals.

Lectin induced aggregation studies by Dynamic Light Scattering (DLS): 300 μL of lectin was added to 300 μL of the glycoAuNPs in disposable a low volume plastic cuvette. Average diameter measurements were taken every 30 seconds for 1 hour at 37 °C.

8.5 References

1.   M. Ambrosi, N. R. Cameron and B. G. Davis, *Org. Bio. Chem.*, 2005, **3**, 1593-1608.

2.   H. Feinberg, D. A. Mitchell, K. Drickamer and W. I. Weis, *Science*, 2001, **294**, 2163-2166.

3.   Y. C. Lee, R. R. Townsend, M. R. Hardy, J. Lonngren, J. Arnarp, M. Haraldsson and H. Lonn, *J. Biol. Chem.*, 1983, **258**, 199-202.

4.   J. J. Lundquist and E. J. Toone, *Chem. Rev.*, 2002, **102**, 555-578.

5.   M. Hartmann and T. K. Lindhorst, *Eur. J. Org. Chem.*, 2011, 3583-3609.

6.   R. J. Pieters, *Org. Biomol. Chem.*, 2009, **7**, 2013-2025.

7.   T. R. Branson and W. B. Turnbull, *Chem. Soc. Rev.*, 2013, **42**, 4613-4622.

8.   M. W. Jones, S. J. Richards, D. M. Haddleton and M. I. Gibson, *Polym. Chem.*, 2013, **4**, 717-723.

9.   S.-J. Richards, M. W. Jones, M. Hunaban, D. M. Haddleton and M. I. Gibson, *Angew. Chem. Int. Ed.*, 2012, **51**, 7812-7816.

10.   C. L. Schofield, B. Mukhopadhyay, S. M. Hardy, M. B. McDonnell, R. A. Field and D. A. Russell, *Analyst*, 2008, **133**, 626-634.

11.   M. Fais, R. Karamanska, S. Allman, S. A. Fairhurst, P. Innocenti, A. J. Fairbanks, T. J. Donohoe, B. G. Davis, D. A. Russell and R. A. Field, *Chem. Sci.*, 2011, **2**, 1952-1959.

12.   J. E. Ghadiali and M. M. Stevens, *Adv. Mater.*, 2008, **20**, 4359-4363.

13.   G. J. Nusz, S. M. Marinakos, A. C. Curry, A. Dahlin, F. Hook, A. Wax and A. Chilkoti, *Anal. Chem.*, 2008, **80**, 984-989.

14.   A. Laromaine, L. L. Koh, M. Murugesan, R. V. Ulijn and M. M. Stevens, *J. Am. Chem. Soc.*, 2007, **129**, 4156-4157.

15.   A. K. Singh, D. Senapati, S. G. Wang, J. Griffin, A. Neely, P. Candice, K. M. Naylor, B. Varisli, J. R. Kalluri and P. C. Ray, *ACS Nano*, 2009, **3**, 1906-1912.

16.   K. M. Mayer, S. Lee, H. Liao, B. C. Rostro, A. Fuentes, P. T. Scully, C. L. Nehl and J. H. Hafner, *ACS Nano*, 2008, **2**, 687-692.

17.   S. H. Huang, *Sens. Actuators, B*, 2007, **127**, 335-340.

18.   A. J. Haes, L. Chang, W. L. Klein and R. P. Van Duyne, *J. Am. Chem. Soc.*, 2005, **127**, 2264-2271.

19.   P. Englebienne, *Analyst*, 1998, **123**, 1599-1603.

20.   N. Ohtake, K. Niikura, T. Suzuki, K. Nagakawa, H. Sawa and K. Ijiro, *Bioconjugate Chem.*, 2008, **19**, 507-515.

21.   P. V. Baptista, M. Koziol-Montewka, J. Paluch-Oles, G. Doria and R. Franco, *Clin. Chem.*, 2006, **52**, 1433-1434.

22.   R. Elghanian, J. J. Storhoff, R. C. Mucic, R. L. Letsinger and C. A. Mirkin, *Science*, 1997, **277**, 1078-1081.

23.   S. Watanabe, K. Yoshida, K. Shinkawa, D. Kumagawa and H. Seguchi, *Colloids Surf., B*, 2010, **81**, 570-577.

24.   Y. J. Chuang, X. C. Zhou, Z. W. Pan and C. Turchi, *Biochem. Biophys. Res. Commun.*, 2009, **389**, 22-27.

25.   L. Otten, S.-J. Richards, E. Fullam, G. S. Besra and M. I. Gibson, *J. Mater. Chem. B*, 2013, **1**, 2665-2672.

26.   C. C. Lin, Y. C. Yeh, C. Y. Yang, G. F. Chen, Y. C. Chen, Y. C. Wu and C. C. Chen, *Chem. Commun.*, 2003, 2920-2921.

27.   H. S. N. Jayawardena, X. Wang and M. Yan, *Anal. Chem.*, 2013, **85**, 10277-10281.

28.   M. J. Marin, A. Rashid, M. Rejzek, S. A. Fairhurst, S. A. Wharton, S. R. Martin, J. W. McCauley, T. Wileman, R. A. Field and D. A. Russell, *Org. Biomol. Chem.*, 2013, **11**, 7101-7107.

29.   S.-J. Richards, E. Fullam, G. S. Besra and M. I. Gibson, *J. Mater. Chem. B*, 2014, **2**, 1490-1498.

30.   M. I. Gibson, E. Froehlich and H.-A. Klok, *J. Polym. Sci. A Polym. Chem.*, 2009, **47**, 4332-4345.

31. J. Chiefari, Y. K. Chong, F. Ercole, J. Krstina, J. Jeffery, T. P. T. Le, R. T. A. Mayadunne, G. F. Meijs, C. L. Moad, G. Moad, E. Rizzardo and S. H. Thang, *Macromolecules*, 1998, **31**, 5559-5562.

32. R. T. A. Mayadunne, E. Rizzardo, J. Chiefari, J. Krstina, G. Moad, A. Postma and S. H. Thang, *Macromolecules*, 2000, **33**, 243-245.

33. CFG, http://www.functionalglycomics.org.

Chapter 9

Glyco-gold nanoparticle libraries for label-free, low-cost and high throughput evaluation of glycan/lectin interactions for affinity measurements and ratiometric biosensing

S-J. Richards, L. Otten and M. I. Gibson, *In Preparation*

This chapter consists of a manuscript to be submitted to a peer-reviewed journal. Using the optimised polymer linker system from Chapter 8, the natural reactivity of reducing sugars towards hydrazide was utilised to obtain carbohydrate functional gold nanoparticles for lectin discrimination. A range of monosaccharides were conjugated to the polymer linker and these were tested for their interaction (determine by a colourimetric response) with a panel of plant lectins. This colourimetric response can be determined spectrophotometrically or by simply using a digital/mobile phone camera and image analysis software. The statistical technique, linear discriminant analysis, was used to differentiate each lectin.

I carried out all the synthesis, characterisation and testing and Lucienne Otten conducted the linear discriminant analysis. I also prepared the manuscript.

9.1 Abstract

Carbohydrate functional gold nanoparticles may find wide applicability as biosensors for infectious diseases and biological warfare agents due to their characteristic aggregation-induced colour change. Here, the ability to discriminate between lectins is determined using simple, natural monosaccharides conjugated to gold nanoparticles. It is shown that the colour change in response to correct lectin-glycan pairings can be determined spectrophotometrically or by using the simple combination of a flatbed scanner and image analysis freeware, providing a low cost route to investigating protein-carbohydrate interactions for low resource settings. These simple, carbohydrate functional gold nanoparticles are powerful tools for probing protein-carbohydrate interactions. Excellent separation is observed when linear discriminant analysis is used to differentiate the panel of lectins used based on the response the glycosylated nanoparticles give.

9.2 Introduction

Carbohydrates coat most cell types in nature and are involved in a multitude of essential biological processes such as cell signalling, cell-cell communication, inflammation and fertilisation.[1-4] However, bacteria, their toxins and viruses can exploit these cell surface oligosaccharides for adhesion to host tissues and is the first step in many infectious diseases.[4, 5] The proteins that mediate these interactions are known as lectins, they interact with carbohydrates non-covalently and reversibly with a high level of specificity.[6, 7] Protein-monosaccharide interactions are typically weak with values for K_d in the range of 10^{-3}-10^{-6} M. This intrinsically weak affinity is circumvented in nature by the involvement of multiple protein-carbohydrate interactions leading to the high affinity and specificity, this is known as the 'cluster glycoside effect', which is regarded as the enhancement in the activity of a

multivalent ligand beyond the simple linear sum of the total number of ligands.[8, 9] This simple, but still not fully understood enhancement effect, presents huge opportunities in macromolecular and nanoscale science to probe glycan function.[4-6, 10]

The ubiquitous nature of carbohydrate-lectin interactions in infectious diseases presents new opportunities in drug design and biosensing. For example, urinary tract infections in humans are strongly associated with *Escherichia coli* producing type I mannose specific adhesins.[5,11] Pulmonary pathogens such as those typically infecting cystic fibrosis (CF) patients such as *Pseudomonas aeruginosa* bind to GalNAcβ1-4Gal residues on lung epithelia.[5, 10] The *Vibrio cholerae* bacteria responsible for cholera releases an AB_5 toxin (cholera toxin) that binds to galactose containing GM1 ganglioside on intestinal epithelial cells.[12-14] Ricin is a toxic lectin found in castor beans from the plant *Ricinus communis,* which is lethal and poses a potential security threat as a biological warfare agent.[15, 16] Also, the nature of cell-surface carbohydrates can differ considerably between diseased and normal cells.[17] Differences in glycosylation have been detected in many cancer cells and it has been suggested that these differences determine the metastatic potential of tumours. Unique glycan markers of diseased cells can be exploited for early diagnosis, prevention and treatment of illnesses.[17] Therefore, rapid detection of various lectin types is required, not only for diagnosis but also for developing effective therapeutics. However, glycans are inherently complex and it is observed that lectins are capable of binding a range of related carbohydrate structures to varying extents, further complicating the challenge of assigning protein-carbohydrate interactions.[3] Carbohydrate microarrays have been developed to aid in the identification of protein-carbohydrate interactions as new drug targets,[18-21] however, they are difficult

to construct and require a protein-labelling step which results in heterogeneity, synthetic complexity and is not a truly native assay. Therefore the development of fast, label-free, easy and inexpensive sensors for the analysis of carbohydrate-protein interactions is highly desirable. The current best methods for this are interferometry, quartz crystal microbalance (QCM) and surface plasmon resonance (SPR). However, all three of these require infrastructure and their throughput is still relatively low, running 10's of samples per hour typically.[22]

Nanoparticle-based materials are attractive alternatives to the fluorescence- or radiolabelled protein substrates, owing to their photo-stability, ease of synthesis and ability to conjugate to biological molecules. Gold nanoparticles (AuNPs) are highly attractive as biosensors, due to exhibiting an intense colour in the visible region as a result of collective oscillation of the conduction-band electrons of the gold core. Factors affecting the optical properties of nanoparticles include, size and shape, degree of aggregation and the dispersion medium.[16] Aggregation of AuNPs leads to a dramatic colour change from red to blue (dependant upon interparticle distance) due to electric dipole-dipole interactions and coupling between the plasmons of neighbouring particles resulting in a broadening and a shift to longer wavelengths of the surface plasmon absorption band. The colour changes associated with AuNP aggregation has been exploited in the development of colourimetric assays for biomolecular interactions by utilising AuNPs functionalised with biomolecules such as proteins, peptides and DNA.[23-27]

Carbohydrate-functionalised AuNPs (glycoAuNPs) are emerging as important tools for the colourimetric determination of carbohydrate-protein interactions as they constitute a good biomimetic model of carbohydrates at the cell surface (glycocalyx). The multivalent presentation of carbohydrates can compensate

for the low affinity of individual protein-carbohydrate interactions and the inherent multivalency of lectins should lead to an optical response as a result of aggregation if the correct lectin-carbohydrate paring is present. GlycoAuNPs have been exploited for the detection of lectins,[16, 28-30] bacteria[31, 32] and influenza.[33] Whilst appealing scaffolds, glycosylated nanoparticles have intrinsic low colloidal stability, resulting in either false-positive aggregation responses or preventing high-throughput application. Gibson *et al*. have recently demonstrated that through precision macromolecular engineering using RAFT (reversible addition-fragmentation chain transfer) polymerisation it is possible to improve colloidal stability, without presenting a steric block to aggregation.[30]

Herein, we describe a polymer-stabilised glycosylated gold nanoparticle platform for the high throughput, label-free screening of carbohydrate-lectin interactions and demonstrate its potential in glycobiology in a range of assays. A mix-and-match synthetic strategy enables huge chemical space to be explored, with the outputs being read in a simple multi-well plate format by both a microplate reader, or simply using a digital camera. Through the use of a training algorithm, with linear discriminant analysis (LDA) it was possible to develop a platform that can correctly identify six distinct lectins from an unknown sample based solely on colourimetric readouts.

9.2 Results and Discussion

GlycoAuNPs were prepared using an optimised polymer coating method we developed recently that produces particles that are stable at physiological salt concentration and gives fast lectin detection.[30] Our synthetic methodology was designed to enable facile and versatile conjugation of the carbohydrates to the gold

nanoparticles using native, underivatised carbohydrates, with the aim of circumventing the need for 'click' type conjugation and the synthetic burden of the introduction of alkynes, azides or thiols.[34, 35] Scheme 9.1 shows the general method employed. *N*-hydroxyethyl acrylamide (HEA) was polymerised by RAFT polymerisation to a targeted degree of polymerisation (DP) of 20, which we have previously shown to give the precise balance between colloidal stability and rapid sensing (See chapter 8).[30] By using a pentafluorophenyl (PFP) containing RAFT agent, the produced telechelic polymers had both an amine-reactive ω-terminus (for conjugation to sugars) and a protected thiol at the α-terminus for subsequent gold particle immobilisation. The PFP functionality is extremely reactive to amines, but has good aqueous stability, compared to NHS esters for example.[36, 37] Scheme 9.1 shows the synthetic route to glycosylated AuNPs. The PFP moiety can be used to install a hydrazide end group for subsequent amidation with reducing sugars.[38] This approach enables the introduction of a range of carbohydrates, which facilitates our later analysis (*vide infra*). During carbohydrate coupling, the trithiocarbonate end-group is aminolysed releasing the thiol enabling coating of 60 nm AuNPs by simple mixing. 60 nm particles were chosen, as we have found that smaller particles give lower colourimetric responses and lower affinities.[32] This post-polymerisation route ensures that all the polymers have the same initial chain length distribution and therefore reduced the variability between particles, but allows versatile end group functionalisation to make libraries of a variety of glycan functional particles.
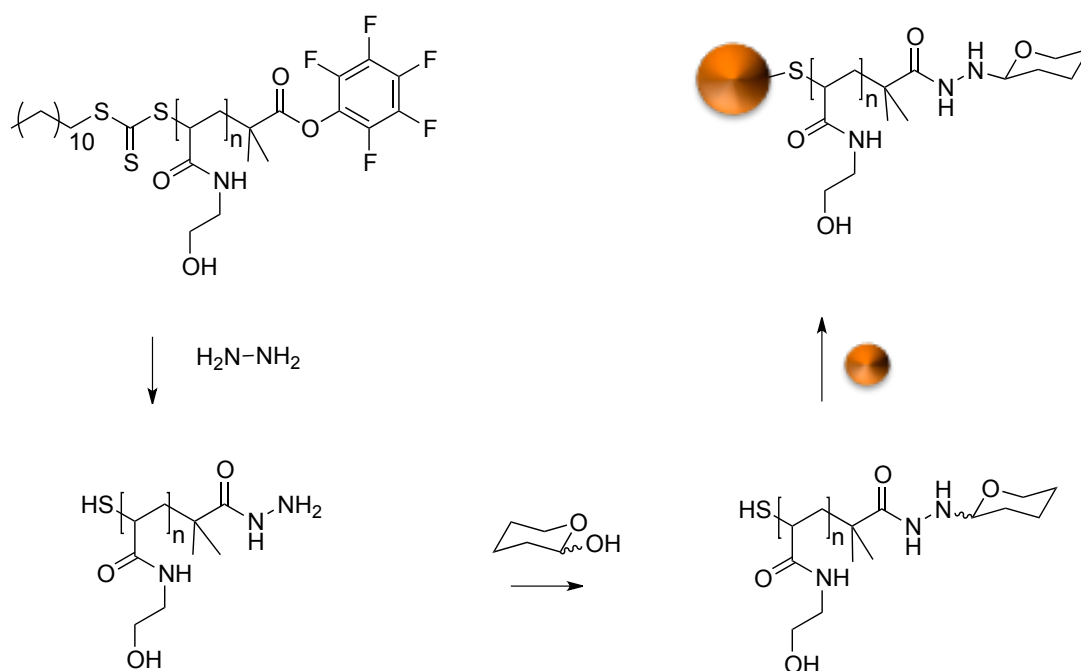
Scheme 9.1: Synthetic routes to carbohydrate functionalised gold nanoparticles.

The intrinsic reactivity of reducing sugars toward hydrazides to form stable *N*-glycoside end-terminated polymers was used. The reaction occurs under mild conditions with good conjugation efficiencies. The reducing sugars react with α-heteroatom nucleophiles (e.g. hydrazide or alkylaminooxy groups) to give mostly cyclic pyranosides, but some ring-opened forms will still form, but is reduced by the reaction conditions employed.[38] AuNPs were functionalised with a library of seven monosaccharides, Man, Gal, Glc, ManNAc, GalNAc, GlcNAc and Fuc. A 5 nm increase in particle size was noted for each polymer as determined by dynamic light scattering (DLS) (Appendix 7) confirming successful functionalisation of the AuNP surface, to give a library of seven glycosylated nanoparticles with identical sensory cores and hydrodynamic diameters.

With this library at hand, the evaluation of their interactions with a panel of six lectins was taken forward; Concavanalin A (Con A), *Ricinus Communis* Agglutinin (RCA$_{120}$, which is a non-toxic variant of Ricin), Soybean Agglutinin

(SBA), Peanut Agglutinin (PNA), Wheat Germ Agglutinin (WGA) and *Ulex Europaeus* agglutinin (UEA). To assess the binding interaction, the glycosylated AuNPs were added to 96-well plate at a concentration of 0.06 M of Au. The appropriate lectins were then added as a dilution series into these wells, and incubated for 30 minutes. After this time, if binding was occurring the particles will crosslink (aggregate) causing a red to blue shift, as shown in the digital photograph of an example plate in Figure 9.1A, where high concentrations of lectins cause an increasing blue shift. This can be monitored using a UV-Vis microplate reader, to give a full spectrum for each sample, Figure 9.1B, which can then be collated to visualise the overall change in as shown in Figure 9.1C. For example, the spectra in Figure 9.1C1 show a sample that has not interacted with the lectin, but in Figure 9.1C2 there is a clear dose dependant response. These curves can then be converted into binding isotherms, based on the change in absorbance at 700 nm, Figure 9.1D.
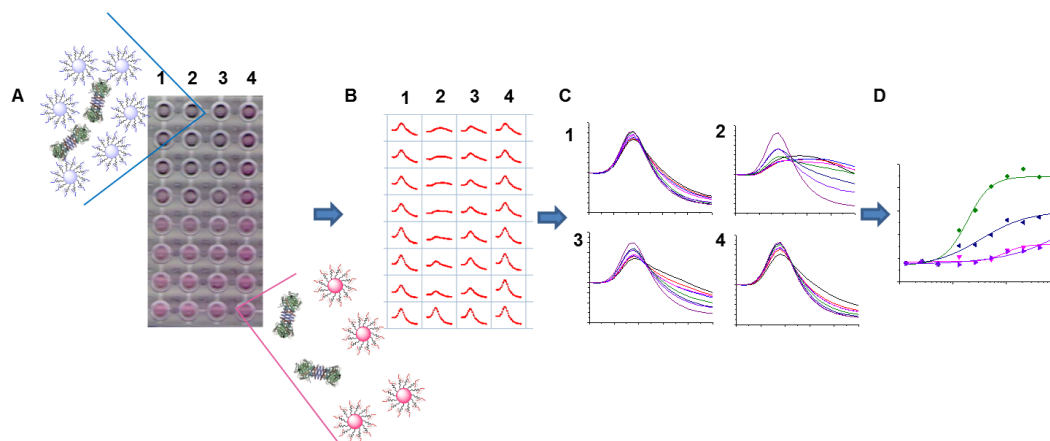
Figure 9.1: Overview of the approach used to allow direct measurement of carbohydrate-lectin interactions by monitoring a colourimetric change (red to blue) due to aggregation of glycoAuNPs bound to lectins.

Using the methodology outlined above, the serial dilutions of each lectin with each nanoparticle was conducted and analysed. In this set, a total of 336 individual, label-free, interaction measurements were conducted (7 sugars, 6 lectins, 8

concentrations). Figure 9.2 summarises the data as dose-dependant binding isotherms for all of these, by plotting the Abs_{700} against protein concentration. As can clearly be seen, a huge amount of data is readily obtained by this method, which would be challenging, expensive and time consuming to extract from SPR type methods, for example.
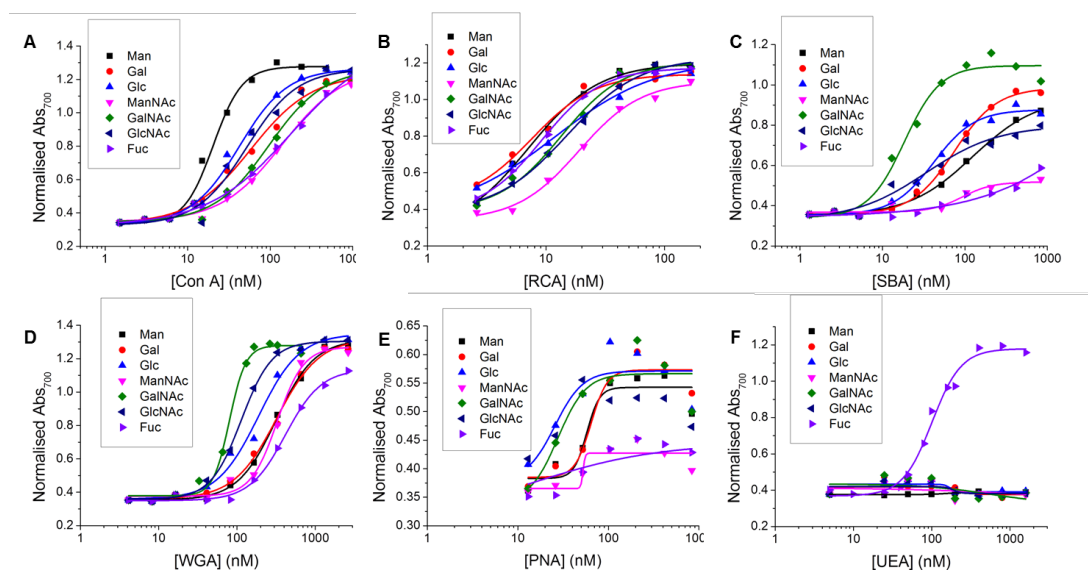
Figure 9.2: Dose-dependent binding isotherms of Man, Gal, Glc, ManNAc, GalNAc, GlcNAc and Fuc functionalised particles with A) Con A B) RCA C) SBA D) WGA E) PNA F) UEA.

To enable these curves to be used to understand their binding interactions, all the data were fitted to Hill functions to obtain the apparent dissociation constants (K_d) as a measure of the relative affinity of each glycan to the lectin partner. These values are summarised in Table 9.1. The selectivity of each lectin for monosaccharide agreed well with microarray data from the Consortium for Functional Glycomics (CFG) database.[39] It is important to highlight that this data shows that monosaccharides (and even more complex glycans) do not bind a single lectin (and that any given lectin can bind many different carbohydrates) and that it is crucial to not study these interactions in isolation, but as a panel of lectins in order to

222

truly probe specificity and affinity. For example, SBA is β-*N*-acetylgalactosamine specific and shows the highest affinity to GalNAc functional particles and Con A is α-mannose/α-glucose specific and shows the highest affinity for mannose and UEA is fucose specific and interacts highly specifically with fucose and showed essentially zero binding to other carbohydrates in the concentration range used here. This broad set of data also shows the challenges intrinsic to developing biosensors based on glycans, due to their broad binding potential that makes specific 'lock and key' style interaction challenging. This particular point is addressed later in the manuscript.

	Con A	RCA	SBA	PNA	WGA	UEA
Man	20.4 ± 1.6	7.6 ± 2.5	124.5 ± 16.5	57.6 ± 16.3	317.3 ± 16.1	N/A
Gal	58.7 ± 8.7	7.1 ± 3.3	74.6 ± 4.2	64.2 ± 14.3	319.9 ± 26.4	N/A
Glc	42.2 ± 3.8	11.7 ± 3.6	42.0 ± 3.7	23.7 ± 19.8	187.7 ± 20.5	N/A
ManNAc	140.2 ± 22.3	19.0 ± 1.9	92.8 ± 22.7	52.5 ± 11.3	326.2 ± 24.0	N/A
GalNAc	96.6 ± 11.1	13.4 ± 2.3	18.5 ± 2.4	27.7 ± 14.9	80.1 ± 4.4	N/A
GlcNAc	52.2 ± 9.0	15.1 ± 1.5	33.7 ± 11.8	26.5 ± 8.8	113.5 ± 4.4	N/A
Fuc	177.8 ± 33.9	9.2 ± 0.8	N/A	N/A	415.6 ± 24.2	100.5 ± 6.9

Table 9.1: Dissociation constant (K_d) in nM for each glycoAuNP and lectin combination determined by Abs_{700}.

9.2.1 Measuring interactions using a scanned image

Due to the strong colouration of the gold particle solutions, the colour change upon binding is obvious to the naked eye (Figure 9.1A). Previously, we demonstrated that citrate stabilised-AuNPs could be used as resolving agents in sorbent assays of lectins to carbohydrates by measuring the amount of non-specifically bound gold to a lectin bound surface, and that a simple mobile phone camera, and image analysis software could be used to measure inhibition.[40] Due to the high extinction coefficient of AuNPs we employed a similar technique here to determine the degree of aggregation and hence affinity from a scanned image of the 96-well plate (Figure 9.3A) and simple, open access visualisation software, ImageJ to obtain pixel

intensity (Figure 9.3B). Figure 9.3C shows the comparison of K_d value determined by UV-Vis and by pixel intensity. Figure 9.3D shows the correlation between the apparent K_d values determined by the two methods. It shows strong positive correlation between the techniques with an R^2 value of 0.977, demonstrating that this analysis is also possible in laboratories without a microplate reader, or in low resource settings. All extracted K_d values are also given in Table 9.2.
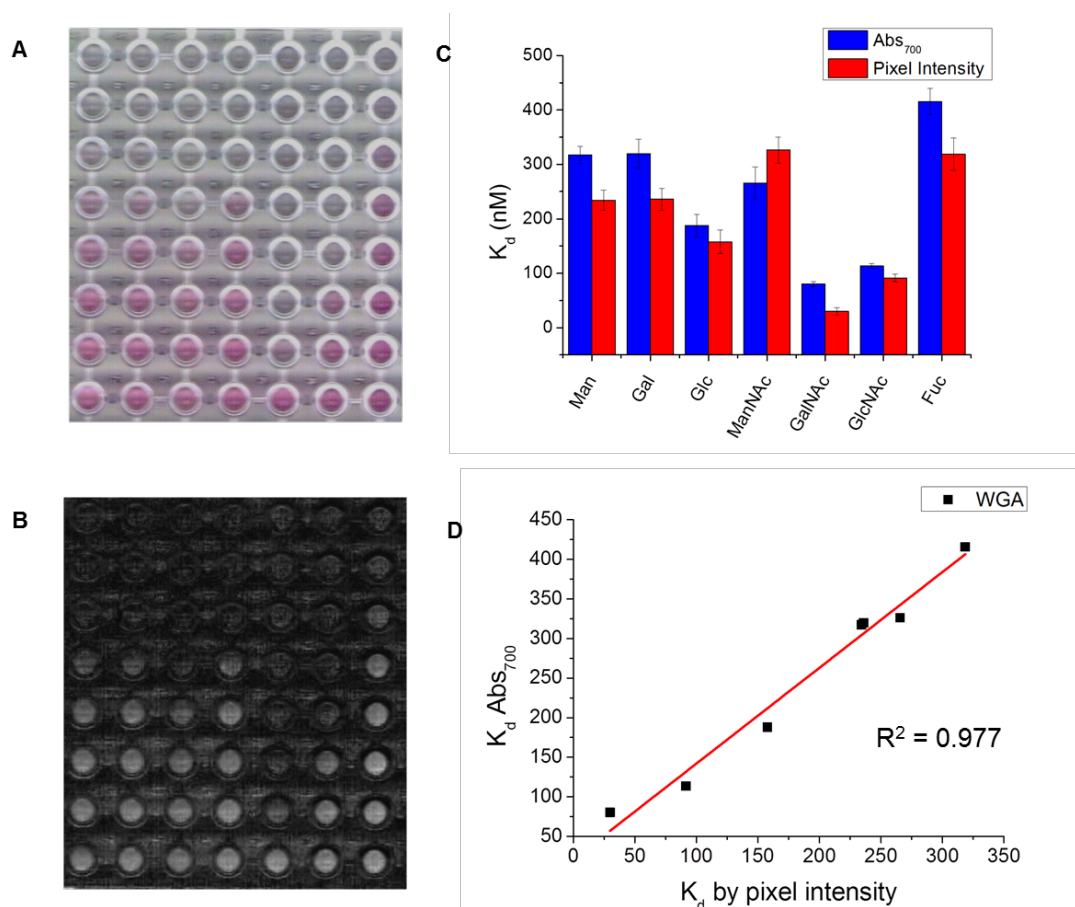
Figure 9.3: Direct optical analysis of protein binding. A) Scanned image of glycoAuNPs with a dilution series of WGA after 30 minutes. B) Saturation image used for pixel intensity measurement (high intensity = red, low intensity = blue). C) Comparison of K_d calculated by Abs_{700} and pixel intensity. D) Correlation between K_d values determined by Abs_{700} and pixel intensity.

Table 9.2: Dissociation constant (K_d) in nM for each glycoAuNP and lectin combination determined by pixel intensity from a scanned image.

	Con A	RCA	SBA	WGA	UEA
Man	18.2 ± 1.2	4.7 ± 0.4	97.6 ± 9.1	234.2 ± 18.3	N/A
Gal	54.4 ± 9.0	1.5 ± 0.1	62.2 ± 22.3	235.9 ± 20.3	N/A
Glc	36.7 ± 6.9	5.5 ± 1.6	57.4 ± 11.6	157.8 ± 22.0	N/A
ManNAc	109.4 ± 10.6	16.1 ± 1.5	N/A	265.6 ± 29.6	N/A
GalNAc	70.1 ± 6.0	7.5 ± 0.4	11.2 ± 0.8	29.8 ± 7.2	N/A
GlcNAc	49.1 ± 14.1	7.9 ± 0.4	30.5 ± 4.4	91.5 ± 6.8	N/A
Fuc	169.5 ± 32.9	6.6 ± 0.6	N/A	318.6 ± 39.7	42.6 ± 3.3

9.2.2 Differentiation of lectins

As a final demonstration of the utility of this methodology, we sought to apply the rapid colour change as a versatile lectin discrimination tool, which could be used in diagnostics. Due to the relatively low specificities of monosaccharides to lectins (compared to complex glycans) glycoconjugates often show a broad range of binding affinities to several lectins (as exemplified in Table 9.1, above). However, we have previously shown that by replacing a single glycoconjugate, with a panel of them, it is possible to use multiplexed (or ratiometric) assays to discriminate between a panel of fluorescently labelled Gal-specific lectins as a 'chemical tongue', based on the differences in relative affinity between sugars. We therefore reasoned that the colour-changing assay described here could be extended to a label free, multiplexed diagnostic platform. Therefore, a panel of six glyconanoparticles with a range of carbohydrates attached, were incubated with our panel of six lectins, and the total change in Abs_{700} recorded, and plotted in Figure 9.4A. As can be clearly seen, any individual lectin binds multiple sugars, and *vice versa*. However, the pattern of binding is unique to each lectin. For example, SBA gives a greater response to GalNAc particles than ManNAc particles whereas Con A gives a greater response to ManNAc than GalNAc. We can mathematically express these differences using linear discriminant analysis (LDA), which is a statistical approached used to separate

two or more classes of objects. LDA takes an input training matrix of the initial

particles bound to the different glyconanoparticles (the data displayed in Figure

9.4A) and generates distinct binding profiles for all the lectins with maximum

separation between groups in order to generate a robust model for identifying

unknown lectin samples without any fluorescent labels (Figure 9.4B).
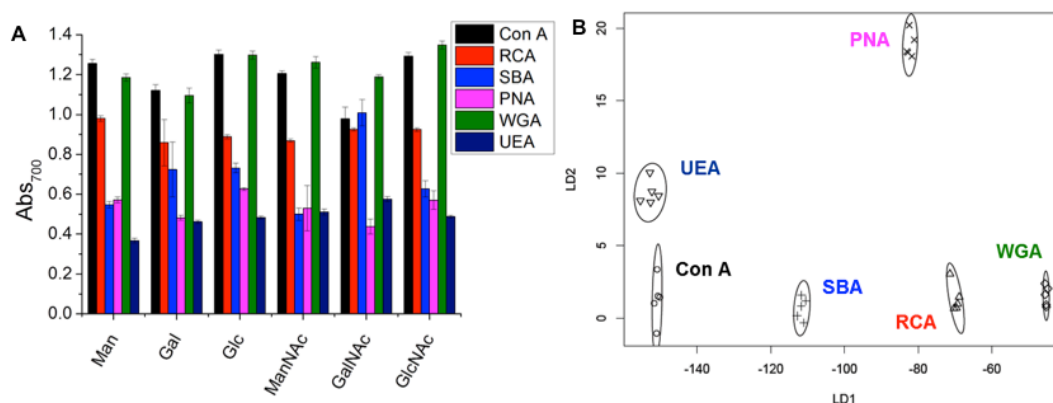
Figure 9.4: Lectin Discrimination A) Absorbance at 700 nm of Man, Gal, Glc, ManNAc, GalNAc, GlcNAc and Fuc functionalised particles with 6.25 μg.mL^{-1} Con A, RCA, SBA, WGA, PNA, UEA. Each is the average of 5 measurements. B) Linear Discriminant plot showing excellent segregation between lectins. The centres of the ellipses represent the mean values of that class and the boundaries of the ellipses are one standard deviation from the mean.

Figure 9.4B clearly shows that excellent segregation between each lectin is achieved.

Using a leave one out approach, where a model is produced from the rest of the data,

all lectins can be correctly identified with a high level of confidence. The minimum

variables required to correctly predict the lectins can be determined. In this instance,

there are a number of two glycoAuNP pairings that will correctly predict all the

lectins, including Man and GalNAc or GlcNAc and GalNAc, however the certainty

decreases with fewer variables. This glycoAuNP technique therefore constitutes a

robust and versatile platform for investigating carbohydrate-protein interactions and

can also be used to identify lectin samples.

9.4 Conclusion

We have developed a high throughput screening technique based on the colourimetric response of glycoAuNPs in response to a panel of plant lectins. A facile conjugation route is used that allows for the incorporation of any reducing sugar onto polymer-stabilised AuNPs. The lectin-induced colourimetric response of these glycoAuNPs can be determined spectrophotometrically or by the simple combination of a flatbed scanner and image analysis software. Good correlation between the values determined by the two techniques suggests that this could be a low cost/low-tech route to the discrimination between lectins. Excellent separation between all the lectins testing was achieved using LDA, allowing successful differentiation of all the lectins using only simple monosaccharide functionalities.

9.5 Experimental Section

9.5.1 Materials

All chemicals were used as supplied unless otherwise stated. Acetone, dichloromethane, toluene, methanol, diethyl ether and dimethylformamide were purchased from Fischer Scientific at laboratory grade. 2-(Dodecylthiocarbonothioylthio)-2-methylpropionic acid pentafluorophenyl ester, (PFP-DMP) was synthesised as previously described (See Chapter 8),[30] *N*-Hydroxethylacrylamide (97 %), 4,4′-Azobis(4-cyanovaleric acid) (98 %), mesitylene (reagent grade), N-(3-Dimethylaminopropyl)-N′-ethylcarbodiimide hydrochloride (≥ 98 %), hydrazine hydrate solution (78-82 %) D-(+)mannose, α-D-glucose, D-(+)galactose, D-galactosamine hydrochloride (98 %), D-mannosamine hydrochloride (98 %), D-glucosamine hydrochloride (< 98 %) and *N*-acetyl-D-mannosamine were

all purchased from Sigma-Aldrich. 2-bromo-2-methylpropionic acid (98 %), 4-(Dimethylamino)pyridine (99 %), pentafluorophenol (99 %), Triethylamine (99 %) were purchased from Acros. Low bind, low volume, clear, flat bottom, microtitre plates were purchased from Greiner Bio-one. *N*-acetylgalactosamine, *N*-acetylglucosamine and fucose were purchased from Carbosynth. 10 mmol HEPES buffer containing 0.05 M NaCl, 0.1 mM $CaCl_2$ and 0.01 mM $MnCl_2$ (pH 7.5, HEPES) was prepared in 200 mL of milliQ water (with a resistance >19 mOhms). 60 nm gold nanoparticles were obtained from BBI Solutions. Concanavalin A, Soybean Agglutinin, *Ricinus Communis* Agglutinin, Peanut Agglutinin, Wheat Germ Agglutinin and *Ulex Europeaus* Agglutinin were purchased from Vector Labs.

9.5.2 Physical and Analytical Methods

NMR spectra were recorded on Bruker DPX-300 and DPX-400 spectrometers for ^{1}H NMR (400 MHz) and ^{13}C NMR (125 MHz). Chemical shifts are reported in ppm relative to the deuterated solvent resonances and spectra analysed with WIN-NMR software. GPC (DMF) was performed on a Varian 390-LC MDS system equipped with a PL-AS RT/MT autosampler, a PL-gel 3 μm (50 × 7.5 mm) guard column, two PL-gel 5 μm (300 × 7.5 mm) mixed-D columns equipped with a differential refractive index, using DMF (with 1 mg.mL^{-1} LiBr) as the eluent with a flow rate of 1.0 mL.min^{-1} at 50 °C. Narrow molecular weight PMMA standards (200 - 1.0 × 106 g.mol^{-1}) were used for calibration using a second order polynomial fit. Infrared absorption spectra were recorded on a Bruker VECTOR-22 FTIR spectrometer using a Golden Gate diamond attenuated total reflection cell. Absorbance measurements were recorded on a BioTek SynergyTM multidetection microplate reader using Gen5

1.11 multiple data collection and analysis software. DLS measurements were carried out using a Malvern Instruments Zetasizer Nano-ZS.

9.5.3 Synthetic procedures

Polymerisation of hydroxyethylacrylamide using PFP-DMP DP20:

Hydroxyethylacrylamide (HEA) (0.5 g, 4.34 mmol), Pentafluorophenyl 2-(Dodecylthiocarbonothioylthio)-2-methylpropionic acid (PFP-DMP) (0.115 g, 0.22 mmol), 4,4′-Azobis(4-cyanovaleric acid) (ACVA) (0.0122 g, 0.043 mmol were dissolved in 50:50 Toluene:Methanol (4 mL). Mesitylene (150 µL) was added as an internal reference. An aliquot was taken for NMR analysis in $CDCl_3$. The solution was degassed under N_2 for 30 mins. The reaction was stirred at 70 °C for 90 mins. An aliquot was taken for NMR analysis in MeOD. The reaction was rapidly cooled in liquid nitrogen and precipitated into diethyl ether. The polymer was reprecipitated into diethyl ether from methanol twice to yield a yellow polymer product, which was dried under vacuum. 90 % conversion by NMR, M_n (Theoretical) = 2800 g.mol^{-1} M_n (SEC) = 4100 g.mol^{-1} M_w/M_n (SEC) = 1.14.

End group modification of PFP-poly(hydroxyethylacrylamide) using hydrazine:
PFP-pHEA (500 mg, 0.18 mmol), hydrazine (50 µL 1.5 mmol) were dissolved in 5 mL DMF. The reaction was stirred at 50 °C for 16 hrs. The polymer was precipitated into diethyl ether from methanol three times and dried under vacuum. IR indicated loss of C=O stretch corresponding to the PFP ester.

Carbohydrate functionalisation of hydrazide-pHEA: In a typical reaction, hydrazide-pHEA (10 mg, 0.0043 mmol), reducing sugar (3 mg) in 1 mL 100 mM acetate containing 1 mM aniline. Left at 50 °C over night. Employed immediately for goldnanoparticle functionalisation

Gold nanoparticle functionalisation using a carbohydrate terminated pHEA:

1 mg of polymer in 100 μL water was added to 1 mL of 60 nm particles (OD_{600} = 1, 0.288 mM Au) and left for 30 minutes at room temperature. Following incubation the particles were centrifuged at 6000 rpm, the supernatant was removed along with any unattached polymer, the particle were then resuspended in water.

Particle size determination by Dynamic Light Scattering (DLS): 400 μL of glycoAuNPs in a disposable low volume cuvette. 3 measurements comprised of 10 runs were made of each sample at 25 °C. Average size and distribution were recorded.

Lectin induced aggregation studies by Absorbance: A 0.1 mg.mL^{-1} stock solution of the lectin was made in 10 nM HEPES buffer with 0.05 M NaCl, 0.1 mM $CaCl_2$ and 0.01 mM $MnCl_2$. 25 μL serial dilution was made up in the same buffer in a 96-well micro-titre plate. 25 μL of the glycoAuNP were added to each well. After 30 minutes an absorbance spectrum was recorded from 450 nm -700 nm with 10 nm intervals.

The plates were then scanned using a canon flatbed scanner, the images were converted to a HSB stack and the saturation image was used for tiff image file uploaded into the open- source image processing package ImageJ (version 1.46a) where a region of interest was drawn around every well. The colour (RGB) image was then converted into a hue saturation and brightness (HSB) stack of images and the saturation image used. The regions of interest drawn on the original image were added to the saturation image using the ROI manager and average pixel intensity in each region of interest was measured using an inbuilt function in ImageJ.

A fixed concentration of 6.25 µg.mL^{-1} lectin was added to glycoAuNPs. 5 repeats were made for each carbohydrate functionalised particle and the absorbance at 450 nm and 750 nm were recorded for linear discriminant analysis.

Linear discriminant analysis: Every lectin was added to every surface as described in the lectin binding assay section. This was repeated 5 times to generate a training data matrix of 6 particles x 6 lectins x 5 replicates, which was then subjected to a classical linear discriminant analysis (LDA) in R (version 2.14.1).

9.6 References

1.   C. R. Bertozzi and L. L. Kiessling, *Science*, 2001, **291**, 2357-2364.

2.   L. L. Kiessling, J. E. Gestwicki and L. E. Strong, *Angew. Chem. Int. Ed.*, 2006, **45**, 2348-2368.

3.   K. T. Pilobello and L. K. Mahal, *Curr. Opin. Chem. Biol.*, 2007, **11**, 300-305.

4.   N. Sharon, *Biochim. Biophys. Acta*, 2006, **1760**, 527-537.

5.   R. J. Pieters, *Org. Biomol. Chem.*, 2009, **7**, 2013-2025.

6.   M. Ambrosi, N. R. Cameron and B. G. Davis, *Org. Bio. Chem.*, 2005, **3**, 1593-1608.

7.   H. Feinberg, D. A. Mitchell, K. Drickamer and W. I. Weis, *Science*, 2001, **294**, 2163-2166.

8.   Y. C. Lee, R. R. Townsend, M. R. Hardy, J. Lonngren, J. Arnarp, M. Haraldsson and H. Lonn, *J. Biol. Chem.*, 1983, **258**, 199-202.

9.   J. J. Lundquist and E. J. Toone, *Chem. Rev.*, 2002, **102**, 555-578.

10.   N. P. Pera and R. J. Pieters, *Med. Chem. Comm.*, 2014, **5**, 1027-1035.

11.   M. Hartmann and T. K. Lindhorst, *Eur. J. Org. Chem.*, 2011, 3583-3609.

12.   T. R. Branson and W. B. Turnbull, *Chem. Soc. Rev.*, 2013, **42**, 4613-4622.

13.   M. W. Jones, S. J. Richards, D. M. Haddleton and M. I. Gibson, *Polym. Chem.*, 2013, **4**, 717-723.

14.   S.-J. Richards, M. W. Jones, M. Hunaban, D. M. Haddleton and M. I. Gibson, *Angew. Chem. Int. Ed.*, 2012, **51**, 7812-7816.

15.   M. Fais, R. Karamanska, S. Allman, S. A. Fairhurst, P. Innocenti, A. J. Fairbanks, T. J. Donohoe, B. G. Davis, D. A. Russell and R. A. Field, *Chem. Sci.*, 2011, **2**, 1952-1959.

16.   C. L. Schofield, B. Mukhopadhyay, S. M. Hardy, M. B. McDonnell, R. A. Field and D. A. Russell, *Analyst*, 2008, **133**, 626-634.

17.   M. C. Galan, D. Benito-Alifonso and G. M. Watt, *Org. Biomol. Chem.*, 2011, **9**, 3598-3610.

18.   J. Hirabayashi, M. Yamada, A. Kuno and H. Tateno, *Chem. Soc. Rev.*, 2013, **42**, 4443-4458.

19.   P. H. Seeberger and D. B. Werz, *Nature*, 2007, **446**, 1046-1051.

20.   S. Park, J. C. Gildersleeve, O. Blixt and I. Shin, *Chem. Soc. Rev.*, 2013, **42**, 4310-4326.

21.   D. N. Wang, S. Y. Liu, B. J. Trummer, C. Deng and A. L. Wang, *Nat. Biotechnol.*, 2002, **20**, 275-281.

22.   G. Safina, *Anal. Chim. Acta*, 2012, **712**, 9-29.

23.   J. E. Ghadiali and M. M. Stevens, *Adv. Mater.*, 2008, **20**, 4359-4363.

24.   A. Laromaine, L. L. Koh, M. Murugesan, R. V. Ulijn and M. M. Stevens, *J. Am. Chem. Soc.*, 2007, **129**, 4156-4157.

25.   A. J. Haes, L. Chang, W. L. Klein and R. P. Van Duyne, *J. Am. Chem. Soc.*, 2005, **127**, 2264-2271.

26. R. Elghanian, J. J. Storhoff, R. C. Mucic, R. L. Letsinger and C. A. Mirkin, *Science*, 1997, **277**, 1078-1081.

27. P. Englebienne, *Analyst*, 1998, **123**, 1599-1603.

28. C. C. Lin, Y. C. Yeh, C. Y. Yang, G. F. Chen, Y. C. Chen, Y. C. Wu and C. C. Chen, *Chem. Commun.*, 2003, 2920-2921.

29. H. S. N. Jayawardena, X. Wang and M. Yan, *Anal. Chem.*, 2013, **85**, 10277-10281.

30. S.-J. Richards and M. I. Gibson, ACS, ACS Macro Lett., 2014, vol. 3, pp. 1004-1008.

31. C. C. Lin, Y. C. Yeh, C. Y. Yang, C. L. Chen, G. F. Chen, C. C. Chen and Y. C. Wu, *J. Am. Chem. Soc.*, 2002, **124**, 3508-3509.

32. S.-J. Richards, E. Fullam, G. S. Besra and M. I. Gibson, *J. Mater. Chem. B*, 2014, **2**, 1490-1498.

33. M. J. Marin, A. Rashid, M. Rejzek, S. A. Fairhurst, S. A. Wharton, S. R. Martin, J. W. McCauley, T. Wileman, R. A. Field and D. A. Russell, *Org. Biomol. Chem.*, 2013, **11**, 7101-7107.

34. A. Dondoni, *Chem. Asian J.*, 2007, **2**, 700-708.

35. A. Dondoni and A. Marra, *Chem. Soc. Rev.*, 2012, **41**, 573-586.

36. M. Eberhardt, R. Mruk, R. Zentel and P. Theato, *Eur. Polym. J.*, 2005, **41**, 1569-1575.

37. P. Theato, *J. Polym. Sci. A Polym. Chem.*, 2008, **46**, 6677-6687.

38. K. Godula and C. R. Bertozzi, *J. Am. Chem. Soc.*, 2010, **132**, 9963-9965.

39. CFG, http://www.functionalglycomics.org.

40. L. Otten, S.-J. Richards, E. Fullam, G. S. Besra and M. I. Gibson, *J. Mater. Chem. B*, 2013, **1**, 2665-2672.

Chapter 10

Conclusions

Glycopolymers with high selectivity may feature in the development of sensitive and precise sensors or anti-adhesive therapies, which has so far limited the application of synthetic glycopolymers. In this work, it is shown that combining structural biology tools with macromolecular chemistry enables the creation of synthetic glycopolymers that can mimic glycan architecture without the need for multi-step oligosaccharide synthesis, could find applications in anti-adhesive therapy and biomolecular sensors.

A series of glycopolymers with varying saccharide density, linker length, and chain length were synthesised by a variety of tandem post-polymerisation modification techniques. These techniques enable precise control over not only chain length (and hence valency), but also carbohydrate-polymer backbone linker distance and the introduction of secondary binding (branched) motifs onto the linker. Firstly, a combination of active esters and alkyne-azide chemistry was used to install variable linkers lengths and carbohydrate density onto a polymer backbone. It was shown that a longer linker resulted in increased inhibition of the B subunit of the cholera toxin (CTxB), which is attributed to the depth of the binding pocket.

Secondly, the versatility of poly(azlactone)s as a scaffold for both direct, and tandem, post-polymerisation modification was explored. In particular, the 100 % atom efficiency and the ability to conduct polymerisation and functionalisation in a one-pot, two-step process are highly favourable. Glycopolymers synthesised using this method showed good inhibitory activity towards CTxB due to the increased linker length.

To mimic the branched structure of the nature CTxB ligand GM1, a new, three-step, tandem post-polymerisation methodology was developed. Sequential variation of this branched motif was found to dramatically alter both the affinity and the selectivity of the glycopolymers towards two lectins; CTxB and PNA.

These measurements demonstrated that in the design of biomimetic macromolecules for anti-adhesion or other therapeutic applications, structural biological information must be considered, in conjunction with using the relevant assays. Therefore, methods to determine the inhibitory activity were compared. It was found that glycopolymers that are sufficiently large to span binding sites, lead to the highest activity in a fluorescent-linked sorbent assay (FLSA) however, as a result of spanning binding sites, these glycopolymers actually showed the *least* total mass binding by quartz crystal microbalance (QCM), which was determined to be due to the formation of a flat film, rather than extended brush structures that are seen for short polymers. Hence, when screening multivalent glycopolymers, single-concentration measurements are unlikely to reveal the highest affinity binders. Therefore, the assays most relevant to the intended application must be used, preferably in combination with others to fully assign the mode of action.

Techniques to investigate protein-carbohydrate interactions can require highly expensive, sophisticated equipment. In this work, citrate-coated AuNPs were used as resolving agents to analyse protein binding to surfaces, as a low-cost, accurate glycomics tool. A strong correlation was found between the AuNP method and more traditional fluorescence techniques; with the AuNP method having the advantage that it does not require labelled proteins. Due to the high extinction coefficient (hence high colouration) of the AuNP resolved surfaces, it was possible to simply use a digital camera to image the microplates combined with image analysis software to extract

binding isotherms, which showed strong correlation to those obtained by fluorescence or absorbance measurements. This presents the opportunity to use AuNP resolving agents for label free, low cost, high-throughput evaluation of carbohydrate-protein interactions that may have diagnostic or screening applications.

Due to the threat of antibiotic resistance, it is important that the limited arsenal of antibiotics left to use are administered correctly. In this work, a sensitive and rapid colourimetric bioassay for the quantitative detection of lectins and type 1 fimbriated bacteria based upon the binding of glycosylated gold nanoparticles (glycoAuNPs) was developed. AuNPs with carbohydrates directly immobilised on their surface showed very rapid responses to both lectins and lectin-expressing bacteria. However, these particles also displayed low saline stability and nonspecific interactions with the bacteria limiting their discriminatory capacity. To overcome this a PEG layer was inserted between the particles and the carbohydrate. This dramatically increased the saline stability of particles. However, these particles took far longer to lectins no red to blue colour change was observed upon lectin binding, which was hypothesised to be due to steric shielding effects of the PEG layer.

Therefore, through an optimisation study, the correct length of polymer to stabilise particles but also give rapid colourimetric response was determined. It was found crucial to ensure that the polymer is sufficiently long to endow saline stability for use in biological media, but must be balanced against the competing effect that if the polymer is too long, no aggregation events occur (in a reasonable time-scale). These optimised particles were then employed to study the binding interactions with three different lectins, including a surrogate for ricin – a biological warfare agent and may form the basis of new point-of-care diagnostics, especially for low-resource

environments. It was also noted that the lectin-induced colourimetric response of these glycoAuNPs could be determined by the simple combination of a flatbed scanner and image analysis software. Good correlation between the values determined by the two techniques suggests that this could be a low cost/low-tech route to the discrimination between lectins. Excellent separation between all the lectins testing was achieved using linear discriminant analysis (LDA), allowing successful differentiation of all the lectins using only simple monosaccharide functionalities.

Appendices

Appendix 1

Supplementary Information: Chapter 2

Synthesis of 1-Azido-1-deoxy-β-D-galactopyranoside

Stereopure $GalN_3$ was synthesis by displacement of the corresponding anomeric bromide with sodium azide. Stereochemistry of each product was confirmed by NMR spectroscopy based on the H_1-H_2 coupling constants.
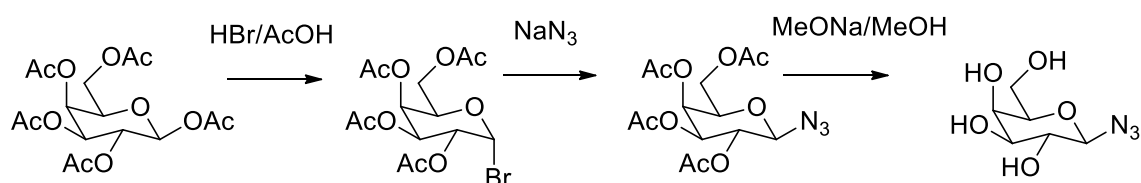
	δ_{ppm} ^{1}H	δ_{ppm} ^{13}C	$H_1 - H_2$ coupling (Hz)	Assignment
Ac_4GalBr	6.65	88.2	4.0	α
Ac_4GalN_3	4.60	88.3	8.8	β
$GalN_3$	4.50	90.5	8.5	β

Table S1.1: Characterisation of the anomeric stereochemistry of $GalN_3$.

Synthesis of Alkyne 2 linker.

The synthetic method is summarised in Scheme S2. 2-(2-Boc-aminoethoxy)ethanol[1] and Tert-butyl 2-(2-(prop-2-ynyloxy)ethoxy)ethylcarbamate[2] were synthesised according to literature methods.
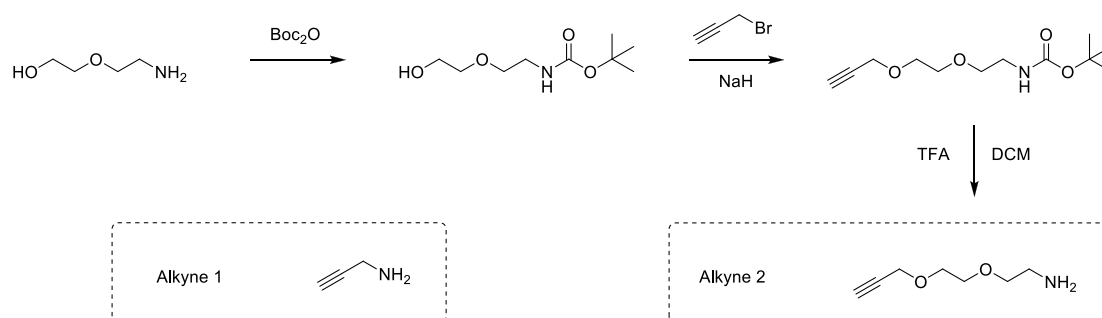
Scheme S1.1: Amino-functionalised alkynes employed in this study.

Alkyne Functional Polymers:

Characterisation of the intermediate scaffolds obtained by aminolysis of poly(pentafluorophenylmethacrylate) are shown in Table 2.1 (Chapter 2). These were used to obtain the glycopolymers shown in Table S2, main text.

Table S1.1: Alkyne/hydropropylamine copolymers.

Polymer	Mol % Alkyne 1[a]	Mol % Alkyne 2[a]	Mol % HOPrNH$_2$[a]	M$_n$[b]	M$_w$/M$_n$[b]
P4	100	-	-	6100	1.24
P5	100	-	-	7000	1.21
P6	100	-	-	9000	1.17
P7	-	100	-	10800	1.29
P8	-	100	-	12700	1.22
P9	-	100	-	13500	1.24
P10	-	50	50	10800	1.20
P11	-	25	75	10700	1.21
P12	-	10	90	10600	1.23

(a) Determined by feed ratio of each amine; (b) Determined by SEC in DMF verses PMMA standards. HOPrNH$_2$ = hydroxypropylamine.

Over the course of the tandem post-polymerization process, there was no evidence of fractionation, and all the polymers obtained were well defined with dispersities below 1.3. Example SEC data showing a series of modifications are shown in Figure S1. It should be noted that due to the differential solubility of each polymer used, it was not possible to use a single SEC eluent system for all polymers.
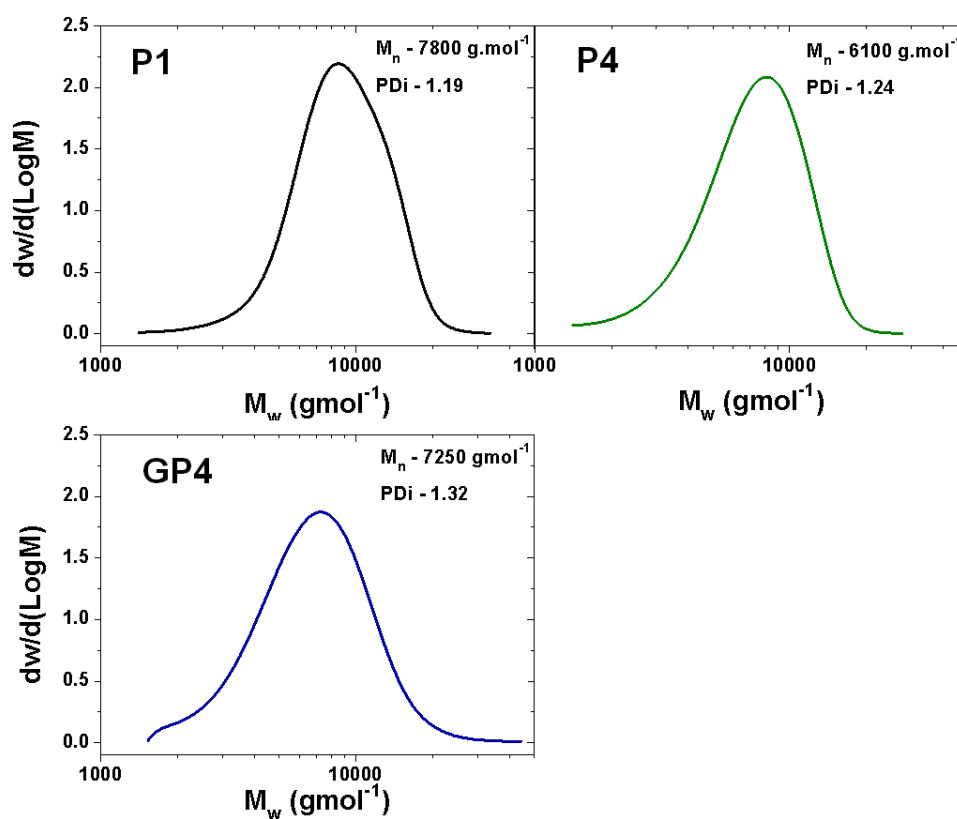
Figure S1.1. Molecular weight distributions obtained by SEC showing tandem-modification procedure.

Fluorescence-linked sorbent assay for inhibitory activity.
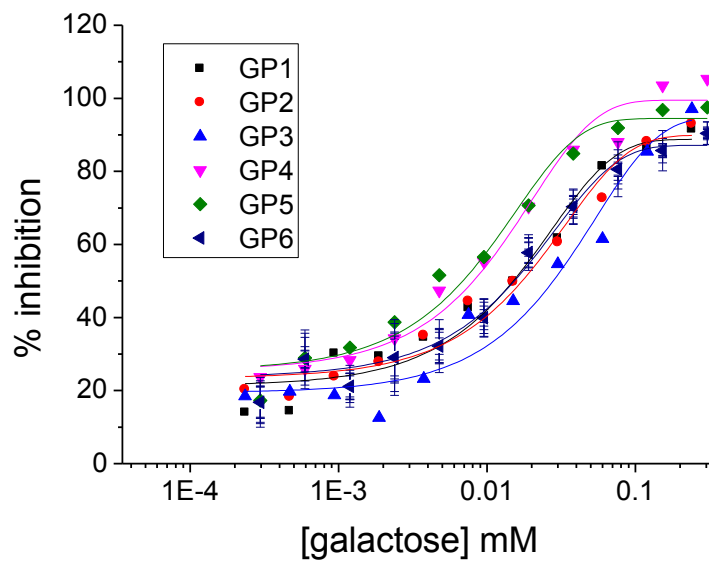
Figure S1.2. Inhibitory curve for **GP1 – 6** against cholera toxin B-subunit.

References

1.   R. B. Greenwald, Y. H. Choe, C. D. Conover, K. Shum, D. Wu, M. Royzen, *J. Med. Chem.* 2000, **43**, 475

2.   S.-Y. Chang, S. J. Bae, M. Y. Lee, S.-H. Baek, S. Chang, S. H. Kim, *Bioorg. Med. Chem. Lett.* 2011, **21**, 727

Appendix 2

Supplementary Information: Chapter 3

Additional Characterisation

N-(2-methyl-1-oxo-1-(prop-2-ynylamino)propan-2-yl)acrylamide
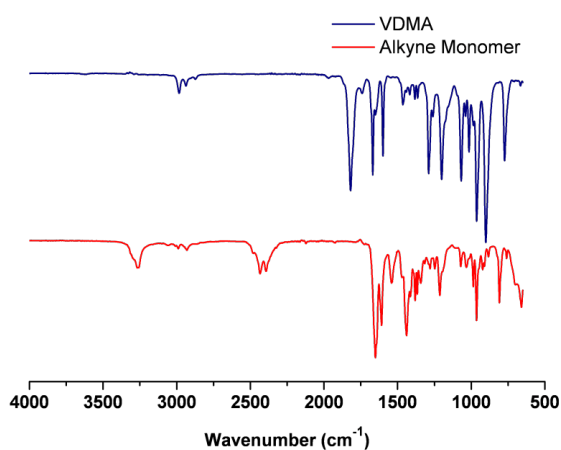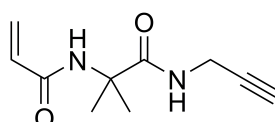
Figure S2.1: IR spectra of VDMA before (blue) and after (red) reaction with propargyl amine
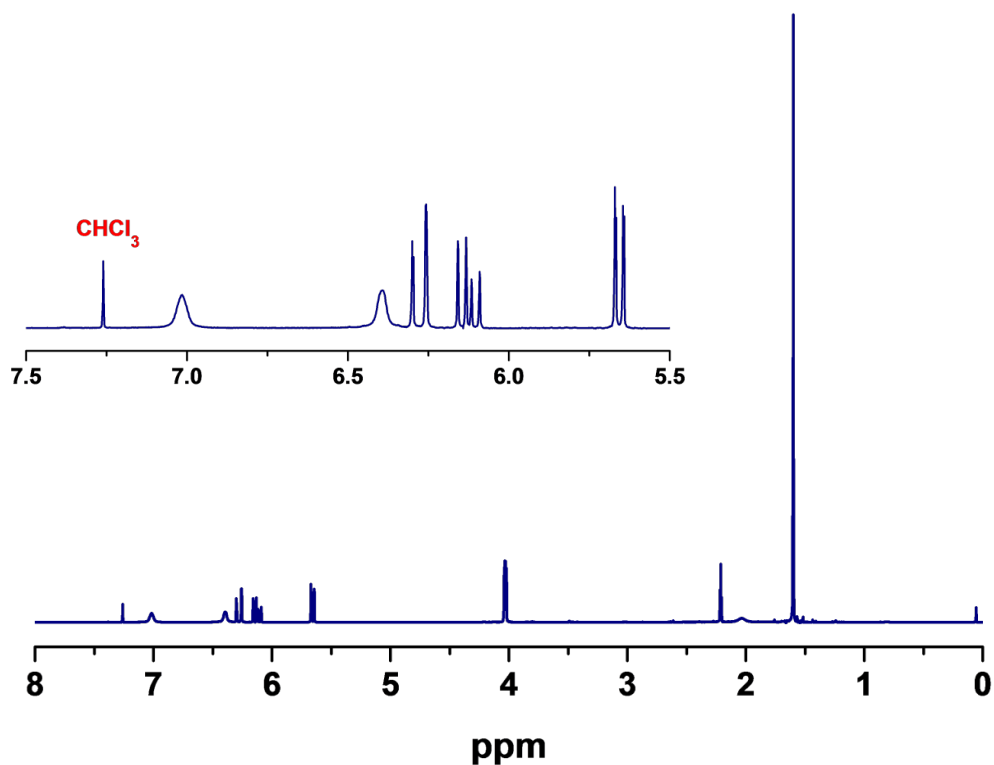
Figure S2.2: NMR analysis of the ring opened product upon treatment of VDMA with propargyl amine.

_N_-(1-(allylamino)-2-methyl-1-oxopropan-2-yl)acrylamide
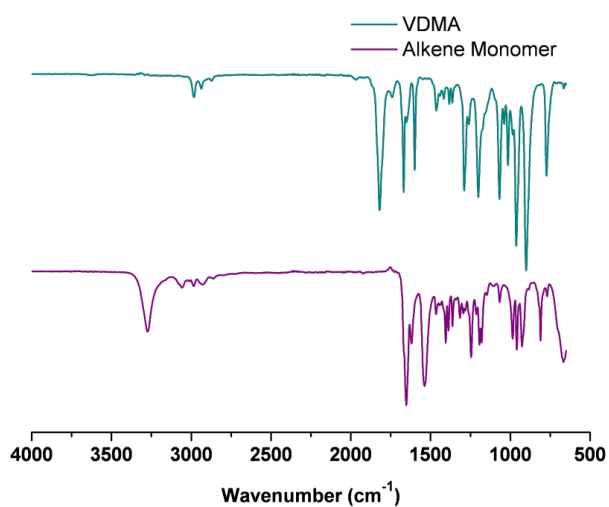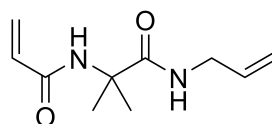
Figure S2.3: IR spectra of VDMA before (blue) and after (red) reaction with allyl amine
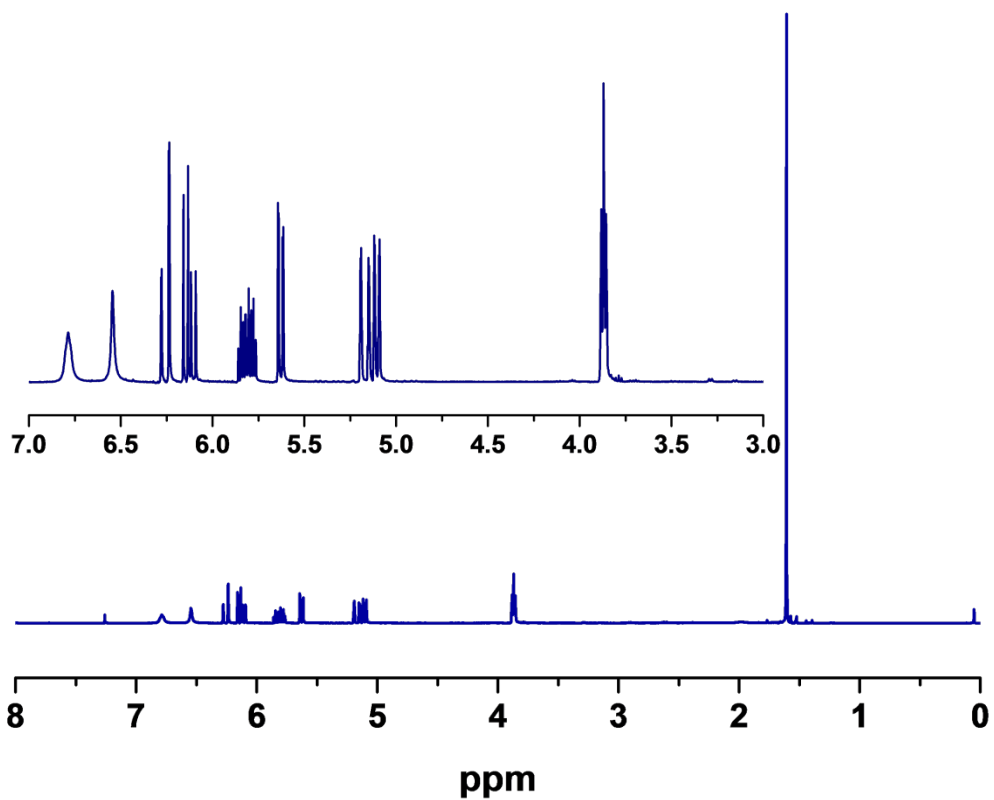
Figure S2.4: IR and NMR analysis of the ring opened product upon treatment of VDMA with allyl amine.

Propargyl Amine Modification of PVDMA
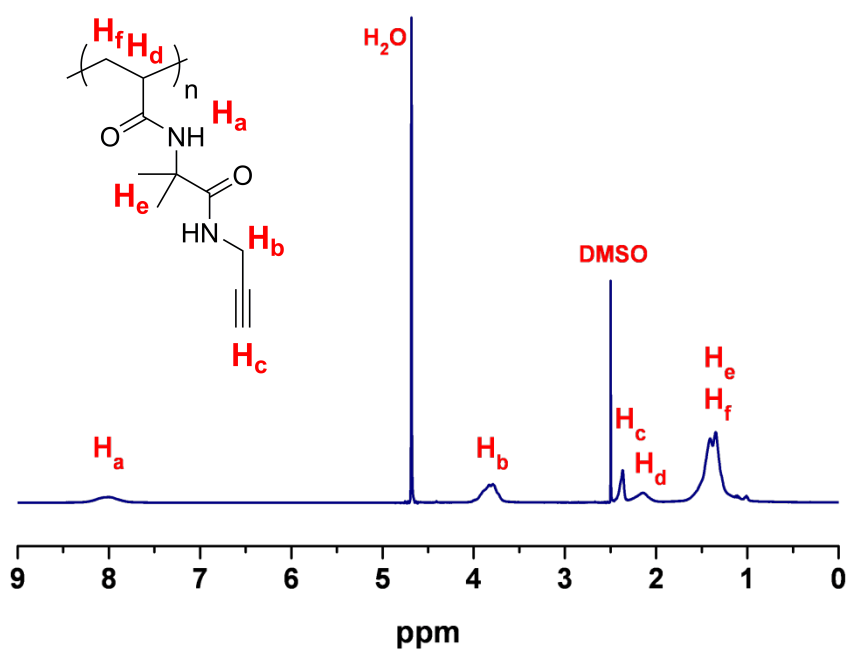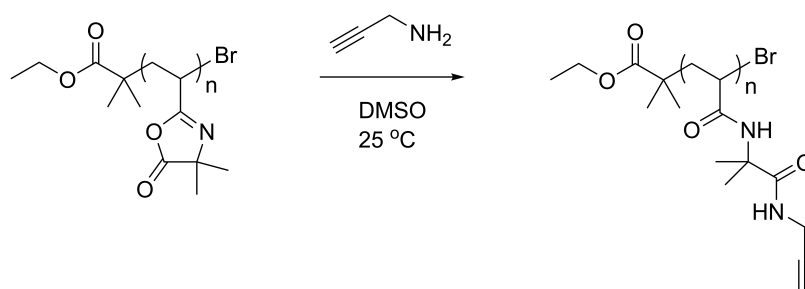
Figure S2.5: ^{1}H NMR analysis of the post polymerisation modification of PVDMA with propargyl amine.

Allyl Amine Modification of PVDMA
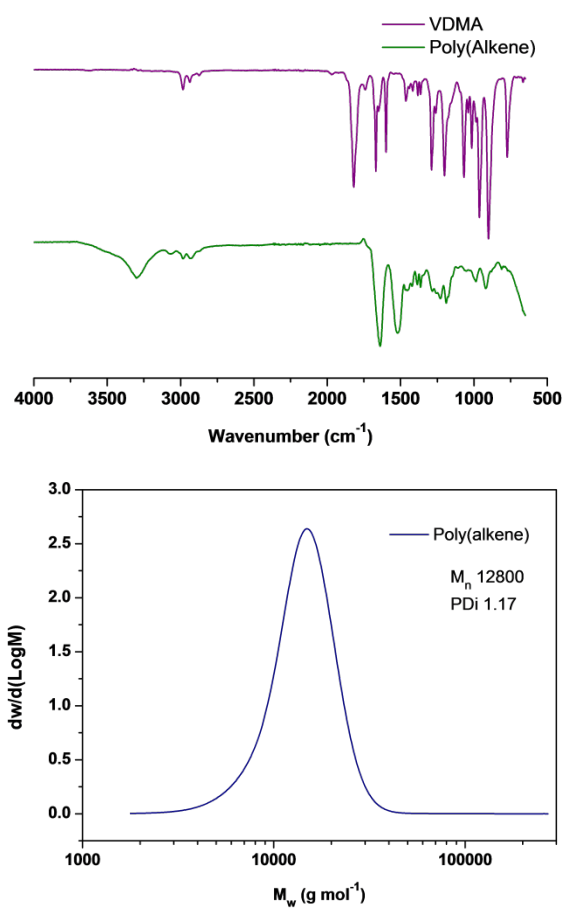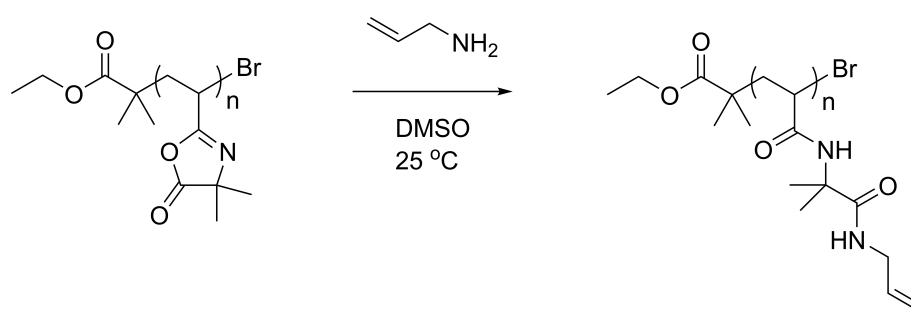
Figure S2.6: IR and SEC analysis of the post polymerisation modification of PVDMA with allyl amine.
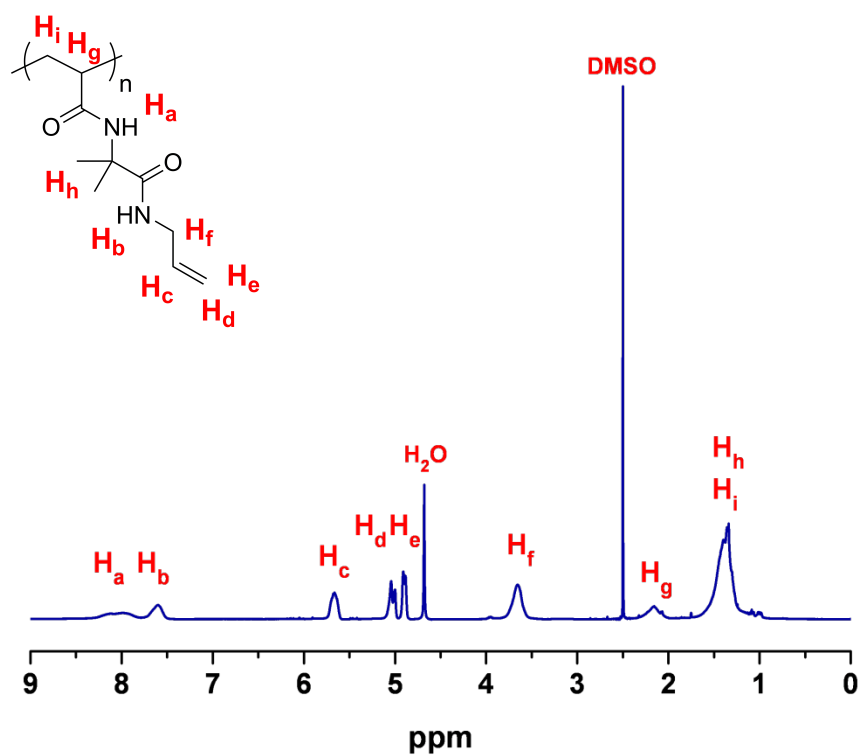
Figure S2.7: ¹H NMR analysis of the post polymerisation modification of PVDMA with propargyl amine.

Tyramine Modification of PVDMA
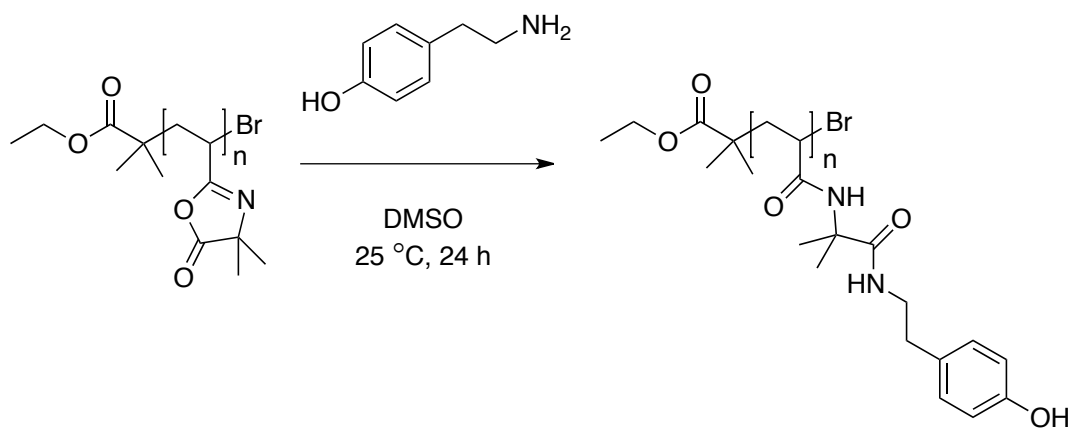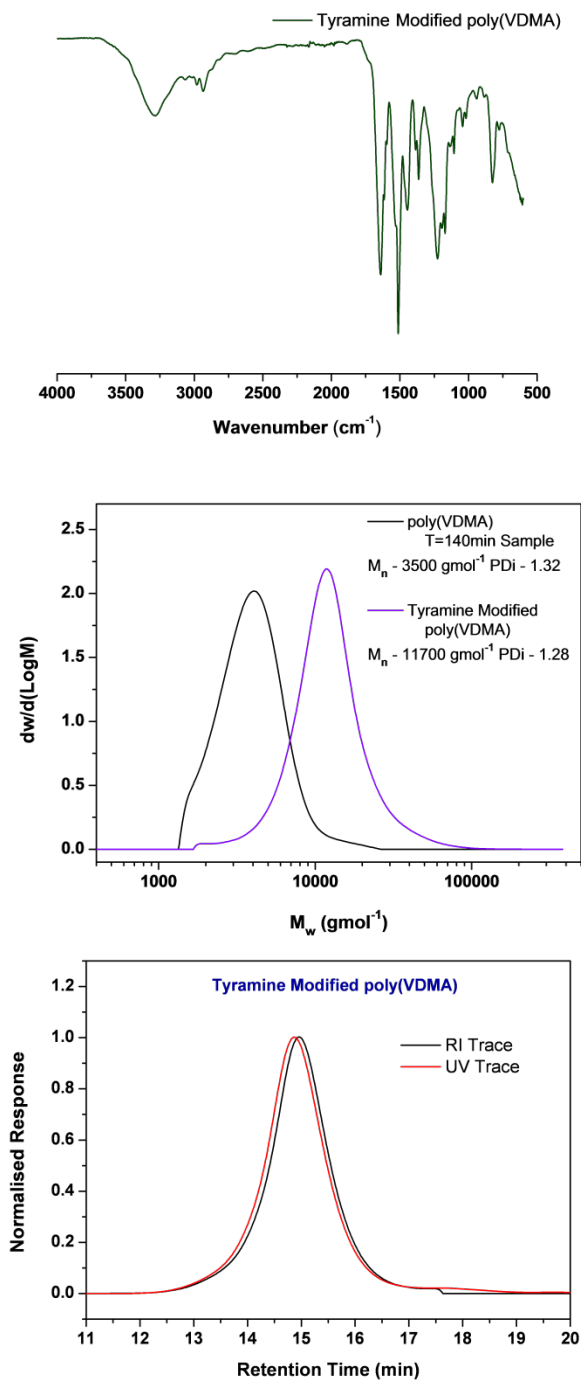
Figure S2.8: IR and SEC analysis of the post polymerisation modification of PVDMA with tyramine.
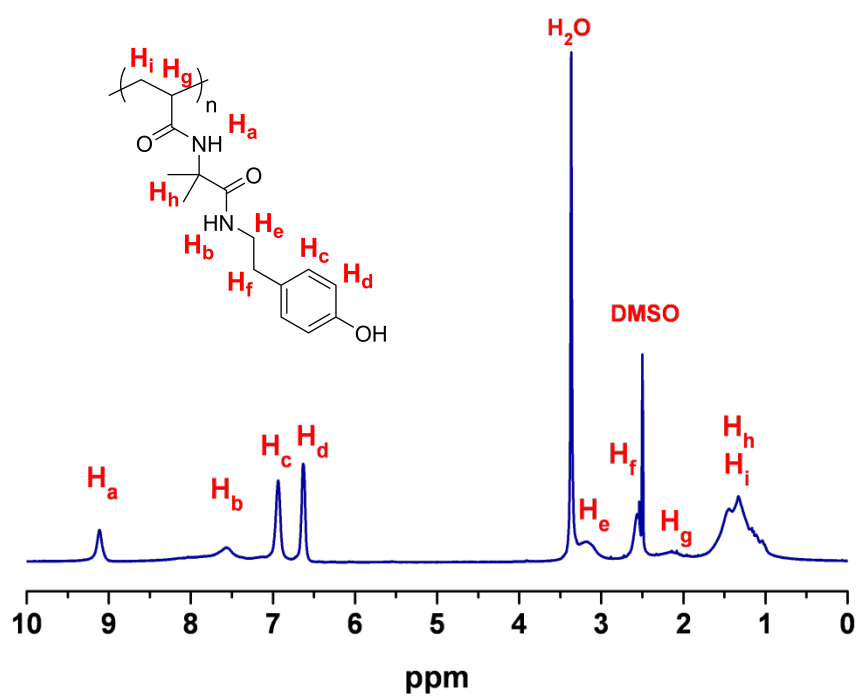
Figure S2.9: ^{1}H NMR analysis of the post polymerisation modification of PVDMA with tyramine.

Furfuryl amine modification of PVDMA
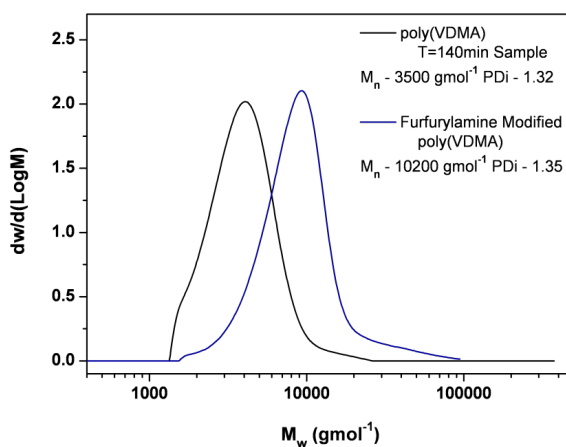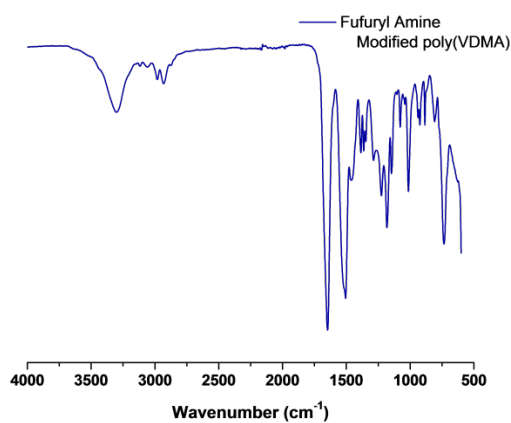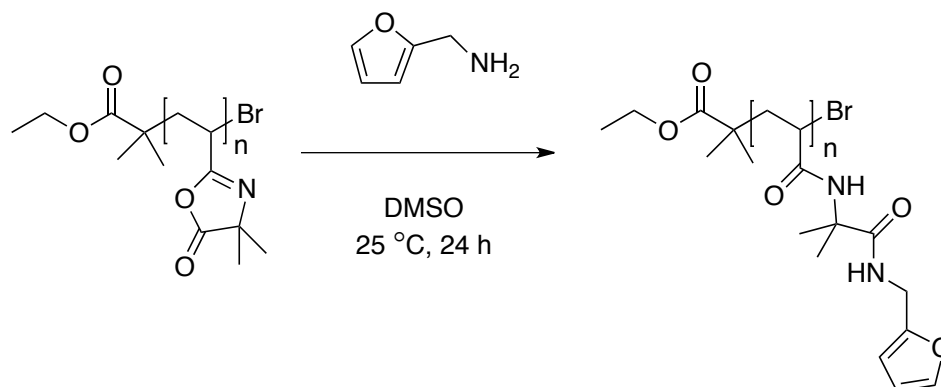
Figure S2.10: IR and SEC analysis of the post polymerisation modification of PVDMA with furfurylamine.
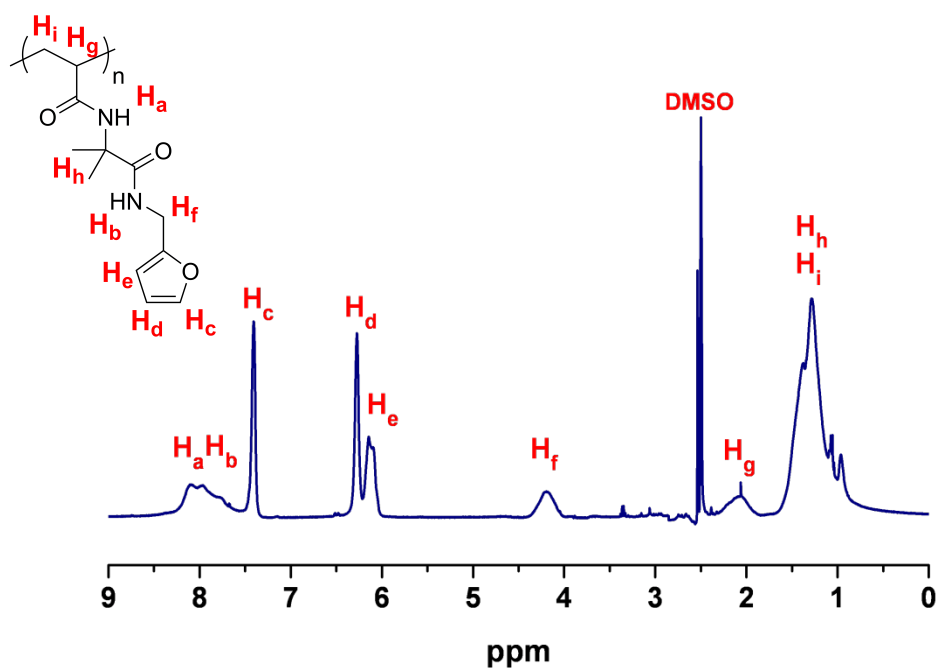
Figure S2.11: ^{1}H NMR analysis of the post polymerisation modification of PVDMA with furfuryl amine.

Glucosamine modified PVDMA

4.5 mL of the crude PVDMA solution (containing 10.8 mmol of azlactone functionality) was added to a round-bottomed flask and diluted with 5 mL of DMSO. Glucosamine hydrochloride (3.487 g, 16.2 mmol) was added to the polymer solution in 10 mL of DMSO, along with triethylamine (1.63 g, 16.2 mmol) and the solution allowed to stir at room temperature overnight. Volatiles were then removed and the crude polymer solution diluted with water and dialysed against water (MWCO 1000 Da) for 3 days to remove low molecular weight species. The water was removed by lyophilisation to yield the product as a white fluffy powder.

Infra-red analysis of the obtained polymer showed complete disappearance of the signals corresponding to the azlactone ring, along with the appearance of a strong signal corresponding to the two amide moieties generated upon ring opening. SEC analysis revealed a clear mass increase upon ring opening with glucosamine. SEC Analysis (Aqueous) – M_n 11,900 gmol^{-1}, PDi 1.40.

Figure S2.12: IR and SEC analysis of the post polymerisation modification of PVDMA with glucosamine.

Galactosamine modified PVDMA

4.5 mL of the crude PVDMA solution (containing 10.8 mmol of azlactone functionality) was added to a round-bottomed flask and diluted with 5 mL of DMSO. Galactosamine hydrochloride (3.487 g, 16.2 mmol) was added to the polymer solution in 10 mL of DMSO, along with triethylamine (1.63 g, 16.2 mmol) and the solution allowed to stir at room temperature overnight. Volatiles were then removed and the crude polymer solution diluted with water and dialysed against water (MWCO 1000 Da) for 3 days to remove low molecular weight species. The water was removed by lyophilisation to yield the product as a white fluffy powder.

Infra-red analysis of the obtained polymer showed complete disappearance of the signals corresponding to the azlactone ring, along with the appearance of a strong signal corresponding to the two amide moieties generated upon ring opening. SEC analysis revealed a clear mass increase upon ring opening with galactosamine, and a well-defined final polymer observed. SEC Analysis (Aqueous) – M_n = 11,400 gmol^{-1}, Đ = 1.44.
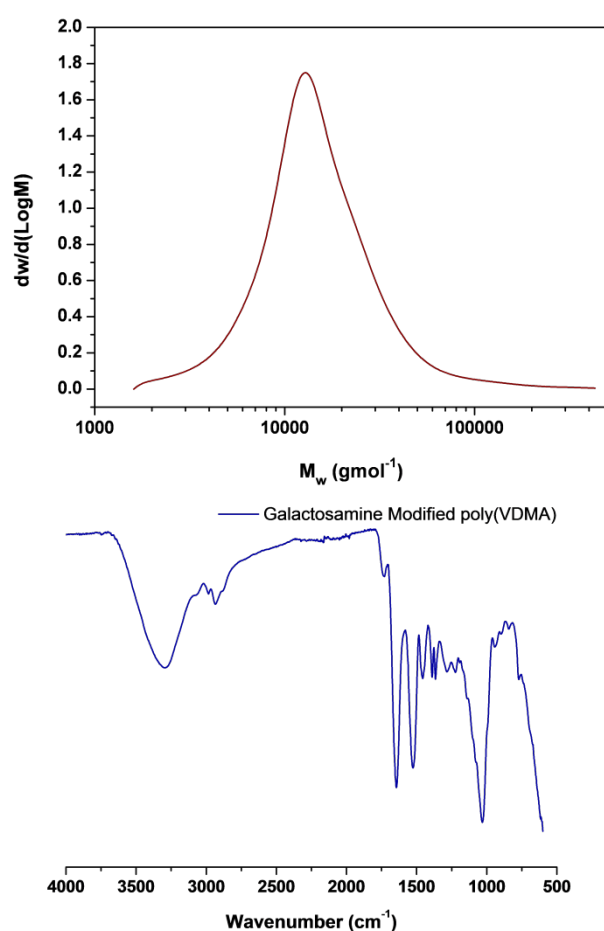
Figure S2.13: IR and SEC analysis of the post polymerisation modification of PVDMA with galactosamine.

Mannosamine modified PVDMA

4.5 mL of the crude PVDMA solution (containing 10.8 mmol of azlactone functionality) was added to a round-bottomed flask and diluted with 5 mL of DMSO. Mannosamine hydrochloride (3.487 g, 16.2 mmol) was added to the polymer solution in 10 mL of DMSO, along with triethylamine (1.63 g, 16.2 mmol) and the solution allowed to stir at room temperature overnight. Volatiles were then removed and the crude polymer solution diluted with water and dialysed against water (MWCO 1000 Da) for 3 days to remove low molecular weight species. The water was removed by lyophilisation to yield the product as a white fluffy powder.

Infra-red analysis of the obtained polymer showed complete disappearance of the signals corresponding to the azlactone ring, along with the appearance of a strong signal corresponding to the two amide moieties generated upon ring opening. SEC analysis revealed a clear mass increase upon ring opening with mannosamine, and a well-defined final polymer observed. SEC Analysis (Aqueous) – M_n = 11,600 gmol^{-1}, Đ = 1.42.
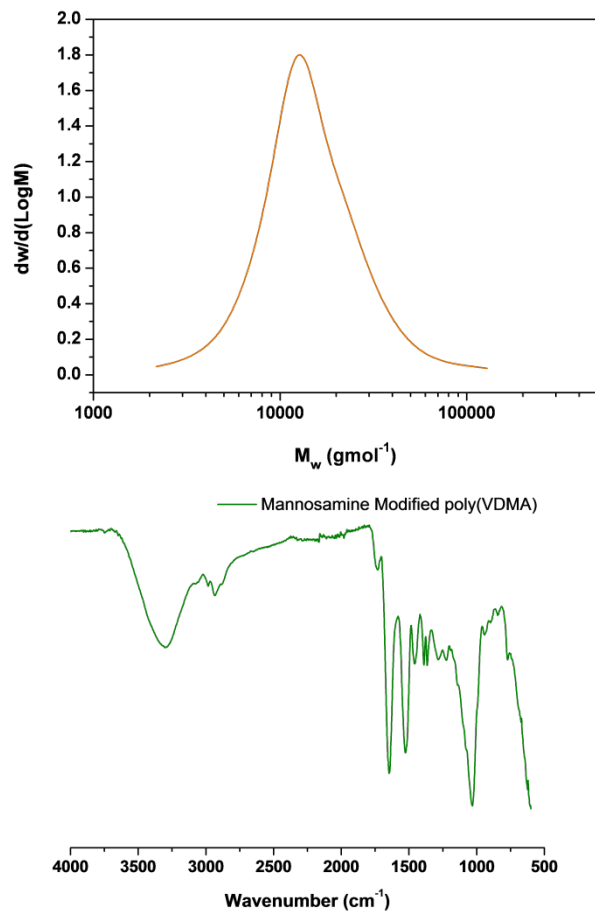
Figure S2.14: IR and SEC analysis of the post polymerisation modification of PVDMA with mannosamine.

Hydrolysis of PVDMA
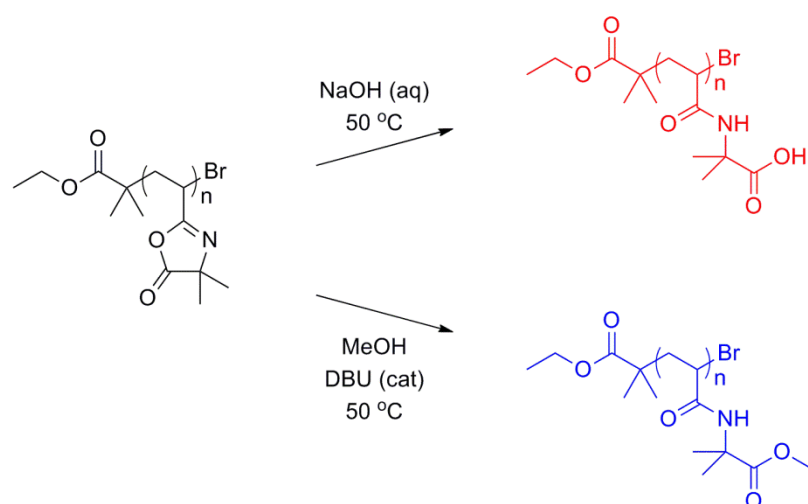
Scheme S2.1: Ring opening of PVDMA with NaOH (red) and methanol (blue) to yield acid- and ester-functional polymers respectively.
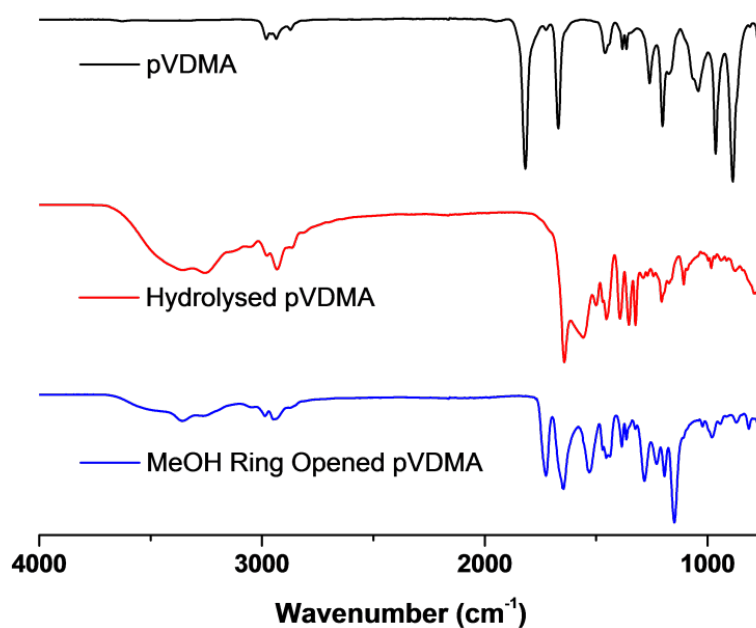
Figure S2.15: IR analysis of the products obtained from ring opening of PVDMA with NaOH (red trace) and methanol (blue trace). The acid functional polymer showed a clear signal at around 1644 cm^{-1}, with the ester functional polymer displaying a signal at 1726 cm^{-1}

Appendix 3

Supplementary Information: Chapter 4
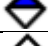
Visualisation of protein structures

Image of one subunit of 2CHB (Merritt, E.A., Sarfaty, S., Jobling, M.G., Chang, T., Holmes, R.K., Hirst, T.R., Hol, W.G. (1997) Structural studies of receptor binding by cholera toxin mutants *Protein Science* 6: 1516-1528) created with CCP4mg (McNicholas, S., Potterton, E., Wilson, K.S., Noble, M.E.M (2011) Presenting your structures: the CCP4mg molecular graphics software *Acta Cryst.* 67: 386-394).

Glycan Notation and Microarray Analysis

Table S3.1. A table of the symbols representing sugar stereochemistries. All symbols as described by the consortium for functional glycomics.

Sugars	Hexoses	N-acetylhexosamines	Hexosamines
Galactose	⬤	◻	◹
Glucose	⬤	◼	◹
Mannose	⬤	◼	◹
Fucose	▲	N/A	N/A
Xylose	☆	N/A	N/A

Acidic sugars	Symbol
NeuAc	◆
NeuGc	◇
KDN	◈
GlcA	⬖
IdoA	⬗
GalA	◈
ManA	◈

To investigate the relative importance of glycan branching and secondary binding site interactions, microarray data for two galactose-binding proteins was extracted from the Consortium for Functional Glycomics database. Figure S1 shows the affinity of 5 sequentially modified carbohydrates to both peanut agglutinin (PNA) and cholera toxin (CTx). Upon changing from Gal (**1**) to GalNAc (**2**) there was no significant difference in lectin affinity for PNA or CTx. However, when Gal(β1-4)GalNAc (**3**) is used PNA's affinity is significantly increased compared to CTx, highlighting that connectivity and presentation of the sugars is crucial. Addition of a neuraminic acid branch (**4**) leads to a 200-fold increase in CTx binding, but has little influence on PNA binding. This is despite the neuaminic acid (**5**) alone having negligible CTx affinity. The increased binding affinity of CTx to (**4**) is attributable to allosteric interactions of the neuraminic with a secondary binding pocket within CTx. While not intended as a complete bioinformatic study, this limited set of glycans demonstrate that controlled branching can improve specific and affinity of glycans by several orders of magnitude, which is more than observed by multivalency alone in many cases.
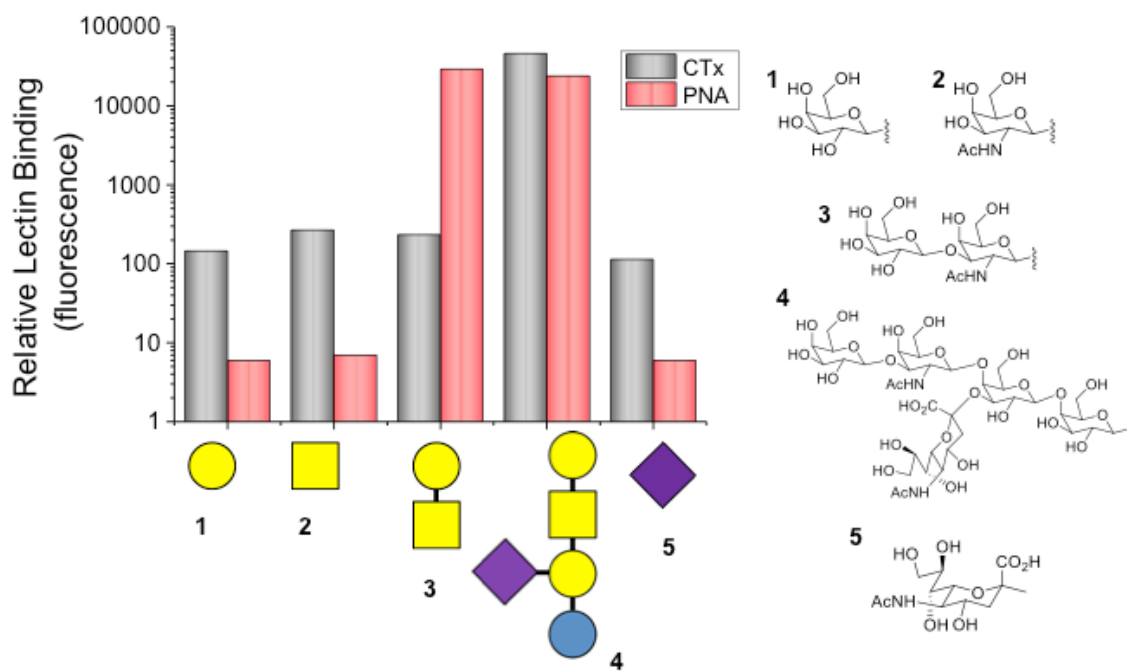
Figure S3.1: Glycan Microarray analysis of galactose-terminated glycans with PNA and CTx lectins taken from the CFG database (values were taken for the assay performed with 10 µg of each lectin).
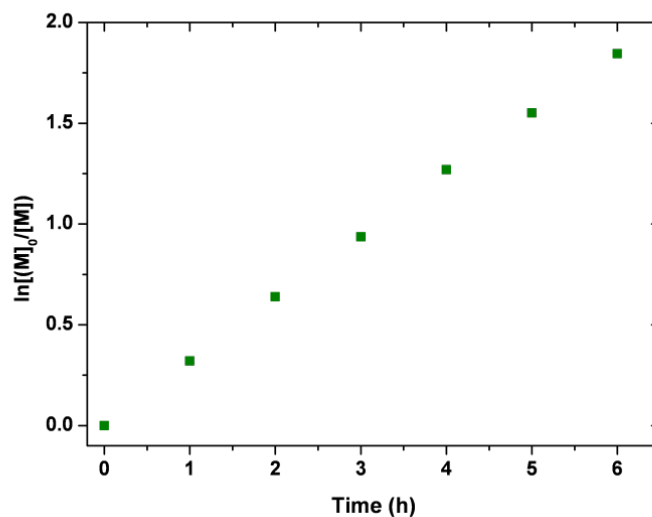
Figure S3.2: First order kinetic plot for the polymerisation of glycidyl methacrylate
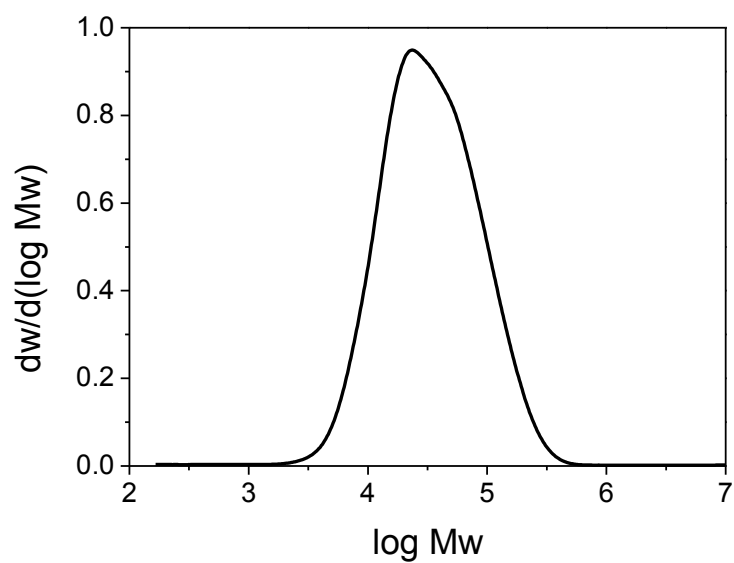
Figure S3.3: Molecular weight distribution curve of poly(glycidyl methacrylate) after 6 hour polymerisation time.
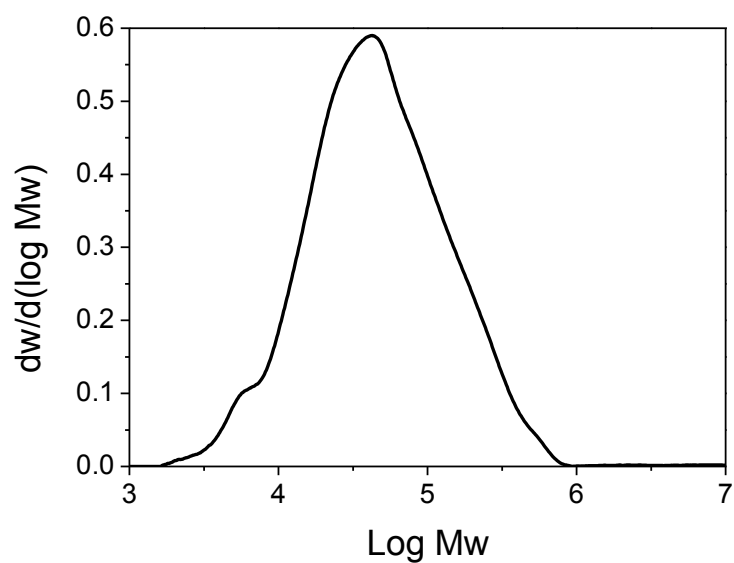
Figure S3.4: Molecular weight distribution curve of poly(2-hydroxy-3-azidopropyl methacrylate).
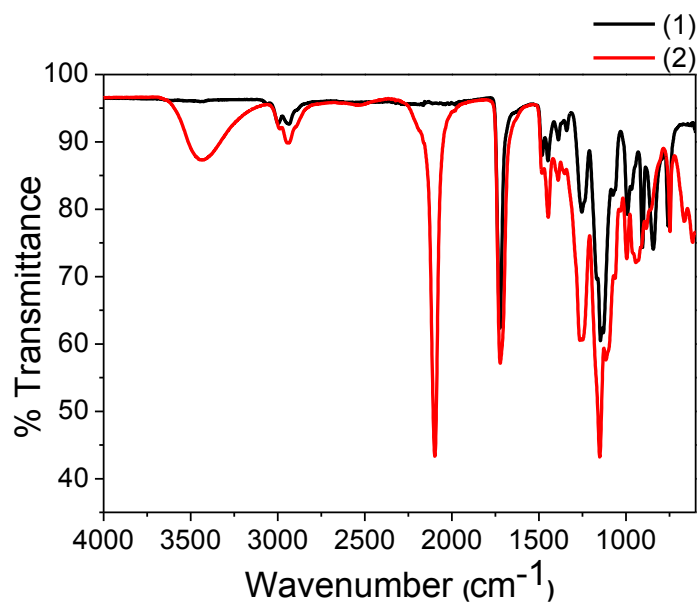
Figure S3.5: Infrared spectra of poly(glycidyl methacrylate), **(1)**, and poly(2-hydroxy-3-azidopropyl methacrylate), **(2)**.

Example: Modification of (2) with acid chlorides

Polymer **(2)** was modified with a series of commercially available acid chlorides and the reaction monitored by IR spectroscopy.
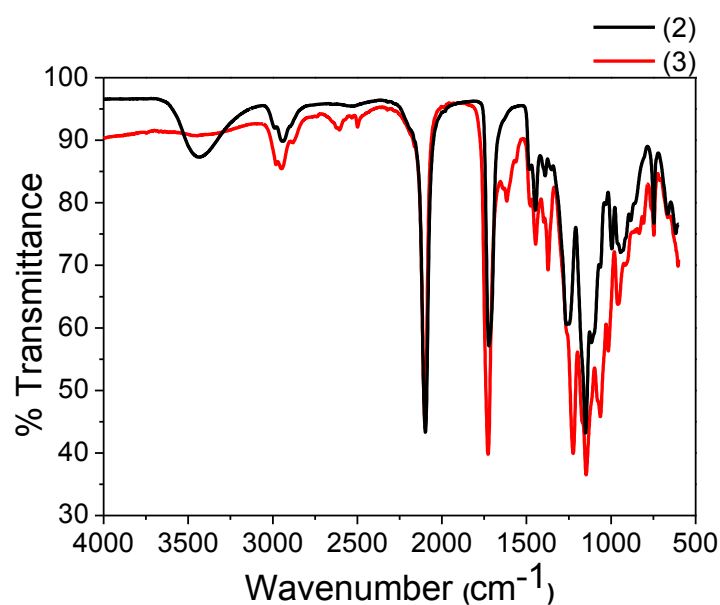
Figure S3.6. Infrared spectra of poly(2-hydroxy-3-azidopropyl methacrylate), **(2)**, and following modification with benzoyl chloride **(3)**.

Example: Reaction of (3) with β-D-1-propargyl galactose
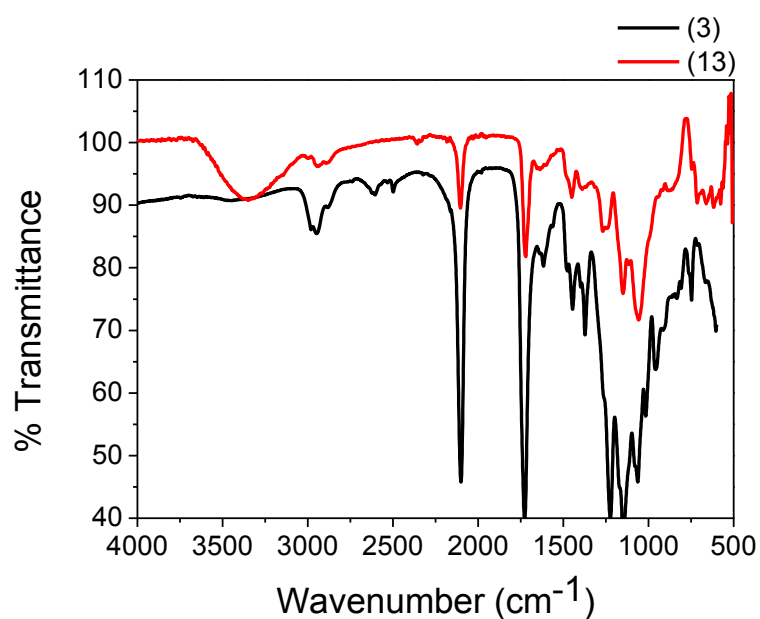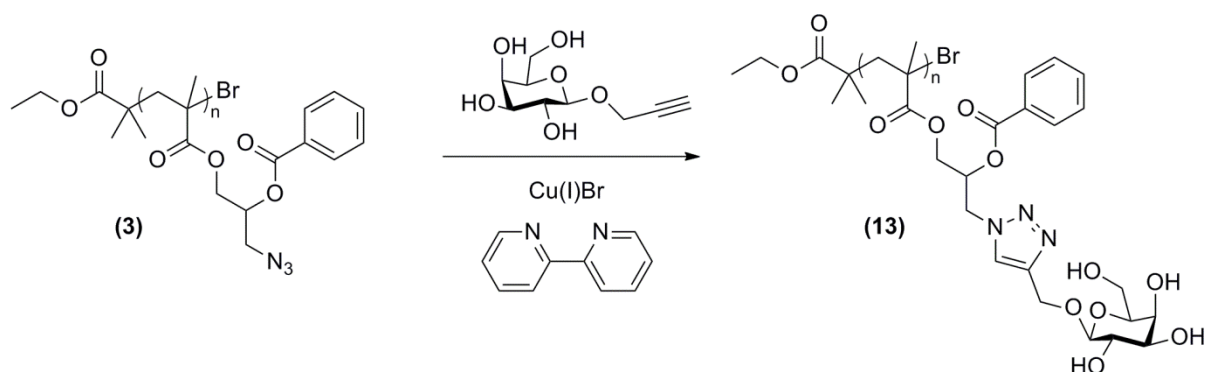
Figure S3.7: Infrared spectra of azide-functional polymer **(3)** and following 1,3-dipolar cycloaddition reaction with β-D-1-propargyl galactose **(13)**.

^{1}H NMR analysis of Post-Polymerisation Modification

The synthetic route employed to obtain the library of polymers was designed to enable each reaction step to be monitored by IR-spectroscopy by the appearance/disappearance of diagnostic peaks, rather than NMR in which there are many overlapping peaks. Potential side reactions (such as the ester linkage being broken into carboxylic acid) would also be visible in IR. To demonstrate the

successfully installation of the azide and carbohydrate groups, representative [1]H

NMR spectra are shown below. The functional polymers obtained here generally

displayed low solubility in most solvents (biochemical assays were undertaken < 1

mg.mL^{-1}). This complicated analysis as DMSO obscured several peaks of interest,

and the intensity was rather low.
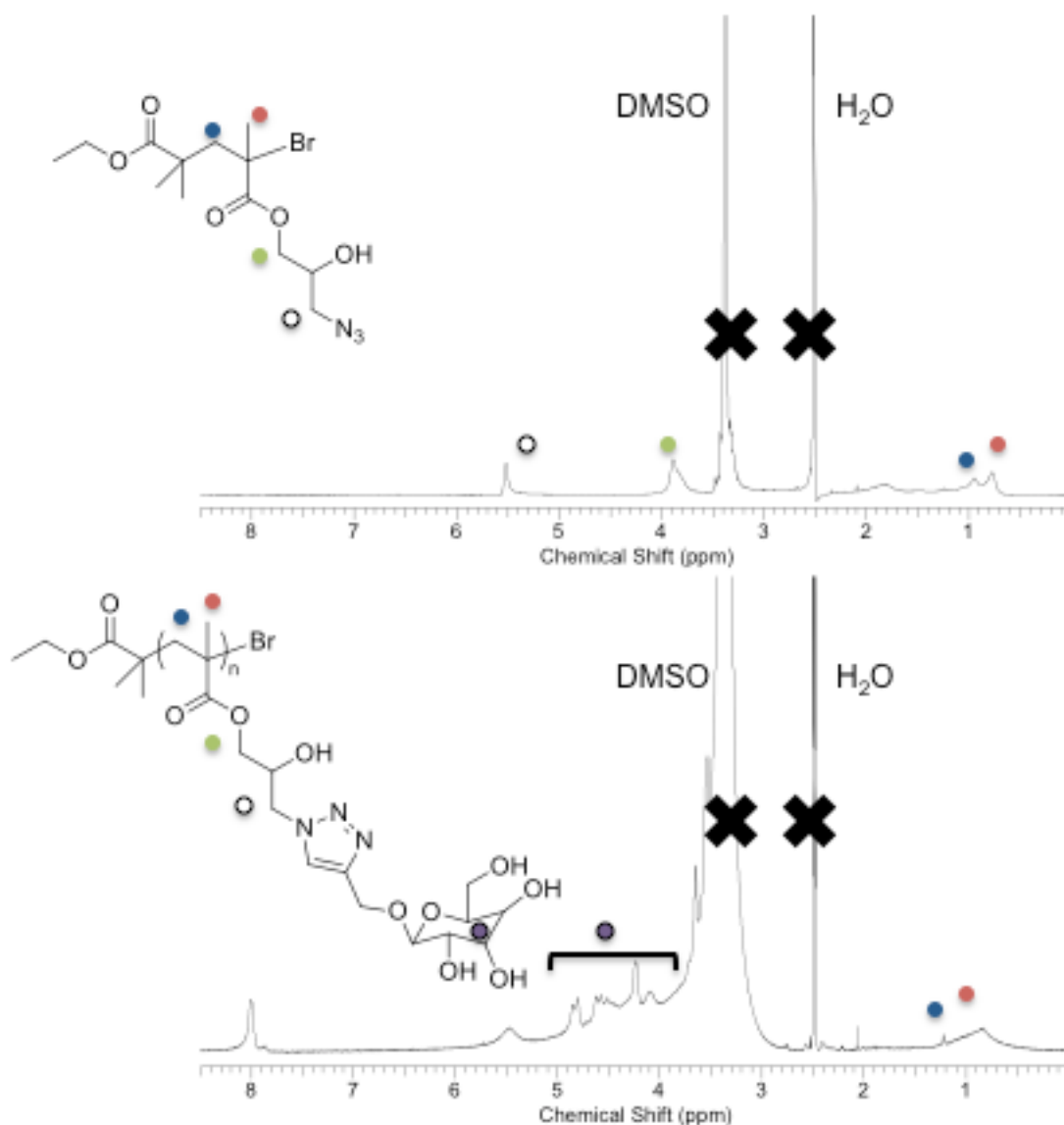
Figure S3.8: ^{1}H NMR analysis of representative polymers showing the successful installation of azide and carbohydrate groups.

Lectin Binding to Galactocerebroside Surface

Binding of each of the lectins to the galactocerebroside-functionalised surface was confirmed by measuring the fluorescence after incubation with a serial dilution of each lectin (Figure S28). As expected, greater binding (higher fluorescence) was observed with increasing lectin concentration.
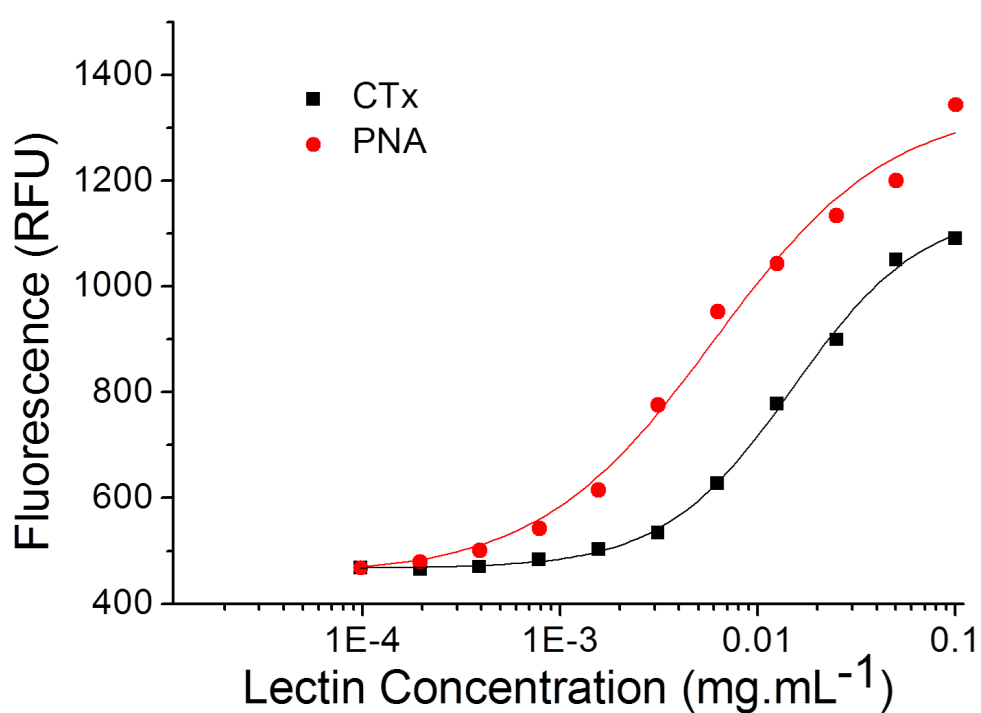
Figure S3.9: Binding curve of a serial dilution of PNA and CTx to a surface functionalised with 0.1 mg/ml of galactocerebroside.

Example glycopolymer inhibition curves

As anticipated, addition of the secondary binding motifs had a dramatic influence on the inhibitory potential of the glycopolymers. Figure S28 shows example inhibition curves for 3 glycopolymers **P1**, **P5** and **P9** against PNA. Addition of 4-chlorobenzyl (**P5**) lead to a dramatic reduction in binding activity with the MIC_{50} value increasing by a factor of 5. Conversely, introduction of a methyl group (**P9**) greatly enhanced inhibitory activity, with the MIC_{50} decreasing by 10-fold.
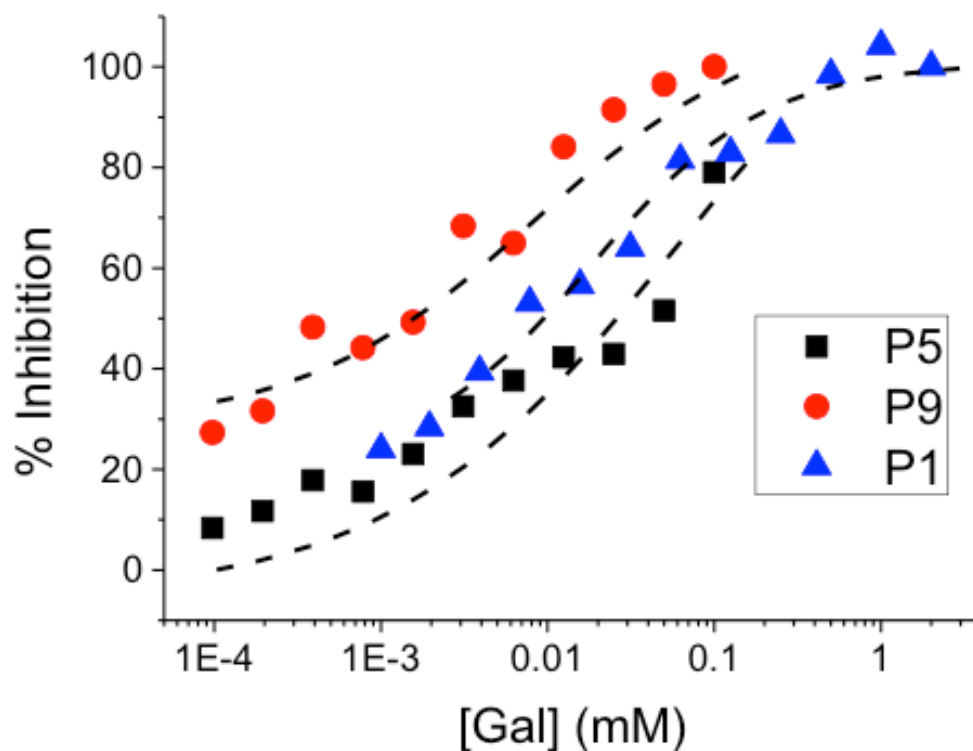
Figure S3.10: Example inhibition curves against PNA. Each point represents the average of 3 fluorescence measurements and the dotted line represents the line of best fit.

Correlation between Inhibition and Partition Coefficient

In small molecule drug design the partition coefficient, which is a measure of hydrophobicity is often used to assign hydrophobic interactions or to predict pharmacokinetics. The partition coefficient of a single repeat unit of each polymer was plotted against the observed MIC_{50} against both lectins, below. There was a peak of lower affinity (higher MIC_{50}) at intermediate values of LogP, but no clear trend emerged.
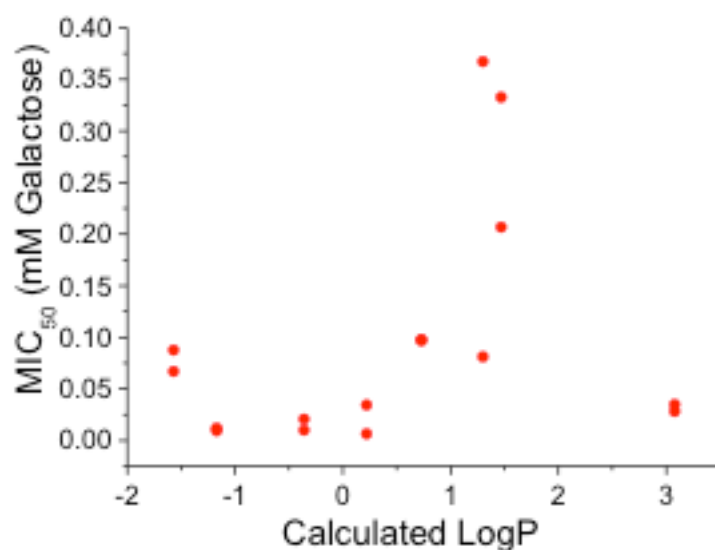
Figure S3.11. Plot showing relationship between (estimated) partition co-efficient of a single repeat unit of the polymers verses the observed MIC_{50} values for both lectins.

RCA_{120} Inhibitory Assay

Table S3.2: RCA_{120} inhibition compared to PNA

Polymer	IC_{50} PNA (mM Gal)	IC_{50} RCA_{120} (mM Gal)
P1	0.087	0.014
P5	0.36	0.017

Comparison of relative affinities of polymer to each lectin

Table S3 shows the relative affinities of each glycopolymer, relative to the control polymer (P1). P5 was selected as the most selective as it maintained its affinity towards CTx, but had significant decreased affinity towards PNA. P8 also demonstrates selectivity. However, this appear due to it have increase affinity towards both lectins.

Table S3.3: Relative affinity of glycopolymers compared to control polymer, **P1**

Polymer	Px/P1 CTx	Px/P1 PNA
P1	1	1
P4	0.52	0.32
P5	1.21	4.20
P6	4.98	2.36
P8	0.10	0.39
P9	0.18	0.11
P10	0.31	0.11
P11	1.45	1.12

Px is the polymer listed in the first column.

Appendix 4

Supplementary Information: Chapter 6

Experimental Section

Glycopolymer Synthesis and Characterisation. The glycopolymers used in this study have been previously reported in a publication (See Chapter 2 and Appendix 1).[1] They were obtained by tandem post-polymerization modification and summarized below for completeness. The reaction scheme used is shown in Scheme S1 and the characterization of the polymers in the subsequent tables. For full details please see the indicated reference.
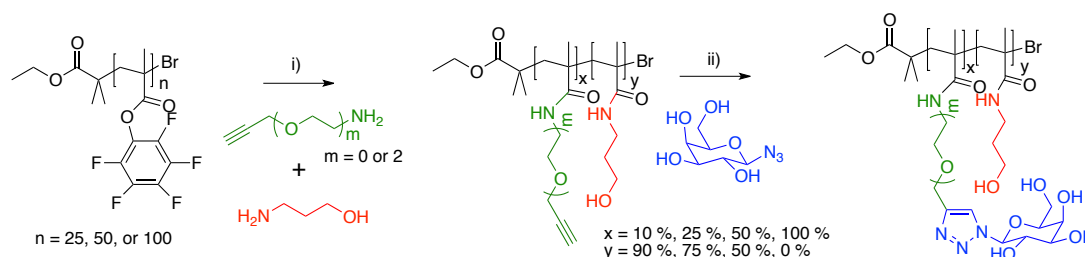
Scheme S4.1: Synthesis of galactose-functional polymers with varying linker length y tandem post-polymerisation modification.

Table S4.1: Molecular characteristics of glycopolymers used in this study

Polymer	DP[a]	Linker[b]	M_n[c] (g.mol^{-1})	M_w/M_n[c]
P1	18	Short m = 0	5100	1.29
P2	33	Long m = 2	10000	1.28
P3	18	Long m = 2	7250	1.32

[a] Theoretical number average degree of polymerization; [b] Alkyne used to modify PPFMA scaffold; [c] determined by SEC in DMF.

Additional Results

Gold Nanoparticle-Linked Measurement of Con A-Mannan Interactions.

Concanavalin A binding to mannan-coated multi-well plates was evaluated as described in the main paper and the data summarized below.
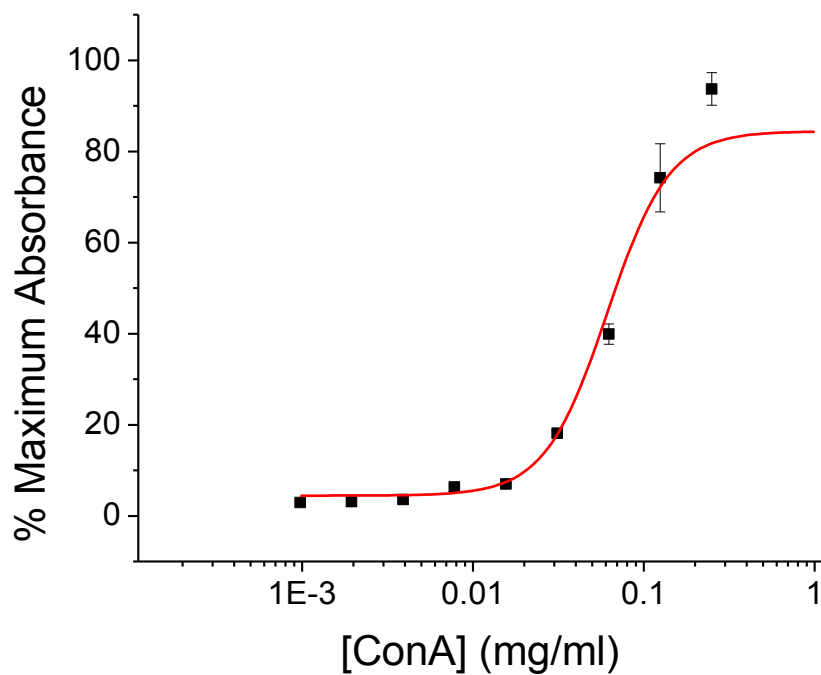
Figure S4.1: Dose dependant binding curves of ConA onto mannam functional surfaces. AuNP absorbance at λ_{max}. Errors bars represent ± standard deviation from a minimum of 3 repeats.

Reference

1.   Richards, S.-J., Jones, M. W., Hunaban, M., Haddleton, D. M., and Gibson, M. I., *Angew. Chem. Int. Ed.* **2012**, *51*, 7812 - 7816.

Appendix 5

Supplementary Information: Chapter 7

Additional Figures

Infrared analysis of PEG-azide before and after cycloaddition reaction. Appearance of O-H stretch at ~ 3500 cm-1 due to sugar can be seen.
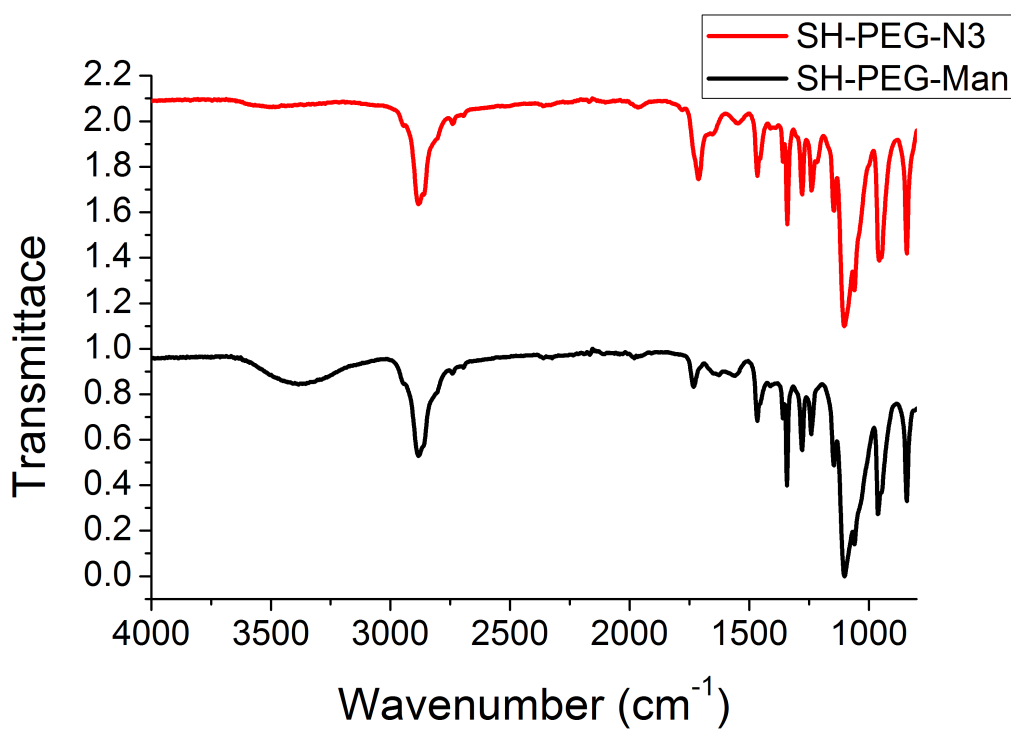
Figure S5.1: Infrared spectra Azido-PEG-thiol (Red) and Mannose-PEG-thiol (Black).

DLS data showing no change in particle size over 2 hour incubation with Con A.
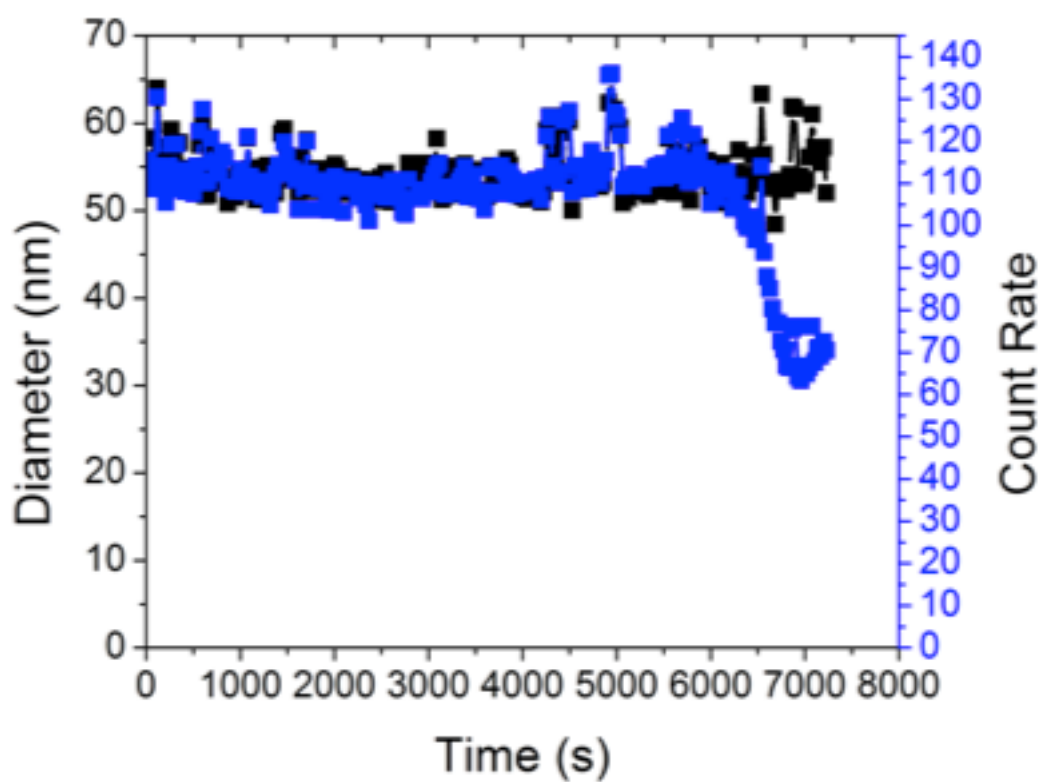
Figure S5.2: Kinetics of **NP-Man** response to Con A by dynamic light scattering
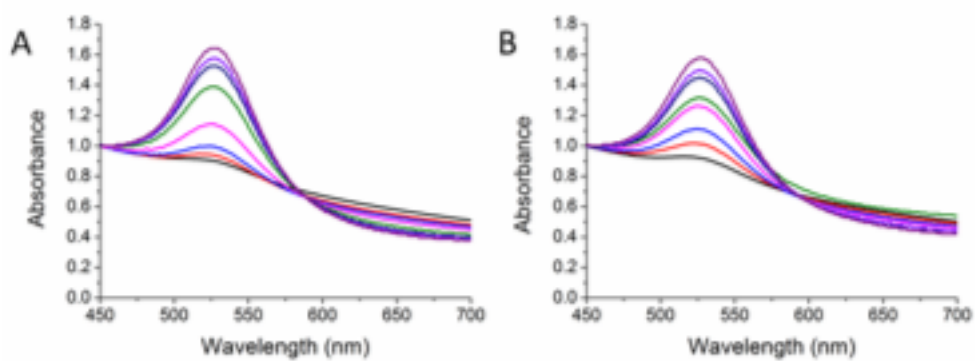
Figure S5.3: UV-visible spectra of **NP-Gal** with K-12 (A) and TOP10 (B)
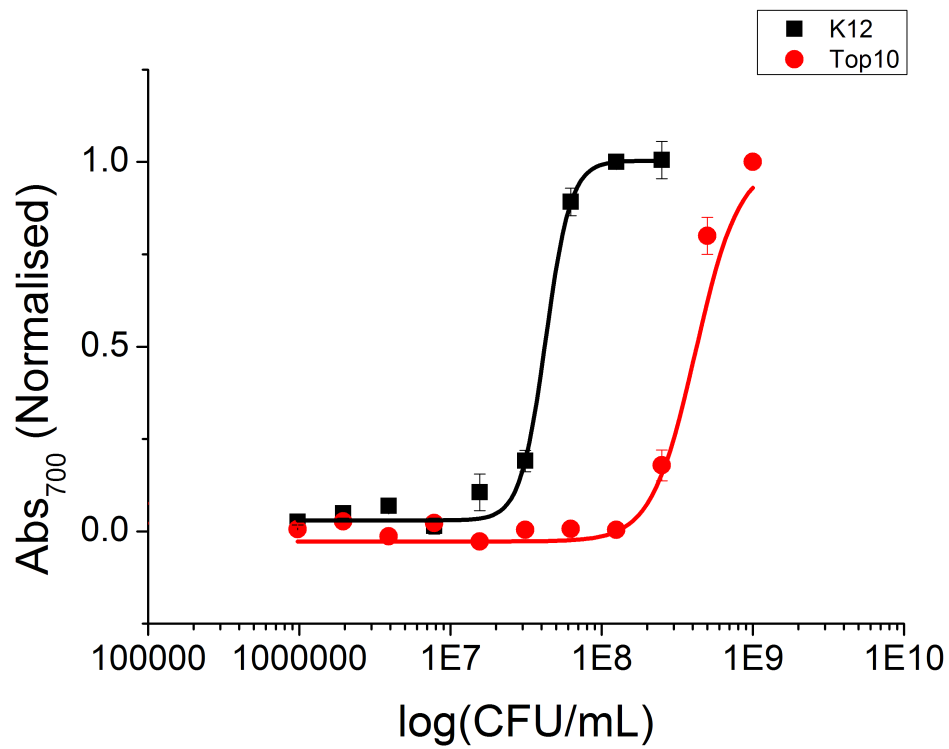
Figure S5.4: Response of NP-Man to bacteria expressed in terms of colony forming units.
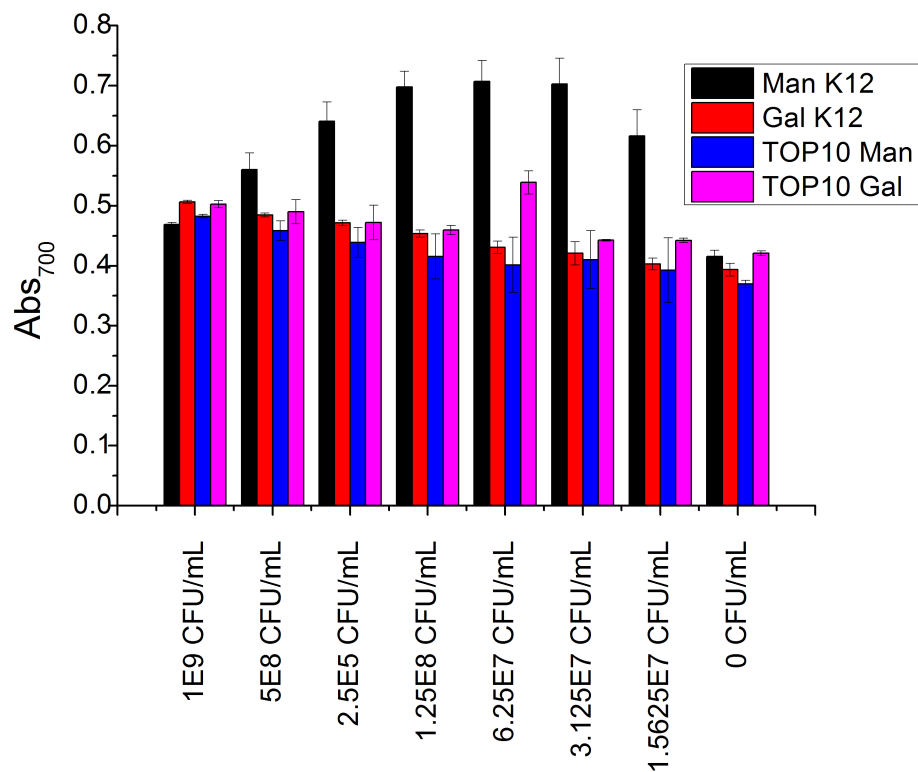
Figure S5.5. Bar chart showing response of mannose and galactose nanoparticles to the different bacteria, expressed in terms of colony forming units.

Appendix 6

Supplementary information: Chapter 8

Additional Figures

Infrared analysis of pHEA before and after reaction of pentafluorophenol end-group with mannosamine. Disappearance of C=O at around 1750 cm^{-1} attributable to the carbonyl associated with the PFP end-group being removed. It was not possible to see appearance of amide peak due to the large number of amides associated with the acrylamide monomer.
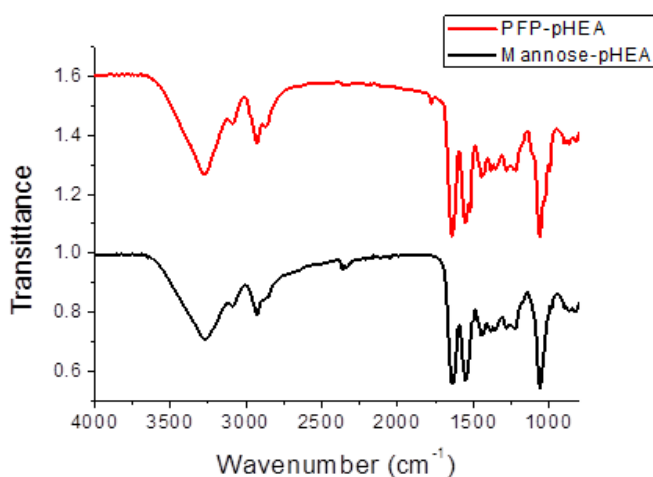
Figure S6.1: Infrared spectra of PFP-pHEA (red) and Mannosamine-pHEA

Differences in percentage functionalisation of DP20:DP10 pHEA-galactosamine polymers on their aggregation behaviour in response to SBA. A 1:1 ratio of DP10:DP20 gives a far lower K_d compared to 1:3 ratio of DP10:DP20. $K_d = 8$ nM for 1:1 and 52 nM for 1:3 DP10:DP20.
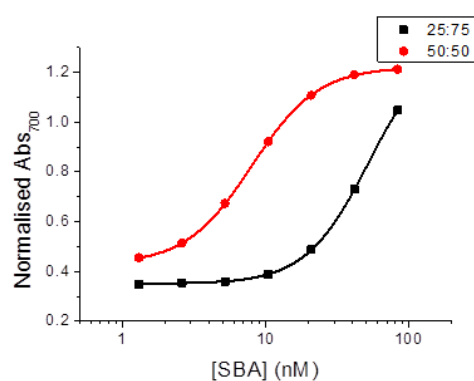

Figure S6.2: Binding isotherms (at 37 °C) of GalNH$_2$-pHEA DP10:DP20 1:3 ratio (black) and GalNH$_2$-pHEA DP10:DP20 1:1 ratio (red) AuNPs with SBA

Dynamic light scattering data to confirm the formation of aggregates upon addition of the correct glycan lectin pairing.
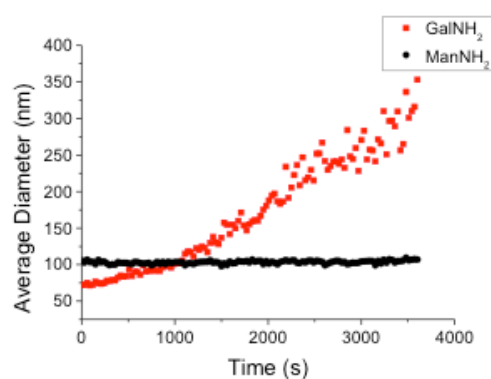
Figure S6.3: Kinetics of AuNP responses to SBA by dynamic light scattering over one hour after addition of 85 nM SBA to GalNH$_2$ functional particles and ManNH$_2$ functional particles.

Aggregation behavior of ManNH$_2$ and GalNH$_2$ particles in response to Con A. K_d

ManNH$_2$ = 109 nM and GalNH$_2$ = 146 nM.
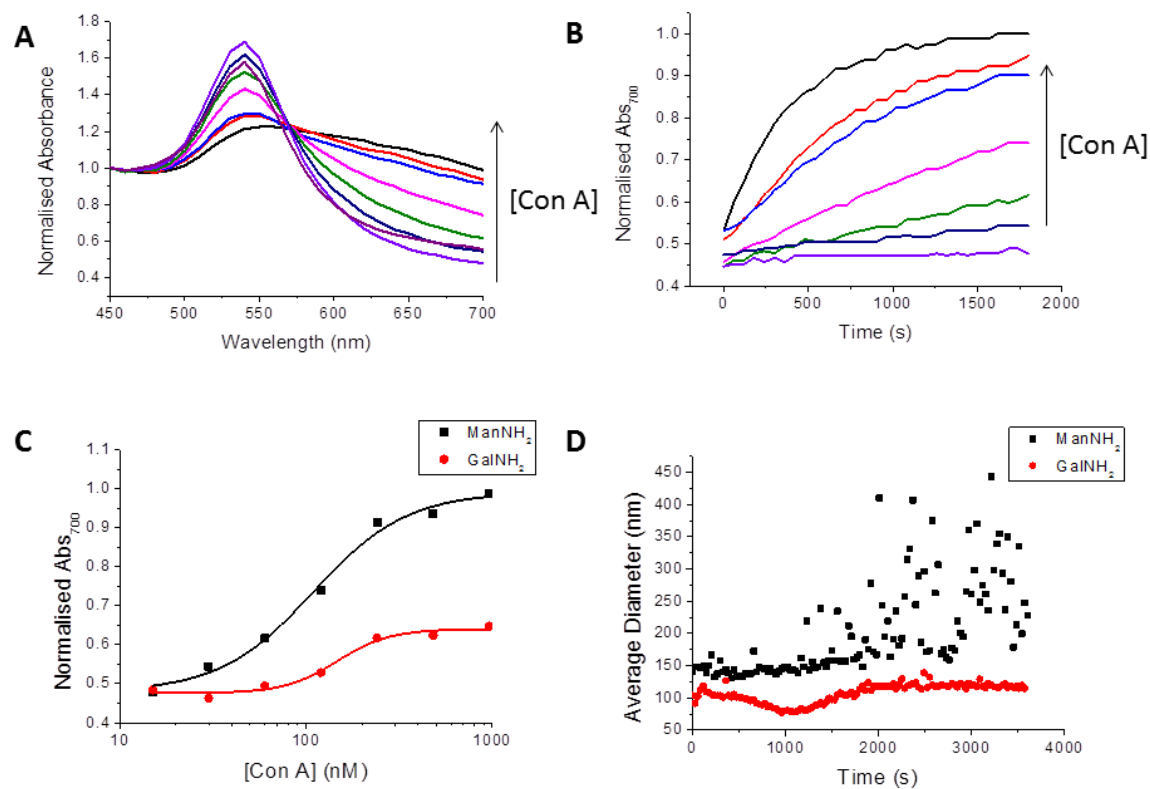
Figure S6.4: Interaction of GalNH$_2$ and ManNH$_2$ functional AuNPs with Con A. (A) UV-Vis spectrum of ManNH$_2$-AuNP upon addition of increasing concentrations of Con A following 30 minutes of incubation. (B) Kinetics of nanoparticle responses to SBA by monitoring Abs$_{700}$ over 30 mins. (C) Binding isotherms (at 37 °C) of ManNH$_2$ and GalNH$_2$ AuNPs with Con A. (D) Kinetics of nanoparticle responses to Con A by dynamic light scattering over one hour.

Aggregation behavior of GalNH$_2$ and ManNH$_2$ particles in response to RCA$_{120}$.
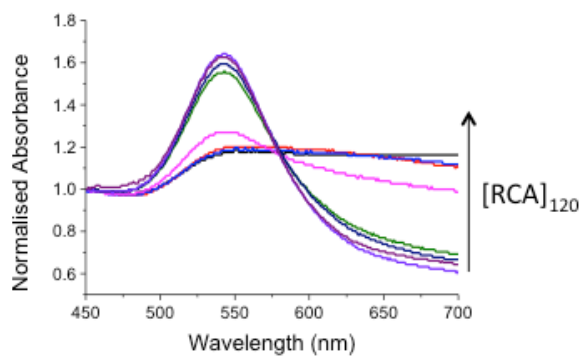
Figure S6.5: Interaction of GalNH$_2$ and ManNH$_2$ functional AuNPs with RCA$_{120}$. UV-Vis spectrum of GalNH$_2$-AuNP upon addition of increasing concentrations of RCA$_{120}$ following 30 minutes of incubation.

Appendix 7

Supplementary Information: Chapter 9
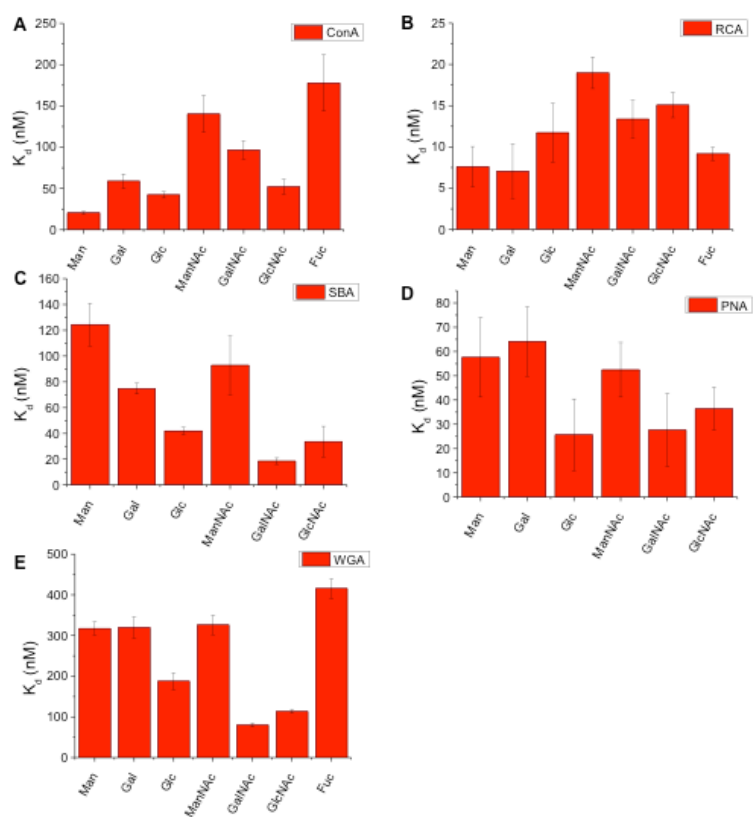
Additional Figures

Size determination of goldnanoparticles by DLS. Before functionalisation (60 nm) and after functionalisation with carbohydrate terminated polymers. There is a size increase of about 5 nm.
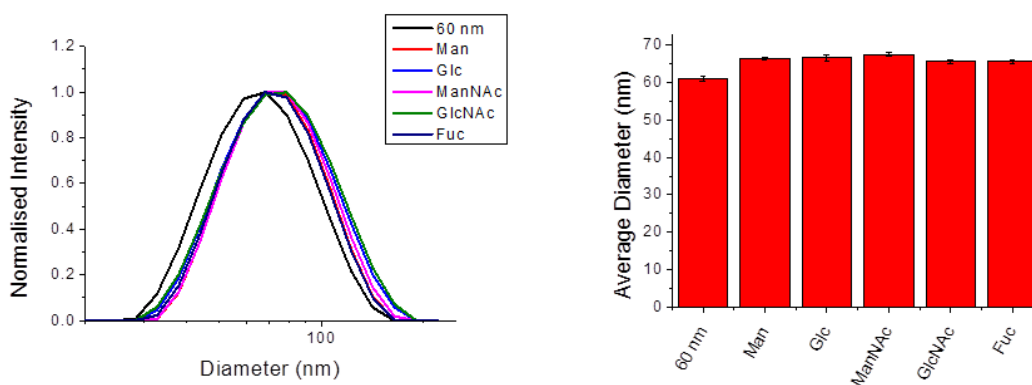
Figure S7.1: Size characterisation of gold nanoparticles after polymer functionalisation.
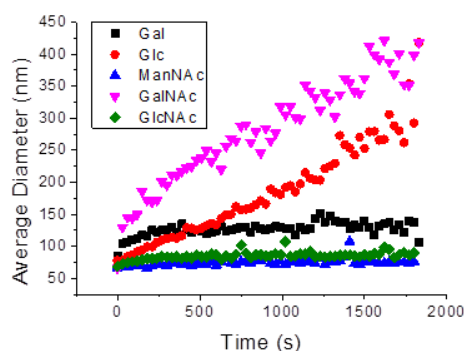
K_d values for each lectin on each surface derived from the hill plots.

Figure S7.2: K_d values of each carbohydrate functionalised gold nanoparticles and lectin pairing.

Size increase of over time of glycogoldnanoparticles upon addition of 200 nM SBA.

Figure S7.3: Kinetics of size increase of gold particles over a 1-hour period in response to SBA by DLS.

Further demonstration of use of pixel intensity to determine apparent K_d values of

protein-carbohydrate interactions using Con A.
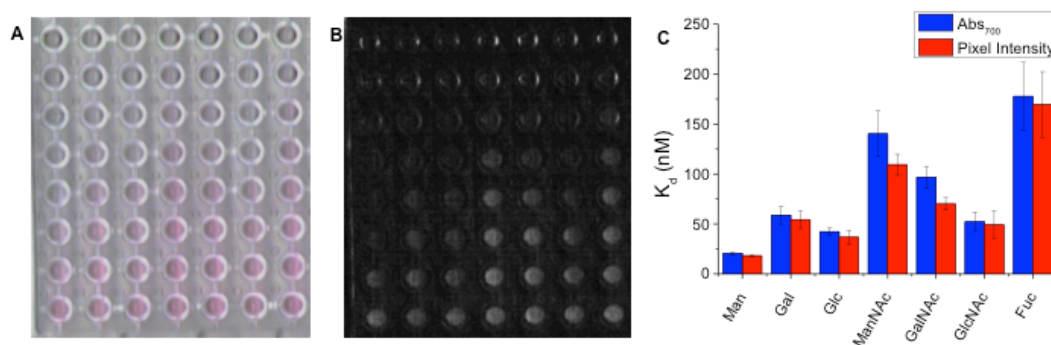
Figure S7.4: Direct optical analysis of protein binding. A) Scanned image of glycoAuNPs with a dilution series of Con A after 30 minutes. B) Saturation image used for pixel intensity measurement (high intensity = red, low intensity = blue). C) Comparison of K_d calculated by Abs_{700} and pixel intensity.

Correlation between K_d values determined by Abs_{700} from UV/Vis spectrometry and pixel intensity for a scanned image and image analysis freeware.